UNIVERSIDADE FEDERAL DE MINAS GERAIS

PROGRAMA DE PÓS-GRADUAÇÃO EM

ENGENHARIA MECÂNICA

PARAGLIDERS FLIGHT DYNAMICS

DIEGO MUNIZ BENEDETTI

Belo Horizonte, 21 de Dezembro de 2012

Diego Muniz Benedetti

PARAGLIDERS FLIGHT DYNAMICS

Dissertação apresentada ao Programa de Pós-Graduação em Engenharia Mecânica da Universidade Federal de Minas Gerais, como requisito parcial à obtenção do título de Mestre em Engenharia Mecânica.

Área de concentração: Projeto Mecânico

Orientador(a): Prof. Dr. Ricardo Luiz Utsch de Freitas Pinto

Universidade Federal de Minas Gerais

Belo Horizonte
Escola de Engenharia da UFMG
2012

UNIVERSIDADE FEDERAL DE MINAS GERAIS

PROGRAMA DE PÓS-GRADUAÇÃO EM

ENGENHARIA MECÂNICA

PARAGLIDER'S FLIGHT DYNAMICS

DIEGO MUNIZ BENEDETTI

Dissertação defendida e aprovada em 21, de dezembro de 2012, pela Banca Examinadora designada pelo Colegiado do Programa de Pós-Graduação em Engenharia Mecânica da Universidade Federal de Minas Gerais, como parte dos requisitos necessários à obtenção do título de "**Mestre em Engenharia Mecânica**", na área de concentração de "**Projeto Mecânico**"

_____

Prof. Dr. Ricardo Luiz Utsch de Freitas Pinto - Orientador

_____

Prof. Dr. Ricardo Poley Martins Ferreira - Examinador

_____

Prof. Dr. Paulo Henriques Iscold Andrade de Oliveira - Examinador

_____

Prof. Dr. Marcos Pinotti Barbosa - Examinador

AGRADECIMENTOS

Agradeço a minha família, amigos e namorada, pelo apoio e compreensão durante os anos de desenvolvimento deste trabalho. Em especial, agradeço a meu irmão André que me apresentou ao vôo livre que hoje é parte fundamental de minha vida.

Finalmente, agradeço especialmente ao professor, orientador e amigo Dr. Ricardo Utsch, que a mais de seis anos tem sido fonte de conhecimento, suporte, e exemplo. E sem o qual, não haveria uma única linha deste trabalho.

CONTENTS

LIST OF FIGURES

LIST OF TABLES

ABBREVIATIONS AND ACRONYMS

AC	Aerodynamic center
AOA	Angle of attack
CG	Center of gravity
DOF	Degrees of freedom

LIST OF SYMBOLS

Latin Letters

a	Tri-dimensional lift coefficient .vs. angle of attack curve slope
a_0	Bi-dimensional lift coefficient .vs. angle of attack curve slope
a_0'	Corrected coefficient .vs. angle of attack curve slope
$\tilde{a}$	Global lift coefficient .vs. angle of attack curve slope
$\bar{a}$	Adjusted local lift coefficient .vs. angle of attack curve slope
AR	Aspect ratio
A_r	Roll arm
A_y	Yaw arm
b	Span
C_0	Central airfoil's length
C_D	Drag coefficient
$C_{D_{CG}}$	CG drag coefficient (Harness and pilot's drag contribution)
$C_{D_{wing}}$	Wing drag coefficient
$C_{D_{total}}$	Total drag coefficient (CG plus wing)
C_L	Lift coefficient
C_m	Pitch moment coefficient
Cm_{x_w}	Roll moment coefficient
Cm_{z_w}	Yaw moment coefficient
C_{m_0}	Bi-dimensional aerodynamic moment coefficient
$\widetilde{C_m}$	Global aerodynamic moment coefficient
$\overline{C_{m_0}}$	Adjusted local aerodynamic moment coefficient
$CTD^{5\%}$	Cycles to damp oscillation up to 5% of initial disturbance
d_{CG}	Central airfoil's aerodynamic center horizontal distance regarding the CG
d_0'	Corrected horizontal distance between CG and global AC
D_0	Bi-dimensional profile drag coefficient

$D_0{}'$	Corrected profile drag coefficient
$\widetilde{D_0}$	Global profile drag coefficient
$D_2{}'$	Corrected induced drag coefficient
D_2	Tri-dimensional induced drag coefficient
$\widetilde{D_2}$	Global induced drag coefficient
$\overline{D_2}$	Adjusted local induced drag coefficient
$e_{(t)}$	Estate variable or dynamic conditions vector
EPI	Endurance performance index
F	Force
G	Gravitational acceleration
$GRPI$	Glide ratio performance index
h_0	Central airfoil's aerodynamic center height regarding the CG
h_0'	Corrected vertical distance between CG and global AC
I_x	Moment of inertia in x-axis
I_y	Moment of inertia in y-axis
I_z	Moment of inertia in z-axis
I_{xy}	Product of inertia in z-axis
I_{yz}	Product of inertia in x-axis
I_{xz}	Product of inertia in y-axis
i_0	Bi-dimensional zero lift angle of attack
$\widetilde{\iota_0}$	Global zero lift angle of attack
L_c	Lateral-coupling modulus
M	Moment
MAC	Mean aerodynamic chord
P	Rotational speed in x-axis
Q	Rotational speed in y-axis
$\bar{Q}$	Dynamic pressure
q_{av}	Average pitch rate in takeoff maneuver
R	Rotational speed in z-axis
r	Glide ratio

S	Wing's reference area
$SM\|_p$	Longitudinal stability static margin
T	Period of oscillation
U	Speed component in x-axis
u_0	Standard disturbance in x-axis speed for stability analysis
U_{min}	Minimum horizontal speed during takeoff maneuver
U_{max}	Maximum horizontal speed during takeoff maneuver
V	Speed component in y-axis
V	Total speed
V_p	Penetration speed
V_{sr}	Sink rate speed
v_0	Standard disturbance in y-axis speed for stability analysis
V_w	Wing speed
W	Speed component in z-axis
w_0	Standard disturbance in z-axis speed for stability analysis

Greek Letters

$\propto$	Angle of attack
$\alpha_{opt.GR}$	Angle of attack for optimum glide ratio
$\alpha_{(L/D)_{max}}$	Angle of attack for maximum wing's efficiency
$\alpha_{opt.Vsr}$	Angle of attack for optimum sink rate
β	Sideslip angle
δ_{B_r}	Brake deflection at right side semi-wing
δ_{B_l}	Brake deflection at left side semi-wing
Φ	Bank angle
ϕ_{max}	Maximum bank due to standard disturbance in y-axis
Γ	Dihedral
Γ_{ef}	Effective dihedral
γ	Path angle

Λ	Seewp
λ	Taper ratio
τ_G	Geometric torsion angle
ρ	Air density
ρ_w	Wing's material surface density parameter
ρ_{air}	Medium air density
Ψ	Yaw angle
$\psi_{\max}$	Maximum yaw due to standard disturbance in y-axis
ω_n	Natural frequency
Θ	Attitude angle or pitch angle
$\theta^{u}_{\max}$	Maximum attitude due to standard disturbance in x-axis
$\theta^{w}_{\max}$	Maximum attitude due to standard disturbance in z-axis
ξ	Damping factor

Subscripts

$()_{min}$	Minimum value
$()_{max}$	Maximum value
$()_{med}$	Medium value
$()_{eq}$	Steady flight (equilibrium) related terms
$()_{sp}$	Short period related terms
$()_{ph}$	Phugoid related terms
$()_{DR}$	Dutch roll related terms
$()_{lp}$	Lateral phugoid related terms
$()_w$	Wing related terms
$()_{CG}$	CG related terms
$()_x$	x-axis related terms
$()_y$	y-axis related terms
$()_z$	z-axis related terms

RESUMO

A prática do vôo de paraglider tem se popularizado nas últimas três décadas, e o desenvolvimento da tecnologia associada ao esporte resultou avanços consideráveis em termos de desempenho e segurança. Entretanto, devido à finalidade desportiva dessas aeronaves, ainda são raros os estudos científicos aplicados ao tema. Os avanços tecnológicos no projeto de paragliders devem-se principalmente aos esforços da indústria , sendo que, apesar de existirem diversos fabricantes com anos de experiência, não é possível encontrar na literatura disponível trabalhos acerca da teoria de projeto de paragliders.

Considerando a falta de informações específicas sobre engenharia de paragliders, uma linha de pesquisa ligada a área de dinâmica de vôo aplicada está sendo desenvolvida no intuito de explicar o vôo de paraglider e, principalmente, relacionar as características de vôo aos parâmetros de projeto dessas aeronaves. Os principais aspectos relacionados à dinâmica de vôo como o desempenho, a estabilidade e a controlabilidade serão investigados aplicando-se conceitos clássicos da engenharia aeronáutica adaptados às singularidades destas aeronaves.

Neste trabalho é feita uma análise completa da dinâmica de vôo dos paragliders. Com isso, tem-se uma base para futuros desenvolvimentos com base em dados de ensaio e um primeiro material no sentido de incentivar a comunidade aeronáutica internacional a dedicar atenção a este campo em particular.

Palavras Chaves: Paragliders, razão de planeio, dinâmica de voo, desempenho, estabilidade, controle.

ABSTRACT

Paragliding has become popular in the last three decades, and the development of modern paragliders has shown considerable improvements on performance and safety. However, due to the sportive purpose of paragliders, scientific studies on this subject are still rare. The achievements on paragliders design are mostly originated from industry, and, although there are many manufactures with years of experience designing paragliders, it cannot be found in the available literature works dedicated on paragliders design theory.

Taking in account the lack of specific information about paragliders engineering, a dedicate work in applied flight mechanics has been developed with the purpose of explain paragliders flight, and specially the relations between flight characteristics and design parameters. The main aspects of flight dynamics as performance, stability, and controllability, are addressed applying the concepts from classical aeronautical engineering adapted to the specificity of these aircrafts.

In this work, a complete theoretical assessment of paragliders flight dynamics is provided. This is supposed to provide a base for future developments using flight test data, and a first focused material in order to incentivize the international aeronautical engineering community to dedicate some attention to this particular branch.

***Key words**:* Paragliders, glide ratio, flight dynamics, performance, stability, controllability.

BIBLIOGRAPHIC REFERENCE

1. Abbott, Ira H.; and Von Doenhoff, Albert E.: Theory of Wing Sections - Dover Publ., Inc., c.1959.

2. Anderson, J., Aircraft Performance and Design, McGraw-Hill, 1999

3. Anderson, John D.: Fundamentals of Aerodynamics – McGraw-Hill, 3º Edition – 2001.

4. Babinsky, H.: Aerodynamic Improvements of Paraglider Performance – AIAA-99-3148 – 1999.

5. Babinsky, H.: The Aerodynamic Performance of Paragliders – The aeronautical journal of the Royal Aeronautical Society - September – 1999.

6. Babister, A.W.: Aircraft Dynamic Stability and Response - Pergamon Pr – 1º edition -1980

7. Bosca, C.O.: Coupled Roll-spiral oscillation – Embry – Riddle Aeronautical University – 01/2010.

8. Chambers, J.R.: Longitudinal Dynamic Modeling and Controlo of Powered Parachute Aircraft - Thesis Submitted in Partial Fulfillment of the Requirement for Master of Science in Mechanical Engineering - Rochester Institute of Technology - Rochester, New York 14623 - April 2007

9. Chapra, S.; Canale, R.: Numerical Methods for engineering – McGraw-hill – 4º edition – 2001

10. Colley, D.P.: Unraveling the mysteries of parachutes. - Compressed Air, 1996. 101(1): p. 12-18.

11. Çengel, Y. A.; Turner, R. H.: Fundamentals of Thermal-Fluid Sciences – McGraw-Hill - 2º edition – 2004

12. Deutscher Hängegleiterverband e.V. in the DAeC.: Airworthiness requirements for hanggliders and paragliders - LTF-2009

13. Etkin B.: Dynamics of Flight: Stability and Control – Wiley – 3º edition – 1995

14. Hattis, P.D. and Benney, R.: Demonstration of precision guided ram-air parafoil airdrop using GPS/INS navigation. Cambridge, MA, USA: Inst of Navigation, Alexandria, VA, USA - 1996.

15. Hiraki, K.: Experimental approach to identify the longitudinal and lateral stability of flexible parafoil – AIAA 2003-2145 – may 2003.

16. Hoerner, S.F; Borst, H.V.: Fluid - Dynamic Lift - Brick Town, N.J., L.A. Hoerner -1975.

17. Hsiao, F. B.; Lin, C. Y.; Liu, Y. C.; Wang, D. B.: Thickness Effect on Low-Aspect-Ratio Wing Aerodynamic Characteristics at Low Reynolds Number – Journal of Mechanics, Vol 24 n□-3, September 2008.

18. Hur, G.B. and Valasek, J.: System Identification of Powered Parafoil-Vehicle from Flight Test Data - AIAA Atmospheric Flight Mechanics Conference and Exhibit. 2003. Austin, Texas, United States.

19. Iosilevskii, G., Center of gravity and minimal lift coefficient limits of a gliding parachute - Journal of Aircraft, 1995. 32(6): p. 1297-1302.

20. Kalro, V. and Tezduyar, T.E.: A parallel 3D computational method for fluid-structure interactions in parachute systems. Computer Methods in Applied Mechanics and Engineering, 2000. 190(3-4): p. 321-332.

21. Kurashova M., Vishnyak A.: Identification of a Paraglider Longitudinal aerodynamic characteristics - Scientific Research Institute of Parachute Constructions - Moscow, Russia – AIAA-95-1560-CP – 1995.

22. Lingard, J. S.: Ram-Air Parachute design - 13th AIAA Aerodynamic Decelerator Systems Technology Conference - May 1995.

23. Lissaman, P.B.S. and Brown, G.J.: Apparent Mass Effects on Parafoil Dynamics - 12th RAeS/AIAA Aerodynamic Decelerator Systems Technology Conference and Seminar. American Institute of Aeronautics and Astronautics: London, England -1993.

24. Mair, W.A.: Aircraft Performance – Cambridge University Press – March 1996.

25. Mashud, M.: Wind Tunnel Test of a Paraglider (flexible) Wing Canopy - International Journal of Mechanical & Mechatronics Engineering Vol: 10 No: 03

26. Massey, B.S.: Mechanics of Fluids – 6th edition – Chapman&Hall - 1989

27. Meier, M.; Stucky, M.: A Pilot's Training Manual – Wills Wing; 7th edition - June 2004.

28. Messinger, M.: "Remote" control. Unmanned Systems, 1994. 12(3): p. 31-2.

29. Mortaloni, P.; Yakimenko, O.; Dobrokhodov, V.; Howard, R.: On the developement of a six-degrees-of-freadom model of low aspect ratio parafoil delivery system - 17th AIAA Aerodynamic Decelerator Systems Technology Conference and Seminar - 19-22 May 2003, Monterey, California

30. Muller, T. J; DeLaurier, J. D.: Aerodynamics of Small Vehicles - Annu. Rev. Fluid Mech. 2003.

31. Munson, B.R.; Young, D. F.; Okiishi, T.H.: Fundamentals of Fluid Mechanics – Wiley – 5º edition 2005.

32. Ogata, k.: Engenharia de Controle Moderno - Prentice-Hall – 4º edition – 2003

33. Pagen, D. The art of Paragliding, Black Mountain Books, 2001

34. Pelletier, A; Muller, T. J.: Low Reynolds Number Aerodynamics of Low-Aspect-Ratio, Thin/Flat/Cambered-Plate Wings – Journal of Aircraft Vol. 37 n□-5, September 2000.

35. Prakash, O; Ananthkrishnany, N.: Modeling and Simulation of 9-DOF Parafoil-Payload System Flight Dynamics - Indian Institute of Technology - Bombay, Mumbai 400076

36. Rogallo, F.M.; Lowry, J.G.; Croom, D. R.; Taylor, R.T.: Preliminary Investigation of a Paraglider –Technical Note D-443 – NASA – 1960.

37. Slegers, N. and Costello M.: Model predictive control of a parafoil and payload system - American Institute of Aeronautics and Astronautics Inc., Reston, VA 20191, United States - 2004.

38. Smith, B. P.; Tanner, C. L.; Mahzari M.; Clark, I. G.; Braun, R. D.: A Historical Review of Inflatable Aerodynamic Decelerator Technology Development - Daniel Guggenheim School of Aerospace Engineering - Georgia Institute of Technology Atlanta, GA 30332-0150 – IEEE 978-1-4244-3888-4 – 2010.

39. Soppa, U., T. Gorlach, and Roenneke A.J.: German contribution to the X-38 CRV demonstrator in the field of guidance, navigation and control (GNC). Acta Astronautica, 2005.

40. Stengel, R.: Advanced Problems of Lateral-Directional Dynamics – MAE 331 -2010

41. Strahan, A.L.: Testing of Parafoil Autonomous GN&C for X-38 - 17th AIAA Aerodynamic Decelerator Systems Technology Conference and Seminar. 2003. Monterey, California, United States.

42. Strickert, G.: Study on the relative motion of parafoil-load-systems - Aerospace Science and Technology, 2004. 8(6): p. 479-488.

43. Subramaniam, V.; Gilat, A.: Numerical Methods with MATLAB- Wiley, 2 edition – 2010.

44. Taylor; John W. R.: Jane's All the World's Aircraft 1987-88 - Jane's Information Group - 1987

45. Tewari, A.: Modern Control Design With MATLAB and SIMULINK – Wiley – 1º edition – 2002

46. Tilley, A.R; Dreyfuss, H.: The measure of man and woman – Human Factors in design - John Wiley & Sons – Revised edition 2002.

47. Toglia, C.; Vendittelli, M.: Modeling and motion analysis of autonomous paragliders - 18th AIAA Aerodynamic Decelerator Systems Technology Conference and Seminar AIAA 2005

48. Toohey, D.: Development of a Small Parafoil Vehicle for Precision Delivery - Massachusetts Institute of Technology -June 2005.

49. Thorpe, A.W.; Curtis, M.F.: Lateral Stability of Tailless Aircraft – Aeronautical Research Council Reports and Memoranda – 1948

50. Walpert, R.A.; Kyle, C.R.: Aerodynamics of the human body in sports – J Biomechanics – 1989.

51. Ware, G.M. and Hassell, J.L.: Wind-Tunnel Investigation of Ram-Air-Inflated All-Flexible Wings of Aspect Ratios 1.0 to 3.0. National Aeronautics and Space Administration: Hampton, VA - 1969.

52. Watanabe, M.; Ochi, Y.: Modeling and Simulation of Nonlinear Dynamics of a Powered Paraglider - AIAA Guidance, Navigation and Control Conference and Exhibit - 18 - 21 August 2008, Honolulu, Hawaii

53. Yamauchi, B.: PackBot: A versatile platform for military robotics - International Society for Optical Engineering, Bellingham, WA 98227- 0010, United States – 2004.

54. Yamauchi, B. and Rudakevych, P.: Griffon: A man-portable hybrid UGV/UAV. Industrial Robot, 2004. 31(5): p. 443-450.

55. Yakimenko, O.: On the Development of a Scalable 8-DoF Model for a Generic Parafoil-Payload Delivery System - 17th AIAA Aerodynamic Decelerator Systems Technology Conference and Seminar - 19-22 May 2003, Monterey, California

56. Yechout, T.R.: Introduction to Aircraft Flight Mechanics – AIAA Education Series – 2003

57. PARA2000 paragliders data source web site: WWW.para2000.org – available in 20/01/2012.

1 INTRODUCTION

A paraglider is an aircraft composed by an inflatable wing linked to a harness by an array of lines as illustrated in figure 1.1 below. Detailed information about paraglider's components and flight principles is provided in chapter 2.

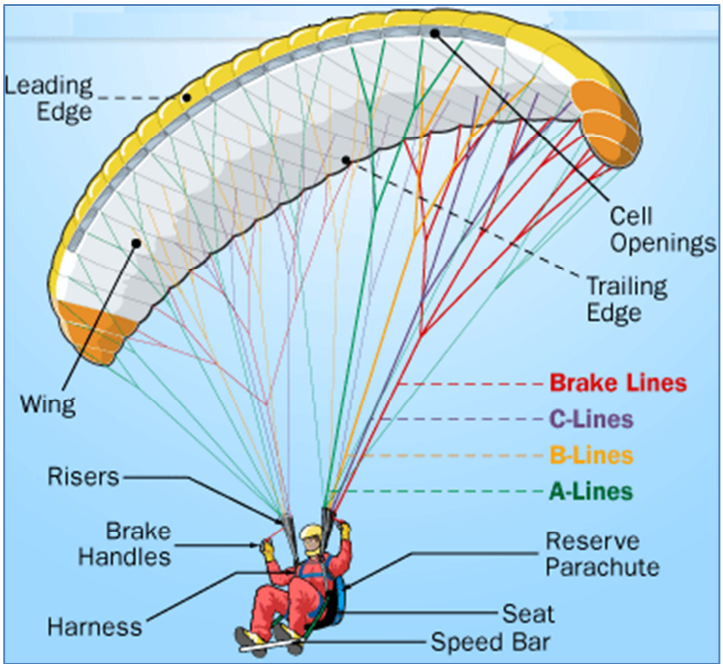

Figure 1.1 – Paraglider sketch

The main characteristics of paragliders flight are the low speed range of operation, the susceptibility to local atmospheric disturbances and the absence of thrust. All these points, allied to the singular geometry and flexible structure, bring major difficulties applying classical theories developed for conventional airplanes flight dynamics.

Paragliding has become popular in the last three decades, and the development of modern paragliders has shown considerable improvements on performance and safety. However, due to the sportive purpose of paragliders, scientific studies on this subject are still rare. The achievements on paragliders design are mostly originated from industry, and, although there are many manufactures with years of experience designing paragliders, it cannot be found in the available literature dedicate works on paragliders design theory.

Some punctual works about paragliders dynamics can be found, however, none of them presents a deep analytical investigation of the paragliders flight characteristics focusing in design

improvements. Anyway, some useful measurements of important characteristics and also some comparisons between different modeling approaches are available, and it constitutes an important source of information which will be widely used in this text. In this way, the basic contents of the most relevant studies available are summarized in section 1.2.

Taking in account the lack of specific information about paragliders engineering, this thesis is part of a on development dedicate work in applied flight mechanics with the purpose of explain paragliders flight, specially the relations between flight characteristics and design parameters. The main aspects of flight dynamics as performance, stability, and controllability, are addressed applying the concepts from classical aeronautical engineering adapted to the specificity of these aircrafts. Also, flight test based validations are being planned for future developments.

The strategy used in this work is mainly based in explain how paragliders works in an engineering viewpoint and parameterize its flight characteristics based in design parameters. This is accomplished by treating each aspect of paragliders flight mechanics starting from a geometry description up to a comprehensive analysis in performance, stability and controllability. The structure of the proposed approach is summarized in chapter 2, which provides a general introductory assessment about all subjects in paragliders flight mechanics addressed in the following chapters.

1.1 Objectives

The main objective of this work is analyzing paraglider's flight dynamics using classic flight mechanics concepts adapted to the singularities of these aircrafts and focusing in conceptual design evaluations. It is intended to explain the flight mechanics of paragliders, especially, the specific phenomena exhibited by these aircrafts. Some conclusive relations between design parameters and flight characteristics are derived, providing a useful tool for theoretical modeling and conceptual design optimizations.

It is necessary to make clear that, it is not the intention of this work to discuss or present piloting techniques, which can be found in many available pilots training manuals. Also, it must be taken in account that the approaches proposed here focus on allowing a reasonable evaluation of flight characteristics without using wind-tunnels tests, flight tests or CFD simulations. Thus, some approximations introduced throughout this text may be reviewed or improved in a second moment using any one of the three tools mentioned above, or even all of them.

Finally, it is expected that the spreading of specialized information about paraglider's engineering may incentivize the development of new technologies leading to improvements on safety and performance of these aircrafts. Being this, beneficial not only for manufactures and pilots, but for the sport itself.

1.2 Bibliographic Revision

Unfortunately there is no specific literature available, which means formally published books, discussing paraglider's flight dynamics. However, some punctual initiatives can be found, as the "Laboratori d'envol" - Laboratory of takeoff - which is a design studio of wings for free flight, placed at 20 km NE from Barcelona. This private initiative comes from a group of engineers interested in developing paragliders and studding its design process. The website provides relevant information about the design process where the practical approach presented is interesting and helpful. Also, it mentions an under-development work in a "paraglider design handbook".

Many relevant pilots training manual can be found in the literature. Those works can be useful to understand the mechanisms involved in paragliders and the piloting techniques. Among these works, the concepts presented by Pagen (2001) are especially helpful to qualitatively understand the principles of paraglider's flight. Also, Meier (2004) provides a very insightful approach about paragliders maneuvering and flying techniques. However, consistently, none of them focus on paraglider's engineering or scientific principles.

A variety of books are available discussing classical flight dynamics, which means, conventional airplanes flight dynamics. These works present the basic concepts necessary to investigate flight characteristics of any specific aircraft. Among them, Yechout (2003) provides a very clear and comprehensive treatment of the entire flight dynamics applied to airplanes. Babister (1980) and Etkin (1995) address the basic concepts in stability and controllability, and Tewari (2002) and Ogata (2003) discuss the concepts of classical and modern control theory. All the knowledge involved in these references is fundamentally necessary for the application of classic flight dynamics concepts in paraglider's design analysis.

Although there are very few works in paragliders dynamics, some important papers addressing subjects related to paragliders flight mechanics or aerodynamics are available. Smith (2010) presents a comprehensive historical review of inflatable aerodynamic decelerator technology development, from which is worthy to mention the developments initiated when NASA Langley

Research Center (LaRC) proposed using inflatable vehicles for manned atmospheric reentry. It incentivized the generation of many different inflatable aerodynamic decelerators (IAD) configurations, which were analyzed and tested for different military and exploration-related applications.

A list of better related references is presented by Chambers (2007) in his thesis, where a complete bibliographic review about the developments in autonomous glided parafoil, unmanned powered parafoils and parafoil's aerodynamics and control literature is provided in details. Although not directly dedicated to paragliders, some works mentioned by Chambers bring important information about devices nearly related to paragliders, and the most relevant among them are summarized below.

Regarding autonomous glided parafoil, some relevant papers were written about the development of the NASA X-38 crew return vehicle (1995 to 2002). Among them are: Strahan (2003) who discusses the results of tests for the autonomous Guidance, Navigation, and Control (GN&C) focusing on the flight test objectives; Soppa (2005), who studied important effects related to wing loading and maximum turn rate; and Hur (2003), who utilizes Texas A & M's modified Buckeye powered parafoil to develop both the longitudinal and lateral/directional models for the vehicle.

Beyond the X-38 project, Hattis and Benney (1996) provided important conclusions about autonomous glided parachutes performance characteristics, in special the lack of accurate parafoil dynamics models available in open literature. This fact is attributed to both the fundamental non-linearity of parafoil performance characteristics and to the difficulty of collecting good empirical data. Also, Slegers and Costello (2004) developed and tested a 6-DOF model for a parafoil-payload system using a model predictive approach. Considering certain restrictions, the model shows itself useful when compared with experimental data. Finally, Strickert (2004) presents a comprehensive study considering relative motions of parafoil and payload, elevating the number of degrees of freedom, and providing a more accurate assessment when compared to other available parachute/payload models.

Considering unmanned powered parafoils, just a few papers can be found up to now. The most useful for the purpose of this work are provided by Messinger (1994), Who briefly introduces his own product, the Remote Aerial Video Assessment Link (RAVAL), and the two works presented by Yamauchi and Rudakevych (2004) describing the "Griffon," a man-portable UAV.

Overall, the most important publications for paragliders are those related to parafoil's aerodynamics and control literature. As a base, Chambers (2007) confirms that: *"Reliable aerodynamic data for wings as in powered parachutes is relatively hard to locate due to the*

challenges presented in testing a flexible airfoil. The large size of a parafoil and its rigging makes a very large wind tunnel a necessity. Inducing changes in angle-of-attack poses additional problems for experimentation". Even though, it is presented important works as: Colley (1996), who provides a general review of parafoil issues in a historical and forward looking perspective; Iosilevskii (1995), presenting a longitudinal model for a gliding parachute and determining limits on the location of the center of gravity; Kalro and Tezduyar (2000) presenting a finite element computational method for three-dimensional analysis of the fluid-structure interaction around a ram-air parachute; And Ware and Hassel (1969) providing, as quoted from Chambers (2007) *"some of the most useful information regarding parafoil aerodynamics"*.

In the 1969 NASA Technical Memorandum SX-1923, Ware and Hassel (1969) tested a variety of large scale parafoils of both constant-wing-area and constant-wing-chord series providing insightful information about the parafoil's flight dynamics, including performance and stability aspects. Also, another very important and widely referenced work is that of Lissaman (1993), in which the "apparent mass" effect is discussed.

Completing the excellent review provided by Chambers (2007), some other papers providing important conclusions about devices nearly related to paragliders can be found. Some works focusing in small UAV (unmanned aerial vehicles), low aspect ratio wings, low Reynolds number flows, aerial delivering systems and others, were very useful developing the many considerations and approximations used in this study. Below are listed the most useful ones:

- Lingard (1995), provides a complete assessment about aerodynamic decelerator systems including a dynamic model and addressing aspects of aerodynamics and control.
- Hsiao (2008), presents the thickness effect on Low-Aspect-Ratio at Low Reynolds Number which provides important tools for the development of an aerodynamic model for paragliders.
- Muller (2003), introduces many concepts applied to aerodynamics of small vehicles which are useful in developing an aerodynamic model for paragliders
- Pelletier (2000), discussed the particularities of low Reynolds number flows over Low-Aspect-Ratio Thin/Flat/Cambered-Plate Wings, providing important conclusions to be taken in account when analyzing paragliders aerodynamics.
- Toohey (2005), developed a small parafoil vehicle for precision delivery presenting many useful approaches to be used when modeling paraglider's dynamics.

- Prakash (2006), discusses the advantages of a 9-DOF Parafoil-Payload System model and presents a comprehensive flight dynamics analysis.
- Bosca (2010), explain the coupled Roll-spiral oscillation, which is a phenomenon pertinent for paragliders, providing a good insight in the related dynamics characteristics.
- Hiraki (2003), presents an experimental approach providing important conclusions about to longitudinal and lateral stability of flexible parafoils.
- Thorpe (1948), provides the basic concepts involved in lateral stability of tailless aircraft, which are completely pertinent to the investigation of lateral-directional stability of paragliders.

Additionally, it is also possible to list some works directly related to paragliders which were very helpful in developing the present work:

- Babinsky (1999) provides an excellent set of tested data and a useful study about paraglider's performance focusing in aerodynamics and constructive improvements.
- Mashud (2010) provides wind tunnel test data of a Paraglider, being very useful for model validation and flight dynamics discussions.
- Toglia (2005), provides an especially useful work modeling an autonomous paragliders and addressing the most relevant issues in dynamics modeling.
- Kurashova (1995), presents useful information about paraglider's longitudinal aerodynamic characteristics, important for longitudinal stability and performance assessments.
- Rogallo (1960), presents a comprehensive discussion about the characteristics of earlier paragliders.

Also, to allow theoretical comparisons, data from manufactures are very useful and can be found openly in the internet. As a major source, it can be indicated the site: WWW.para2000.org which provides a wide range of paraglider's data listing a variety of models.

Finally, it is possible to conclude that many related works done separately by many contributors are available as references and can be used to drive further investigations in paraglider's studies. However, it is also noticeable that paraglider's science needs to be incentivized in order to

increase the number of dedicated works leading to the development of a new dedicated branch in aeronautical engineering.

2 PARAGLIDERS FLIGHT MECHANICS OVERVIEW

A paraglider flight is an excellent demonstration of the principles of aerodynamics. Also, the physics involved in paragliders flight is the same one as in airplanes or gliders. However, due to the flexible structure, the low speed range of operation, and the specific geometry, paragliders presents some relevant particularities that make it a separate subject to be studied as an unconventional aircraft.

The paraglider's flight normally takes place at hills or cliffs where the takeoff is executed with or without the help of a wind component. The wind plays a very important part in takeoff and landings, and it is very important to observe some limits regarding to wind speed and direction. A minimum wind speed is desirable to help wing's inflation. However, an excessive wind speed in takeoff is extremely dangerous increasing the possibilities of loss of control and backward flight, and at landing, contributing for an aggressive wind gradient near to the ground. Another necessary consideration is the wind direction. Takeoff and landings must be always executed with headwind. Also, although flight controls allows some directional compensations, aggressive crosswind components can cause hazardous wing twists and asymmetric collapses, as well as loss of control at takeoff and landing.

After takeoff, the paraglider may flies beneficiating from orographic lift or thermals. Orographic lift flights are easier to perform but some attention must be given to excessive proximities to the terrain. On the other hand, thermals flight is always susceptible to turbulences which sometimes cause violent disturbances of the steady glide demanding a more active piloting. In flight, the basics pilot's tasks consist in defining heading, executing turns and reacting to eventual disturbances in order to bring the paraglider back to the steady glide condition. Finally, the landing is just a controlled steady glide, preceded by a careful approximation over a suitable area, and finalized with a decisive application of brakes in order to stall the wing.

In this chapter the main aspects of paraglider's flight are qualitatively discussed in the same order as they appear in the text. It is presented basic explanations about the paraglider's flight mechanics, providing a necessary background to better understands the approaches and strategies used to investigate each specific proprieties addressed in the future chapters. Also, in each section, some noticeable singularities of paragliders are presented and discussed using basic concepts from classical flight theory and practical observation of paraglider's flight.

2.1 Paragliders Geometry and Constructive Aspects

A paraglider can be designed using innumerous shapes, and the different geometries will result different flight characteristics. Important aspects of performance, stability and control are deeply affected by geometrical proportions. Then, some geometrical relations becomes important parameters for design optimization, as a few examples it can be cited, the ratio between CG height and CG to AC horizontal distance, the ratio between CG height and span, the ration between span and wing area.

In chapter 3, a systematic parameterization of paraglider's geometry is proposed, presenting the advantage of allowing free creation of different wing forms and providing a formulation to calculate geometric proprieties for any kind of design. Using the presented parameterization it is defined the geometric proprieties, most of them already used to characterize airplanes geometry and some other specifically applicable to paragliders.

It will be defined as "constructive aspects" any particularities associated to lines subdivisions, type of sewers, number of internal divisions, possible ribs or wing stiffeners, types of links, harness or materials. It is known that the constructive aspects have important effects in aerodynamics coefficients, especially drag, and also in some flight characteristics as the ability to recover from a collapse or inflation capability. However, it is possible to accounting for the final effects of constructive aspects in an indirect manner using adapted factors and coefficients. In this way, constructive aspects are not directly taken in account in this work.

The geometric proprieties are defined considering the wing fully inflated and behaving as a rigid body structure. Such hypothesis is strong but reasonable as will be substantiated in chapter 5. As a matter of fact, the practical observation allied to other available studies shows that a paraglider in steady glide, or even submitted to small disturbances, behaves as a rigid body. Especially when there are no deficiency of kinetic energy and the lines are fully tensioned.

2.2 Paragliders Aerodynamics and Steady Flight Principles

For any aircraft the aerodynamics aspects are extremely important. In paragliders, the aerodynamics aspects are very hard to be determined due to the specificities of the flexible wing and the low-speed flow. It is noticeable that paragliders presents a combination of high anhedral, low

aspect ratio, flexible wing flying at low Reynolds numbers, which makes the analysis considerably complex.

Anyway, to investigate paraglider's proprieties and dynamic behavior it is necessary to define aerodynamic coefficients. Therefore, in chapter 4 the main aspects of paraglider's aerodynamics are extensively discussed and a methodology to predict aerodynamics coefficients from basic design parameters is provided.

Based on the developments in chapter 4, it is shown that paraglider's steady flight condition is determined by a specific equilibrium angle of attack, which is closely related to the combination of some geometric and aerodynamic proprieties. This equilibrium angle of attack (AOA) is found solving the pitch moment equation for a particular set of design parameters, and presents some applicable limits related to stall and frontal collapse.

The definition of the equilibrium angle of attack leads to the definition of other two variables which completes the set of variables necessary to fully represent the steady flight condition: The flight speed and flight path. The pitch moment equation does not take in account pilots-harness drag or total weight. Thus, using the two longitudinal translational equilibrium equations, related respectively to vertical and horizontal force resultants, it is found the combination of speed and flight path angle which equilibrates the system. Therefore, it can be concluded that three independent variables defines the equilibrated flight condition. Alternatively it can also be expressed also as: penetration speed, sink rate and attitude angle.

2.3 Paragliders Motion and General Dynamics

Considering paraglider in steady flight and even in low bank turns or slightly disturbed conditions, the use of rigid body equations of motion to represent paraglider's movements is shown to be accurate enough for flight dynamics evaluations. The many reasons which corroborate such statements are presented in details in chapter 5, in which a complete dynamic model is developed to mathematically describe paraglider's dynamics.

The analysis of paragliders motion can become as complex as desired. Evaluating the dynamics involved in aggressive maneuvers or strongly disturbed situations is probably an unnecessary and extremely hard task, especially because it demands considerations about wing geometric distortions and unsteady aerodynamics. Therefore, in order to get reasonable results to be

used driving design optimization considerations, using the conventional approaches normally found in classical airplanes modeling theory is shown to be the best option.

Also, the possibility to simulate paraglider's movements makes very important the development of a linear model. This simplified model is derived considering constant wing resultants derivatives obtained near to equilibrium, almost like in classical airplanes stability and control theory, but with some dedicate adaptations due to the fact that for paragliders the parameterization of the in-flight dynamic variables by speed components is more suitable them using wind-axis angles.

It is important to add a special consideration about the utilization of the linear model for paragliders. Due to the increased relevance of some second order terms already mentioned by other authors, the use of constant stability derivatives is quite inaccurate for situations going far from equilibrium. Anyway, the use of simulations to represent paragliders motion can be very helpful identifying many important flight characteristics and revealing the nature of the movements.

By inspecting some different cases, it is possible to see that the paraglider's movements are basically composed by longitudinal and lateral-directional oscillations which cause related variations in flight speed and flight path angle.

2.4 Paragliders Performance Characteristics

Paraglider's performance is usually parameterized by glide ratio, what is a logical approach since glide ratio will allow a more efficient thermal hunting and also provides a better range. It can be seen that in the last two decades paraglider's glide ratio has improved dramatically. This is mostly due to the decrease in drag and increase in aerodynamic efficiency accomplished with the development of new manufacturing techniques and special materials. However, the definition of basic geometric proprieties has a fundamental effect in optimizing glide performance, and then, much can be done by working with geometry based design optimization.

Chapter 6 presents a comprehensive discussion about paragliders performance principles and methods to improve performance. It is provided important relations between design parameters and performance index, and a useful methodology for performance based design optimization. It is shown that paraglider's performance may be improved both by refining aerodynamics coefficients as by optimizing the CG position.

2.5 Paragliders Stability Characteristics

Paragliders presents especially interesting behavior regarding stability. It can be shown that, due to the singular geometry, the modes of motion exhibited by paragliders present relevant differences from those normally found in conventional airplanes. Some effects as the induced phugoid and the roll-spiral coupling constitute important subjects for analysis.

Chapter 7 presents a general view of the classical concepts of stability applied to paragliders focusing on longitudinal stability aspects, presenting a very comprehensive analysis of both static and dynamic stability. Some important stability proprieties are derived using state-space modeling strategy, and also, some simplified approaches are introduced describing analytically the longitudinal modes of motions in order to better explain it.

It is shown that, for paragliders, any disturbance in AOA is rapidly suppressed as a dead-bit short-period oscillation but generates a low-damped attitude oscillation named the induced phugoid. Such oscillation presents period and amplitude depending mostly on the flight speed which is closely linked to wing load. It is possible to show that, although there is a low damping capability, the combination of extended periods and low amplitudes makes these oscillations mostly harmless.

Chapter 8 presents an important discussion about the lateral-directional stability of paragliders, where the main aspects of lateral and directional motion are qualitatively discussed and some basic parameters are defined allowing relate lateral-directional stability proprieties to design parameters.

The results from chapter 8 show that paragliders in general presents good lateral stability characteristics, what is confirmed by practical observation. About directional stability, it can be seen that any effect of the low yaw inertia is dynamically overridden by the strong level of lateral stability.

2.6 Paragliders Controllability and Maneuverability

Controllability and maneuverability are necessary capabilities of any aircraft. The term controllability denotes the ability to maintain controlled or stable flight, change heading, vary speed or recover from an abnormal situation. And, the term maneuverability denotes the ability of

efficiently change flight condition or direction, executing normal tasks as takeoff, turns and Landing, or complex maneuvers as spirals, longitudinal oscillations, or any other possible movement.

The three command mechanisms available in a paragliser are: The brakes, the accelerator, and the CG shifting.

The brakes are composed by two separate array of lines linked to the trailing edge of each semi-wing and works simultaneously as flaps and ailerons.

The accelerator, also called speed bar, is a connection between the frontal lines linked to the leading edge and a bar positioned near to pilot's feet. It allows pilot to reduce wing incidence by shorting the frontal lines.

The CG shifting mechanism is quite simple, and consists in pilot's lateral movements used to dislocate the center of gravity improving turn efficiency.

Chapter 9 discussed the aspects related to controllability and maneuverability of paragliders focusing in the basic maneuvers and control capabilities. The available flight controls are explained and analyzed in order to provide some evaluative parameters, and also some important assessments about the trade-off between controllability and stability.

It is shown that constructive parameters as wing's material specific weight and also geometric proprieties have important effects on takeoff capability. Also, it is shown that wind speed and direction plays a very important part in providing a safe and effective takeoff. A qualitative analysis of the landing maneuver shows that some concerns about wind gradients must be taken in account when defining equilibrium flight conditions and brakes authority in order to provide good landing characteristics. Finally, an analysis of turning performance is made showing the main aspects affecting paraglider's maneuvering capability.

3 PARAGLIDERS GEOMETRY

Both the performance and handling qualities of a paraglider are deeply dependent of the geometric parameters involved in paragliders design. The wing`s shape, the harness position and size, the distribution of lines and risers, the air intakes, and the number of cells, are some of the geometry-related variables that will directly affect the aerodynamics of the system. Therefore, to understand and modeling paragliders flight dynamics it is mandatory to systematically describe paraglider geometry.

It is notable the fact that paraglider's geometry changes in flight. Pilot's control actuations, pressure losses and wing twists can cause momentary or permanent geometric changes. However, it is useful, and precise enough, to define a basic geometry considering the wing fully inflated and the lines fully tensioned, what allows assuming a rigid body structure. Some considerations about structural stability and controls actuations will be addressed in future chapters, however, in this work, all the modeling will be made upon this "assumed" rigid-body basic geometry. Although it might seems like a misleading consideration, for flight mechanics analysis this shall not result relevant deviations. In fact, excluding collapses and some transient situations, the rigid-body behavior can be actually observed in the large majority of a paraglider flight. Toglia and Vendittelli (2005) corroborate this last affirmation by showing that the dynamic behavior observed using a model with 6 degrees-of-freedom (which is analogous to assume a rigid-body structure) presents only a drift from that considering a fully articulated model with 9 degrees-of-freedom. Finally, a more comprehensive explanation about the implications of the rigid-body hypothesis in flight dynamics analysis is provided in chapter 5, showing that this approach is completely sufficient for conceptual design analysis and optimization.

The paraglider geometry can be analyzed considering two complementary terms: the "wing geometry" and the "system geometry". The wing geometry denotes the wing`s shape itself, comprehending the overall wing's curvatures, the wing-section`s profiles, and the air intakes. The system geometry simply denotes the previously defined wing integrated to the harness through the array of lines, including the risers, brake mechanisms, speed bar and the pilot. An important consideration is that, for geometric description purposes, the pilot-harness assembly will be treated as a solid sphere considered to be the center of gravity of the system. Such consideration does not represent an expressive deviation because the "body-drag" and the weight, which represent the main influences of this part in system's dynamics, will be considered properly.

To start the description of paraglider's geometry it is necessary to define the reference coordinate system to be used. It will be applied the concept of "body-coordinate-system" as in classical airplanes design theory (Babister, 1980).

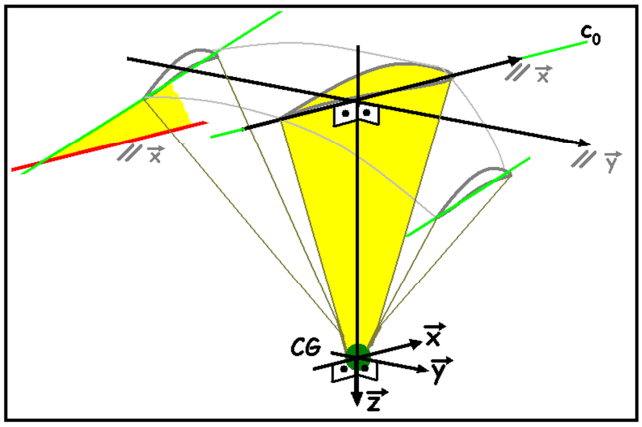

Figure 3.1 – Body coordinate system definition

Observing figure 3.1 above, the "body-coordinate-system", with the origin on the center of gravity, can be defined as follows:

- Axis X: Is the axis contained in paraglider's symmetry plan, parallel to the chord of the central airfoil, passing through the center of gravity, with positive direction going from the trailing edge to the leading edge.

- Axis Z: Is the axis contained in paraglider's symmetry plan, perpendicular to the chord of the central airfoil, passing through the gravity center, with positive direction downwards.

- Axis Y: Is the axis that forms the direct trihedral XYZ. It is perpendicular to paraglider's symmetry plan, passing through the center of gravity, with positive direction towards the right-hand half of the wing.

With the definition of the reference coordinate system it is possible to describe the basic longitudinal body-profile, or, for an obvious reason, the basic triangle:

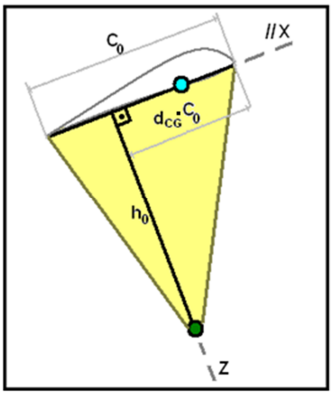

Figure 3.2 – Basic triangle

As shown in figure 3.2, the basic triangle is defined by de central chord length and the position of the center of gravity relatively to this chord. Automatically becomes defined a height of the central airfoil relative to the CG and a projected distance between the center of gravity and the leading edge. Those three parameters (c_0,h_0,d_{CG}) define the basic triangle, representing the fundamental variables necessary to describe the system's longitudinal geometry.

Some authors use different approaches to describe this same geometry. For example, it is common to define a "rigging angle" as in Lingard (1995), which denotes the angle formed by the line connecting the AC to the CG and a line normal to the central chord passing through the CG. However, the parameterization proposed here was understood to be more meaningful for conceptual design investigations because some parameters obtained by combinations of the three variables established above present themselves as important design parameters directly affecting some flight characteristics.

It is important to notice that some other geometry-related variables as the line distribution, harness shape, and flight controls mechanisms do not affect the geometric description. Because of that, each one of these items will be considered separately when applicable.

The array of lines is carefully designed to give the wing the stiffness necessary to keep the intended shape, thus, the lines distribution must be planned taking in account the pressure distribution over the wing managing the wing load wisely. However, assuming it done successfully, the array of lines can be considered only as a source of drag proportional to the amount of lines used.

The flight controls mechanisms are basically defined by an available length of brakes and accelerator (speed-bar). It will be pertinent for flight dynamics modeling, and it shall result two more geometry-related variables which will be introduced in chapter five. In fact, when a flight control device is applied the geometry as described here will change because the "basic triangle" will be

slightly modified, however, it is reasonable to assume that the change in geometry is negligible comparing to the intended effects of such mechanisms in flight dynamics.

In this way, it can be said that for a specific wing the positioning of the center of gravity, the lines distribution and the type of harness selected completely defines the geometry of the paraglider. Nevertheless, it is important to have in mind that, among these three items, only the CG positioning has a practical effect on geometric description.

3.1 Wing's Geometry Parameterization

To describe the wing geometry a set of mathematical functions shall be used in order to allow many different shapes design. As much flexible or comprehensive this parameterization became more different shapes will be possible to analyze. However, the complexity of the mathematical functions grows with model's flexibility. In this way, a tradeoff between comprehensiveness and complexity must be taken in account.

Observing figure 3.1 it is possible to notice some important aspects included in wing parameterization. These functions must be able to describe:

- Different wing curvatures and variable dihedral
- Different and variable sweep angle
- Different chord length distributions
- Different airfoil incidence angles (geometric torsion)

3.1.1 Wing frame definition:

Taking into account the discussion until this point, using the body coordinate system defined in figure 3.1, the wing´s frame geometry can be defined by a set of 4 functions as follows:

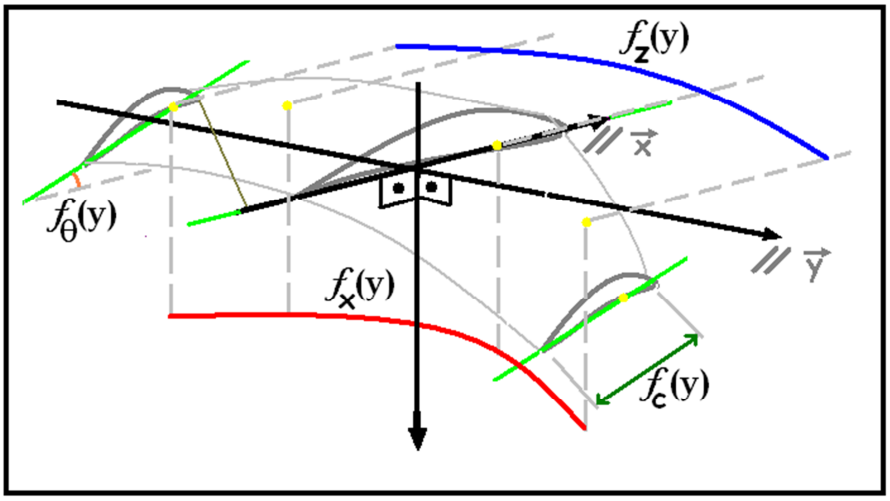

Figure 3.3 – Wing frame geometry definitions

- $f_z(y)$ – The projection of the ¼ chord points in the frontal plane (Z-Y), or, the height of the aerodynamic center of each airfoil relative to the CG as a function of the position along the span.

- $f_x(y)$ – The projection of the ¼ chord points in the horizontal plane (X-Y), or, the horizontal distance of the aerodynamic center of each airfoil relative to the spam as a function of the position along the span.

- $f_c(y)$ – The chord length of each airfoil section as a function of the position along the span.

- $f_\Theta(y)$ – The angle between the chord of a particular airfoil section and the chord of the central airfoil projected in the airfoil's plane, or, the angle of each airfoil chord relative to an axis parallels to axis X contained in the airfoil's plane as a function of the position along the span.

With these four functions it is possible to sketch the wing. Notice that the basic triangle's parameters will be incorporated in those functions.

3.1.2 Airfoil's profile definition:

To completely define the wing it is necessary to define the airfoil shape of each section along the span. To describe the airfoil it can be used the classical methodology defining mathematical functions to represent the center camber line and the thickness of the airfoil as shown in figure 3.4(a) below:

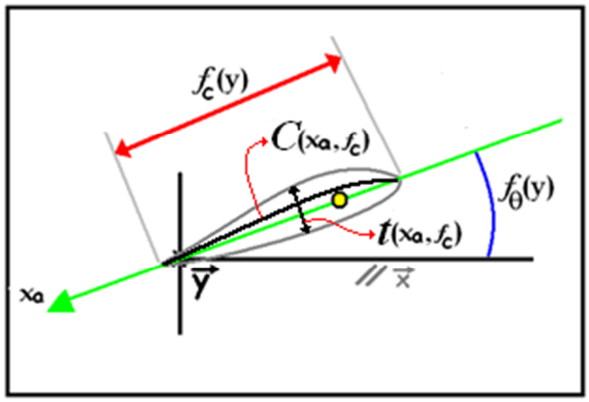

Figure 3.4(a) – Airfoil geometry definitions

Observing figure 3.4(a) above, there are two functions defining the airfoil geometry:

- $C(x_a, f_c)$ – Airfoil center camber line as a function of the position on the airfoil chord.
- $t(x_a, f_c)$ – Airfoil thickness as a function of the position on the airfoil chord.

However, in order to make easy future analytical assessments about the airfoil geometry and related proprieties, it is useful to adopt an alternative airfoil description defining mathematical functions for the upper camber line and lower camber line as shown in figure 3.4(b) below:

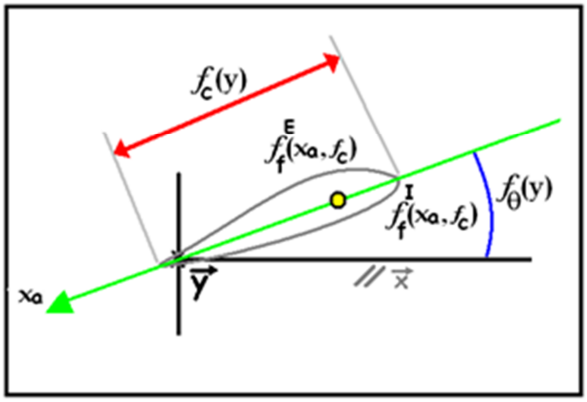

Figure 3.4(b) – Airfoil alternative description

Observing figure 3.4(b) above, the new two functions defining the airfoil geometry can be defined as:

- $f_f^E(x_a, f_c)$ – Airfoil upper camber line as a function of the position on the airfoil chord.
- $f_f^I(x_a, f_c)$ – Airfoil lower camber line as a function of the position on the airfoil chord.

Observe that these functions can be easily obtained from the center camber line and thickness functions previously presented.

Considering aerodynamic torsion the airfoil functions can be different for each wing`s section, it brings a major complexity in the calculation process, however, the benefits of aerodynamic torsion can be very representative for paragliders, and thus, it is useful to mention this feature. Another observation related to those functions is that they will be important for inflation analysis, moment of inertia's calculation and aerodynamic coefficients estimation.

In all examples presented in this text, for simplicity, it will be chosen to use NACA-4-digits airfoils, because it is easy to find basic aerodynamic data and also to mathematically describe its geometry. However, the developments made throughout this text are valid for any kind of airfoil.

3.1.3 General point coordinates calculation for wing sketching:

It is important to be able of calculate general point coordinates using the defined coordinate system. This is especially useful for drawing the wing. Below is shown a wing-section sketch and some notable points.

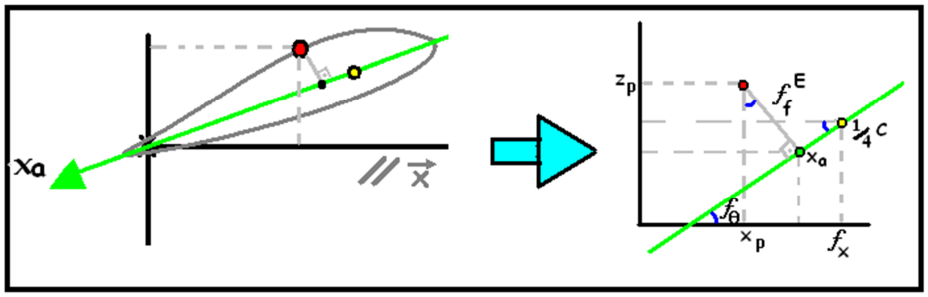

Figure 3.5 – Airfoil section sketch

The airfoil sections are not parallel, but rotate following the wing´s curvature. Because of that, the term $\delta = \text{atan}\left(\frac{\mathrm{d}f_z}{\mathrm{dy}}\Big|_y\right)$ that denotes the dihedral angle in each point of the wing should be taking in account. It is possible to derive the following relations:

For the upper camber line:

$$X_p(x_a, y) = f_x(y) + \left(\frac{1}{4}\cdot f_c(y) - x_a\right)\cdot cos\left(f_\theta(y)\right) - f_f^E\left(x_a, f_c(y)\right)\cdot sen\left(f_\theta(y)\right) \tag{3.1}$$

$$Y_p(x_a, y) = y + \left[\left(\frac{1}{4}\cdot f_c(y) - x_a\right)\cdot sen\left(f_\theta(y)\right) + f_f^E\left(x_a, f_c(y)\right)\cdot cos\left(f_\theta(y)\right)\right]\cdot sin(\delta)$$

(3.2)

$$\left|Z_p(x_a, y)\right| = -f_z(y) + \left[\left(\frac{1}{4}\cdot f_c(y) - x_a\right)\cdot \text{sen}\left(f_\theta(y)\right) + f_f^E\left(x_a, f_c(y)\right)\cdot \cos\left(f_\theta(y)\right)\right]\cdot \cos(\delta)$$

(3.3)

For the lower camber line:

$$X_p(x_a, y) = f_x(y) + \left(\frac{1}{4}\cdot f_c(y) - x_a\right)\cdot cos\left(f_\theta(y)\right) + f_f^I\left(x_a, f_c(y)\right)\cdot sen\left(f_\theta(y)\right)$$

(3.4)

$$Y_p(x_a, y) = y + \left[\left(\frac{1}{4}\cdot f_c(y) - x_a\right)\cdot sen\left(f_\theta(y)\right) + f_f^I\left(x_a, f_c(y)\right)\cdot cos\left(f_\theta(y)\right)\right]\cdot sin(\delta)$$

(3.5)

$$\left|Z_p(x_a, y)\right| = -f_z(y) + \left[\left(\frac{1}{4}\cdot f_c(y) - x_a\right)\cdot \text{sen}\left(f_\theta(y)\right) + f_f^I\left(x_a, f_c(y)\right)\cdot \cos\left(f_\theta(y)\right)\right]\cdot \cos(\delta)$$

(3.6)

*the only reason to use absolute values to the Z axis, is that, in fact, using the defined body coordinate axis, the values in Z are always negative and, for drawing, this is not relevant or desirable.

It is useful to have a tool to draw the designed wing, and to build such tool a good approach is to divide de upper and lower surface in discrete sections of the wingspan. This can be done as follows:

- Divide the wing in M span sections, with M being an even number, that will give us M-1 airfoils through the span with a central airfoil in y=0.
- Divide each airfoil in N chord sections, that will result in N+1 points trough the chord, with one in each edge.
- In this way, for each surface, will be defined (M-1)x(N+1) points.
- Using the equations defined above, it is possible to calculate the two surfaces defined by [Xp,Yp,Zp] as a function of y and Xa, where:
- y=-b/2+k*dy, where dy=b/M, with k from 1 to M-1
- Xa=(j-1)*dXa, where dXa=Fc(y)/N, with j from 1 to N+1

- Finally, it is possible to plot these 2x(M-1)x(N+1) points and visualize the wing.

3.2 Wing's Geometric Proprieties

"Design parameters" are all input variables necessary to define the system under analysis, including: geometry, atmospheric conditions, loads, material or aerodynamic proprieties, etc... In this way, all parameters used to compose the geometric functions previously presented fit in this definition. However, the geometric design parameters can be better represented by using geometric proprieties. These proprieties are more meaningful and will be especially useful to correlate the wing's geometry with paraglider flight characteristics.

The main geometric proprieties are:

- Reference area
- Aspect ratio
- Mean aerodynamic chord
- Dihedral (medium and maximum)
- Sweep angle (medium and maximum)
- Geometric torsion

Although the last three proprieties above are already design parameters, the other three proprieties must be calculated. It is useful to mention that paragliders usually present negative dihedral angle or "anhedral", however, the dihedral concept will be adopted as the design parameter to keep coherence with the classic aeronautical definition.

To derive these proprieties from the definitions presented, it follows:

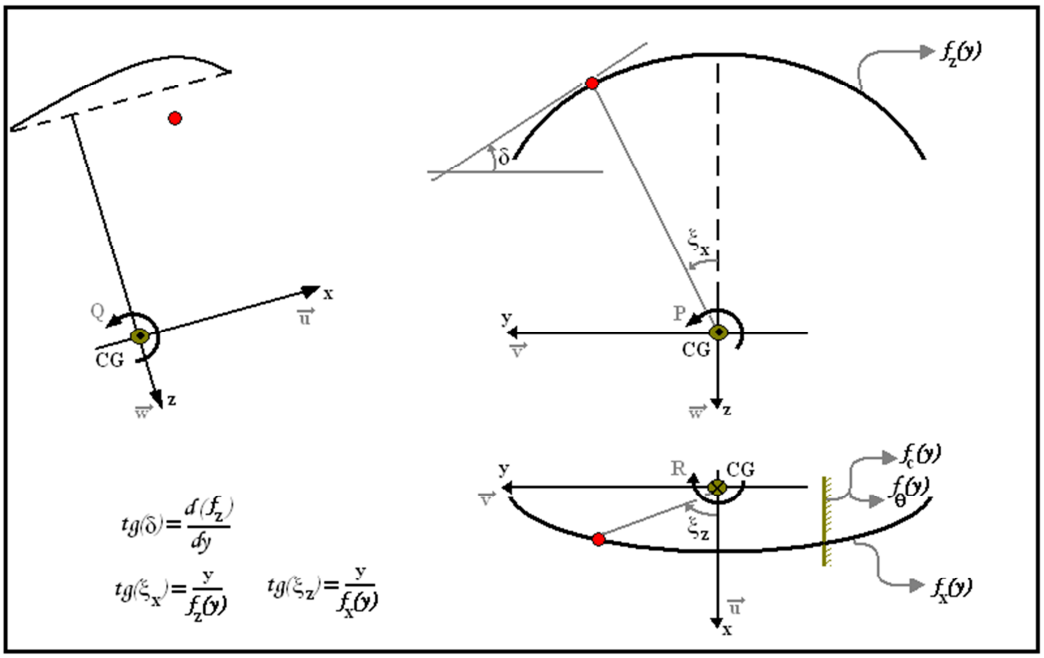

Figure 3.6 – Geometry parameterization

Observing figure 3.6 it is possible to derive the relations presented in table 3-1 below:

Table 3-1: Mathematical relations of geometrical parameterization

Function	Sketch	Parameters	Fundamental relations
$f_z(y)$	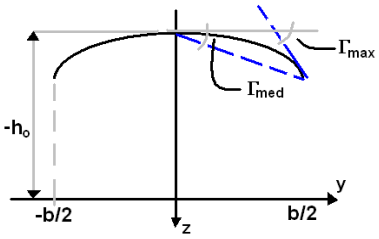	Γ_{med} Γ_{max} h_0 b	$tg(\Gamma_{med}) = \frac{-f_z(b/2) - h_0}{b/2}$ $tg(\Gamma_{max}) = -\frac{df_z(y)}{dy}\|_{b/2}$ $f_z(0) = -h_0$ $\frac{df_z(y)}{dy}\|_0 = 0$
$f_x(y)$	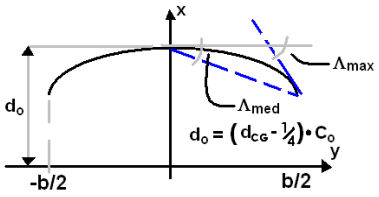	Λ_{med} Λ_{max} d_{CG} C_0 b	$tg(\Lambda_{med}) = \frac{-f_x(b/2) + (d_{CG} - \frac{1}{4}) \cdot C_0}{b/2}$ $tg(\Lambda_{max}) = -\frac{df_x(y)}{dy}\|_{b/2}$ $f_x(0) = \left(d_{CG} - \frac{1}{4}\right) \cdot C_0$ $\frac{df_x(y)}{dy}\|_0 = 0$
$f_c(y)$	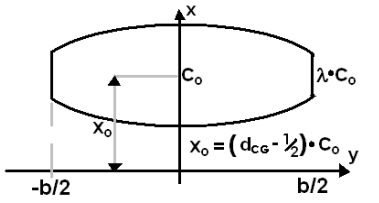	λ C_0 b	$f_c(0) = C_0$ $f_c(b/2) = \lambda \cdot C_0$ $\frac{df_c(y)}{dy}\|_0 = 0$
$f_\theta(y)$	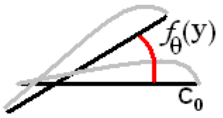	τ_G	$\frac{\tau_G}{2} = \frac{\int_0^{b/2} f_\theta(y) \cdot dy}{b/2}$

To calculate the geometric proprieties it is necessary to define mathematically the previously listed wing`s geometry functions. The above relations are valid for any set of functions, and the mathematical definitions can be done in many different ways; however, in this text, it will be presented three basic approaches as fundamental options:

- The parabolic functions: The use of parabolic functions makes simple the calculation process; however, it is quite limited in terms of design flexibility.
- The elliptical functions: The use of elliptical functions expands flexibility allowing a good range of variations in wing's shape. However the calculation becomes more complex with those functions.
- The elliptical planform: This is a particular case of using elliptical functions. From the classical finite wings design theory (Anderson, 1999), it is know that the elliptical form gives the minimum level of induced drag, and this will be shown to be especially important for paragliders. In this way, some constraint relations can be applied to the elliptical functions to resulting in a elliptical planform;

For the "angle-of-incidence" function, it is enough to define a linear variation as follows: $f_\theta(y) = 2 \cdot \frac{\tau_G}{b} \cdot |y|$, were, τ_G is the geometric torsion on the tips relatively to the root or center.

3.2.1 Parabolic functions

The mathematical relations of table 3-1 applied for parabolic functions gives:

Table 3-2: Geometrical parameterization using parabolic functions

Final function	Param.	Constant definitions
$f_z(y) = A_z \cdot y^2 + C_z$	Γ_{med} h_0 b	$A_z = -\frac{2 \cdot tg(\Gamma_{med})}{b}$ $C_z = -h_0$
$f_x(y) = A_x \cdot y^2 + C_x$	Λ_{med} d_{CG} C_0 b	$A_x = -\frac{2 \cdot tg(\Lambda_{med})}{b}$ $C_x = \left(d_{CG} - \frac{1}{4}\right) \cdot C_0$
$f_c(y) = A_c \cdot y^2 + C_c$	λ C_0 b	$A_c = \frac{C_0 \cdot (\lambda - 1)}{\left(b/2\right)^2}$ $C_c = C_0$

For parabolic functions, it results that:

$$tg(\Gamma_{max}) = 2 \cdot tg(\Gamma_{med}) \tag{3.7}$$

$$tg(\Lambda_{max}) = 2 \cdot tg(\Lambda_{med}) \tag{3.8}$$

3.2.2 Elliptical functions

The mathematical relations of table 3-1 applied for elliptical functions gives:

Table 3-3: Geometrical parameterization using elliptical functions

Final function	**Param.**	**Constant definitions**
$f_z(y) = B_z \cdot \sqrt{1 - \frac{y^2}{{A_z}^2}} + C_z$	Γ_{med} Γ_{max} h_0 b	$A_z = \frac{b}{2} \cdot \frac{\left(1 - \frac{tg(\Gamma_{med})}{tg(\Gamma_{max})}\right)}{\sqrt{1 - 2 \cdot \frac{tg(\Gamma_{med})}{tg(\Gamma_{max})}}}$ $B_z = \frac{b}{2} \cdot tg(\Gamma_{med}) \cdot \frac{\left(1 - \frac{tg(\Gamma_{med})}{tg(\Gamma_{max})}\right)}{\left(1 - 2 \cdot \frac{tg(\Gamma_{med})}{tg(\Gamma_{max})}\right)}$ $C_z = -B_z - h_0$
$f_x(y) = B_x \cdot \sqrt{1 - \frac{y^2}{{A_x}^2}} + C_x$	Λ_{med} Λ_{max} d_{CG} C_0 b	$A_x = \frac{b}{2} \cdot \frac{\left(1 - \frac{tg(\Lambda_{med})}{tg(\Lambda_{max})}\right)}{\sqrt{1 - 2 \cdot \frac{tg(\Lambda_{med})}{tg(\Lambda_{max})}}}$ $B_x = \frac{b}{2} \cdot tg(\Lambda_{med}) \cdot \frac{\left(1 - \frac{tg(\Lambda_{med})}{tg(\Lambda_{max})}\right)}{\left(1 - 2 \cdot \frac{tg(\Lambda_{med})}{tg(\Lambda_{max})}\right)}$ $C_x = -B_x + \left(d_{CG} - \frac{1}{4}\right) \cdot C_0$
$f_c(y) = B_c \cdot \sqrt{1 - \frac{y^2}{{A_c}^2}}$	λ C_0 b	$A_c = \frac{b/2}{\sqrt{1 - \lambda^2}}$ $B_c = C_0$

3.2.3 Elliptical Planform Wings

The formulation for elliptical planform is shown below:

Table 3-4: Geometrical parameterization for elliptical planform

Final Functions	Param.	Constant definitions	Consequences
$f_x(y) = B_x \cdot \sqrt{1 - \frac{y^2}{{A_x}^2}} + C_x$	d_{CG} C_0 b	$A_x = \frac{b}{2}$ $B_x = \frac{C_0}{4}$ $C_x = \left(d_{CG} - \frac{1}{2}\right) \cdot C_0$	$\Lambda_{med} = tg^{-1}\left(\frac{C_0}{2 \cdot b}\right)$ $\Lambda_{max} \to 90°$
$f_c(y) = B_c \cdot \sqrt{1 - \frac{y^2}{{A_c}^2}}$	C_0 b	$A_c = \frac{b}{2}$ $B_c = C_0$	$\lambda = 0$
$f_\theta(y) = 0$	–	–	$\tau_G = 0$

3.2.4 Geometric proprieties calculation

With the geometric functions defined, the main geometric proprieties can be calculated as follows:

Table 3-5: Geometric proprieties mathematical definition

Reference Area	Aspect Ratio	Mean Aerodynamic Chord
$S = \int_{-b/2}^{b/2} f_c(y) \cdot cos(f_\theta(y)) \cdot dy$	$AR = \frac{b^2}{S}$	$MAC = \frac{\int_{-b/2}^{b/2} f_c(y)^2 \cdot dy}{S}$

Considering the geometric torsion negligible for area calculation, these proprieties can be simplified and algebraically calculated for each type of parameterization proposed:

Table 3-6: Geometric proprieties algebraic expressions

Reference Area	Aspect Ratio	Mean Aerodynamic Chord
Parabolic functions		
$S = A_c \cdot \frac{b^3}{12} + B_c \cdot \frac{b^2}{4} + C_c \cdot b$	$AR = \frac{3 \cdot b}{C_0 \cdot (\lambda + 2)}$	$MAC = \frac{6 \cdot \left(3 \cdot {A_c}^2 \cdot \left({}^{b}/_{2}\right)^4 + 10 \cdot A_c \cdot C_c \cdot \left({}^{b}/_{2}\right)^2 + 15 \cdot {C_c}^2\right)}{15 \cdot \left(2 \cdot A_c \cdot \left({}^{b}/_{2}\right)^2 + 6 \cdot C_c\right)}$
Elliptical functions		
$S = C_0 \cdot \frac{b}{2} \cdot \left[\lambda + \frac{arcsen\left(\sqrt{1-\lambda^2}\right)}{\sqrt{1-\lambda^2}}\right]$	$AR = \frac{2 \cdot b}{C_0 \cdot \left[\lambda + \frac{arcsen\left(\sqrt{1-\lambda^2}\right)}{\sqrt{1-\lambda^2}}\right]}$	$MAC = \frac{\frac{2}{3} \cdot C_0 \cdot (2 + \lambda^2)}{\left[\lambda + \frac{arcsen\left(\sqrt{1-\lambda^2}\right)}{\sqrt{1-\lambda^2}}\right]}$
Elliptical planform functions		
$S = \frac{\pi \cdot C_0 \cdot b}{4}$	$AR = \frac{4 \cdot b}{\pi \cdot C_0}$	$MAC = \frac{8}{3} \cdot \frac{C_0}{\pi}$

Finally, it is worthy to mention that these are the most relevant geometric parameters for flight dynamics analysis. In fact, there are other geometric parameters often presented as geometric characteristic by wings manufacturers. However those secondary parameters can be easily derived from the basic geometric parameterization presented here. Below follows some additional parameters commonly used:

- The “flat area”: It means the “real” area and may be used for constructive purposes. It can be calculated as follows:

$$S_{flat} = \int_{-{}^{b}/_{2}}^{{}^{b}/_{2}} f_c(y) \cdot \left(\sqrt{\left(\frac{df_z(y)}{dy}\right)^2 + 1}\right) \cdot dy \tag{3.9}$$

- The “flat span”: it represents the actual wing length and can be indirectly related to the medium dihedral:

$$b_{flat} = \int_{-b/2}^{b/2} \left(\sqrt{\left(\frac{df_z(y)}{dy} \right)^2 + 1} \right) \cdot dy \approx \frac{b}{cos(\Gamma_{med})} \tag{3.10}$$

- The "flat aspect ratio": it represents the aspect ratio considering the flat span and flat area, and the calculation is obvious:

$$AR_{flat} = \frac{{b_{flat}}^2}{S_{flat}} \tag{3.11}$$

- The "Flattening": It is the percentage of area correspondent to the difference between flat and projected (reference) area. It gives an idea of how curved is the canopy, and it can be calculate as:

$$\Upsilon = \left(1 - \frac{S_{ref}}{S_{flat}} \right) \cdot 100\% \tag{3.12}$$

- The "Smoothness": It is a measurement of how smooth is the wing's curvature (applicable for dihedral and sweep angle). A wing presenting a flat center and abruptly curved tips has low smoothness and a wing with an almost constant or well distributed curvature presents high smoothness. This concept is specially applicable for the elliptical parameterization and can be presented in percentage of possible smoothness, it can be calculated as:

$$\Upsilon = \left(1 - \frac{|\Gamma_{max}| - |\tilde{\Gamma}|}{\pi/2 - |\tilde{\Gamma}|} \right) \cdot 100\% \tag{3.13}$$

Where $|\tilde{\Gamma}|$ is the minimum acceptable value for the maximum dihedral/sweep angle based on the parameterization constraints. Notice that the expressions in table 3-3 results a minimum limitation on the dihedral and sweep angle, given by:

$$\Gamma_{max} > 2 \cdot \Gamma_{med} \tag{3.14}$$

$$\Lambda_{max} > 2 \cdot \Lambda_{med} \tag{3.15}$$

3.3 Wing's Moments of Inertia

Using the parameterization defined and considering that the wing's geometric torsions are negligible for inertial effects, the moments of inertia of the paraglider can be derived as using ρ_w, which is the wing's material surface density, and $\overline{\rho_{air}}$, which is a parameter to account for the inside air. This last parameter can be approximated as:

$$\overline{\rho_{air}} = \rho \cdot MAC \cdot \frac{t}{3} \tag{3.16}$$

Where "t" is the airfoil's maximum thickness, and for NACA 4-digits airfoils can be calculated as:

$$t = \frac{fix\left[NACA - 100 * fix\left(\frac{NACA}{100}\right)\right]}{100} \tag{3.17}$$

where $fix(x)$ gives the integer part of x.
Finally the moments of inertia can be calculated as follows:

$$I_x = (\rho_w + \overline{\rho_{air}}) \cdot \int_{-\frac{b}{2}}^{\frac{b}{2}} \int_{f_x(y)-\frac{3}{4}f_c(y)}^{f_x(y)+\frac{1}{4}f_c(y)} (y^2 + f_z(y)^2) \cdot dx \cdot dy$$
$$I_x = (\rho_w + \overline{\rho_{air}}) \cdot \int_{-b/2}^{b/2} (y^2 + f_z(y)^2) \cdot f_c(y) \cdot dy \tag{3.18}$$

$$I_y = (\rho_w + \overline{\rho_{air}}) \cdot \int_{-b/2}^{b/2} \int_{f_x(y)-\frac{3}{4}\cdot f_c(y)}^{f_x(y)+\frac{1}{4}\cdot f_c(y)} (x^2 + f_z(y)^2) \cdot dx \cdot dy$$

$$I_y = \frac{(\rho_w + \overline{\rho_{air}}) \cdot}{6} \cdot \int_{-b/2}^{b/2} \left(3 \cdot f_x(y)^2 - f_x(y) \cdot f_c(y) + \frac{7}{32} \cdot f_c(y)^2 + 6 \cdot f_z(y)^2\right) \cdot f_c(y) \cdot dy$$

(3.19)

$$I_z = (\rho_w + \overline{\rho_{air}}) \cdot \int_{-b/2}^{b/2} \int_{f_x(y)-\frac{3}{4}\cdot f_c(y)}^{f_x(y)+\frac{1}{4}\cdot f_c(y)} (x^2 + y^2) \cdot dx \cdot dy$$

$$I_z = \frac{(\rho_w + \overline{\rho_{air}}) \cdot}{6} \cdot \int_{-b/2}^{b/2} \left(3 \cdot f_x(y)^2 - f_x(y) \cdot f_c(y) + \frac{7}{32} \cdot f_c(y)^2 + 6 \cdot y^2\right) \cdot f_c(y) \cdot dy$$

(3.20)

$$I_{xy} = (\rho_w + \overline{\rho_{air}}) \cdot \int_{-b/2}^{b/2} \int_{f_x(y)-\frac{3}{4}\cdot f_c(y)}^{f_x(y)+\frac{1}{4}\cdot f_c(y)} (x \cdot y) \cdot dx \cdot dy$$

$$I_{xy} = (\rho_w + \overline{\rho_{air}}) \cdot \int_{-b/2}^{b/2} y \cdot \frac{1}{4} \cdot \left(f_c(y) - 2f_x(y)\right) \cdot f_c(y) \cdot dy$$

(3.21)

$$I_{yz} = (\rho_w + \overline{\rho_{air}}) \cdot \int_{-b/2}^{b/2} \int_{f_x(y)-\frac{3}{4}\cdot f_c(y)}^{f_x(y)+\frac{1}{4}\cdot f_c(y)} \left(y \cdot f_z(y)\right) \cdot dx \cdot dy$$

$$I_{yz} = (\rho_w + \overline{\rho_{air}}) \cdot \int_{-b/2}^{b/2} y \cdot f_z(y) \cdot f_c(y) \cdot dy$$

(3.22)

$$I_{xz} = (\rho_w + \overline{\rho_{air}}) \cdot \int_{-b/2}^{b/2} \int_{f_x(y)-\frac{3}{4}\cdot f_c(y)}^{f_x(y)+\frac{1}{4}\cdot f_c(y)} \left(x \cdot f_z(y)\right) \cdot dx \cdot dy$$

$$I_{xz} = (\rho_w + \overline{\rho_{air}}) \cdot \int_{-b/2}^{b/2} \left(2 \cdot f_x(y) - \frac{f_c(y)}{2}\right) \cdot f_z(y) \cdot f_c(y) \cdot dy$$

(3.23)

Observe that, due to the wing symmetry, the I_{yz} and I_{xy} products will be null.

3.4 Paragliders geometry definition summary:

At this point the paraglider's geometry parameterization is almost complete. With the parameters defined here the geometric proprieties can be calculated and analyzed, however, four geometry-related items remain uncovered and will be introduced separately in future chapters:

- The flight control devices (accelerator/brakes) geometry: As will be discussed in chapter 5 and chapter 9, an available length must be defined for both brakes and accelerator (speed bar). This definition is useful for controllability analysis but has no effects on geometric proprieties.

- The air entrance opening geometry: As will be discussed in chapter 4, a "cut" in the airfoil leading edge exists for wing inflation. This opening must be defined by a position and an angle relative to the profile chord. This will be useful to analyze structural stability and aerodynamic issues but it has no effects on geometric proprieties.

- The number of cells and the array of lines: The number of cells and the array of lines are construction definitions. The same geometry can be built using different number of cells and lines distribution. Therefore, although it has important effects on structural stability and aerodynamics issues, it has no effects on geometric proprieties.

- The harness connections wideness: The distance between the carabineers connecting each semi-wing to the harness is important for controllability and lateral stability effects. Although some difference in the final canopy's curvature may result from different settings of this distance, the effects in geometric proprieties are still negligible.

Observing the geometric parameters introduced in this chapter, fourteen variables define the wing-frame geometry which is sufficient to calculate the main geometric proprieties. Other four variables will be added, as explained above, to complete the design definitions. Thus, the paraglider`s geometry can be fully defined with eighteen variables.

It is important to notice that for calculate the inertias it is also necessary a "material" propriety – the wing surface density – and an environmental propriety – the air density. These are initial design definitions, thus it is supposed to be selected based on fundamental design objectives.

Some illustrations of particular design cases using the parameterization proposed in this chapter is shown in figure 3.7 below:

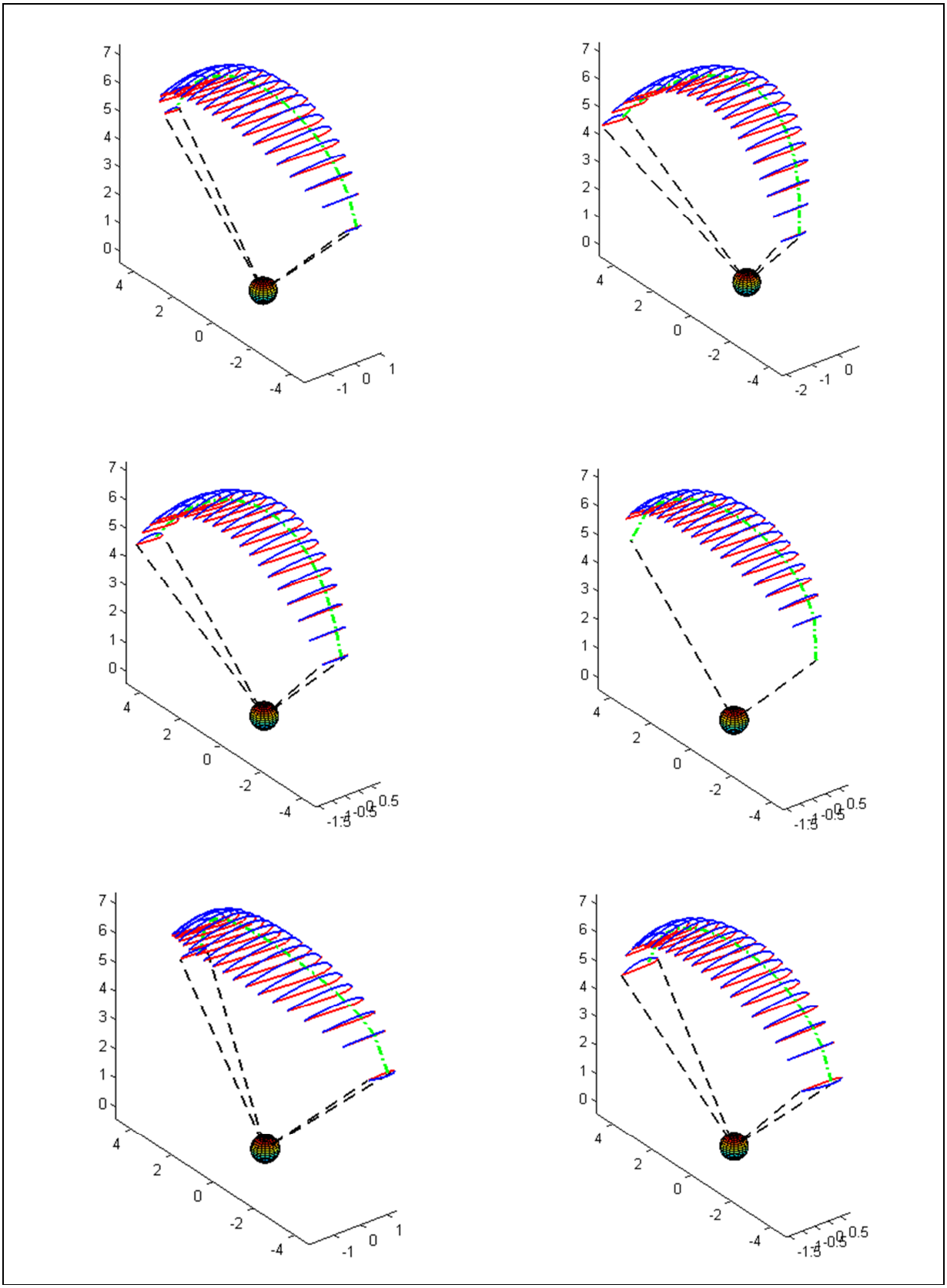

Figure 3.7 – paragliders illustrations

4 PARAGLIDERS AERODYNAMICS

Among the various aspects involved in paraglider's flight mechanics, the aerodynamics of paragliders is a specially important and challenging one. In this chapter it is presented a qualitative and quantitative analysis of the fundamentals of paraglider's aerodynamics, including a practical method to estimate aerodynamic coefficients based on design parameters.

In any aircraft, the aerodynamic proprieties are of first importance determining flight characteristics. The dynamic behavior of the aircraft is tightly linked to its aerodynamics proprieties, because of that, the understanding of the particularities involved in paraglider`s aerodynamics is completely necessary to allow a deeper understanding of paraglider`s flight mechanics. In this way, the results obtained here will be used in all future analysis.

The aerodynamic proprieties are usually represented by the aerodynamic coefficients well established in classical aerodynamic theory as presented, for example, in Anderson (2001). The usual approaches to accurately obtain these coefficients are mostly based in experimentation. However, in the initial stages of a design process is quite hard to predict the aerodynamics coefficients efficiently. Although some theoretical simplified formulations and computational tools can provide a good estimative, the methodology available was mainly developed for airplanes and the direct application for paragliders may drive to non-realistic values and misleading conclusions.

Unlikely conventional airplane's wings, paragliders presents textile material wings with low aspect ratio, aggressive and variable anhedral, frontal air intakes, flying at moderate Reynolds numbers. Then, as the aerodynamic proprieties are deeply affected by all these characteristics, paraglider's particularities directly affect the complexity of the aerodynamic analysis and significant deviations could be expected using classical formulations. Because of that, a dedicate analysis focusing on the most relevant singularities of these aircrafts, capable of explain the fundamentals of paraglider's flight and relating the aerodynamic proprieties to wing`s geometric design parameters, is of great utility for conceptual design evaluations.

A comprehensive aerodynamic model specifically developed for paragliders which would take in account all particularities of those wings are not available yet. Some papers with important developments for flexible wings and ram-air parachutes are available, but generally they are not completely applicable for paragliders. Some available works (Hsiao, 2008; Lingard, 1995; Muller, 2003; Ware, 1969), present dedicate approaches to estimate aerodynamic coefficients for different aircrafts presenting each one of them some characteristics similar to paragliders. In these works it is possible to found explanations for some interesting aerodynamic behaviors observed in

paraglider's flight. Also, efforts were made deriving aerodynamic coefficients based in experimentations or in adaptations of classical formulations. However, the singular characteristics of paraglider's wings strongly contribute for additional deviations using such general approaches. It is worthy to mention that among the available bibliography the works presented by Babinsky (1999) are especially useful. In these papers the author presents a very good analysis of the fundamentals of paraglider's aerodynamics and also provides some experimental data obtained by wind-tunnel tests of some planar wing models.

Although the development of an accurate aerodynamic model for paragliders would be an important achievement, it would require an entirely dedicated work comprehending many complex subjects as: considerations about constructive techniques, effects of local distortions due to wing's flexibility, and others items demanding experimentation. Therefore, this is beyond the scope of this text. On the other hand, as the main objective of this work is to analyze the influence of the design parameters on flight characteristics and to understand paraglider's aerodynamics, the direct application of simplified formulations is not accurate enough. Because of that, an alternative approach will be developed to calculate the wing's aerodynamic forces and moments in each wing section providing a better understanding about how aerodynamics forces and moments act throughout the wing and how the lift and drag distribution changes according to wing's geometry. This shall allow sufficiently deep analysis and a more accurate assessment of aerodynamic proprieties to be used in conceptual design developments. As listed below, five main aspects of paraglider's aerodynamics are addressed:

- In-flight structural stability constraints.
- Paraglider's specific limitations using classical aerodynamics theory.
- Estimation of aerodynamic coefficients based on design parameters.
- Wing's forces and moments calculation and analysis.
- Conceptual design aerodynamics improvements.

4.1 Wing's Structural Stability Preliminary Evaluation:

When studying paraglider's flight mechanics and aerodynamics it is common to deal with the wing as a rigid-body structure, which means, assuming that the wing is always fully inflated. This fundamental consideration deserves a dedicated analysis to explore its consistency and implications. Although it might seem to be a strong assumption, it does not represent a relevant deviation for the present purposes. Indeed, in equilibrium and also in maneuvers were there are no kinetic energy deficiency, this assumption is clearly confirmed.

The capability to maintain the wing's shape is also a design goal because the structural stability is obviously an important characteristic for safety. Therefore, a relevant concern is to sustain the pressure differential that keeps the wing inflated. The airfoil shape and thickness and also the operational speeds have special importance in this task.

Accordingly classical fluid dynamics principles it is easy to show that the pressure differential between the inside and outside surfaces of a caved body immersed in a fluid is directly related to the dynamic pressure applied by the flow.

Practical observation shows that paragliders with large air entrances have better structural stability. That's because the pressure imposed by the incoming flow inside the wing is what keep it inflated. This practical observation can be easily repeated by experimentation. However, it is interesting to investigate the inflation of the wing in a qualitative sense to understand how the characteristics of the airfoil will affect this essential capability.

In order to keep the wing inflated, the pressure differential between the inside and outside surfaces must generate a force at least grater then the weight of the wing's material acting in each section of the wing.

For paragliders in steady flight, it can be assumed that the fluid inside the wing is at rest. Therefore, the incoming airflow hits the cavities of the leading edge applying pressure on the inside air. This pressure is distributed around the inside surface. If no losses were involved in this process, the resultant inside pressure would equals airflow total pressure, or stagnation pressure. However, the geometry of the air entrances plays a relevant part determining the amount of total pressure effectively transferred to the inside air.

The outside surface is submitted to a specific pressure distribution that is a function of airfoil characteristics, angle of attack and speed. In general, the pressure around an airfoil is lower than the reference static pressure (local atmospheric pressure). Therefore, for a preliminary evaluation, it can be conservatively considered that each point in the outside surface is submitted to

atmospheric pressure, what will result an inside-outside pressure differential over each section substantially lower than that expected in practice.

At this point it is interesting to define a "structural stability factor – SSF" that can be calculated dividing the estimated minimum available surface pressure differential by the surface load due to wing's weight.

Quantitatively, this factor can be calculated using an objective approach to compare the wing's material surface load and a minimum effective surface pressure differential. This approach must also to take in account the wing openings geometry as an efficiency factor.

Knowing the total weight of the wing, a wing surface density ρ_w in mass per surface area can be estimated and the load that must be counterbalanced by the inside-outside pressure differential can be calculated as follows:

$$L_{surf} = \rho_w \cdot g \tag{4.1}$$

Where g denotes the gravitational acceleration and ρ_w the "wing surface density" considering the total weight of the wing including ribs, lines, or any other components directly attached to the textile material.

Conservatively, considering external static pressure around the airfoil in each point, the inside-outside pressure differential can be described as a portion of the available airflow dynamic pressure:

$$\Delta P = \varepsilon_A \cdot \left(\frac{1}{2} \cdot \rho \cdot V^2\right) \tag{4.2}$$

Where "ε_A" represents an efficiency factor to account for losses related to the air entrances geometry, which reduces the total airflow dynamic pressure effectively transmitted to the inside air.

In order to estimate ε_A it is necessary to have the wing geometry fully defined. Then, it must be determined the frontal opening size and shape that will form the air intakes. Figure 4.1 below illustrates the main parameters involved in wing inflation:

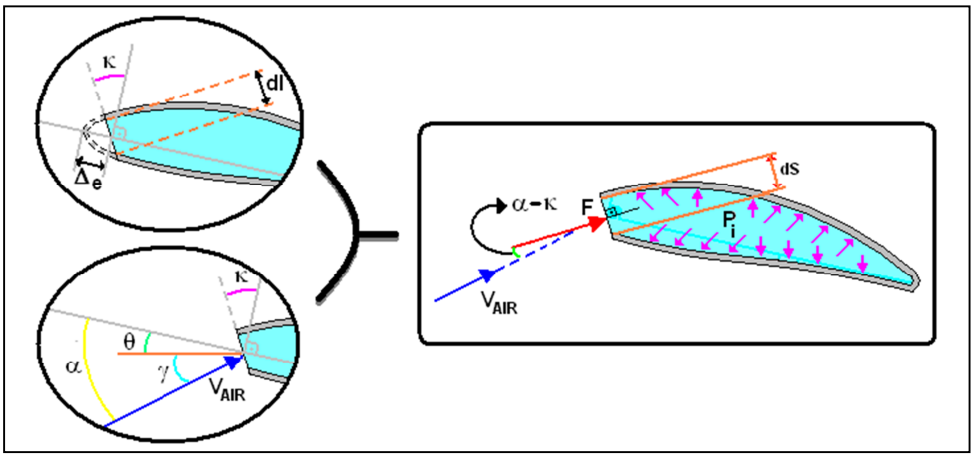

Figure 4.1 – Wing inflation sketch

It is possible to notice that the portion of the incoming air that makes effective pressure inside of the wing depends on the incidence angle and size of the openings. To calculate the incoming area it is proposed the following approach:

In addition to the basic airfoil functions explained in section 3.1.2, the following geometric parameters must be defined:

- Δ_e=The position of the intersection between the frontal opening reference plan and the airfoil chord in percentage of the chord.
- κ=The angle of the frontal opening plan relative to a plan normal to the airfoil chord.

With those parameters it is possible to estimate the air incoming area, as follows:

$$S_f = \int_{-\frac{b}{2}}^{\frac{b}{2}} \left(\left[f_f^E(\Delta_e, f_c(y)) - f_f^I(\Delta_e, f_c(y)) \right] \cdot cos(\kappa) \right) \cdot dy \tag{4.3}$$

Notice that in this equation it is included the airfoil thickness inside the airfoil surfaces definition functions already introduced in Chapter 3.

Considering the main variables involved, the following efficiency factor will be proposed as a preliminary design parameter, allowing a safe initial evaluation of the inflation capability:

$$\varepsilon_A = cos(\alpha - \kappa) \cdot \frac{S_f}{S} \tag{4.4}$$

Naturally, experimentation is necessary to precisely define an efficiency factor.

Finally, the structural stability factor can be calculated dividing the minimum available pressure differential by the wing surface load:

$$SSF = \frac{\Delta P}{L_{surf}} \tag{4.5}$$

That can be rewritten as:

$$SSF = \frac{1}{2 \cdot g} \cdot \frac{\rho_{air}}{\rho_w} \cdot \frac{S_f}{S} \cdot V^2 \cdot cos(\alpha - \kappa) \tag{4.6}$$

By analysis of some theoretical models it can be seen that a safe value for the structural stability factor must be above 1.3 using this simplified approach.

An investigation of inflatable wings proprieties was presented by Mashud (2010) highlighting the importance of the air intakes for wing inflation and providing an experimental visualization of the external and internal pressure distribution over the wing section for different angles of attack. As commented, it is expected that manufacturing proprieties as the number of cells, ribs and the sewing type also affect the inflation proprieties. However, no work on this subject was found. Taking in account the pre-design evaluation objective, the approach proposed here shows to be enough to allow a safe and efficient airfoil selection and wing design.

Finally, with the proposed formulation it is possible to vary the flight speed and the angle of attack in a representative range to evaluate the variation of the SSF for a particular wing design. An exemplification of such analysis is shown below for a generic wing model considering a speed range from 20 to 60 Km/h and an AOA variation between -5 and 25º:

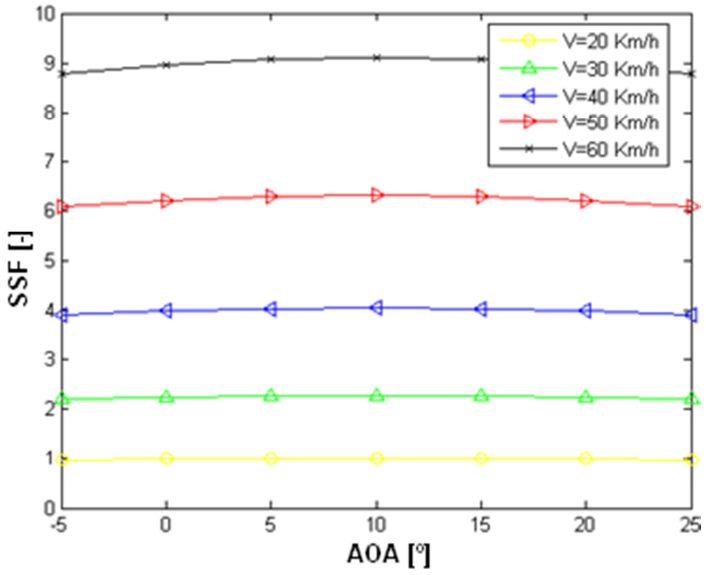

Figure 4.2 – Structural stability factor variation

Figure 4.2 suggests the SSF is basically determined by the speed and present just a small variation with the AOA. In this way, the AOA influence can be neglected and the SSF for a particular wing can be seen as a function of the flight speed calculated using a medium expected equilibrium AOA. Then, It can be plotted the SSF variation with respect to flight speed for a typical AOA of 8 degrees to represent the SSF behavior:

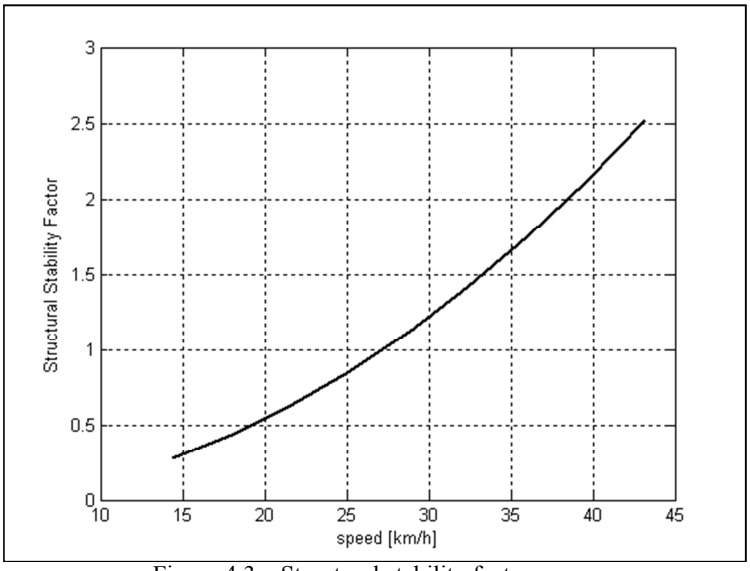

Figure 4.3 – Structural stability factor curve

For a particular wing's geometry, with a specific air entrance design, the graph above can provide an idea of the acceptability of a designed wing model, taking in account the minimum flight speed necessary to provide an acceptable level of wing stiffness.

4.2 Classical Aerodynamic Theory Limitations:

Even considering the wing fully inflated, due to the many singularities and some fundamental differences between paragliders and conventional airplanes, some common used assumptions and approximations from classical aerodynamic theory cannot be immediately applied. Because of that, a dedicate analysis about some of the most relevant aspects of paraglider's aerodynamics is important to drive future considerations when dealing with the development of a methodology for aerodynamics coefficients estimation. Below it is presented an assessment about the most relevant aspects that might be taken in account:

4.2.1 Low Aspect ratio and Low Reynolds numbers

A first constraint in using the classical aerodynamic theory is the flow characteristics over the wing. The known formulation commonly applied for coefficient calculations has been tested for many years and it is shown to be very efficient for high values of both aspect ratio and Reynolds numbers. However when Reynolds number decreases below 2.10^5, and aspect ratio decreases below 7, the change in flow characteristics has important effects on the aerodynamic coefficients.

Paragliders usually have low aspect ratio (between 3 and 5) and flies at a moderate Reynolds numbers (around 1.10^6), therefore, its characteristics would be between small UAV`s and small aircrafts. Fortunately it is possible to find some papers (Muller, 2003; Pelletier, 2000) dealing with those kinds of flows. In those works it is possible to understand how the low aspect ratio and low Reynolds number affect the aerodynamic characteristics. However a relevant observation is that for paragliders the Reynolds number is slightly lower than for usual aircrafts (around 1.10^7), but the referred studies deals with micro air vehicles – MAV that presents Reynolds number values really low (down to 1.10^4). Anyway, those references are still useful to drive some considerations in dealing with paraglider's aerodynamics, thus, it is important to mention the main conclusions presented.

The low Reynolds number results that the flow over the wing can develop a relevantly different boundary layer. This flow regime results an increase in drag, and thus, a loss of airfoil efficiency. As shown experimentally by Pelletier (2000), although an increase in drag is clear for low Reynolds number when compared with usual values, it does not seems to affect significantly the lift coefficient.

The low aspect ratio has extremely important effects on the wing`s aerodynamics characteristics. As shown experimentally by Pelletier (2000) and Muller (2003), due to a vortex-lift effect originated by the great influence of the tip`s flown over the entire wing, it is possible to notice a expressive non-linearity in the lift versus angle of attack curve. Also, it is observed that the lift coefficient in general is decreased. However, it is notable that the stall angle strongly increases. Therefore, those low aspect ratio wings presents a lower lift coefficient but a higher angle of stall that trespass 20 degrees, what is a great advantage for paraglider`s flight because it can be submitted to more aggressive disturbances in angle-of-attack without approaching the stall region.

4.2.2 High thickness airfoil and air intakes

Classic analytical theory is basically developed for thin airfoils; therefore, high thickness airfoils present some deviations especially relevant for airflows at low Reynolds numbers. A comprehensive study in this subject is presented by Hsiao (2008), which shows that a slight increase in lift and a considerable increase in drag occur for high thickness airfoils. Generally, paragliders use high thickness airfoils because the air penetration inside the wing is an important factor to maintain the wing structural stability and the airfoil must be sufficiently thick to provide a good air intake.

Also, classic aerodynamics deals always with continuous airfoils. In this way, the air intakes (or frontal openings) constitute a major difference that could probably cause some changes in airfoil's characteristics. Because of the cut in the leading edge region, alteration in the pressure distribution profile could be expected. However, Babinsky (1999) shows that the contribution of the air intakes in drag is small compared to other sources.

4.2.3 Wing's geometry and finite wing coefficients corrections

The classical aerodynamics theory deals mostly with rigid structure, trapezoidal or elliptical wings, with constant low dihedral and sweep angle. Therefore, it is obvious that paraglider's wings are considerable different to these standards. Allied to that, the flexible nature of paraglider's wing contributes for unaccounted aerodynamic effects difficult to be determined analytically.

It must be noticed that the high curvature of the wing, associated to the low speed range of operation, makes the angle of attack varying considerably along the wing sections. In consequence, the direction of each aerodynamic force components changes throughout the span, demanding a complex summation of each local contribution to calculate the total aerodynamic

forces. Therefore, the classical finite-wings corrections for tridimensional flow effects using lift-line theory approximations are not enough to provide reasonable estimations for paragliders. Because of that, an adaptation of the classical formulations taking in account the wing's specific curvature is for sure necessary.

4.3 Wing's aerodynamic coefficients estimation methodology:

As already established, the main objective of the method to be proposed here is to estimate aerodynamic coefficients based on basic design parameters achieving an acceptable level of accuracy, but without the pretention of predict the exact values. A methodology focusing on wing's geometry based corrections will be adopted to explore, in special, the effect of the wing's shape on aerodynamics. Also, to develop a functional method, previous results from some available works will be used to guide some basic definitions and to crosscheck the analytical results with reported experimental data and manufacture`s published information.

4.3.1 Wing's section bi-dimensional coefficients estimation

The first step to determine the aerodynamics coefficients is to obtain the values of the bi-dimensional coefficients for the airfoil selected as wing section. This can be done using any source of airfoil's data available (see Abbott , 1959 as an example). Also, some computational tools are very useful to generate theoretical data for customized airfoils and it can be used as well. Whichever be the source of data, it shall provide:

- The lift-AOA curve slope (a_0)
- The zero-lift AOA (i_0)
- The profile basic drag (D_0)
- The moment coefficient on the aerodynamic center (Cm_0).

It must be remembered that, using these data sources, the profile is considered continuous and rigid. Although these data are quite representative for conventional wing sections, comparing it to the experimental results shown by Babinsky (1999), it is easy to see that a considerable difference exists in the amount of profile drag observed in a paraglider's wing. Figures 4.4 and 4.5 below shows wind tunnel results for a classic NACA-4412 airfoil and the results obtained by Babinsk for its wing tunnel models:

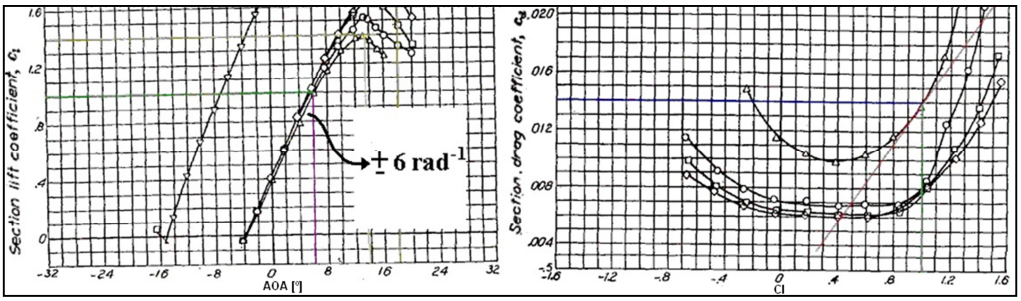

Figure 4.4 – NACA 4412 airfoil wind-tunnel data (Abbott,1959)

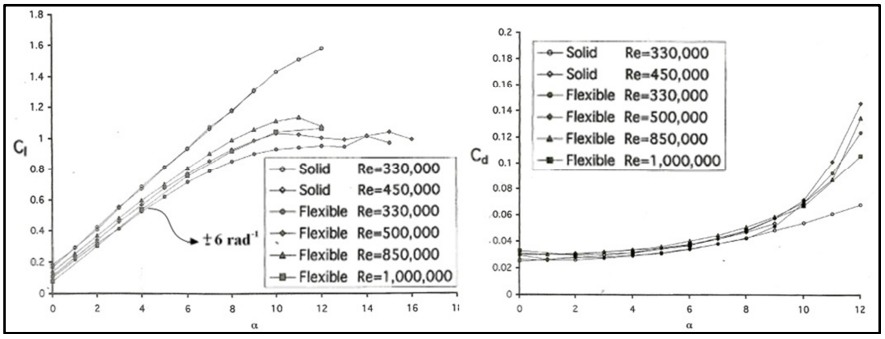

Figure 4.5 – Paraglider's planar wings wind-tunnel data from Babinsky (1999)

It is notable that, although the lift-curve slope is quite similar, the amount of profile drag presents very different levels. This was already expected, since the air intakes, the flexible material, the thicker airfoil, and the low Reynolds number are factors that contributes for an increase in drag. Therefore, as a second step, the profile drag coefficient must be corrected using further considerations.

4.3.2 Bi-dimensional coefficients corrections

Added to the basic profile drag, there are two other drag components to be considered: the drag due to the profile surface proprieties and the drag caused by the air intakes. Both components are essentially experimental and will be estimated here using results previously obtained.

The surface roughness term can be added using the proposition made by Ware and Hassel (1923, 1969) which indicates an addition of 0.004 in drag coefficient due to surface characteristics. The air intakes influence can be modeled as suggested by Babinsk (1999) using an adaptation of the given formula " $0.07 \cdot \frac{h}{c}$ ", (where "h" represents the size of the opening and "c" is the chord length) to use the previously defined parameters of air intake geometry.

Finally, adding both terms discussed above, the final expression proposed to calculate the profile drag term for paraglider's wings becomes:

$$D_0{}' = D_0 + 0.07 \cdot t(\Delta_e) + 0.004 \tag{4.7}$$

Where "$t(\Delta_e)$" means the airfoil thickness, at the position of the air intake, measured in fractions of chord length as introduced in section 4.1.

4.3.2.1 - Averaged bi-dimensional coefficients adjustments for aerodynamic torsion

As paragliders flight controls principles relay on airfoil's curvature and incidence changing, central airfoils and tip airfoils are submitted to different variations in angle of attack. Therefore, it could be useful to differentiate the type of airfoil using airfoils with better stall characteristics on the tips and high lift airfoils at the center of the wing. Whichever be the objective, any aerodynamic torsion can be supposed to present a linear transition of aerodynamic proprieties

between different airfoils type sections, what is naturally expected and accurate enough for conceptual design calculations.

To extract an averaged coefficient from different airfoil profiles, supposing a linear variation in the transition areas, the following formulation can be applied:

- For a specific coefficient C^i (ex: i_0, a_0, Cm_0, etc...), the function defining the linear variation throughout the span can be written as:

$$C^i(y) = C^i{}_i + \frac{C^i{}_f - C^i{}_i}{y_f - y_i} \cdot (y - y_i) \tag{4.8}$$

Where:

- $C^i{}_i$= Coefficient value on the initial section.
- y_i= Initial section position.
- $C^i{}_f$= Coefficient value on the final section.
- y_f= Final section position.
- For each coefficient the averaged value can be calculated as follows:

$$\overline{C^i} = \frac{\int_{y_i}^{y_f} [C^i(y) \cdot f_c(y)] \cdot dy}{\int_{y_i}^{y_f} f_c(y) \cdot dy} \tag{4.9}$$

4.3.3 Finite wing preliminary coefficients integration

With the bi-dimensional coefficients adjusted, the third step is to take in account the wing's curvature effect. Two main effects are expected from wing's curvature, one due to the variable dihedral and another in case of geometric torsion. For both features the aerodynamics components in each wing section acts in a different direction, resulting different components of lift and drag considering the reference coordinate-system. Then, by proceeding with an integration of each wing-section's contribution for lift and drag, it is possible to extract the total aerodynamic forces and moments and to derive corrected finite-wing's aerodynamic coefficients.

To calculate the total forces and moments acting on the wing it is necessary to calculate the exactly speed components acting on each airfoil section throughout the span. A visualization of this decomposing process is shown below:

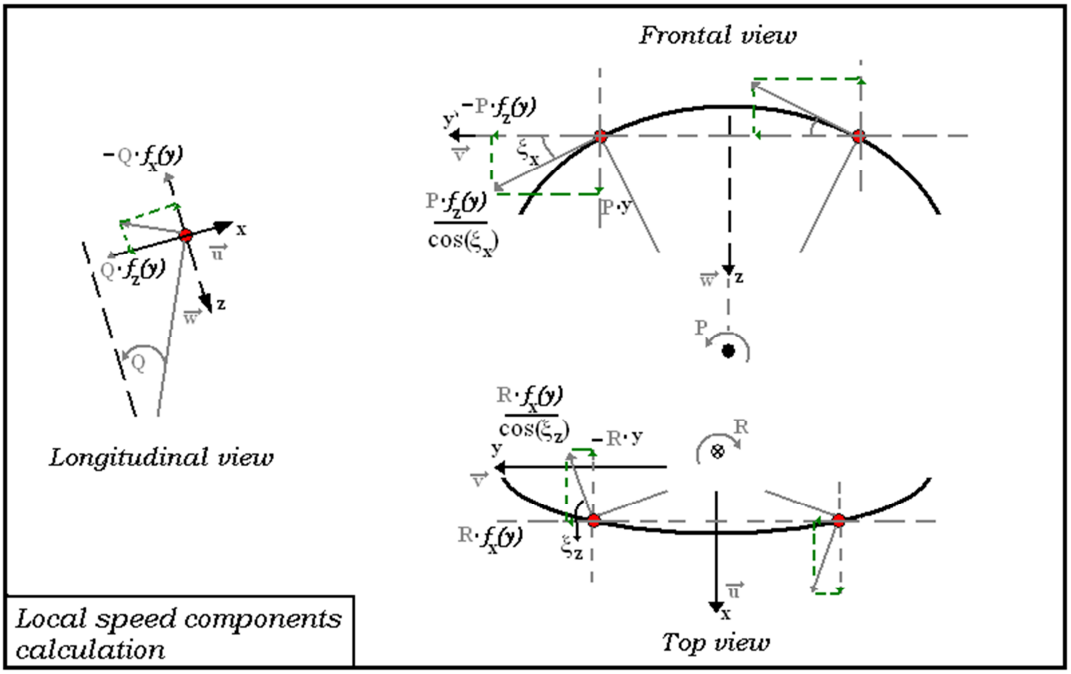

Figure 4.6 – Local speed components

Using the body-coordinate-system, the speed components in each wing section are calculated as follows:

$$u_L = U + f_z(y) \cdot Q - y \cdot R \tag{4.10}$$

$$v_L = V - f_z(y) \cdot P + f_x(y) \cdot R \tag{4.11}$$

$$w_L = W + y \cdot P - f_x(y) \cdot Q \tag{4.12}$$

To allow using basic aerodynamics formulations, these velocities must be projected on the airfoil`s plan. For that, the local orientation of each cell can be modeled using the wing's curvature as illustrated in figure 4.7 below:

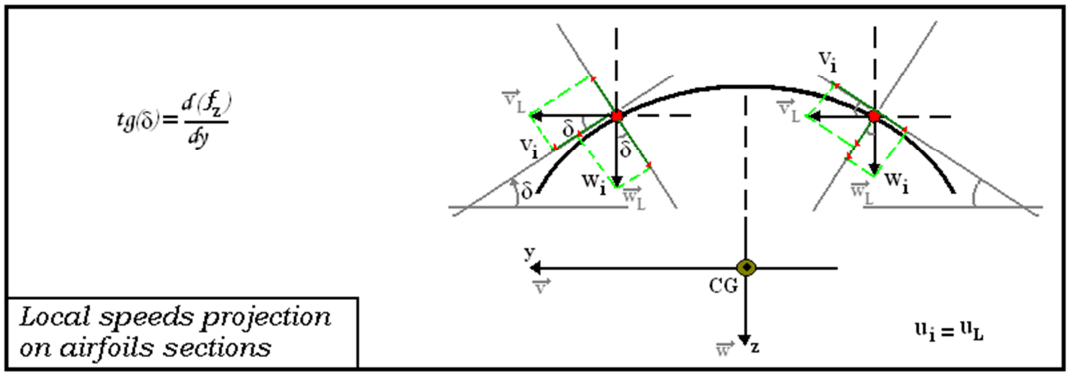

Figure 4.7 – Airfoil section speeds components

The curvature angle of each wing section can be expressed as:

$$\delta = atan\left(\frac{df_z(y)}{dy}\right) \tag{4.13}$$

Using this definition, the local speed components necessary to calculate aerodynamic resultants are:

$$u_i = u_L \tag{4.14}$$

$$w_i = w_L \cdot cos(\delta) - v_L \cdot sen(\delta) \tag{4.15}$$

In consequence, the local angle of attack can be described as:

$$\propto_i = arctg\left(\frac{w_i}{u_i}\right) + f_\theta(y) \tag{4.16}$$

Adding a possible contribution of brakes actuation using the model that will be discussed in section 5.1.3, the angle of attack can be rewritten as:

$$\propto_i = arctg\left(\frac{w_i}{u_i}\right) + f'_\theta(y) \tag{4.17}$$

Where:

$$f'_\theta(y) = f_\theta(y) + \delta_{B_r} \cdot \delta_M \cdot \left(\frac{100}{\delta_f}\right)^{\left(\frac{y}{b}-\frac{1}{2}\right)} + \delta_{B_l} \cdot \delta_M \cdot \left(\frac{100}{\delta_f}\right)^{\left(-\frac{y}{b}-\frac{1}{2}\right)} \tag{4.18}$$

Although this definition is being introduced here, it has no effect in coefficients estimation, because all the calculations to define de aerodynamic coefficients will be made considering the wing in steady glide with no control actuation. However, the inclusion of this term it is important to allow a subsequent useful analysis about aerodynamic forces distribution in flight controls actuation situations.

At this point, using the bi-dimensional aerodynamic coefficients for the airfoil selected, the local lift, drag and moment components can be calculated following classical aerodynamics formulations:

$$L_i = \frac{\rho}{2} \cdot ({u_i}^2 + {w_i}^2) \cdot a_0 \cdot (\propto_i - i_0) \cdot f_c(y) \cdot \frac{dy}{cos(y)} \tag{4.19}$$

$$D_i = \frac{\rho}{2} \cdot ({u_i}^2 + {w_i}^2) \cdot D_0 \cdot f_c(y) \cdot \frac{dy}{cos(y)} \tag{4.20}$$

$$m_{0_i} = \frac{\rho}{2} \cdot ({u_i}^2 + {w_i}^2) \cdot c_{m_0} \cdot \left(f_c(y)\right)^2 \cdot \frac{dy}{cos(y)} \tag{4.21}$$

It must be observed that the lift equation is valid only if the angle of attack is between the angle for zero lift and the stall angle. A mathematical method to account for non-negative lift consideration is applying the multiplicative factor below:

$$L_i = \left[\left(\frac{1}{10^5}\right)^{\left(1-\frac{(\propto_i - i_0)}{|\propto_i - i_0|}\right)}\right] \cdot L_i \tag{4.22}$$

At this point, it is mandatory to notice that each airfoil section will generate lift and drag aligned with the “local” relative wind, which is a function of the local angle of attack. Therefore, it is necessary to correct these forces to make them aligned with the global angle of attack, which means, the drag force in the direction opposite to the longitudinal projection of the flight path and the lift force normal to it.

The first applicable correction is to find the forces and moments components aligned to the central wing section as shown in figure 4.8.

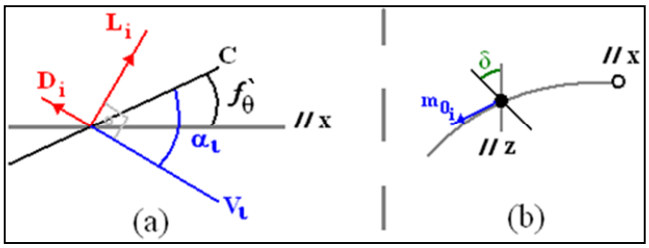

Figure 4.8 – Wing section's forces and moments components

Still considering the airfoil plan, the Lift and drag forces can be decomposed in the direction parallel to axis X and the respective perpendicular (as indicated by "a" in figure 4.8), yielding:

$$F_{\parallel x} = L_i \cdot sin\left(\propto_i - f'_\theta(y)\right) - D_i \cdot cos\left(\propto_i - f'_\theta(y)\right) \tag{4.23}$$

$$F_{\llcorner x} = L_i \cdot cos\left(\propto_i - f'_\theta(y)\right) + D_i \cdot sin\left(\propto_i - f'_\theta(y)\right) \tag{4.24}$$

However, the component normal to "X" presents components parallel to "Y" and "Z" (as indicated by "b" in figure 4.8) that can be calculated respectively as:

$$F_{\parallel y} = F_{\llcorner x} \cdot sin(\delta) \tag{4.25}$$

$$F_{\parallel z} = F_{\llcorner x} \cdot cos(\delta) \tag{4.26}$$

There is also a necessary decomposition of the aerodynamic moment:

$$m_{i_{\parallel y}} = m_{0_i} \cdot cos(\delta) \tag{4.27}$$

$$m_{i_{\parallel z}} = -m_{0_i} \cdot sin(\delta)$$

(4.28)

However, as the yaw moment generated by differences in lift and drag between the semi-wings is much more representative them some yaw components generated in asymmetric flight conditions due to the decomposition of wing's aerodynamic pitch moment, this last term can be neglected without further considerations.

Finally, the reactions on the wing section projected in a plan parallel to the symmetry plan can be decomposed again to give the local components of lift and drag aligned with the global relative wind as illustrated in figure 4.9 below:

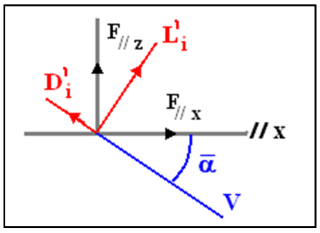

Figure 4.9 – Wing section's lift and drag contribution

The lift and drag contribution can be calculated as:

$$L'_i = F_{\parallel z} \cdot cos(\bar{\alpha}) + F_{\parallel x} \cdot sin(\bar{\alpha})$$

(4.29)

$$D'_i = -F_{\parallel x} \cdot cos(\bar{\alpha}) + F_{\parallel z} \cdot sin(\bar{\alpha})$$

(4.30)

Where, $\bar{\alpha}$ denotes the global angle of attack given by "$\bar{\alpha} = \text{atan}\left(\frac{W}{U}\right)$".

At this point it is possible to find the preliminary total lift and drag forces integrating the components over the wing and also obtain the aerodynamics coefficients as follows:

$$C_L = \frac{\int_{-b/2}^{b/2} L'_i}{\frac{\rho}{2} \cdot (U^2 + W^2) \cdot S}$$

(4.31)

$$C_D = \frac{\int_{-b/2}^{b/2} D_i'}{\frac{\rho}{2}\cdot(U^2+W^2)\cdot S} \tag{4.32}$$

$$C_{m_0} = \frac{\int_{-b/2}^{b/2} m_{i_{\parallel y}}}{\frac{\rho}{2}\cdot(U^2+W^2)\cdot MAC\cdot S} \tag{4.33}$$

From these coefficients, assuming no changes on the zero-lift angle of attack and profile drag term due to geometrical decomposition, it can be derived a preliminary lift curve slope and a preliminary induced drag term as follows:

$$a_0' = \frac{C_L}{(\overline{\alpha}-i_0)} \tag{4.34}$$

$$D_2{}' = \frac{C_D}{{C_L}^2} - D_0{}' \tag{4.35}$$

These values are preliminary because a correction to account for tridimensional effects is still required. Although a new lift-curve slope term has been calculated and a parcel of induced drag has already being found as a result of the wing's curvature, the downwash effect requires another correction on the lift curve slope and the addition of a new component of induced drag. Using the well-known formulation from lift-line theory, both the lift-curve slope and the induced drag parameters can be corrected as follows:

$$a = \frac{a_0'}{1+\frac{a_0'}{\pi\cdot AR}} \tag{4.36}$$

$$D_2 = D_2{}' + \frac{1}{\pi\cdot AR} \tag{4.37}$$

With these final coefficients the total lift and drag forces must be re-calculated as follows:

$$L = \frac{\rho}{2} \cdot \bar{V}^2 \cdot S \cdot a \cdot (\bar{\alpha} - i_0) \tag{4.38}$$

$$D = \frac{\rho}{2} \cdot \bar{V}^2 \cdot S \cdot [D_2 \cdot a^2 \cdot (\bar{\alpha} - i_0)^2 + D_0] \tag{4.39}$$

Where, $\bar{V}$ denotes the total flight speed that can be calculated as: $\bar{V} = \sqrt{U^2 + W^2}$, and the resultant aerodynamic moment can be written as:

$$M_{y_{AC}} = \frac{\rho}{2} \cdot \bar{V}^2 \cdot S \cdot MAC \cdot C_{m_0} \tag{4.40}$$

These are the final estimative for lift, drag and pitch moment acting on the wing for a specific flight condition.

4.3.4 Wing's global aerodynamics coefficients

Up to here it was possible to derive the aerodynamic coefficients and calculate the aerodynamic forces and moments for a specific flight condition; however, it is true that some variation in those coefficients due to changes in flight conditions are expected, in special for different angles of attack. Therefore, a fourth step it is necessary to harmonize the estimated coefficients to cover a reasonable range of angles of attack.

Repeating the calculations presented in step 3 for an expected range of angles of attack, a lift-AOA curve and the drag polar can be generated. Then, using polynomial fittings of these curves it is possible to extract global averaged aerodynamic coefficients for the wing.

From a linear fitting of the lift-AOA curve it is obtained the lift-curve slope "$\tilde{a}$" and the zero-lift angle of attack "$\widetilde{i_0}$". From a parabolic fitting of the drag polar it is obtained a corrected profile drag term "$\widetilde{D_0}$"and an induced drag term "$\widetilde{D_2}$". The moment coefficient "$\widetilde{C_m}$"can be assumed to be equal to the median of the values obtained.

At this point, the estimation of the wing's aerodynamics coefficients is completed. With the values obtained here it is already possible to visualize the classical aerodynamic curves for a specific wing. Figure 4.10 below, present the data obtained following this process for a generic paraglider's wing:

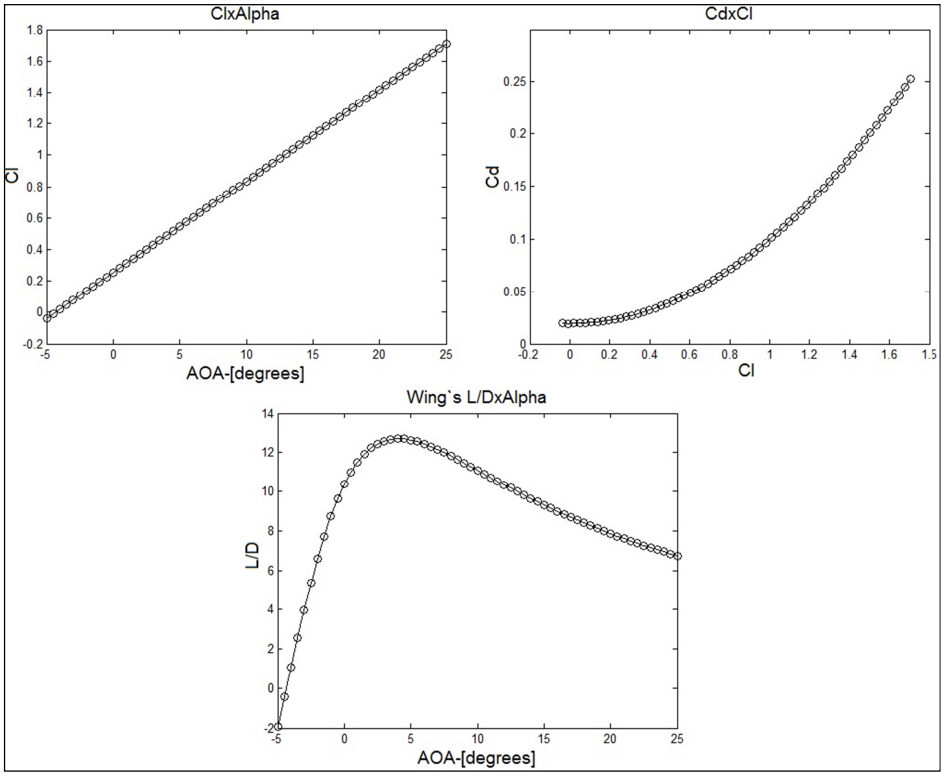

Figure 4.10 – Estimated aerodynamic curves for a specific wing

In Figure 4.10 above, the wing designed uses a NACA-4412 airfoil as wing sections and presents aspect ratio of 4 and a medium dihedral of -30º. It is possible to see that the degradation based in the bi-dimensional lift-curve slope is quite representative, as well the representativeness of the induced drag for high angles of attack. Considering figure 4.10, it can be noticed that both lift curve and drag polar present reasonable values. And, in special, that the efficiency curve (L/D) presents results very near to the range of operation of paraglider`s wing without considering the other sources of drag not related to the wing as the line array, harness and pilot. Up to this point, this is an important evidence to support the proposed approach as a practical method for the established purposes.

4.3.5 Local coefficients adjustment

The four steps of calculation presented up to this point results the intended coefficients necessary to characterize the wing's aerodynamics. Notice that, to reach these results it was applied some concepts involving bi-dimensional and tridimensional corrections and also some numerical integration processes. This is necessary and justified to allow a good approximation of the aerodynamics proprieties tanking in account all the geometric particularities of those wings.

However, these final global coefficients are not enough to allow a deep investigation about the force distribution over the wing or to permit the calculation of forces and moments acting on the wing in non-steady situations. Because of that, a complementary step will be added to define new constant "local coefficients" to be used in future calculations of wing's forces and moments with a "local effect" approach.

It can be assumed that both the zero-lift AOA and the profile drag in each wing section corresponds exactly to those calculated in step four, and so, a local lift-curve slope and a local induced drag term can be adjusted in order to make the integration of all local contributions results the same values calculated with the previously derived global coefficients for steady flight.

4.3.5.1 - Derivation of the local coefficients

To comply with the basic hypotheses established above, the integration of each cells contribution, considering local constant coefficients, must result the same value of lift, drag and moment obtained with the process carried out up to step four. This condition can be mathematically presented as:

$$\begin{cases} \frac{\rho}{2} \cdot V^2 \cdot S \cdot a \cdot \left(\propto_{eq} - \widetilde{i_0}\right) = \int_{-b/2}^{b/2} L_i' \\ \frac{\rho}{2} \cdot V^2 \cdot S \cdot \left(D_2 \cdot {C_{L_{eq}}}^2 + \widetilde{D_0}\right) = \int_{-b/2}^{b/2} D_i' \\ \frac{\rho}{2} \cdot V^2 \cdot S \cdot MAC \cdot \widetilde{C_{m_0}} = \int_{-b/2}^{b/2} {M_y}_i' \end{cases} \tag{4.41}$$

Where, the aerodynamic resultants in each wing section are calculated as:

$$L_i' = \frac{\rho}{2} \cdot ({u_i}^2 + {w_i}^2) \cdot \bar{a} \cdot (\propto_i - \widetilde{i_0}) \cdot f_c(y) \cdot \frac{dy}{cos(\delta)} \tag{4.42}$$

$$D_i' = \frac{\rho}{2} \cdot ({u_i}^2 + {w_i}^2) \cdot \left[\overline{D_2} \cdot \left(\bar{a} \cdot (\propto_i - \widetilde{i_0})\right)^2 + \widetilde{D_0}\right] \cdot f_c(y) \cdot \frac{dy}{cos(\delta)} \tag{4.43}$$

$${m_0}_i' = \frac{\rho}{2} \cdot ({u_i}^2 + {w_i}^2) \cdot MAC \cdot \overline{C_{m_0}} \cdot f_c(y) \cdot \frac{dy}{cos(\delta)} \tag{4.44}$$

As the speed component in X-axis is much more representative for the total speed then the Z-axis component, and taking in account that in steady flight there are no rotation contributing for local speed variations, it is reasonable to consider:

$$V_i \approx U_i \approx V \tag{4.45}$$

Also, based on the same considerations, it is easy to derive the relation:

$$\propto_i \approx \propto_{eq} \cdot cos(\delta) + f_\theta(y) \tag{4.46}$$

The same geometry related correction applied in section 4.3.3 and illustrated in figures 4.8 and 4.9 are necessary. Then, assuming $\bar{a}$ constant, applying the first correction, and using some algebraic manipulation it is possible to obtain:

$$F_{\|x} = \frac{\rho}{2} \cdot V^2 \cdot [\bar{a} \cdot K_x^1 + \overline{D_2} \cdot \bar{a}^2 \cdot K_x^2 + K_x^3] \tag{4.47}$$

$$F_{\|z} = \frac{\rho}{2} \cdot V^2 \cdot [\bar{a} \cdot K_z^1 + \overline{D_2} \cdot \bar{a}^2 \cdot K_z^2 + K_z^3] \tag{4.48}$$

$$m_{i_{\|y}} = \frac{\rho}{2} \cdot V^2 \cdot S \cdot MAC \cdot \overline{C_{m_0}} \tag{4.49}$$

Where:

$$K_x^1 = \left[\left(\frac{1}{10^5}\right)^{\left(1-\frac{(\propto_i - i_0)}{|\propto_i - i_0|}\right)}\right] \cdot (\propto_i - \widetilde{i_0}) \cdot \frac{sin(\propto_i - f_\theta(y))}{cos(\delta)} \cdot f_c(y) \cdot dy \tag{4.50}$$

$$K_x^2 = -(\propto_i - \widetilde{i_0})^2 \cdot \frac{cos(\propto_i - f_\theta(y))}{cos(\delta)} \cdot f_c(y) \cdot dy \tag{4.51}$$

$$K_x^3 = -\widetilde{D_0} \cdot f_c(y) \cdot \frac{cos(\propto_i - f_\theta(y))}{cos(\delta)} \cdot f_c(y) \cdot dy$$

(4.52)

$$K_z^1 = \left[\left(\frac{1}{10^5}\right)^{\left(1-\frac{(\propto_i - i_0)}{|\propto_i - i_0|}\right)}\right] \cdot (\propto_i - \widetilde{\imath_0}) \cdot cos(\propto_i - f_\theta(y)) \cdot f_c(y) \cdot dy$$

(4.53)

$$K_z^2 = (\propto_i - \widetilde{\imath_0})^2 \cdot sin(\propto_i - f_\theta(y)) \cdot f_c(y) \cdot dy$$

(4.54)

$$K_z^3 = \widetilde{D_0} \cdot f_c(y) \cdot sin(\propto_i - f_\theta(y)) \cdot f_c(y) \cdot dy$$

(4.55)

Applying the correction indicated in figure 4.9, the lift and drag contribution of each cell can be calculated as:

$$L_i' = \frac{\rho}{2} \cdot V^2 \cdot [\bar{a} \cdot K_L^1 + \overline{D_2} \cdot \bar{a}^2 \cdot K_L^2 + K_L^3]$$

(4.56)

$$D_i' = \frac{\rho}{2} \cdot V^2 \cdot [\bar{a} \cdot K_D^1 + \overline{D_2} \cdot \bar{a}^2 \cdot K_D^2 + K_D^3]$$

(4.57)

Where, for "i" from 1 to 3:

$$K_L^i = K_z^i \cdot cos(\propto_{eq}) + K_x^i \cdot sin(\propto_{eq})$$

(4.58)

$$K_D^i = K_z^i \cdot sin(\propto_{eq}) - K_x^i \cdot cos(\propto_{eq})$$

(4.59)

Finally, the two first equations from system (4.41) become a fully defined system of equations:

$$\begin{cases} S \cdot a \cdot (\propto_{eq} - \widetilde{\imath_0}) = \bar{a} \cdot \Sigma_L^1 + \overline{D_2} \cdot \bar{a}^2 \cdot \Sigma_L^2 + \Sigma_L^3 \\ S \cdot \left(D_2 \cdot {C_L}_{eq}^{\ 2} + \widetilde{D_0}\right) = \bar{a} \cdot \Sigma_D^1 + \overline{D_2} \cdot \bar{a}^2 \cdot \Sigma_D^2 + \Sigma_D^3 \end{cases}$$

(4.60)

Where the "Σ_j^i" coefficients depends only on the assumed equilibrium angle of attack and wing's geometry. Each one of these coefficients can be calculated as:

$$\Sigma_j^i = \int_{-b/2}^{b/2} K_j^i \tag{4.61}$$

Thus, solving the system of equation, it is possible to find the local coefficients:

$$\bar{a} = \frac{S\cdot\left(\frac{\Sigma_D^2}{\Sigma_L^2}\cdot a\cdot(\propto_{eq}-\widetilde{i_0})-\left(D_2\cdot {C_{L_{eq}}}^2+\widetilde{D_0}\right)\right)-\left(\frac{\Sigma_D^2}{\Sigma_L^2}\cdot\Sigma_L^3-\Sigma_D^3\right)}{\left(\frac{\Sigma_D^2}{\Sigma_L^2}\cdot\Sigma_L^1-\Sigma_D^1\right)} \tag{4.62}$$

$$\overline{D_2} = \frac{S\cdot a\cdot(\propto_{eq}-\widetilde{i_0})-\bar{a}\cdot\Sigma_L^1-\Sigma_L^3}{\bar{a}^2\cdot\Sigma_L^2} \tag{4.63}$$

$$\overline{C_{m_0}} = \widetilde{C_{m_0}} \tag{4.64}$$

It is important to have in mind that, despite of some simplifications involved, these theoretical final coefficients will allow a wide range of evaluations of wing's aerodynamic behavior. By working with some hypothetic models it is possible to show that the differences in lift and drag forces obtained using these "local coefficients" or using the process from section 4.3.3 are less them 1%.

Furthermore, the preliminary results obtained from those calculations of the local contributions in lift and drag can be very useful for developing the wing, because it allows the designer to have an initial idea of how the wing-load will be distributed, and then, to get some clues about in-flight dynamic behaviors.

Nevertheless it is true that this is an approximation and the aerodynamic coefficients are not really constant all over the wing, and nether for different flight conditions. However, it can be shown that the effect of differences in these coefficients is expected to be harmless for flight dynamics characteristics evaluation, because the effect of the wing load distribution due to the wing's geometry, specially chord length distribution and dihedral variation, are much more

significant to define the amount of force and moment generated in the system then some quantitative deviation in the locals aerodynamic components.

4.4 Wing's Forces and Moments Calculation:

Using the local aerodynamics coefficients derived in section 4.3.5, the total wing`s forces and moments can be calculated for any flight condition as presented below:

Exactly as presented in section 4.3.3, the first step to calculate wing's forces and moments is to find the exactly speed components acting on each airfoil section throughout the span. Using these speeds the aerodynamic forces and moment in each wing section can be calculated using the coefficients derived in section 4.3.5 as follows:

$$L_i = \frac{\rho}{2} \cdot ({u_i}^2 + {w_i}^2) \cdot \bar{a} \cdot (\propto_i - \widetilde{\iota_0}) \cdot f_c(y) \cdot \frac{dy}{cos(\delta)} \tag{4.65}$$

$$D_i = \frac{\rho}{2} \cdot ({u_i}^2 + {w_i}^2) \cdot \left[\overline{D_2} \cdot \left(\bar{a} \cdot (\propto_i - \widetilde{\iota_0})\right)^2 + \widetilde{D_0}\right] \cdot f_c(y) \cdot \frac{dy}{cos(\delta)} \tag{4.66}$$

$$m_{0_i} = \frac{\rho}{2} \cdot ({u_i}^2 + {w_i}^2) \cdot \widetilde{C_m} \cdot \left(f_c(y)\right)^2 \cdot \frac{dy}{cos(\delta)} \tag{4.67}$$

As considered in section 4.3.3, the same mathematical method to account for non-negative lift is applicable. Also the geometric corrections illustrated in figures 4.8 and 4.9 must be used to reach the local force components in each wing section given in the body-coordinate-system as:

$$\{X_i = F_{\|x};\ Y_i = F_{\|y};\ Z_i = -F_{\|z}\} \tag{4.68}$$

Then, the total forces can be calculated by:

$$F_{x_w} = \int_{-b/2}^{b/2} X_i \tag{4.69}$$

$$F_{y_w} = \int_{-b/2}^{b/2} Y_i \tag{4.70}$$

$$F_{z_w} = \int_{-b/2}^{b/2} Z_i \tag{4.71}$$

Applying basic mechanics as illustrated in figure 4.11, it is possible to calculate the component of moment generated on the center of gravity by each local forces and aerodynamic moment components acting on the wing sections:

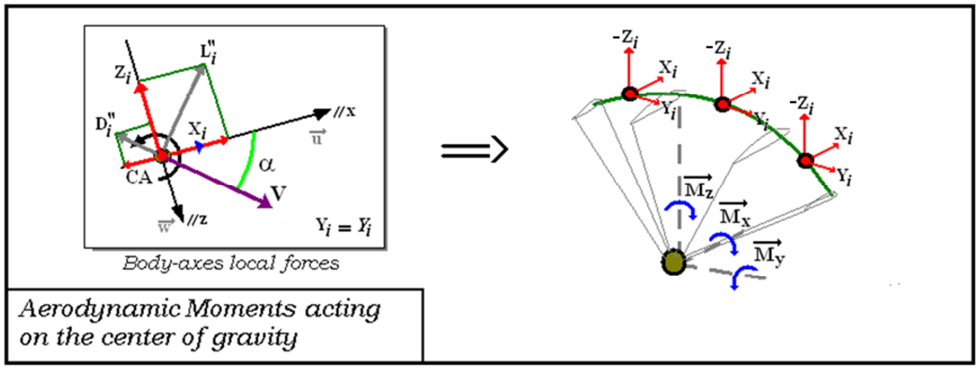

Figure 4.11 – Wing`s moments calculation

The expressions for the wing`s moments are given by:

$$M_{x_w} = \int_{-b/2}^{b/2} -Y_i \cdot f_z(y) + Z_i \cdot y \tag{4.72}$$

$$M_{y_w} = \int_{-b/2}^{b/2} X_i \cdot f_z(y) - Z_i \cdot f_x(y) + m_{i_{\parallel y}} \tag{4.73}$$

$$M_{z_w} = \int_{-b/2}^{b/2} -X_i \cdot y + Y_i \cdot f_x(y) \tag{4.74}$$

4.4.1 The steady flight condition

As can be concluded from the basic formulation presented, the wing's aerodynamic moment must be counterbalanced by the moments generated by the lift and drag forces to keep the paraglider statically equilibrated. It can be shown that for each CG position there will be a specific angle of attack capable of equilibrate the system. Therefore, it is important to assure an adequate equilibrium AOA selecting a reasonable CG position. A simplified sketch of a paraglider in straight steady flight is shown in figure 4.12 below, where some general geometric variables are presented:

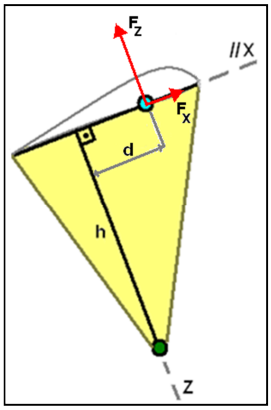

Figure 4.12 – Paraglider`s simplified sketch

The equation to calculate the longitudinal moment is given by:

$$M_y = \frac{\rho}{2} \cdot V^2 \cdot S \cdot \left(C_{Z_{(\propto)}} \cdot d - C_{X_{(\propto)}} \cdot h + C_{m_0} \cdot MAC \right) \tag{4.75}$$

Where:

$$C_{Z_{(\propto)}} = C_L \cdot cos(\propto) + C_D \cdot sin(\propto) \tag{4.76}$$

$$C_{X_{(\propto)}} = C_L \cdot sin(\propto) - C_D \cdot cos(\propto) \tag{4.77}$$

Then, the expression to represent longitudinal moment equilibrium can be derived as:

$$C_{Z_{(\propto)}} \cdot d - C_{X_{(\propto)}} \cdot h + C_{m_0} \cdot MAC = 0 \tag{4.78}$$

The above equation is often complex, demanding numerical solution. In most cases it looks like a third order polynomial function, potentially presenting three roots. However, commonly, only one root will be in the range of interest, which means, presenting a reasonable angle of attack. It is also important to observe that, as mentioned before the equation shows that for a given set of aerodynamic proprieties, which means a defined wing, the equilibrium AOA will be a function of the position of the center of gravity. Therefore, assuming the wing defined but the CG position still undefined, the above equation provides a map for CG positioning as follows:

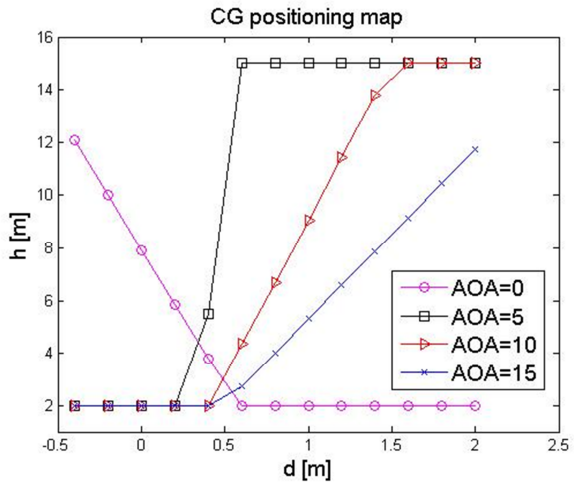

Figure 4.13 – CG positioning map

The map shown in Figure 4.13 can be a useful tool to refine paraglider's geometric definitions in order to extract the best performance achievable. This can be done selecting the equilibrium AOA equal or near that one for maximum aerodynamic efficiency (L/D), which can be obtained from basic aerodynamic curves as presented in section 4.3.4. Further assessments on aerodynamic related design constraints will be presented in chapters 6 and 7, for now, it is enough to observe that for a specific CG height, the operational AOA increases as the center of gravity moves backward.

4.4.2 Wing's forces and moments distribution visualization

With the mathematical model proposed above it is also possible to visualize the aerodynamic local resultants acting on the wing for particular flight conditions. This is useful to explore local effects and analyze the forces and moments distribution profile.

In order to exemplify this kind of analysis, below is presented four different calculation cases using the wing presented in figure 4.14:

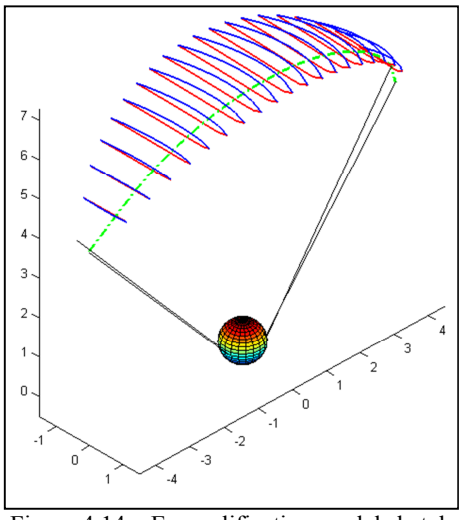

Figure 4.14 – Exemplification model sketch

Figure 4.14 represents a typical paraglider with an elliptical plan-form wing using NACA-4412 airfoils with a 25º anhedral, 9m span, 21m^2 projected area, and CG height of 7m. Below it is presented the visualization of forces and moments distributions in different situations:

1. Straight flight at 30km/h forward speed and 4 km/h sink rate.

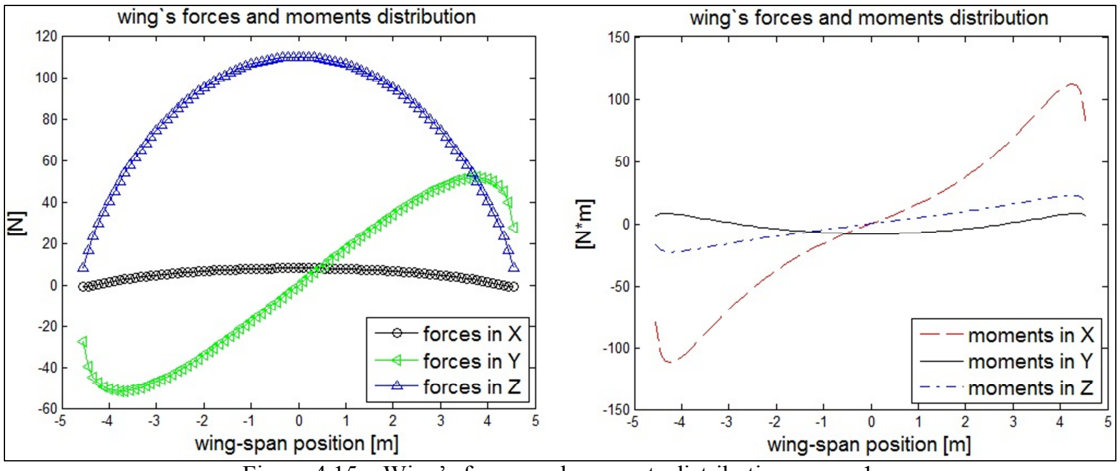

Figure 4.15 – Wing's forces and moments distribution – case 1

Notice that the force distribution is continuous and looks like usual distributions for conventional elliptical wings, and that the lateral and directional moments in each semi-wing cancel each other. Finally, observes that the resultant pitch moment coherently near to zero.

2. Right Brakes actuation in initial straight flight condition.

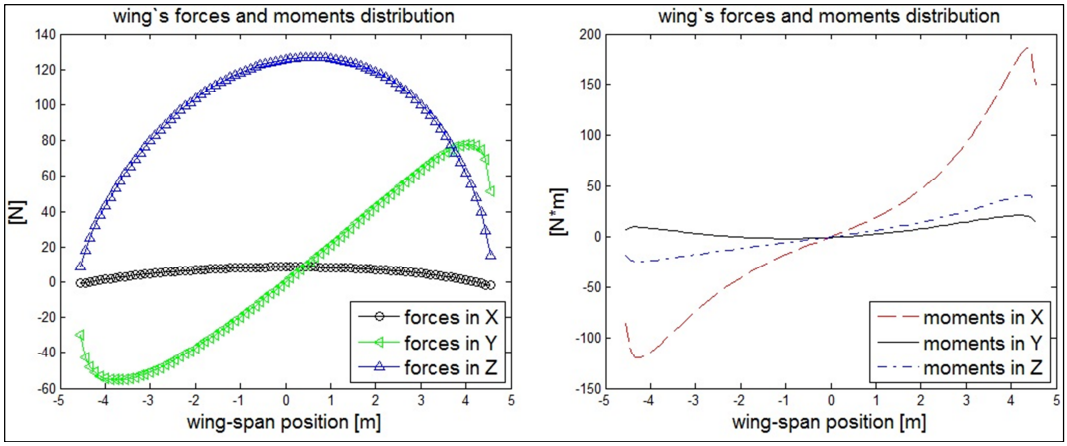

Figure 4.16 – Wing's forces and moments distribution – case 2

The illustration above represents the situation where brakes are fully applied on the right hand side with the paraglider initially in straight flight. Notice that, coherently, the vertical and lateral forces on the right side increases, but the effect of the lateral momentum is more representative, then, resulting a positive rolling moment. Also, it can be seen that the horizontal forces on the right side become more negative, indicating a subsequent slowdown of the inbound semi-wing and leading to a positive yaw. For paragliders, usually the increase in lateral forces is more relevant then some lift gain due to brakes application causing an effective roll response. This behavior is mainly due to the high vertical distance between the wing and the center of gravity and also because of the expressive anhedral. However, depending on model's geometric characteristics, at the beginning of a turn, a phenomenon felt as a minor delay in wing's response can be perceptible for the pilots.

3. Non-steady flight at 45km/h forward speed and 3km/h sink rate with a 30º bank angle and 6°/s yaw rate.

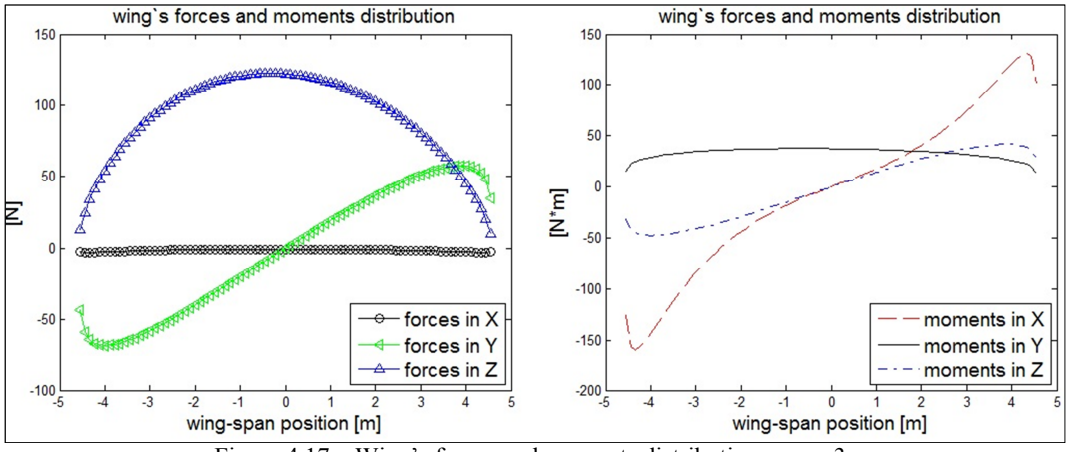

Figure 4.17 – Wing's forces and moments distribution – case 3

The situation above can describe the instant of brakes releasing in a turn, when the wing still have some rotational speed and bank, but the brakes are no longer applied. Notice that, this time, the vertical force distribution is dislocated to the outside half-span regarding the "turning path". Without right brakes applied on the inbound portion, the increased lateral force on the faster side results a reactive rolling moment trying to level the wings.

4. Wings with geometric torsion in steady flight.

This final case shows the effects of geometric torsion to exemplify the kind of analysis that might be useful for conceptual design optimizations. It will be considered the same wing, except that a geometric torsion of ±3° will be applied.

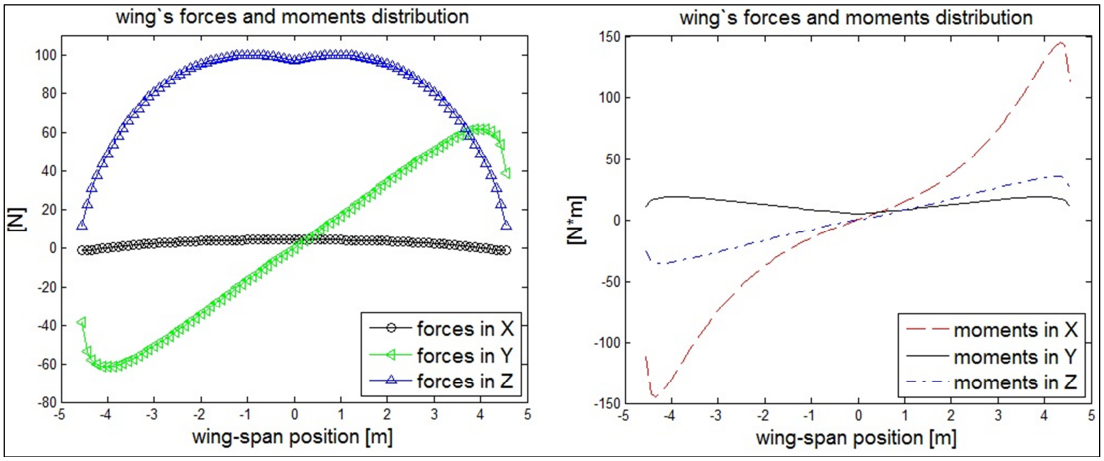

Figure 4.18(a) – Forces and moments for wings with geometric positive torsion

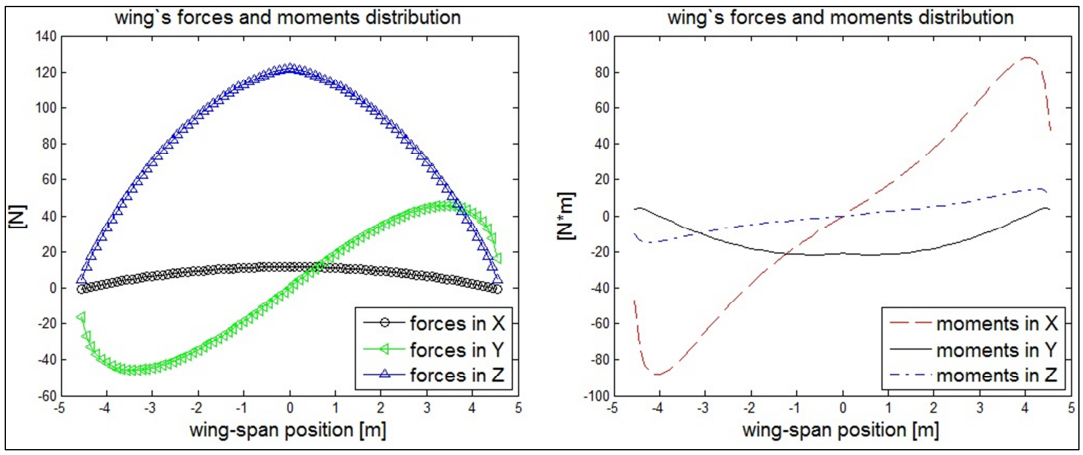

Figure 4.18(b) – Forces and moments for wings with geometric negative torsion

Notice that, as expected the lift is concentrated in the center of the wing for negative torsion and more uniformly distributed for positive torsion. That`s because the combination of chord length distribution and local dihedral is counterbalanced with AOA increasing for positive torsion, and the opposite applies for negative torsion. Additionally, observes that the absolute local moments acting on the wing decreases with negative torsion, what means a slower response to lateral disturbances.

These are just a few examples of what can be done with this mathematical model. Actually there are many other useful purposes for this kind of analysis. Some relevant investigations that could be done using this tool are listed below:

- Investigations of geometric design parameters effects on forces and moments distribution and control characteristics.
- Investigation of operational speeds effects on forces and moments distribution.
- Investigation of local structural stability issues.
- Investigations of forces and moments distributions in maneuvering situations

4.5 Harness, pilot and lines aerodynamic contribution

Up to this point only the wing's aerodynamics was considered. However, it is quite obvious that the others parts of the paraglider shall severely contribute with drag. These other drag components can be divided in two main sources: the line array and the pilot-harness assembly.

For the purposes of this work it is enough to consider that the drag from the line array, pilot and harness acts all on the center of gravity. That's because any neglected distance between the CG and the point of action for each of these drag components are unable to produce a relevant amount of moment that could compromise the flight dynamics analysis. Notice that due to the considerable distance between aerodynamic center and center of gravity, and also due to the dominance of the forces generated on the wing, a residual moment generated by the other sources of drag are for sure negligible.

The drag generated by the lines can be calculated as suggested by Massey (1989) using the formula:

$$log\left(C_{D_{lines}}\right) = 0.342 - 0.114 \cdot log(Re) \tag{4.79}$$

Where the Reynold's number can be calculated using the total line length "l"as follows:

$$Re = \frac{V \cdot l}{\mu} \tag{4.80}$$

Variations of this coefficient are securely negligible for the range of interest, and also, in the early stages of the design process, the total line length can be calculated multiplying the CG height by the expected number of lines.

For the drag generated by the harness-pilot assembly, an adaptation using previously published data in a comparative basis can be used for an initial estimation. Data are available (Çengel, 2004), (Hoerner, 1975), (Munson, 2005), for some typical bodies and shapes like: an average person in a seated position, large birds, cyclists in different configurations, and others. Then, taking in account that the development of modern optimized harnesses revealed considerable improvement in drag reduction, it is quite reasonable to work with averaged coefficients divided in two classes as follows:

Table 4-1: Harness and pilot drag coefficient

Harness type	***Drag coefficient*** $\left(C_{D_{Harness}}\right)$
Conventional	0.8
Performance	0.4

Also, to calculate the area of the assembly, it can be used some basic human proportions (Tilley, 2002; Munson, 2005; Walpert, 1989), to establish the following three classes based on the total weight of the harness-pilot assembly:

Table 4-2: Harness and Pilot cross-sectional area

Payload Weight	***Reference area (m²) - S_{CG}***
Up to 80kg	0.5
Between 80kg and 100kg	0.6
Above 100kg	0.7

Proceeding as proposed, the final drag supposed to act on the center-of-gravity due to the contributions of lines, harness and pilot, can be calculated as:

$$C_{D_{CG}} = \frac{S_{lines}}{S_{CG}} \cdot C_{D_{lines}} + C_{D_{Harness}} \tag{4.81}$$

Consequently, it is easy to see that the final drag coefficient will be the summation of the wing drag and the CG drag. Then, using the reference area as the basic geometric parameter, it follows:

$$C_{D_{total}} = C_{D_{wing}} + \frac{S_{CG}}{S} \cdot C_{D_{CG}} \tag{4.82}$$

As will be better assessed in chapter 6, the addition of a CG drag term can be seen as an unavoidable lost of wing's performance. Recalculating the aerodynamic efficiency curve taking in account this new drag component it can be found the paraglider's efficiency curve as presented in figure 4.19 below:

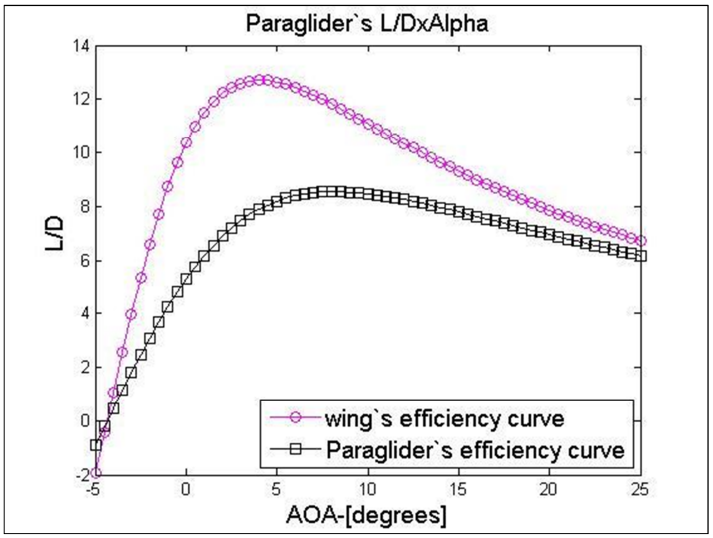

Figure 4.19 – Paraglider's efficiency curve .vs. Wing's efficiency curve

Analyzing figure 4.19 above, it is possible to see that the degradation of the wing's aerodynamic potential by the other sources of drag is quite representative. Also it can be seen that the maximum glide ratio indicated in figure 4.19 matches the average values published by manufactures (modern paragliders usually presents glide ratio between 7 and 11. A considerable amount of data is available on the internet (www.para2000.org)).

4.6 Conceptual design Aerodynamics Improvements:

As discussed throughout this chapter, it is possible to improve the aerodynamic characteristics of a paraglider selecting carefully the design parameters, including wing's geometry and center of gravity position. In order to summarize the main effects of the most common features used in paraglider's design, below is presented an assessment about how some geometric proprieties may affects aerodynamic characteristics.

4.6.1 The CG positioning and the operational condition

As presented in section 4.4.1, the steady flight condition (not considering flight controls actuation) is a single defined condition, determined by the union of a specific wing and the relative position of the center of gravity. This basic "design condition", for which the main aspects of paraglider's flight dynamics are optimized, is defined by a flight speed, an angle of attack and a flight attitude.

The equilibrium angle of attack is particularly important for many reasons, including the determination of the relation between flight speeds and glide ratio. For conventional airplanes in cruise flight, the aerodynamic efficiency represented by the factor L/D diminishes when speed increases. Observing figure 4.19, this means that airplanes operate most time at the left side of the L/D curve. However, for paragliders this is not always true. Depending on some design characteristics the opposite may occurs and the best glide will be achieved by speeding up the wing. Figure 4.20 shows typical aerodynamic efficiency curves for three different classes of aircrafts plotted both as a function of speed and angle of attack:

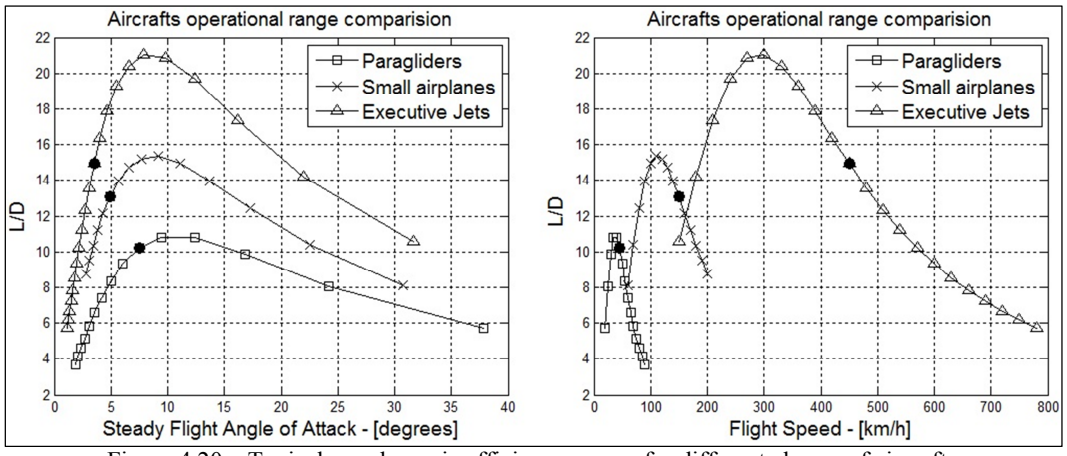

Figure 4.20 – Typical aerodynamic efficiency curves for different classes of aircrafts

In this figure it is possible to notice that paraglider's curve is considerable narrow in terms of speed, and that expected in-service variations may allow operation in different regimes. It can be concluded that by carefully selecting the CG position, and thus the equilibrium AOA, this characteristic can be managed as desired.

Also, the definition of the operational AOA has an important relation to safety. By flying at higher angles of attack the paraglider become susceptible to approaching the stall when submitted to moderate disturbances. On the other hand, by flying at a too low angle of attack the wing may become susceptible to frontal collapses. Therefore, the wise selection of the equilibrium angle of attack is an important feature to improve paraglider`s flying qualities.

4.6.2 Wing's Geometry Influence on Aerodynamic Proprieties

As discussed in sections 4.2 and 4.3, wing's geometry are completely relevant to determine the aerodynamic proprieties. Unfortunately, a simple methodology to analytically define the effects of geometric proprieties in aerodynamics is not practical. Therefore, as a way to qualitatively identify the main influences and relevancy of the most common geometric features, a comparative inspection of the aerodynamic coefficients for different wings can be done leading to very useful conclusions.

Using the developments of section 4.3, below it is presented an assessment about the effects of some common geometric features on aerodynamic coefficients. To analyze the effects of each geometric characteristic it was defined an initial standard design, and then, some geometric proprieties where changed as illustrated in figure 4.21 below:

	Basic Airfoil Bi-dimensional proprieties: a_0=5.73 rad^{-1} i_0=-2º D_0=0.007 Cm_0=-0.05	**NACA-2415** (Used in all wings) 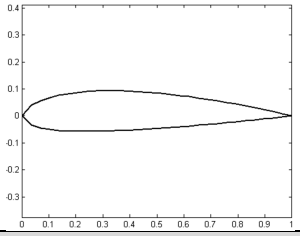
Wing Sketch:	**Basic geometric proprieties:**	**Aerodynamic Proprieties (global):**
****Maximum glide ratio referring to wing`s L/D – not accounting for other sources of drag.***		
Standard Wing: 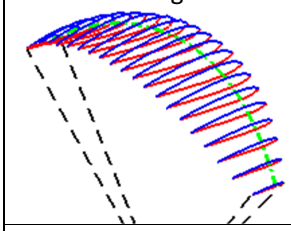	Reference Area=20.8m^2 Mean aerodynamic chord=2.4m Aspect Ratio=3.9 Taper Ratio=0.4 Medium Dihedral=-20º Medium Sweep angle=10º	a=3.71 rad^{-1} i=-2.1º D_0=0.017 D_2=0.081 Cm_0=-0.05 Max. Glide Ratio=13.5 AOA for best GR= 5º
Increased anhedral: 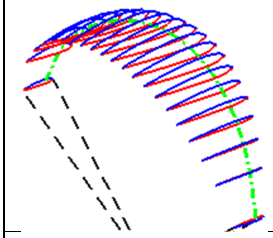	Reference Area=20.8m^2 Mean aerodynamic chord=2.4m Aspect Ratio=3.9 Taper Ratio=0.4 Medium Dihedral=**-35º** Medium Sweep angle=10º	a=**3.51** rad^{-1} i=-2.2º D_0=**0.018** D_2=0.081 Cm_0=-0.05 Max. Glide Ratio=**13.1** AOA for best GR= **5.5º**
Increased sweep angle: 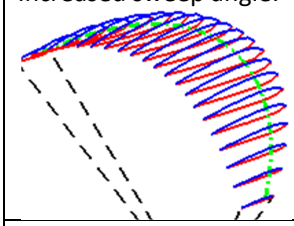	Reference Area=20.8m^2 Mean aerodynamic chord=2.4m Aspect Ratio=3.9 Taper Ratio=0.4 Medium Dihedral=-20º Medium Sweep angle=**25º**	a=3.71 rad^{-1} i=-2.1º D_0=0.017 D_2=0.081 Cm_0=-0.05 Max. Glide Ratio=13.5 AOA for best GR= 5º
Increased aspect ratio: 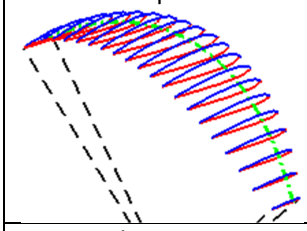	Reference Area=20.6m^2 Mean aerodynamic chord=2.2m Aspect Ratio=**4.9** Taper Ratio=0.4 Medium Dihedral=-20º Medium Sweep angle=10º	a=**4.01 rad^{-1}** i=-2.1º D_0=0.017 D_2=**0.065** Cm_0=-0.05 Max. Glide Ratio=**15** AOA for best GR= 5º
Increased taper ratio: 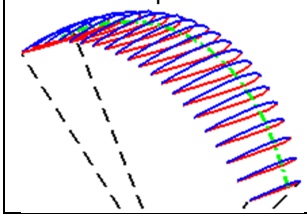	Reference Area=20.0m^2 Mean aerodynamic chord=2.3m Aspect Ratio=4.0 Taper Ratio=**0.6** Medium Dihedral=-20º Medium Sweep angle=10º	a=3.71 rad^{-1} i=-2.1º D_0=0.017 D_2=0.081 Cm_0=-0.05 Max. Glide Ratio=13.5 AOA for best GR= 5º

Figure 4.21 – Aerodynamic coefficients estimated for different geometries

Analyzing figure 4.21, some relevant aspects about the effect of different geometric features can be listed:

4.6.2.1 – The anhedral

The anhedral effect reducing the lift-curve slope and degrading glide ratio is completely understandable. To present increased anhedral the wing must have more flat area for a specific reference area, however this extra surface do not contribute considerably with vertical force, but instead it contributes significantly with horizontal and lateral forces. Therefore, although wing`s anhedral is extremely important for lateral-directional stability and controllability, it is true that increased anhedral will cause a loss of wing`s performance.

4.6.2.2 – The sweep angle

As should be expected, sweep angle has no direct effect in aerodynamics coefficients. Coherently, this is a feature commonly used for high speed airplanes and its effect on low speed aircrafts is often negligible. However, it must be noticed that it will be important for the equilibrium AOA. That’s because the sweep angle will impact the amount of pitch moment generated by each wing-section contribution, and then, a careful adjustment between CG position and sweep angle may allow reaching specific operational angles of attack.

4.6.2.3 – The Aspect ratio

The aspect ratio is for sure the most important geometric parameter to be adjusted. As can be observed, the increasing in aspect ratio allows a sensible improvement on glide ratio. This occurs because the increasing in aspect ratio diminishes the degradation caused by the tip-vortex effect. However, it is important to make clear that a superior limit exist due to both structural issues and handling qualities constraints.

4.6.2.4 – The Taper ratio

Considering a wing with fixed area and aspect ratio, the taper ratio will adjust the chord lengh distribution throughout the wing. Then, although the Taper ratio has no direct effect on aerodynamic proprieties, it is quite representative defining forces distributions over the wing.

Because of that, just like the geometric torsion exemplified in section 4.4.2, the taper ratio can be managed to provide good lateral stability and control characteristics.

4.7 Final Comments:

In this chapter it was analyzed the main aspects of paraglider's aerodynamics using an approach based on design parameters. As can be checked on the various examples provided, the method presented here provides reasonable estimations about paraglider's aerodynamic proprieties, and can be useful in the initial phases of the design process.

The developed investigation leads to some basic conclusions that should be taken in account for conceptual design evaluations:

- Any paraglider's wing model must present a reasonable combination of air intakes geometry, wing`s weight and flight speed to sustain its shape in flight.

- Some adaptations are necessary using classical aerodynamics formulations when estimating aerodynamic coefficients for paragliders. In special, it must be taken in account paraglider's expressive curvature and the low-speed range of operation.

- Paraglider's wing geometry will define the force distribution profile over the wing, which directly affect important aspects of stability and controllability. Therefore, previous visualization of the forces and moments profile may allow the improvement of basic flight qualities.

- The positioning of the center of gravity relatively to the wing defines the operational angle of attack. Therefore, wisely selecting CG position the steady flight condition may be optimized.

- Degradation in wing's performance is perceptible due to the contributions in drag from lines, harness, and pilot. Then, developments in aerodynamically optimized harness or modern line-array arrangements may improve glide ratio considerably.

5 PARAGLIDERS DYNAMICS MODEL AND MOTION SIMULATION

Modeling aircrafts motion is fundamental to investigate flight dynamics characteristics, in special aspects related to stability and controllability. Usually, aircrafts dynamics models are developed based on an extensive set of wind-tunnel and flight test data. However, in the initial stages of the design process, when such data are not available yet, a simplified theoretical model is very useful for conceptual design optimizations and flight characteristics prediction. In this chapter, a mathematical model to describe paragliders motion is developed using basic concepts from classical flight mechanics together with the previous developments presented in chapter 4.

The main objective of the dynamic model to be developed here is to allow the investigation of basic in-flight characteristics of a theoretical paraglider based only in design parameters. With a representative model, simulations of paraglider motion can be run, yielding useful information about paragliders in-flight responses and general flight characteristics.

The derivation of the equations of motion is the first step to describe paragliders dynamics. Obviously the parameters potentially involved in these equations are similar to those present in classical airplanes modeling theory (Yechout, 2003). However, it is important to have in mind that paragliders present some singularities that may impact the set of equations derived. Then, to develop a useful model, considerations about the physics involved in paragliders flight and its particularities must be taken in account as introduced below:

An initial relevant constraint is the rigid body hypothesis, necessary to allow using basic rigid body dynamics equations. This means to use a six degree-of-freedom model which does not take in account relative motion between the harness and the wing. Although this seems to be a strong assumption, in section 5.1.1 it will be shown that this is the most adequate approach for flight characteristics investigations in initial design phases.

Another consideration is that, for paragliders, apparent mass and apparent inertia would have to be considered. This phenomenon is supposed to be important for low wing-load aircrafts as shown by Lissaman and Brown (1993). However, this kind of consideration increases the complexity of the equations of motion and requires additional simplifications resulting a undesirable new source of inaccuracy. Therefore, in section 5.1.2, it will be presented a rationale to analytically explain what would be the apparent mass effect, and also how it could be used for further improvements of the dynamic model.

Finally, to account for pilot's inputs, the flight controls system is mathematically modeled, what for paragliders raises a major issue, because the control mechanism directly conflict with the rigid body hypothesis previously established.

5.1 Flight Dynamics Model Assumptions and Limitations

Any mathematical model designed to represent a physical system contain some assumptions and approximations. Simplifications are especially needed when physical proprieties requiring experimental measurement are not available. Also, additional considerations are normally used to simplify the model in order to obtain a functional tool capable of deeper analytical investigations.

The methods for calculating wing's forces and moments presented in chapter 4, which will be used in the model to be proposed, already constitute a first approximation. In this chapter, other considerations necessary to develop a useful dynamic model will be added. Therefore, the following sub-sections address some relevant assumptions to be used accessing their effects on model's accuracy and evaluating how it could impact the proposed objectives.

5.1.1- 6 degrees-of-freedom model

It is possible to find some papers (Mortaloni, 2003; Prakash, 2006; Yakimenko, 2003), dedicated to develop dynamic models with different levels of complexity for parafoil-payload systems. These are good references to be used as a base for paraglider's dynamics investigations. In these papers, models with 6, 8 and 9 degrees of freedom were developed and tested providing important results and allowing very relevant conclusions about the better modeling strategy. As expected, the 9DOF models present improved accuracy, however, 9DOF models are more restrictive for analytical design evaluations because, usually, it is useful only if flight test data are available to fulfill the parameters precisely.

It can be seen from some papers (Toglia, 2005; Watanabe, 2008) that, for paragliders, simulations using 6DOF models present the same dynamic behavior, adding just some "drift", when compared with 9DOF models. The great advantage of such modeling strategy is the flexibility for working with predictable design parameters. It is important to add that the deviations between 6DOF and 9DOF models are more expressive for fully articulated parafoil-payload systems, especially if

you have considerable distance between the payload's center of gravity and system's articulation point. This last consideration is illustrated in Figure 5.1 below:

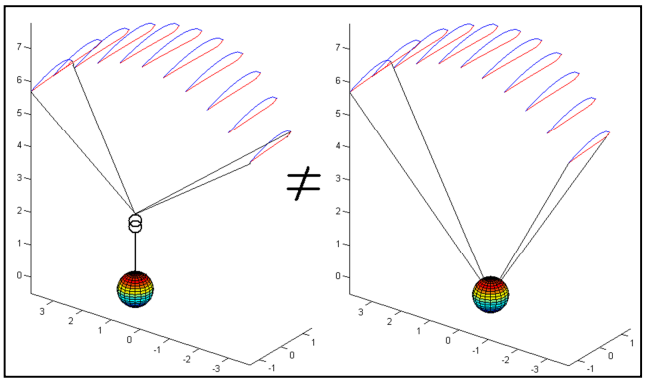

Figure 5.1 – Parafoil-payload system and Paraglyders comparission

Notice that, for paragliders, the joint point can be considered coincident with the center of gravity, and also, the dual side connection apply additional restrictions for payload relative motions. These observations are important showing that for paragliders two of the three degrees-of-freedom added by relative motion can be neglected. Figure 5.2 illustrates these three degrees of freedom dismissed in the 6DOF model.

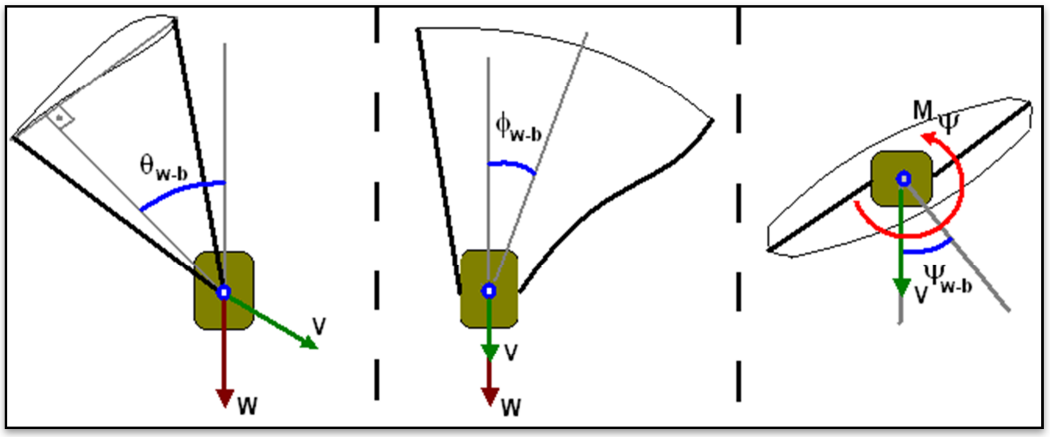

Figure 5.2 – Non-considered degrees of freedom (DOF)

For the longitudinal flight, the first movement not considered is a relative pitch motion between the harness and the wing. As the CG is considered to be on the "joint" point, and as there is no thrust component, the relative pitch movement does not add or change any force or moment component acting on the system. The weight remains vertical, the drag is always in the opposite direction of the velocity vector, both passing through the CG, which means, the forces and moments acting on the system are the same independently of the relative pitch. The only limitation imposed by

not considering this motion is that it will be unknown the exact pilot's angle of attitude, but the only consequence of it would be a minor restriction for ergonomics or human factors assessments.

The second possible movement not taken in account in the 6DOF model is a relative roll between the harness and the wing. For paragliders in normal flight it is hardly observed relative roll motion. It can be seen that any noticeable relative bank angle between wing and pilot's assembly implicates directly in non compliance with the rigid body hypothesis, because the lines in one side would be not fully tensioned. Small relative bank angles may occur, but even though, considering the CG on the roll axis, for the same reasons presented in the last paragraph above, there are no changes in dynamic components acting on the system. Therefore, this movement can be automatically excluded without further considerations. Actually, as can be seen in Yakimenko (2003), it is logical to eliminate this component and use an 8DOF model for parafoil-paylod systems with dual point connection or similar.

The only relevant dynamic component neglected by the 6DOF model is a potential yawing moment due to wing twist or relative yaw. This situation is expected to happen in dynamics maneuvers or in response to violent lateral gusts. It can be identified a new internal dynamic components acting on the system, which is a reactive torque generated by the tension on the lines when twisted, and a change in aerodynamic resultants due to the sudden changing on heading and also due to wing geometric distortions. The twist moment could be modeled as a combined spring-damper component, however, would be necessary establish the physical proprieties of these idealized components, what would be very difficult in a conceptual design phase. Also, effects on aerodynamics coefficients due to wing geometry deformation would require additional considerations. Then, it seems not to be practical to add such considerations in a model intended for conceptual design evaluations. Finally, analyzing situations near to equilibrium or even smooth maneuvers, no relevant twist are expected to be representative. Finally, it is worthy to mention that maneuvers involving wing twist can be evaluated in a second phase when the design is already defined and experimental data can be obtained and applied in more comprehensive models focusing on specific investigations.

5.1.2- Apparent mass and inertia effects

One of the most important and desired characteristics of paragliders is the light weight. It can be noticed that paragliders present very low wing-load (around 4kg/m2) when compared with conventional aircrafts (above 100kg/m2 for small airplanes (Taylor, 1987)), on the other hand, the wing volume is quite representative. This combination makes airflow accelerations to become

representative as an external source of forces and moments. There are some interesting studies available about apparent mass effects on parafoils, the most relevant and useful was proposed by Lissaman and Brown (1993). This paper defines a methodology for apparent mass and inertia coefficients estimation using approximated geometric proprieties.

The principle of apparent mass effect is related to the reactions of the fluid responding to system acceleration. These reactions can be mathematically modeled as “directional” added mass and inertia components. This “added” mass or inertia is not isotropic and strongly depends on system geometry. It is already difficult to evaluate quantitatively those components even using flight tests data. It is even more complicated to apply some “general” model to try taking in account such effect on a design phases, because it would represent another relevant source of inaccuracy. Also, the inclusion of apparent mass terms into the equations of motion elevates the complexity of the model and compromises its applicability.

However it is useful to evaluate how the model proposed is being affected by neglecting the apparent mass. In fact, the apparent mass effect acts basically as a “damper”. When, for some reason, a paraglider initially in equilibrate flight is disturbed, an acceleration component shall appear. The apparent mass will react to this component and diminish the acceleration felt by the system. Therefore, it is expected that the response amplitudes are diminished by this effect. In this way, disregarding apparent mass effects, we are investigating the basic characteristics imposed by aerodynamics and gravitational forces, which will present the same overall dynamic behavior but with augmented amplitudes.

It must be observed that this effect is completely negligible for equilibrated flight analysis and, as consequence, for performance evaluations. It is also negligible for small disturbances near to equilibrium. This subject could mainly affect the long term dynamics analysis, which is already affected by other relevant sources of error as forces and moments derivatives linearization or aerodynamic coefficients estimation. Even though, a fast calculation using approximated coefficients (Lissaman, 1993) can show that the increase in total mass and inertia are quite small and it is not supposed to be relevant for previewing paragliders in-flight behavior. In this way, it is considered better for the presented purposes not taking in account apparent mass effect. Proceeding that way, the conclusions regard the influence of design parameters in flight dynamics characteristics remains valid and further improvements can be applied in a posterior phase using experimental adjustments to refine the dynamic model.

5.1.3- Flight controls modeling

As paragliders do not present independent command surfaces, the main flight controls mechanisms are the "brakes", which are a set of lines linked to the end of the wing's trailing edge in each half-span. The simultaneous or differential actuation of the brakes works as flaps and ailerons, but to add an accurate mathematical modeling of such device into the system dynamic model is far complicated. When brakes actuation is present the wing deforms, and the geometry is no longer as parameterized in chapter 3. Therefore, rigorously, any modeling based on that initial geometric description would be corrupted.

However, a model for brake actuation effects will be presented to allow controllability characteristics investigations and in-turning flight conditions analysis in a predictive approach.

Below is shown a sketch of the brake actuation mechanism. As can be seen, for analytical purposes, the brake actuations can be modeled as a increasing in the local angle of attack.

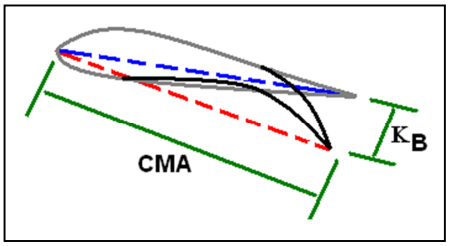

Figure 5.3 – Brakes actuation sketch

The gain in angle of attack is supposed to varies throughout the span due to chord distribution and lines mechanism design. However, it can be estimated a standardized maximum AOA using more representative design parameters and a standard deflection distribution profile.
The standardized maximum AOA variation can be estimated using the maximum brake actuation length κ_B and the mean aerodynamic chord (MAC) as follows:

$$\delta_M = atan\left(\frac{\kappa_B}{MAC}\right) \tag{5.1}$$

Where κ_B is a design parameter defining the maximum available brake length, and MAC is the mean aerodynamic chord that can be easily calculated as presented in chapter 3.

Therefore, the maximum AOA variation for a particular situation of brakes application can be written as:

$$\Delta\propto_{MAX} = \delta_B \cdot \delta_M \tag{5.2}$$

Where δ_B ($0<\delta_B<1$) is the fractional break actuation, representing pilot's relative input between 0 and 100%. It must be considered one input for each side, thus, it must be defined δ_{B_r} for the right side and δ_{B_l} for the left side.

The deflection distribution defines how the local wing-section deflection develops itself throughout the span, decreasing from the tip on the commanded side up to a residual value on the opposite tip. It can be considered an exponential decay where the residual deflection on the opposite tip is the definition parameter. Mathematically this approach can be written as follows:

$$\Delta\propto (y) = \delta_{B_r} \cdot \delta_M \cdot \left(\frac{100}{\delta_f}\right)^{\left(\frac{y}{b}-\frac{1}{2}\right)} + \delta_{B_l} \cdot \delta_M \cdot \left(\frac{100}{\delta_f}\right)^{\left(-\frac{y}{b}-\frac{1}{2}\right)} \tag{5.3}$$

Where:

- δ_{B_r} and δ_{B_l} are the pilot's input, which means, the fractions of available brake length applied in each side ($0<\delta_B<1$).
- δ_M is the standardized AOA variation, in radians, for maximum brake actuation, and can be derived from design parameters.
- δ_f is the residual deflection on the non-actuated tip in percentage of the maximum AOA variation on the actuated side. (A reasonable value is 10%).

Observe that the adjustment added by the parameter δ_f dictates the shape of the distribution curve. This is a design characteristic that depends on many design proprieties as line mechanisms, materials, flight speeds, wing geometry, etc... Obviously, it requires flight test data to define a representative value. However, to allow conceptual design analysis, a standard value of 10% will be used. With a 10% residual deflection it is possible to observe a reasonable variation of AOA for common design parameters. Below is presented a graph showing the AOA variation distribution for a wing with a 10m span, 3m MAC, maximum brake length of 25cm, and residual deflection of 10%:

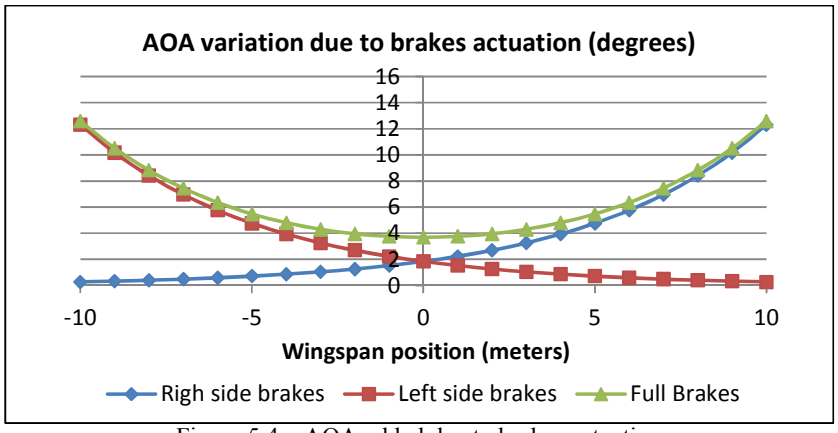

Figure 5.4 – AOA added due to brakes actuation

Notice that, coherently, the deflection develops itself smoothly throughout the span. Also, it can be seen reasonable AOA values. The control characteristics are dependent of the geometry of the wing and of the brakes design proprieties as well. The considerations and adaptations introduced here will be not accurate enough to evaluate the "brake" system design; however, it will be enough to evaluate the controllability characteristics imposed by the other design parameters. A deeper investigation in brakes design proprieties will be addressed in chapter 9.

5.2 Paraglider's Equations of motion

Taking in account the discussions in previous section, considering the paraglider a rigid body, the classical equations of motion commonly used for aircraft movement modeling applies (Yechout, 2003). The illustration below summarize the main parameters involved in paragliders motion using the geometric parameterization established in chapter 3:

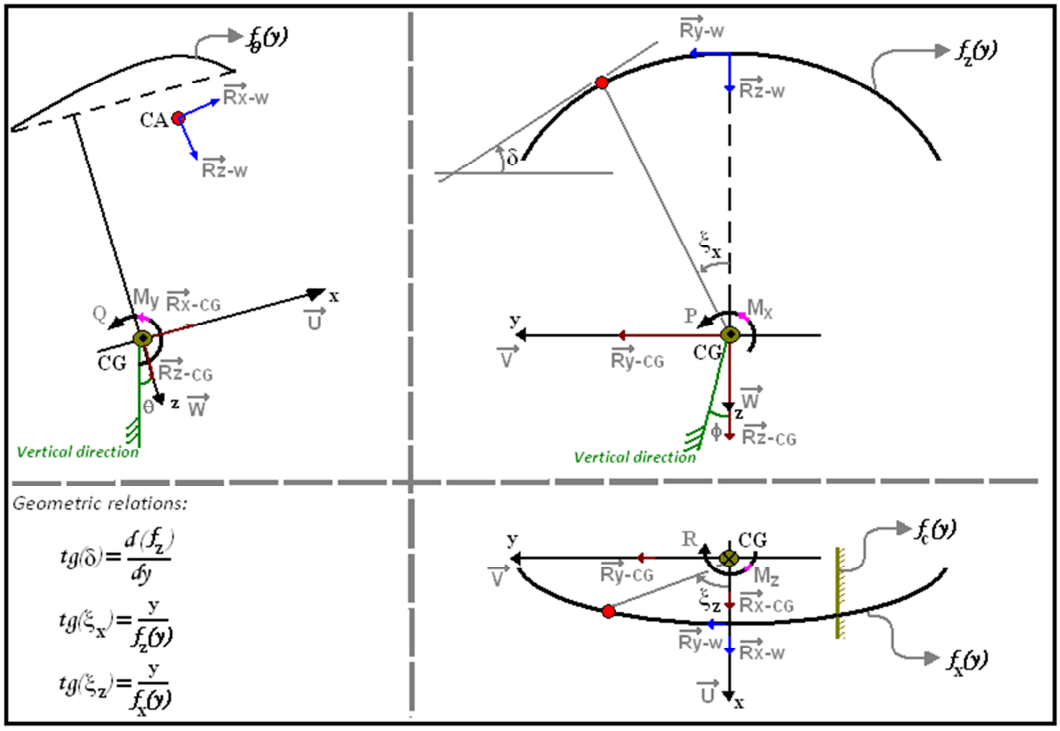

Figure 5.5 – System's dynamics tree-view sketch

The instantaneous dynamic conditions of the system can be fully defined with the following variables:

- θ = Angle between the X axis and the horizontal plan, or attitude.
- ϕ = Angle between the Z axis and the vertical plan, or bank angle.
- U = CG translational speed component in X axis.
- V = CG translational speed component in Y axis.
- W = CG translational speed component in Z axis.
- P = Rotational speed towards X axis, or roll rate.
- Q = Rotational speed towards Y axis, or pitch rate.
- R = Rotational speed towards Z axis, or yaw rate.
- δ_{B_r} and δ_{B_l} =Fraction of available brake applied at each side (pilot's input).

As in classical airplane modeling theory, it can be shown that the heading do not affect the dynamic condition. That's because there are no force component related to this variable. This parameter will be useful only for motion trajectory generation.

The above presented variables will be necessary to determine the instantaneous resultants, which are defined as follows:

- Wing's aerodynamic forces in each axis.
- Moments acting on the CG around each axis, generated by the wing's aerodynamic forces and moments.
- Gravitational forces and drag forces acting on the CG in each axis.

Notice that, applying the concepts of basic mechanics, the wing and CG forces can be combined to give the total resultant for each axis. However it is useful to define those forces separately due to the complex formulation necessary to modeling the wing's resultants shown in section 4.4.

The equations that represent paragliders Kinematics and dynamics are presented below in its matrix format:

Kinematic equations:

$$\begin{bmatrix} \dot{\Phi} \\ \dot{\theta} \\ \dot{\Psi} \end{bmatrix} = \begin{bmatrix} 1 & sen(\Phi)\cdot tan(\Theta) & cos(\Phi)\cdot tan(\Theta) \\ 0 & cos(\Phi) & -sen(\Phi) \\ 0 & sen(\Phi)/cos(\Theta) & cos(\Phi)/cos(\Theta) \end{bmatrix} \begin{bmatrix} P \\ Q \\ R \end{bmatrix} \tag{5.4}$$

$$\begin{bmatrix} \dot{x} \\ \dot{y} \\ \dot{z} \end{bmatrix} = \begin{bmatrix} \cos(\Theta)\cdot\cos(\Psi) & sen(\Phi)\cdot sen(\Theta)\cdot\cos(\Psi) - \cos(\Phi)\cdot sen(\Psi) & \cos(\Phi)\cdot sen(\Theta)\cdot\cos(\Psi) + sen(\Phi)\cdot sen(\Psi) \\ \cos(\Theta)\cdot sen(\Psi) & sen(\Phi)\cdot sen(\Theta)\cdot sen(\Psi) + \cos(\Phi)\cdot\cos(\Psi) & \cos(\Phi)\cdot sen(\Theta)\cdot sen(\Psi) - sen(\Phi)\cdot\cos(\Psi) \\ -sen(\Theta) & sen(\Phi)\cdot\cos(\Theta) & \cos(\Phi)\cdot\cos(\Theta) \end{bmatrix} \begin{bmatrix} U \\ V \\ W \end{bmatrix} \tag{5.5}$$

Dynamic equations:

Translational dynamics:

$$\frac{1}{m}\cdot\begin{bmatrix} X_{RES} \\ Y_{RES} \\ Z_{RES} \end{bmatrix} = \begin{bmatrix} \dot{U} \\ \dot{V} \\ \dot{W} \end{bmatrix} + \begin{bmatrix} 0 & -R & Q \\ R & 0 & -P \\ -Q & P & 0 \end{bmatrix} \begin{bmatrix} U \\ V \\ W \end{bmatrix} \tag{5.6}$$

Rotational dynamics:

$$\begin{bmatrix} M_x \\ M_y \\ M_z \end{bmatrix} = \begin{bmatrix} I_x & 0 & -I_{xz} \\ 0 & I_y & 0 \\ -I_{xz} & 0 & I_z \end{bmatrix} \begin{bmatrix} \dot{P} \\ \dot{Q} \\ \dot{R} \end{bmatrix} + \begin{bmatrix} 0 & -R & Q \\ R & 0 & -P \\ -Q & P & 0 \end{bmatrix} \begin{bmatrix} I_x & 0 & -I_{xz} \\ 0 & I_y & 0 \\ -I_{xz} & 0 & I_z \end{bmatrix} \begin{bmatrix} P \\ Q \\ R \end{bmatrix} \tag{5.7}$$

Although the matrix format is useful for automatic calculations, representing the system in classical format is usually better to visualize system dynamics. Therefore, below is presented the equations of motion separated per axis:

Translational dynamics:

$$\dot{U} = \frac{X_{RES}}{m} + R \cdot V - Q \cdot W \tag{5.8}$$

$$\dot{V} = \frac{V_{RES}}{m} - R \cdot U + P \cdot W \tag{5.9}$$

$$\dot{W} = \frac{W_{RES}}{m} + Q \cdot U - P \cdot V \tag{5.10}$$

Rotational dynamics:

$$\dot{P} = \frac{(I_z \cdot M_x + I_{xz} \cdot M_z)}{(I_x \cdot I_z - {I_{xz}}^2)} + \frac{I_{xz} \cdot (I_x - I_y + I_z)}{(I_x \cdot I_z - {I_{xz}}^2)} \cdot Q \cdot P + \frac{(I_z \cdot (I_y - I_z) - {I_{xz}}^2)}{(I_x \cdot I_z - {I_{xz}}^2)} \cdot Q \cdot R \tag{5.11}$$

$$\dot{Q} = \frac{1}{I_y} \cdot M_Y + \frac{(I_z - I_x)}{I_y} \cdot P \cdot R + \frac{I_{xz}}{I_y} \cdot R^2 - \frac{I_{xz}}{I_y} \cdot P^2 \tag{5.12}$$

$$\dot{R} = \frac{(I_{xz} \cdot M_x + I_x \cdot M_z)}{(I_z \cdot I_x - {I_{xz}}^2)} - \frac{(I_x \cdot (I_y - I_x) - {I_{xz}}^2)}{(I_z \cdot I_x - {I_{xz}}^2)} \cdot Q \cdot P - \frac{I_{xz} \cdot (I_x - I_y + I_z)}{(I_z \cdot I_x - {I_{xz}}^2)} \cdot Q \cdot R \tag{5.13}$$

Kinematic equations for spatial orientation:

$$\dot{\Phi} = P + sen(\Phi) \cdot tan(\Theta) \cdot Q + \ cos(\Phi) \cdot tan(\Theta) \cdot R \tag{5.14}$$

$$\dot{\theta} = cos(\Phi) \cdot Q - sen(\Phi) \cdot R \tag{5.15}$$

$$\dot{\Psi} = \frac{sen(\Phi)}{cos(\Theta)} \cdot Q + \frac{cos(\Phi)}{cos(\Theta)} \cdot R \tag{5.16}$$

As can be seen on the set of equation above, it is presented fourteen dynamically relevant parameters (translational speed, rotational speed, resultant force and moment for each axis and the two orientation angles). However, it is important to clarify that there are eight dynamic inputs and six dynamic outputs expressed in those equations (considering a fixed brake actuation position). The resultant forces and moments are direct functions of the other parameters; therefore, with the forces and moments modeled, these correlations can be substituted into the mathematical system.

The forces and moments on the set of equations above are given by the sum of two set of components: The aerodynamic components on the wing and the CG resultants (aerodynamic and gravitational). Therefore, these terms can be rewritten splitting the total resultants in its components.

The total resultants are given by:

$$\begin{bmatrix} X_{RES} \\ Y_{RES} \\ Z_{RES} \end{bmatrix} = \begin{bmatrix} F_{x_w} \\ F_{y_w} \\ F_{z_w} \end{bmatrix} + \begin{bmatrix} F_{x_{CG}} \\ F_{y_{CG}} \\ F_{z_{CG}} \end{bmatrix} \text{,and, } \begin{bmatrix} M_x \\ M_y \\ M_z \end{bmatrix} = \begin{bmatrix} M_{x_w} \\ M_{y_w} \\ M_{z_w} \end{bmatrix} \tag{5.17}$$

The forces and moments due to the aerodynamic reactions on the wing can be calculated as proposed in chapter 4. For the CG forces, using basic physics and classical aerodynamics (Anderson, 2001), the following applies:

$$F_{x_{CG}} = -\frac{\rho}{2} \cdot U^2 \cdot C_D \cdot S_{CG} - m \cdot g \cdot sen(\Theta) \tag{5.18}$$

$$F_{y_{CG}} = -\frac{\rho}{2} \cdot V^2 \cdot C_D \cdot S_{CG} + m \cdot g \cdot cos(\Theta) \cdot sen(\Phi)$$

(5.19)

$$F_{z_{CG}} = -\frac{\rho}{2} \cdot W^2 \cdot C_D \cdot S_{CG} + m \cdot g \cdot cos(\Theta) \cdot cos(\Phi)$$

(5.20)

Notice that based both on the developments in chapter 4 and on the equations above, the resultants are functions of the dynamic condition (speeds and spatial orientation). In this way, using a compacted format, the previous equations can be rewritten as follows:

Forces and moments:

$$[F_W] = f_{F_W}([v], [\omega], [\delta]); \ [M_W] = f_{M_W}([v], [\omega], [\delta]); \ \ [F_{CG}] = f_{F_{CG}}([v], [\Omega])$$

(5.21; 5.22; 5.23)

Translational dynamics equation:

$$[\dot{v}] = \left[m \cdot [I]\right]^{-1} \cdot \left\{[F_w] + [F_{CG}] - [\omega] \times \left[m \cdot [I] \cdot [v]\right]\right\}$$

(5.24)

Rotational dynamics equation:

$$[\dot{\omega}] = [I_T]^{-1} \cdot \left\{[M_w] - [\omega] \times \left[[I_T] \cdot [\omega]\right]\right\}$$

(5.25)

Kinematics rotational equation:

$$\left[\dot{\Omega}\right] = f_R([\Omega]) \cdot [\omega]$$

(5.26)

Where:

$$[v] = \begin{bmatrix} U \\ V \\ W \end{bmatrix}; [\dot{v}] = \begin{bmatrix} \dot{U} \\ \dot{V} \\ \dot{W} \end{bmatrix}; [\omega] = \begin{bmatrix} P \\ Q \\ R \end{bmatrix}; [\dot{\omega}] = \begin{bmatrix} \dot{P} \\ \dot{Q} \\ \dot{R} \end{bmatrix}; [\Omega] = \begin{bmatrix} \phi \\ \theta \\ \psi \end{bmatrix}; [\dot{\Omega}] = \begin{bmatrix} \dot{\phi} \\ \dot{\theta} \\ \dot{\Psi} \end{bmatrix}; [\delta] = \begin{bmatrix} \delta_{B_r} \\ \delta_{B_l} \end{bmatrix};$$

$$[F_w] = \begin{bmatrix} F_{x_w} \\ F_{y_w} \\ F_{z_w} \end{bmatrix}; [F_{CG}] = \begin{bmatrix} F_{x_{CG}} \\ F_{y_{CG}} \\ F_{z_{CG}} \end{bmatrix}; [M_w] = \begin{bmatrix} M_{x_w} \\ M_{y_w} \\ M_{z_w} \end{bmatrix};$$

$$[I_T] = \begin{bmatrix} I_x & 0 & -I_{xz} \\ 0 & I_y & 0 \\ -I_{xz} & 0 & I_z \end{bmatrix}$$

$$f_R([\Omega]) = \begin{bmatrix} 1 & sen(\Phi) \cdot tan(\Theta) & cos(\Phi) \cdot tan(\Theta) \\ 0 & cos(\Phi) & -sen(\Phi) \\ 0 & sen(\Phi)/cos(\Theta) & cos(\Phi)/cos(\Theta) \end{bmatrix}$$

$$[I] = \begin{bmatrix} 1 & 0 & 0 \\ 0 & 1 & 0 \\ 0 & 0 & 1 \end{bmatrix}$$

This is the set of equations that mathematically represents paraglider motion. It is easy to notice the high complexity involved in this formulation. In the following chapters, this model will be reassessed using new considerations to allow more conclusive analysis.

5.3 Paragliders Motion Simulation Algorithm

With the previously defined equations of motion, using numerical integration procedures, it is possible to simulate paraglider movements. A classical method applicable for such calculations is the 4º-order Runge-Kutta method (Subramaniam, 1987). This method presents a very good level of precision and can be applied to complex formulations.

The basic methodology relays on calculating instantaneous accelerations for punctual dynamic conditions, using the dynamic model. And for a defined time-interval, the next dynamic condition is determined. In this way, with a sufficient set of points calculated, system motion can be visualized.

Following classical system modeling theory the instantaneous flight conditions can be understood as a vector of estate variables:

$$e_{(t)} = [U \quad V \quad W \quad P \quad Q \quad R \quad \Phi \quad \Theta \quad \psi \quad \delta_{B_r} \quad \delta_{B_l}]$$

Below is presented the procedure for motion simulations:

- Initial condition definition - It must be defined the initial conditions of the simulation, which are the values of the state variables at the beginning of the observation period or, mathematically, the initial vector e_0.

- Time interval definition – The time interval is mandatory for accuracy and must be low enough to give smooth results but not so low that would result immeasurable variations. It can be shown that a good range of time intervals is from 0.1s to 1s.

- Time of observation definition – The total time allied to the time interval will implicate the number of points to be calculated. This time must be enough to allow an efficient observation of the movement, in order to minimize the calculation time.

- Calculation of the simulation points – For each point the previously developed equations of motion can be used to calculate accelerations ($[\dot{v}]$, $[\dot{\omega}]$ and $[\dot{\Omega}]$), which combined in a fourth order Runge-Kutta method (Subramaniam, 1987), result the next dynamic condition or state-vector $[e]_{n+1}$.

- Plotting the results – The results can be presented divided by longitudinal and lateral-directional flight parameters for better visualization. Also the flight trajectory can be generated using the kinematic translational equation (5.5).

The algorithm below exemplifies the above procedure translated into a mathematical format:

For each condition established:

$$e_{(t)} = [\mathrm{U} \quad \mathrm{V} \quad \mathrm{W} \quad \mathrm{P} \quad \mathrm{Q} \quad \mathrm{R} \quad \Phi \quad \Theta \quad \psi \quad \delta_{\mathrm{B}_r} \quad \delta_{\mathrm{B}_l}]$$

The punctual acceleration can be calculated as:

$$A(e_{(t)}) = [\dot{U} \quad \dot{V} \quad \dot{W} \quad \dot{P} \quad \dot{Q} \quad \dot{R} \quad \dot{\Phi} \quad \dot{\theta} \quad \dot{\Psi}]$$

Notice that $A = \left[[\dot{v}]^{\mathrm{T}}, [\dot{\omega}]^{\mathrm{T}}, [\dot{\Omega}]^{\mathrm{T}}\right]$, which is basically a function of $e_{(t)}$.

The Runge-Kutta interaction is used to obtain the next point condition as follows:

$$K_1 = A\left(e_{(t)}\right) \tag{5.27}$$

$$K_2 = A\left(e_{(t)} + \frac{\Delta t}{2} \cdot K_1\right) \tag{5.28}$$

$$K_3 = A\left(e_{(t)} + \frac{\Delta t}{2} \cdot K_2\right) \tag{5.29}$$

$$K_4 = A\left(e_{(t)} + \Delta t \cdot K_3\right) \tag{5.30}$$

$$e_{t+\Delta t} = e_{(t)} + \frac{\Delta t}{6} \cdot (K_1 + 2 \cdot K_2 + 2 \cdot K_3 + K_4) \tag{5.31}$$

The process is repeated until the total time is accomplished.

This procedure presents a practical limitation relative to the difficulties of calculating the wing related aerodynamic forces and moments, and thus, to obtain the punctual accelerations through the equations of motion. For each point of calculation, four accelerations cases must be calculated in the runge-kutta interaction and each one of these have six integrals to be solved numerically for wing's resultants determination as presented in section 4.4. Therefore, for 5 seconds observation with a time interval of 0.5s would be necessary to numerically solve 240 integrals. This is obviously time consuming and mostly unpractical for design phase investigations.

5.4 Linear Model Approximation

In order to make practical the investigations using paraglider motion simulation, it is useful to develop a simplified model not requiring numerical integrations in the calculation process. Starting from the wing forces and moments expressions derived in section 4.4, the forces and moments can be remodeled as a linear approximation of those expressions using a classical Taylor series expansion.

A basic definition about the Taylor series expansion is around which point it would be considered. Taking in account that one of the most important objectives of having a simulation tool is to visualize wing's responses to in-flight disturbances, it is an obvious choice to work around the equilibrium point, or, the steady flight condition. An important comment is that this point is unique for a defined command deflection, and so, the obvious choice is to consider the paraglider flying hands-off.

The following sections present the development of the simplified model and the considerations involved. The first part shows a efficient method to calculate the steady flight condition and the second part shows how can be obtained the linear approximations for the wing`s resultants. Finally, with the model fully defined, a comparison between results using the linear model and the original formulations will be made to access the level of deviations expected using the proposed simplification.

5.4.1 The Steady Flight Condition:

The equilibrium or steady flight condition is defined as the situation where there is no acceleration on the system and no lateral-directional movements. In such situation the paraglider flies stabilized with a specific set of speed, flight path and attitude. Applying basic mechanics, the condition for being in equilibrium is that the sum of the resultants must be null. Mathematically the equilibrium can be expressed as follows:

Steady flight constraints:

- $U = U_{eq}$; $V = 0$; $W = W_{eq}$
- $P = Q = R = 0$
- $\emptyset = 0$; $\Theta = \Theta_{\mathrm{eq}}$
- $\delta_{\mathrm{B}_r} = \delta_{\mathrm{B}_l}$ (Considered null for hands-off flight)

Following the definition of steady flight, the equilibrium equations (5.24) e (5.25) becomes:

- $[\dot{v}] = 0$; and, $[\dot{\omega}] = 0$

By applying the steady flight constraints to the set of equations presented in section 5.2 the equilibrate flight equations are reduced to the following relations:

$$[F_w] + [F_{CG}] = 0 \tag{5.32}$$

$$[M_w] = 0 \tag{5.33}$$

The equations above can be expanded as:

$$F_{x_w} - \frac{\rho}{2} \cdot {U_{eq}}^2 \cdot C_D \cdot S_{CG} - m \cdot g \cdot sen(\Theta_{eq}) = 0 \tag{5.34}$$

$$F_{z_w} - \frac{\rho}{2} \cdot {W_{eq}}^2 \cdot C_D \cdot S_{CG} + m \cdot g \cdot cos(\Theta_{eq}) = 0 \tag{5.35}$$

$$M_y = 0 \tag{5.36}$$

Using the aerodynamic model established in chapter 4 for a specific combination of wing's aerodynamics proprieties, the moment equation in steady flight can be written as a function of the angle of attack and the relative position between CG and AC as follows:

$$C_{Z(\propto)} \cdot d_0' - C_{X(\propto)} \cdot h_0' + C_{m_0} \cdot MAC = 0 \tag{5.37}$$

Where "$C_{Z(\propto)}$" and "$C_{X(\propto)}$" are derived from the wing's global aerodynamics coefficients as proposed in section 4.4.1. And, "d_0'" and "h_0'" represents the horizontal and vertical distances between CG and AC as illustrated in figure 5.7, which are two important geometric parameters to be calculated using model's geometric and aerodynamic proprieties.

Although the CG position is a directly defined design parameter, it is necessary to calculate the wing's global aerodynamic center (AC) position. The approximation of the ¼ chord position can be successfully applied for each wing section, however, due to the complex geometry of the paragliders wings, especially if sweep and dihedral angles are present, each wing section's ¼ chord points will be at a different distances from the CG. This is exactly the conceptual definition of the "aerodynamic center positions line" presented in section 3.1 by the functions $f_x(y)$ and $f_Z(y)$. Therefore, as the main objective in defining a generalized aerodynamic center point is to analyze

pitch moment effects, it is useful and accurate enough to define “pitch moment reference arms” as suggested in section 5.4.1.1 below. This definition will be further applied for performance, stability and controllability analysis.

5.4.1.1. The Pitch Moment Reference Arms

A reference pitch moment arm is a particular distance that multiplied by the appropriated component of the total wing’s aerodynamic forces would lead to the same pitch moment as calculated by integrating each wing-section contribution. This modeling strategy is equivalent to generate an abstract planar, straight, constant-sections wing with the same area and flying at the same speed and angle of attack to represent the actual wing. Figure 5.6 illustrates the concept presented:

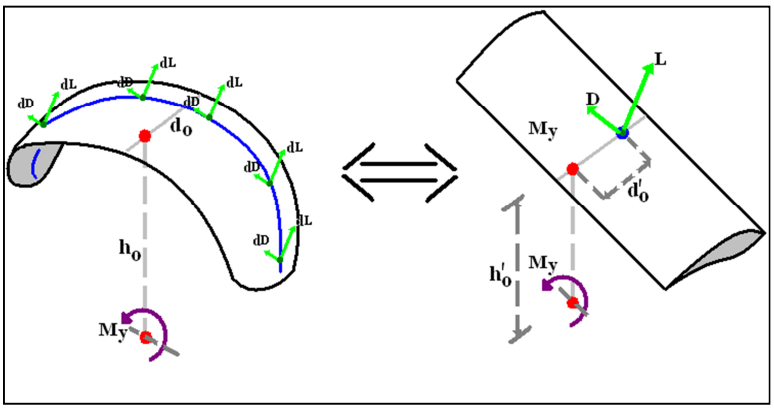

Figure 5.6 – Pitch moment reference arm sketch

With this approach, it is defined a point located in space which can be considered the application point of the aerodynamic forces. This consideration allows to define the global aerodynamic center position for the steady flight condition, and to concentrate the steady flight forces and moments components as presented in figure 5.7 below:

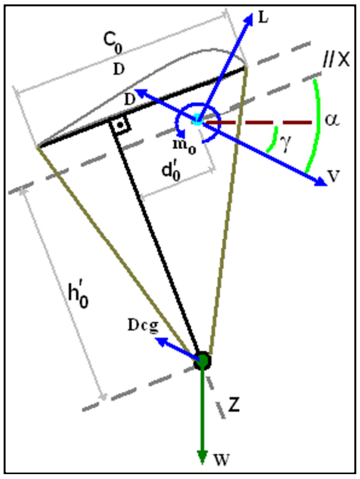

Figure 5.7 – Longitudinal Flight Parameters

To define the distances h_0' and d_0' using the equations derived in section 4.4, the basic definition of pitch moment reference arms can be translated in a mathematical format as:

$$F_{z_w} \cdot d_0' = \int_{-b/2}^{b/2} [-Z_i \cdot f_x(y)]$$

(5.38)

$$F_{x_w} \cdot h_0' = \int_{-b/2}^{b/2} -[X_i \cdot f_z(y)]$$

(5.39)

Where F_{x_w} and F_{z_w} are the wing's total forces calculated using global aerodynamic coefficients as suggested in chapter 4 section 4.3.4:

$$F_{x_w} = \frac{\rho}{2} \cdot V^2 \cdot \left[\widetilde{C_L} \cdot sin(\propto_{eq}) - \widetilde{C_D} \cdot cos(\propto_{eq})\right] \cdot S$$

(5.40)

$$F_{z_w} = \frac{\rho}{2} \cdot V^2 \cdot \left[\widetilde{C_L} \cdot cos(\propto_{eq}) + \widetilde{C_D} \cdot sin(\propto_{eq})\right] \cdot S$$

(5.41)

And, X_i and Z_i are the local components of aerodynamic forces in each wing-section calculated using local aerodynamic coefficients as suggested in chapter 4 section 4.3.5:

$$X_i = \frac{\rho}{2} \cdot V^2 \cdot \left[C_{L_i} \cdot sin(\propto_i) - C_{D_i} \cdot cos(\propto_i)\right] \cdot f_c(y) \cdot dy$$

(5.42)

$$Z_i = \frac{\rho}{2} \cdot V^2 \cdot \left[C_{L_i} \cdot cos(\propto_i) + C_{D_i} \cdot sin(\propto_i)\right] \cdot f_c(y) \cdot dy$$

(5.43)

Finally, applying some reasonable simplifications, the expressions above can be combined with equations (5.38) and (5.39) yielding:

$$d'_0 = \frac{\int_{-b/2}^{b/2} \left[C_{L_i} \cdot cos(\propto_i) + C_{D_i} \cdot sin(\propto_i)\right] \cdot f_x(y) \cdot f_c(y) \cdot dy}{\left[\widetilde{C_L} \cdot cos(\propto_{eq}) + \widetilde{C_D} \cdot sin(\propto_{eq})\right] \cdot S}$$

(5.44)

$$h'_0 = -\frac{\int_{-b/2}^{b/2} \left[C_{L_i} \cdot sin(\propto_i) - C_{D_i} \cdot cos(\propto_i)\right] \cdot f_z(y) \cdot \frac{f_c(y)}{cos(\delta)} dy}{\left[\widetilde{C_L} \cdot sin(\propto_{eq}) - \widetilde{C_D} \cdot cos(\propto_{eq})\right] \cdot S}$$

(5.45)

It is important to understand that the precise solution of the above equations demands iterative calculation, because the equilibrium AOA is a function of the calculated pitch moment reference arms and vice-versa. Notice that for a wing without sweep angle or dihedral the AC position is exactly at the ¼ chord point. Also it can be seen that by increasing the sweep angle the horizontal reference pitch moment arm diminishes and by increasing the anhedral the vertical reference pitch moment arm diminishes.

It must be clear enough that the CG position reference ratio (h'_0/d'_0) is a consequence of both CG positioning and wing aerodynamic proprieties. However, for designs presenting low anhedral and sweep angle, the CG position reference ratio can be successfully approximates as:

$$d'_0 \approx \left(d_{CG} - \frac{1}{4}\right) \cdot C_0 = d_0$$

(5.46)

$$h'_0 \approx h_0$$

(5.47)

This approximation can be very useful in initial design phases, and was sub-textually applied in section 4.4.1.

5.4.1.2 Steady flight parameters calculation

The first steady flight parameter to be determined is the equilibrium AOA, which can be obtained with an iterative calculation process using equations (5.37), (5.44) and (5.45). Many classical numerical methods can be easily applied (Subramaniam, 1987), thus further considerations about this process is unnecessary.

With the angle of attack defined equation (5.32) can be rewritten using the formulation established in chapter 4, as follows:

$$\frac{\rho}{2} \cdot V^2 \cdot \left[S \cdot C_{X_{(\propto_{eq})}} - \left(cos(\propto_{eq}) \right)^2 \cdot S_{CG} \cdot C_{D_{CG}} \right] - m \cdot g \cdot sen(\Theta_{eq}) = 0 \tag{5.48}$$

$$\frac{\rho}{2} \cdot V^2 \cdot \left[-S \cdot C_{Z_{(\propto_{eq})}} - \left(sin(\propto_{eq}) \right)^2 \cdot S_{CG} \cdot C_{D_{CG}} \right] + m \cdot g \cdot cos(\Theta_{eq}) = 0 \tag{5.49}$$

The system of equations above can be easily solved resulting:

$$\Theta_{eq} = atan\left(\frac{C_{X(\propto_{eq})} - \left(cos(\propto_{eq}) \right)^2 \cdot \frac{S_{CG} \cdot C_{D_{CG}}}{S}}{C_{Z(\propto_{eq})} + \left(sin(\propto_{eq}) \right)^2 \cdot \frac{S_{CG} \cdot C_{D_{CG}}}{S}} \right) \tag{5.50}$$

$$V = \sqrt{\frac{m \cdot g \cdot sen(\Theta_{eq})}{\frac{\rho}{2} \cdot \left[S \cdot C_{X(\propto_{eq})} - \left(cos(\propto_{eq}) \right)^2 \cdot S_{CG} \cdot C_{D_{CG}} \right]}} \tag{5.51}$$

And the parameters above can be algebraically combined to present some other usual flight parameters as:

The flight path:

$$\gamma_{eq} = -(\propto_{eq} - \Theta_{eq})$$

(5.52)

The penetration or horizontal speed:

$$V_p = V \cdot cos(\gamma_{eq})$$

(5.53)

The sink rate or vertical speed:

$$V_{SR} = -V \cdot sin(\gamma_{eq})$$

(5.54)

The glide ratio:

$$r_{eq} = \frac{1}{tg(-\gamma_{eq})}$$

(5.55)

Finally, having the steady flight parameters calculated it is possible to evaluate these five important characteristics of paraglider steady flight:

- The equilibrium angle of attack (α_{eq}) – This parameter represents the "central" angle of attack, it is useful to evaluate safety issues related to performance and stability.
- The equilibrium angle of attitude (θ_{eq}) – This parameter shows the attitude angle in steady flight. It is useful for ergonomy and other human-factors assessments.
- The equilibrium penetration speed (V_p) – This parameter gives the most representative operational speed and it is important for every aspects of paraglider flight including stability, control, performance and other safety concerns.
- The equilibrium sink rate (V_{SR}) – This parameter shows how fast the paragliders come down, therefore, it is related to safety especially for landing.
- The equilibrium glide ratio (r_{eq}) – This parameter is immediately related to the maximum range and is the main performance indicative parameter.

5.4.2 Non-equilibrated Flight Conditions:

In any situation where the paraglider flies out-of-equilibrium, which means, at least one of the ten state variables which defines paraglider's flight condition deviates from the equilibrated flight value, there will be non-null accelerations on the system. Mathematically this situation can be expressed in the form:

Flight conditions variables:

$$U = U_{eq} + dU \qquad P = P_{eq} + dP$$
$$V = V_{eq} + dV \qquad Q = Q_{eq} + dQ$$
$$W = W_{eq} + dW \qquad R = R_{eq} + dR$$
$$\theta = \theta_{eq} + d\theta \qquad \phi = \phi_{eq} + d\phi$$
$$\delta_{B_R} = \delta_{B_{R_{eq}}} + \delta_{B_R} \qquad \delta_{B_L} = \delta_{B_{L_{eq}}} + \delta_{B_L}$$

* The environmental conditions (altitude and temperature) are supposed to be a design parameter, and thus, it is supposed not to vary. Therefore there is no need of listing it.

The approach here will be slightly different comparing to airplanes modeling. To define an instantaneous dynamic condition, classical aircraft theory chooses to deal with a single velocity vector and the angles relating body-coordinate-axis and wind axis. This is convenient for airplanes because normally the velocity is mostly in the longitudinal axis, or, in other words, the sink rate and sideslip components are comparatively small. Also, flight controls actuation is the most relevant kind of perturbations. On the other hand, for paragliders, the sink rate are much more representative relatively to the total speed, also, the perturbations originated by gusts in all directions are so important as brakes actuations as a source of disturbance and have special importance for stability analysis. This approach do not change any basic concept for modeling physical phenomenon, it just establishes different dynamic inputs.

Following the proposed definitions, the forces and moments acting on the wing can be calculated using the linear approximation as follows:

$$\begin{bmatrix} F_{x_w} \\ F_{y_w} \\ F_{z_w} \end{bmatrix} = \begin{bmatrix} F_{x_{w_{eq}}} \\ 0 \\ F_{z_{w_{eq}}} \end{bmatrix} + \begin{bmatrix} \frac{\partial F_{x_w}}{\partial U}|_{eq} & \frac{\partial F_{x_w}}{\partial V}|_{eq} & \frac{\partial F_{x_w}}{\partial W}|_{eq} & \frac{\partial F_{x_w}}{\partial P}|_{eq} & \frac{\partial F_{x_w}}{\partial Q}|_{eq} & \frac{\partial F_{x_w}}{\partial R}|_{eq} & \frac{\partial F_{x_w}}{\partial \delta_{B_r}}|_{eq} & \frac{\partial F_{x_w}}{\partial \delta_{B_l}}|_{eq} \\ \frac{\partial F_{y_w}}{\partial U}|_{eq} & \frac{\partial F_{y_w}}{\partial V}|_{eq} & \frac{\partial F_{y_w}}{\partial W}|_{eq} & \frac{\partial F_{y_w}}{\partial P}|_{eq} & \frac{\partial F_{y_w}}{\partial Q}|_{eq} & \frac{\partial F_{y_w}}{\partial R}|_{eq} & \frac{\partial F_{y_w}}{\partial \delta_{B_r}}|_{eq} & \frac{\partial F_{y_w}}{\partial \delta_{B_l}}|_{eq} \\ \frac{\partial F_{z_w}}{\partial U}|_{eq} & \frac{\partial F_{z_w}}{\partial V}|_{eq} & \frac{\partial F_{z_w}}{\partial W}|_{eq} & \frac{\partial F_{z_w}}{\partial P}|_{eq} & \frac{\partial F_{z_w}}{\partial Q}|_{eq} & \frac{\partial F_{z_w}}{\partial R}|_{eq} & \frac{\partial F_{z_w}}{\partial \delta_{B_r}}|_{eq} & \frac{\partial F_{z_w}}{\partial \delta_{B_l}}|_{eq} \end{bmatrix} \cdot \begin{bmatrix} dU \\ dV \\ dW \\ dP \\ dQ \\ dR \\ \delta_{B_r} \\ \delta_{B_l} \end{bmatrix} \tag{5.56}$$

$$\begin{bmatrix} M_x \\ M_y \\ M_z \end{bmatrix} = \begin{bmatrix} 0 \\ 0 \\ 0 \end{bmatrix} + \begin{bmatrix} \frac{\partial M_x}{\partial U}|_{eq} & \frac{\partial M_x}{\partial V}|_{eq} & \frac{\partial M_x}{\partial W}|_{eq} & \frac{\partial M_x}{\partial P}|_{eq} & \frac{\partial M_x}{\partial Q}|_{eq} & \frac{\partial M_x}{\partial R}|_{eq} & \frac{\partial M_x}{\partial \delta_{B_r}}|_{eq} & \frac{\partial M_x}{\partial \delta_{B_l}}|_{eq} \\ \frac{\partial M_y}{\partial U}|_{eq} & \frac{\partial M_y}{\partial V}|_{eq} & \frac{\partial M_y}{\partial W}|_{eq} & \frac{\partial M_y}{\partial P}|_{eq} & \frac{\partial M_y}{\partial Q}|_{eq} & \frac{\partial M_y}{\partial R}|_{eq} & \frac{\partial M_y}{\partial \delta_{B_r}}|_{eq} & \frac{\partial M_y}{\partial \delta_{B_l}}|_{eq} \\ \frac{\partial M_z}{\partial U}|_{eq} & \frac{\partial M_z}{\partial V}|_{eq} & \frac{\partial M_z}{\partial W}|_{eq} & \frac{\partial M_z}{\partial P}|_{eq} & \frac{\partial M_z}{\partial Q}|_{eq} & \frac{\partial M_z}{\partial R}|_{eq} & \frac{\partial M_z}{\partial \delta_{B_r}}|_{eq} & \frac{\partial M_z}{\partial \delta_{B_l}}|_{eq} \end{bmatrix} \cdot \begin{bmatrix} dU \\ dV \\ dW \\ dP \\ dQ \\ dR \\ \delta_{B_r} \\ \delta_{B_l} \end{bmatrix} \tag{5.57}$$

Where, the steady flight related terms presented by the first term in the right side of the above equations can be directly obtained with the formulation presented in the previous section 5.4.1. The vector of disturbances is completely defined by the dynamic condition and the steady flight conditions, and the matrix of wing's derivatives can be obtained numerically as proposed in section 5.4.2.1 below.

Then, using the wing forces and moments linear model developed here, the calculation process to generate motion simulations do not demands numerical integrations and becomes fast and practical.

5.4.2.1. Wing's forces and moments derivatives

As presented in section 4.4 the calculation of forces and moments involves many complexes expressions, and then, it would be an unreasonable effort trying to obtain analytical expressions for the derivatives terms. Because of that, a numerical approach is indicated.

The numerical calculation of the derivatives can be done using the previous calculated equilibrium condition and applying normally expected variations in each dynamic variable separately as synthesized in the formula below:

$$\frac{\partial \vec{R}}{\partial j}|_{eq} = \frac{\vec{R}_{(e_{eq}+\Delta j)} - \vec{R}_{(e_{eq}-\Delta j)}}{2 \cdot \Delta j} \tag{5.58}$$

In this expression "$\vec{R}$" represents the resultants forces and moments varying from F_{x_w} to M_{z_w} and can be calculated using the method presented in section 4.4. The term "j" means the different dynamic variables that may affect the wing's aerodynamic resultants, which are:

$$[\mathrm{U} \quad \mathrm{V} \quad \mathrm{W} \quad \mathrm{P} \quad \mathrm{Q} \quad \mathrm{R} \quad \delta_{\mathrm{B}r} \quad \delta_{\mathrm{B}l}]$$

In order to cover a comprehensive range of interest, the definition of the variation interval for each one of the dynamic variables must take in account the commonly expected in-flight disturbances. It can be shown that the linear approximation provides good results for dynamic situations near to equilibrium, however, as the deviations increase the accuracy of the simplified model decreases considerably.

5.4.3. Limitations of the linear model and derivative analysis

Below is presented for a typical paraglider, the error introduced by the simplified model on the values of forces and moments previously calculated with the non-linear model in different situations:

Table 5-1: Unsteady flight forces and moments

	longitudinal disturbance dU=4m/s		***lateral disturbance dV=1m/s***	
	non-linear	***linear***	***non-linear***	***linear***
FX (N)	**-8,4**	**-7,9**	**0,6**	**0,2**
FY (N)	**0,0**	**0,0**	**-28,8**	**-28,8**
FZ (N)	**-98,9**	**-90,2**	**2,8**	**2,1**
MX (N*m)	**0,0**	**0,0**	**-51,8**	**-51,8**
MY (N*m)	**69,4**	**63,1**	**-2,0**	**0,2**
MZ (N*m)	**0,0**	**0,0**	**8,7**	**8,7**

It can be seen that the error introduced by the linear approximation is manageable. However it is important to have in mind that above a certain level of deviation from equilibrium the results obtained can become non-realistic. Because of that, investigations based in motion simulation for extreme situations must use the non-linear model.

Also, the analysis of the derivatives terms provides relevant conclusions about system's flight dynamics and can define some further constraints for flight dynamics analysis using the simplified model. Table 5-2 below presents the derivatives for a typical paraglider:

Table 5-2: Typical paraglider's wing forces and moments derivatives

	dU	dV	dW	dP	dQ	dR	dBr	dBrl
dFX	-3	1	91	3	-45	0	8	8
dFY	0	-103	0	-187	0	-176	61	-61
dFZ	-83	0	-348	0	830	-4	-188	-188
dMX	0	-187	0	-362	0	-308	109	-109
dMY	55	-4	-359	-14	-125	0	79	79
dMZ	0	31	0	43	0	-72	36	-36

Analyzing table 5-2 above, important observations can be made:

There are some crossed derivatives presenting non-null values ("$\frac{\partial M_y}{\partial V}|_{eq}$", "$\frac{\partial M_y}{\partial P}|_{eq}$"), which mean that lateral-directional and longitudinal disturbances may become coupled in some situations. This is a relevant complication in using classical flight dynamics modeling theory, because usually these terms are considered null, allowing treating the longitudinal and lateral-directional movements separately.

In paragliders the terms relative to roll rate and lateral speed component has considerable impact in pitch moment because of the distance between the aerodynamic center and the center of gravity. As the vertical distance between the wing and the CG is expressive, a small roll rate is capable of generate a considerable component of lateral speed on the wing, and consequently, this lateral component will cause variations in total lift and drag forces, which will be potentiated by the CG height resulting perceptible pitch moment. Chapter 8 will address further considerations in this subject. For now, it is enough to mention that this kind of effect leads to some interesting behaviors observed in flight.

It can also be noticed that, coherent with the previous observations, the most representative derivatives are that related to the rolling and pitching movements. The high value associated to these terms indicates very good lateral and longitudinal responsiveness. On the other hand, the low values of the terms related to yaw reveals a lack of directional stability, typically observed on tailless aircrafts.

Conclusively, by respecting the limitations pointed, and taking in account the main characteristics of the system, the simplified model can be a very useful tool driving considerations and evaluations about flight dynamics and generating methods for design optimization.

5.5 Dynamic Model Applications

The dynamic model is especially useful to explore dynamic behaviors of a specific design model. The non-linear model is a powerful tool to evaluate instantaneous reactions and situations expressively far from the steady flight condition. However, using the linear approximation for forces and moments calculation, a wide range of investigations can be accomplished, in special, dynamic stability characteristics investigations, controllability assessments and any moderate disturbance evaluation that makes itself necessary.

Having in mind the above discussion, the following items exemplifies some useful analysis using the developed dynamic model.

5.5.1. Disturbance analysis examples:

To illustrate the applicability of a simulation tool, below is presented two different simulations using the same paraglider model. The first disturbance chosen was a frontal gust of 10km/h supposed to act in the paraglider as a “speed impulse input”. The second simulation applies the same gust in the lateral direction.

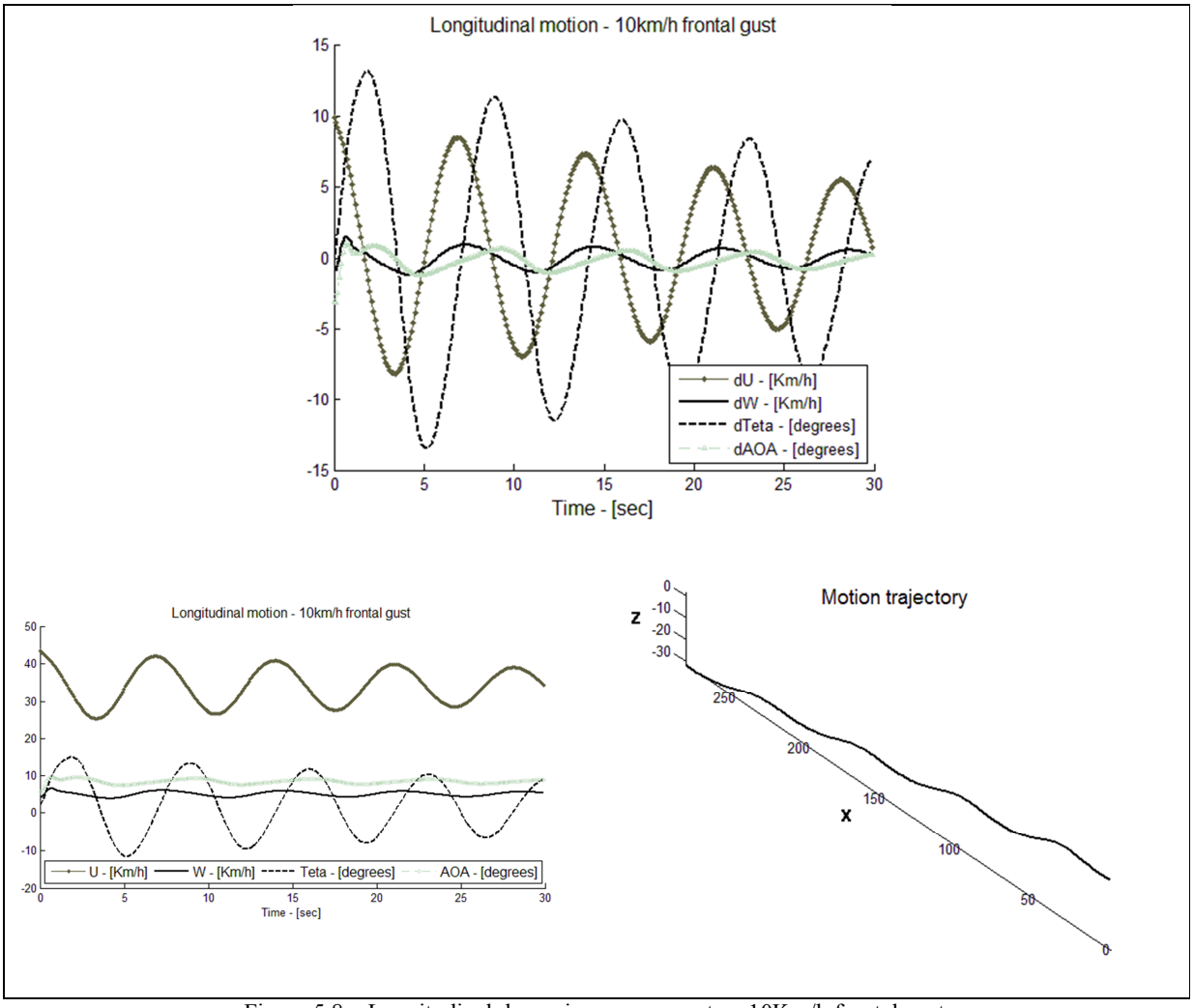

Figure 5.8 – Longitudinal dynamics – response to a 10Km/h frontal gust

Observe that the graph shows an expected behavior accordingly to practical observation (Pagen, 2001). The wing initially pitches up and starts to oscillate around the equilibrated condition. The oscillations characteristic strongly depends on paraglider's geometric proprieties. These relations will be explored in chapter 7. For now it is useful to say that the longitudinal oscillations normally presents lower damping coefficients then lateral ones but also presents an adequate period of oscillation, allowing pilots to stop them. Notice here that the AOA remains inside an acceptable range, what indicates no approximation to the stall or frontal collapse regions.

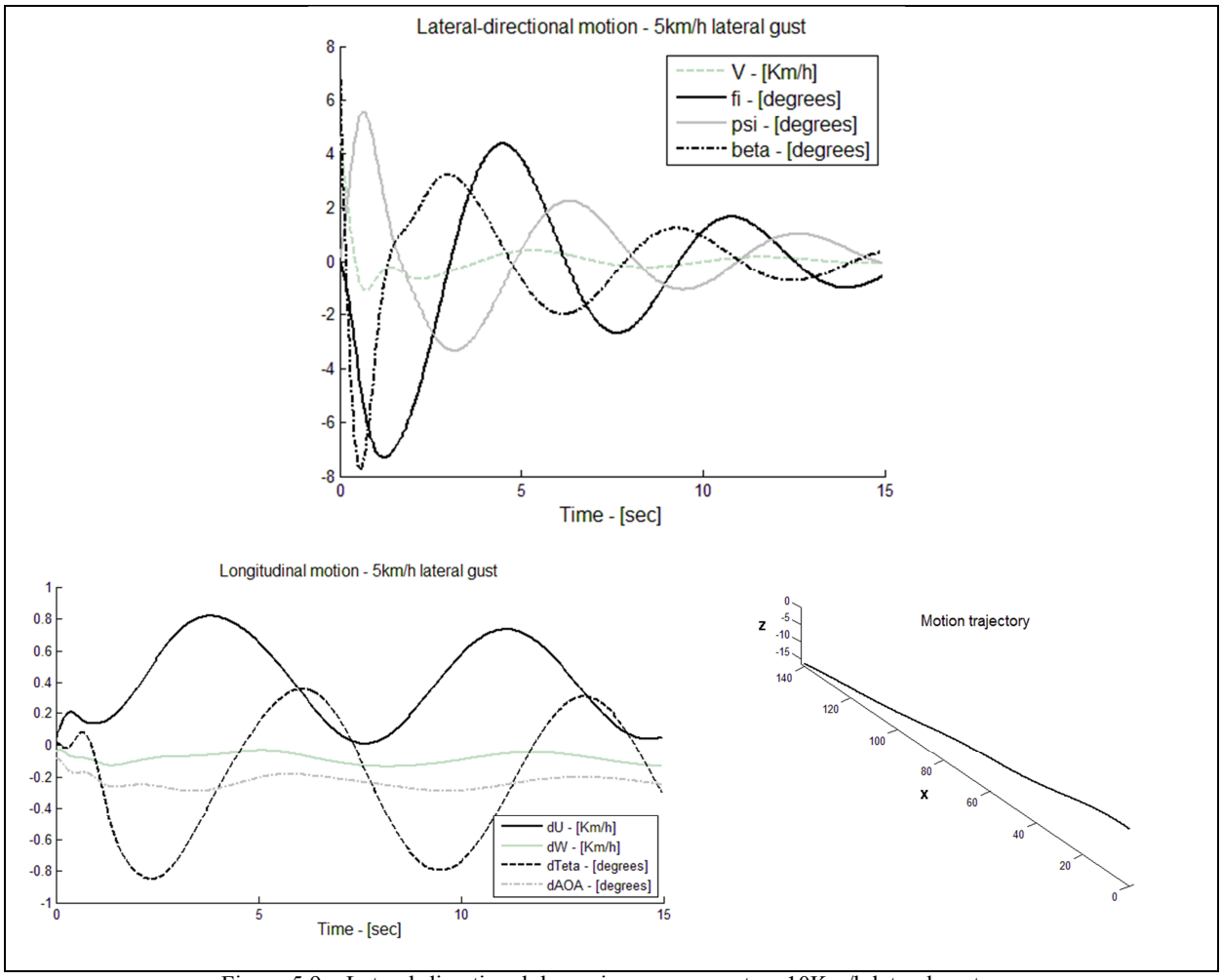

Figure 5.9 – Lateral-directional dynamics – response to a 10Km/h lateral gust

For the lateral-directional case, again, the graph shows an expected behavior. The wing reacts trying to eliminate sideslip. In this case it is possible to notice a good level of damping, consistent with practical observations. It can also be noticed that the lateral oscillation cause some longitudinal disturbance, but with moderate amplitude. This is the previously mentioned effect of wing curvature and vertical CG-AC distance not common for conventional airplanes.

5.5.2. Turning flight motion simulation

With the linear model derived for disturbed flight conditions, even in-turn flight simulations can be done. It must be remembered that the developed model has an accuracy constraint related to the level of deviation from equilibrium. However, it is very useful to evaluate command actuation response characteristics.

The plots below shows the motion simulation for the situation proposed above. Here, full right brakes are applied with initials steady flight conditions:

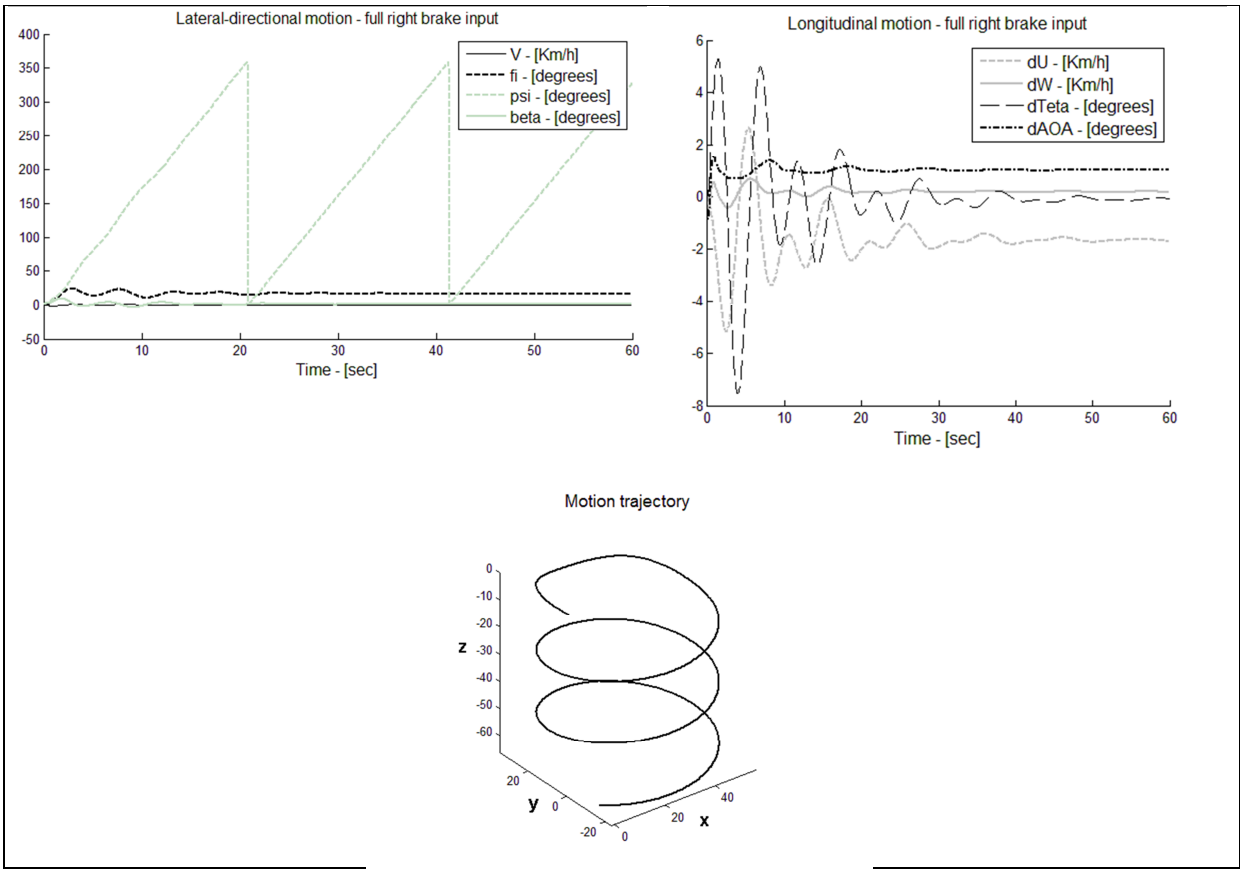

Figure 5.10 – Paraglider's response to right brakes application

As can be seen in figure 5.10 the bank angle increases and the wing pitches down until find a new equilibrium point which is a descendent spiral movement with a high sink rate. Although the absolute values can present some relevant deviations because of the simplifications used by the linear model, the dynamic behavior is physically coherent and, therefore, qualitative optimization analysis can be done using this tool.

The same simulation can be repeated using the non-linear model. The results for such calculation, considering a 15 seconds interval is shown below:

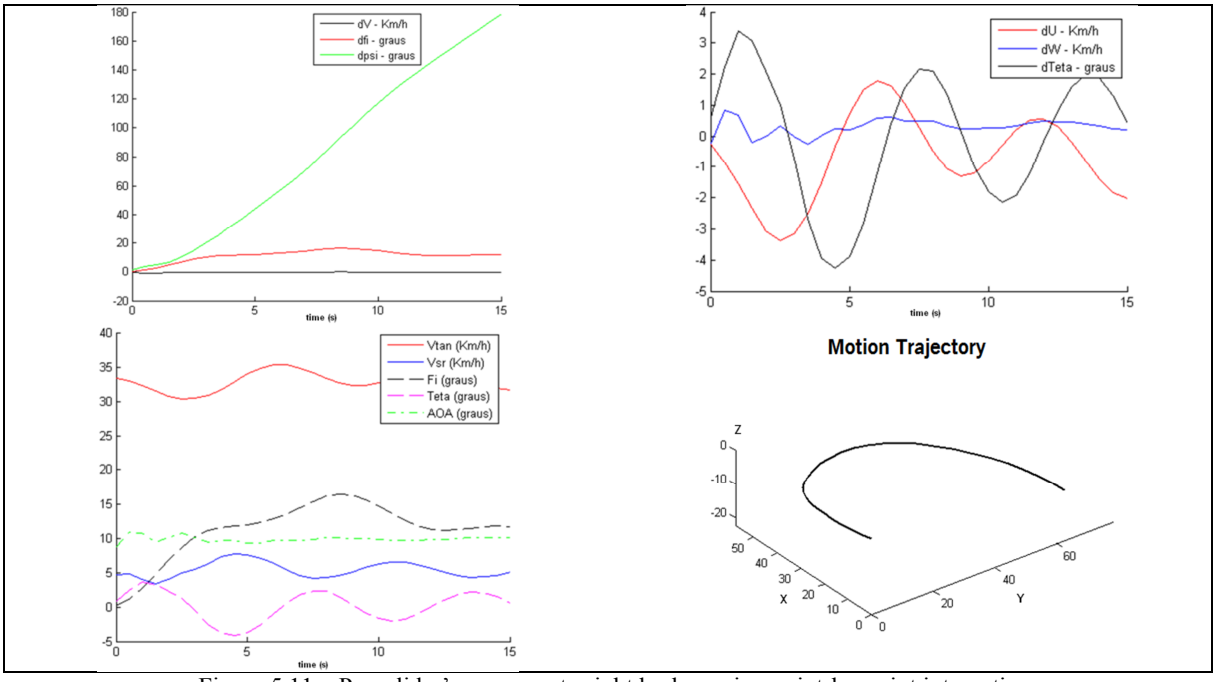

Figure 5.11 – Paraglider's response to right brakes using point-by-point integration

Notice that the overall dynamic behavior remains the same. However observing the values obtained with the non-linear simulation it is possible to see diminished amplitudes in wing's response. Also, curve radius is increased. Below is shown the motion trajectory and the turning parameters graph for both calculations methodology:

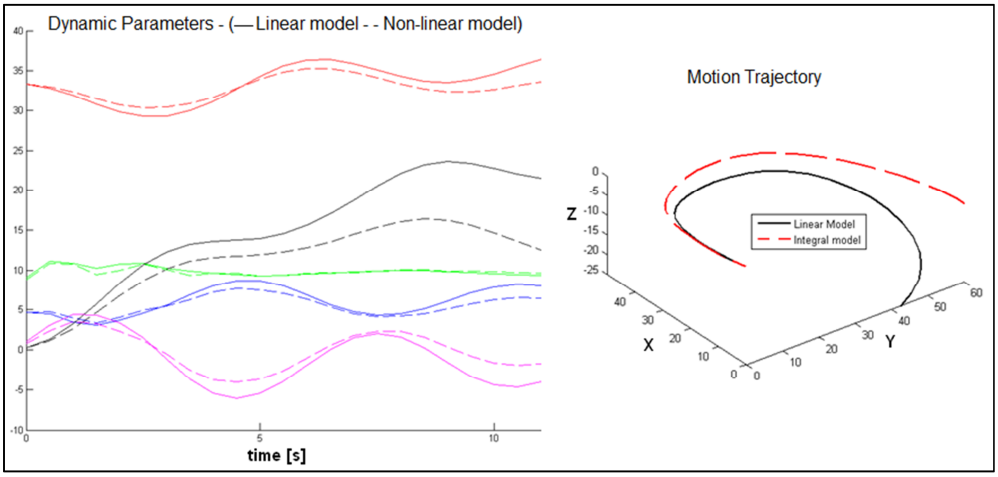

Figure 5.12 – Paraglider's turn analysis using linear and integral models

Again, notice that the overall dynamic behavior remains the same. The "drift" presented do not affect qualitative conclusions about the influence of design parameters on flight controls

characteristics, therefore, the model generated can be considered sufficient for such assessments. Further investigations on paragliders controllability and turn maneuvers will be done in chapter 9 assessing both “brakes” and “accelerator” flight controls.

5.5.3. Exceptional situations assessment:

To exemplify a situation where the application of the linear model would not be suitable, and thus the basic set of equations must be used, it can be analyzed a collapse recovering situation.

This situation can be defined as the moment when the wing completely re-inflates after a complete collapse. In such condition the sink rate is expressively high and there is almost no penetration speed.

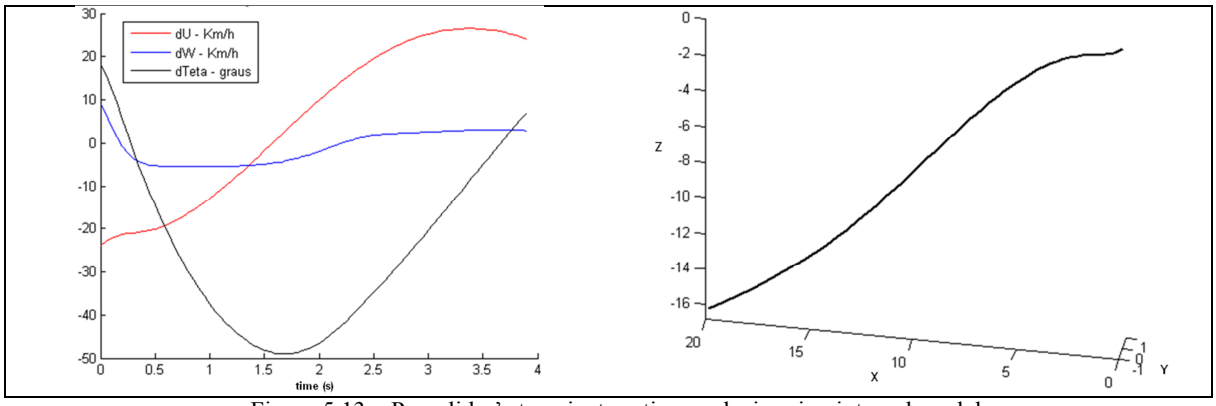

Figure 5.13 – Paraglider’s transient motion analysis using integral model

The above graph shows the penetration and vertical speeds variation relative to the equilibrium condition. As expected, the paraglider try to rebalance, notice that all three longitudinal parameters oscillates around zero deviation presenting a damped behavior. However, notice that the changing in the flight parameters at the first second of movement is very representative. This kind of situation requires a very small time increment in a range of values far away from the steady flight condition. In this way, for these situations the linear model usually result a calculation error or give unrealistic results.

Finally, it can be seen that the linear model developed is a powerful tool to investigate paragliders disturbances response. In the following chapters specific analysis will be held using this model to explore how the design parameters affect the dynamic behavior.

5.6 Final Comments:

In this chapter it was developed a dynamic model to represent paraglider's motion, which was fully based in design parameters. Some simplifications and assumptions where adopted in order to build a useful model for conceptual design investigations and still, a good characterization of paraglider movement can be seen on the many simulations presented.

It was analyzed the main particularities that makes problematic the application of classical airplanes modeling theory to paragliders, and each particularities was addressed in order to overcome or understand eventual deviations in flight dynamics representation.

Among other important achievements in this chapter, the dynamic model developed will be very useful to investigate the effects of the various design features in paraglider flight characteristics. Also, the equations of motion derived here will serve as a base for future developments in stability and controllability analysis.

Furthermore, the motion simulation, and the consequent visualization of paraglider's response to different disturbances, is of primary interest studying paragliders flight mechanics because allows reaching important conclusions about the in-flight behavior of these aircrafts.

6 PARAGLIDERS PERFORMANCE

For any aircraft, the performance characteristics are fundamental design goals which can be represented by specific quantitative parameters to be used in conceptual design optimization. This kind of evaluation varies because the concept of "performance" is linked to the aircraft mission and operational characteristics.

Airplanes performance parameters are normally related to climb capability, range of operation, ceiling, takeoff and landing field limitations and fuel consumption. In this way, conventional airplanes have their performance strongly affected by engine power, brake capability, and other systems characteristics. These features are not pertinent for paragliders, which present a very restricted range of performance parameters, basically determined by the aerodynamic proprieties and system geometry.

A paraglider flight may have different goals for different users at different moments. Basically, the three flight objectives that should be considered are:

- Endurance - Common in leisure flights, when pilots look for keep flying the longest time they can. Although the glide ratio can also indirectly improve flight time, the flying time is nearly related to the sink rate.

- Range – Common in either competitions or weekend flights, it means to reach great distances. It is directly related to the glide ratio, the ratio between penetration speed and sink rate. This characteristic is also important for improve flight time, because, the ability of reach great distances with a minimum height lost improves the thermal-hunting efficiency.

- Acrobatic – The acrobatic flight is much rare and demands special pilot skills. In this kind of flight it is desirable to have a fast and maneuverable wing, because most maneuvers depend on a great amount of kinetic energy and angular momentum.

Whichever be the flight purpose, the three capabilities listed above can be translated in three basic performance parameters: The glide ratio, the sink rate and the flight speed. It can be noticed that these parameters are direct consequences of two basic steady flight characteristics: Flight-speed and Flight-path, therefore the performance analysis corresponds to an expanded analysis of the steady flight condition. In this chapter it will be investigated the performance characteristics and their relations with design parameters.

6.1. Performance Parameters Calculations

For trajectory analysis purposes, a paraglider in steady flight can be treated as a point moving through the air. The equilibrium condition can be then illustrated as shown in figure 6.1 below:

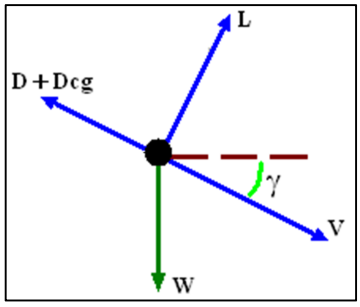

Figure 6.1 – Paraglider's CG in steady glide

Using basic mechanics (Yechout, 2003), the translational equilibrium can be expressed by the two equations below:

$$L \cdot cos(\gamma) + (D + D_{CG}) \cdot sin(\gamma) - W = 0 \tag{6.1}$$

$$L \cdot sin(\gamma) - (D + D_{CG}) \cdot cos(\gamma) = 0 \tag{6.2}$$

Using classical formulation for the aerodynamic forces, the concept of dynamic pressure and considering that the flight path angle are small enough to allow the usual approximation tan(γ)=sin(γ)=angle and cos(γ)=1, the system of equations above can be rewritten as:

$$\bar{Q} \cdot \left[C_L + \left(C_D + \frac{S_{CG} \cdot C_{D_{CG}}}{S}\right) \cdot \gamma\right] = w_l \tag{6.3}$$

$$\bar{Q} \cdot S \cdot \left[C_L \cdot \gamma - \left(C_D + \frac{S_{CG} \cdot C_{D_{CG}}}{S}\right)\right] = 0 \tag{6.4}$$

With some algebraic manipulation of the second equation, the flight path can be expressed as:

$$\gamma = \left(\frac{C_D}{C_L} + \frac{S_{CG} \cdot C_{D_{CG}}}{S \cdot C_L}\right) \tag{6.5}$$

By substituting the above relation in the first equation, its yields:

$$\bar{Q} \cdot \left[\frac{{C_L}^2 + \left(C_D + \frac{S_{CG} \cdot C_{D_{CG}}}{S}\right)^2}{C_L}\right] = w_l \tag{6.6}$$

For normal design parameters it is possible to simplify the above expression by neglecting the drag term on the numerator. With this, the flight speed can be approximated as:

$$V = \sqrt{\frac{w_l}{\frac{1}{2}\rho \cdot C_L}} \tag{6.7}$$

With an statistical investigation it is possible to shown that the simplification above results errors below 2% in flight speed, what makes it completely acceptable considering that flight speed for paragliders are between 25 and 70 km/h and an error of 1.4km/h is absolutely not relevant.

Equations (6.5) and (6.7) define the basic steady flight trajectory parameters as functions of the aerodynamic coefficients and some geometry related parameters. Notice that the only parameter affected by the wing-load is the flight speed. It means that for a specific design model, a change in pilot's weight will affect the flight speed but not the flight path.

6.1.1. The Glide Ratio

The main performance indicative parameter is the glide ratio. The glide ratio can be visualized as the relation between horizontal and vertical displacement, or, the ratio between horizontal and vertical speeds. In this way, it is easy to see that the glide ratio can be mathematically defined as the inverse of the tangent of the flight path angle (Mair, 1996).
Using equation (6.5), it follows:

$$r = \frac{1}{\gamma} = \frac{C_L}{C_D}\Big|_{\alpha_{eq}} \cdot \left(\frac{1}{1+\frac{S_{CG} \cdot C_{D_{CG}}}{S \cdot C_D|_{\alpha_{eq}}}} \right)$$

(6.8)

It can be seen that paraglider's glide ratio is directly related to the wing's efficiency parameter (L/D). A degradation factor "f" multiplies the wing efficiency parameter resulting the paraglider glide ratio:

$$f = \left(\frac{1}{1+\frac{S_{CG} \cdot C_{D_{CG}}}{S \cdot C_D|_{\alpha_{eq}}}} \right)$$

(6.9)

Notice that this degradation factor is a function of the ratio between CG drag and wing drag. In this way, as much representative is the CG drag for the overall drag more relevant will be the wing efficiency degradation factor.

By expanding the aerodynamic coefficients as proposed in chapter four, the glide ratio can be expressed as a function of the design parameters and the equilibrium angle-of-attack (AOA) as follows:

$$r = \frac{a \cdot (\alpha_{eq} - i_0)}{D_2 \cdot [a \cdot (\alpha_{eq} - i_0)]^2 + D_0} \cdot \left(\frac{1}{1+\frac{S_{CG} \cdot C_{D_{CG}}}{S \cdot \left(D_2 \cdot [a \cdot (\alpha_{eq} - i_0)]^2 + D_0 \right)}} \right)$$

(6.10)

In this formula it can be seen that the glide ratio depends basically on aerodynamics proprieties with a light influence of the wing area. Figure 6-2 shows the wing efficiency (L/D) and glide ratio (r) curves for a range of angle-of-attack using basic proprieties of a typical paragliders (presented in table 6-1).

Table 6-1: Basic-design parameters for the exemplification model.

Paraglider's basic proprieties				
Geometric proprieties ->	Reference area = $20m^2$		Wing-load = $4Kg/m^2$	
Wing's Aerodynamic proprieties ->	I_0=-2°	a=3.6 rad^{-1}	D_0=0.017	Cm_0=-0.009
CG's proprieties ->	S-cg = $1m^2$		CD-cg = 0.8	

The proprieties shown in table 6-1 will be used as a basic-design definition for the exemplifications and graphs throughout this chapter. These are reasonable values of these variables and the performance parameters analysis can be understood valid for any model. The only effect of changing those basic design variables will be some repositioning of the presented curves with no relevant changes on the overall behavior or analytical conclusions.

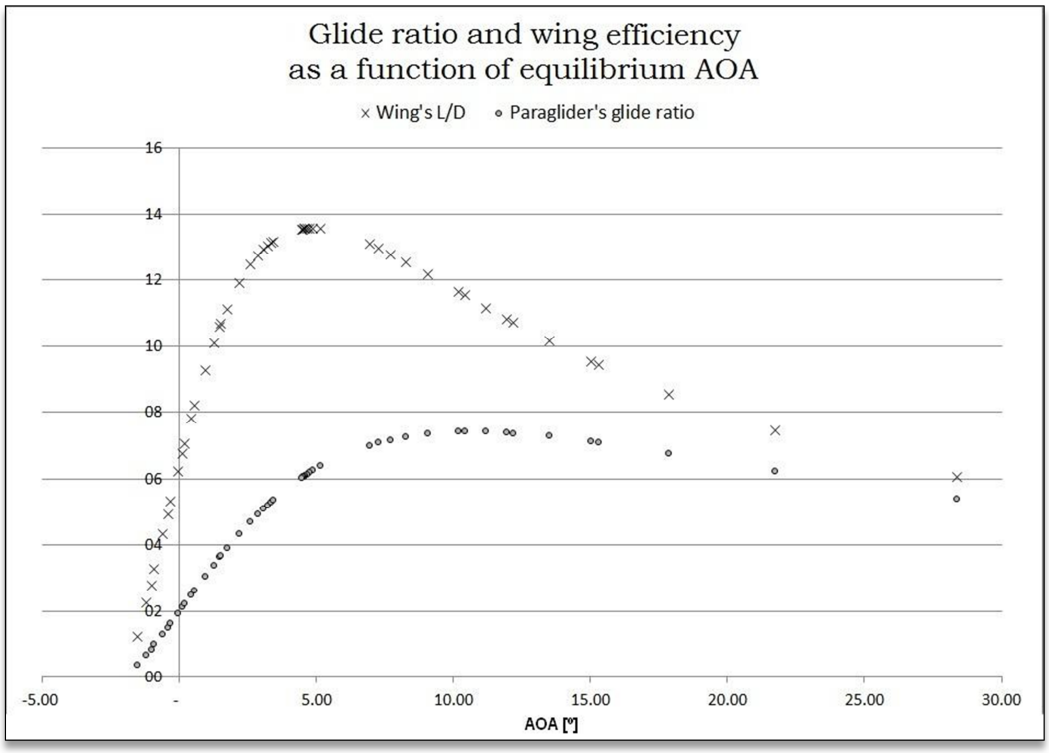

Figure 6.2 – Glide ratio and wing efficiency as a function of equilibrium AOA

As can be seen the wing's efficiency degradation is quite representative, especially for low AOA values. This is expected since in low AOA the induced drag is diminished and the CG drag becomes more representative increasing the degradation factor.

An obvious objective is to reach the best glide ratio for a particular model, for that, it is necessary to determine the AOA for optimum glide ratio or maximum range by differentiating equation (6.10):

$$\alpha_{opt.GR} = i_0 + \sqrt{\frac{\left(D_0 + \frac{S_{CG} \cdot C_{D_{CG}}}{S}\right)}{D_2 \cdot a^2}} \tag{6.11}$$

Coherently, eliminating the center of gravity drag contribution this expression gives the angle of attack for the maximum wing's efficiency (L/D):

$$\alpha_{(L/D)_{max}} = i_0 + \frac{1}{a} \cdot \sqrt{\frac{D_0}{D_2}} \tag{6.12}$$

and substituting the optimum glide AOA into equation (6.10), it yields:

$$r_{max} = \frac{1}{2 \cdot \sqrt{D_2 \cdot \left(\frac{S_{CG} \cdot C_{D_{CG}}}{S} + D_0\right)}} \tag{6.13}$$

The above expression gives the maximum achievable glide ratio as a function of the design parameters. As can be seen, the maximum glide ratio can be improved by attenuating the sources of drag and also by adjusting the wing area. Figure 6.3 below shows glide ratio variation with AOA for different wing areas taking as a base the design parameters specified on table 6-1.

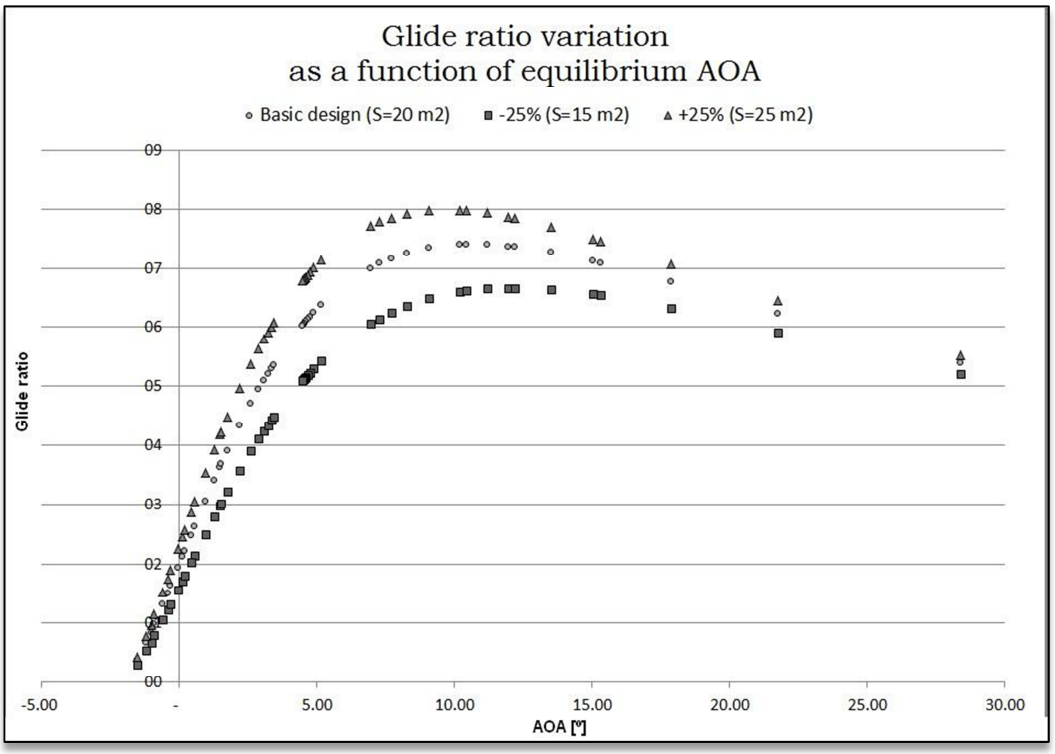

Figure 6.3 – Glide ratio variation

Actually the maximum glide ratio can be difficult to reach in some cases due to some design limitations. Therefore, it is useful to define a "Glide Ratio Performance Index - (GRPI)" as:

$$GRPI = \left[\frac{r_{eq}}{r_{max}}\right] \cdot 100\% \tag{6.14}$$

This index measure how optimized the actual glide ratio is for a particular model, and can be used as an indication of the design optimization level regarding glide ratio. Normally the design variables are adjusted to maximize this index, but ratings above 85% can be considered already an acceptable level of optimization.

6.1.2. The Flight Speed

The total flight speed is not directly a performance parameter; however it is very important in many aspects. There are some design limits associated to the flight speed as the structural stability minimum and the maximum safe landing speed. Another important consequence of this parameter is the maneuverability characteristics, and, therefore, an evaluation of the variation of the steady flight speed for a particular model is primarily important for flight characteristics evaluations. By expanding the lift coefficient as proposed in chapter four, equation (6.7) becomes:

$$V = \sqrt{\frac{w_l}{\frac{1}{2}\rho \cdot a \cdot (\alpha_{eq} - i_0)}} \tag{6.15}$$

Notice that the velocity depends on the wing-load which relates weight and area; therefore, in this expression it is included aerodynamics, geometrics and load parameters. Also it is interesting to point out that there is no drag terms directly involved in this expression, however, the definition of the equilibrium AOA depends on drag parameters. Figure 6.4 below shows the steady flight speed variation with AOA for a range of wing-loads:

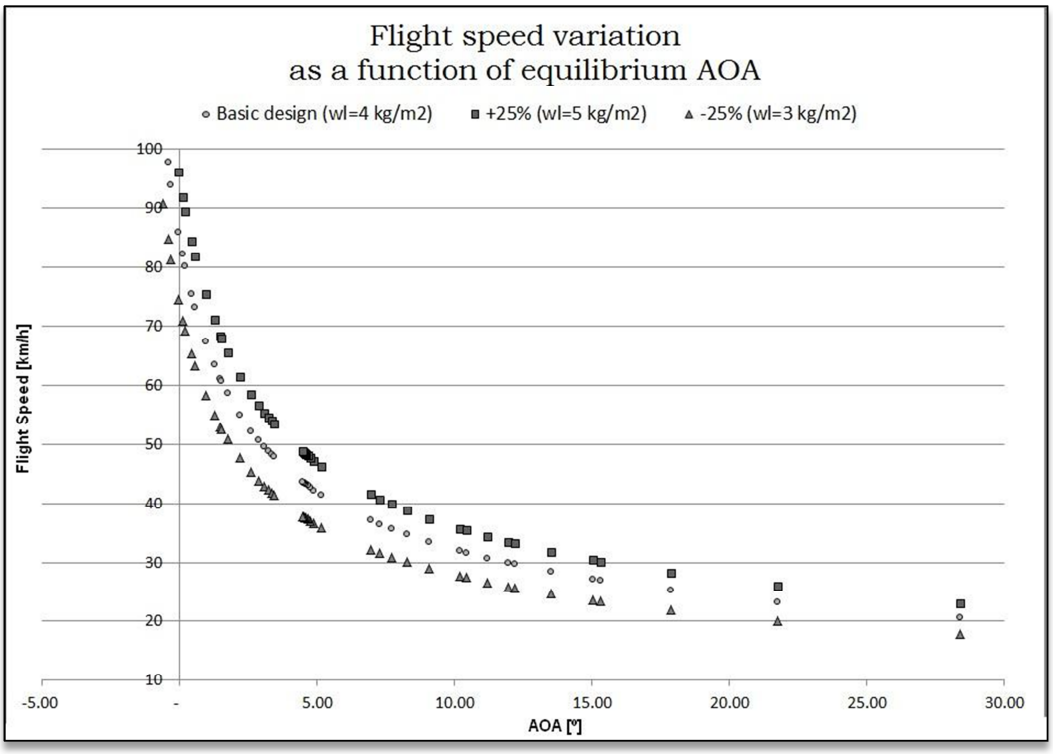

Figure 6.4 – Steady flight speed

Notice that the variation of steady flight speed with angle-of-attack and wing-load is really representative. As presented before, the flight path and glide ratio is a function of the equilibrium AOA and do not depends on wing-load. In this way, by fixing a steady flight AOA it can be evaluated on a graph similar to figure 6.4 how the predicted in-service variations of wing-load will affect the flight speed and then check for structural and safety limitations.

6.1.3. The Sink Rate (Descent speed)

The sink rate or descent speed is a direct consequence of the total flight speed and the glide path. Figure 6.5 below shows an illustration of this geometric relation:

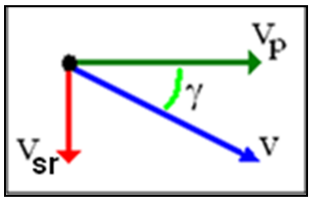

Figure 6.5 – Longitudinal flight speeds

The above relation can be mathematically expressed as:

$$V_{sr} = V \cdot sin(\gamma) \approx V \cdot \gamma = \frac{V}{r}$$

(6.16)

Substituting the equations (6.7) and (6.10) on the above relation the, sink rate or vertical speed can be written as:

$$V_{sr} = \left(\sqrt{\frac{w_l}{\frac{1}{2}\rho}}\right) \cdot \frac{\left(\left(D_2 \cdot [a \cdot (\alpha_{eq} - i_0)]^2 + D_0\right) + \frac{S_{CG} \cdot C_{D_{CG}}}{S}\right)}{\left(a \cdot (\alpha_{eq} - i_0)\right)^{3/2}}$$

(6.17)

Notice that for the sink rate both wing-load and wing area are independently included into the expression. Figure 6.6 below shows the sink rate variation with angle-of-attack for a range of wing-load and wing-area combinations.

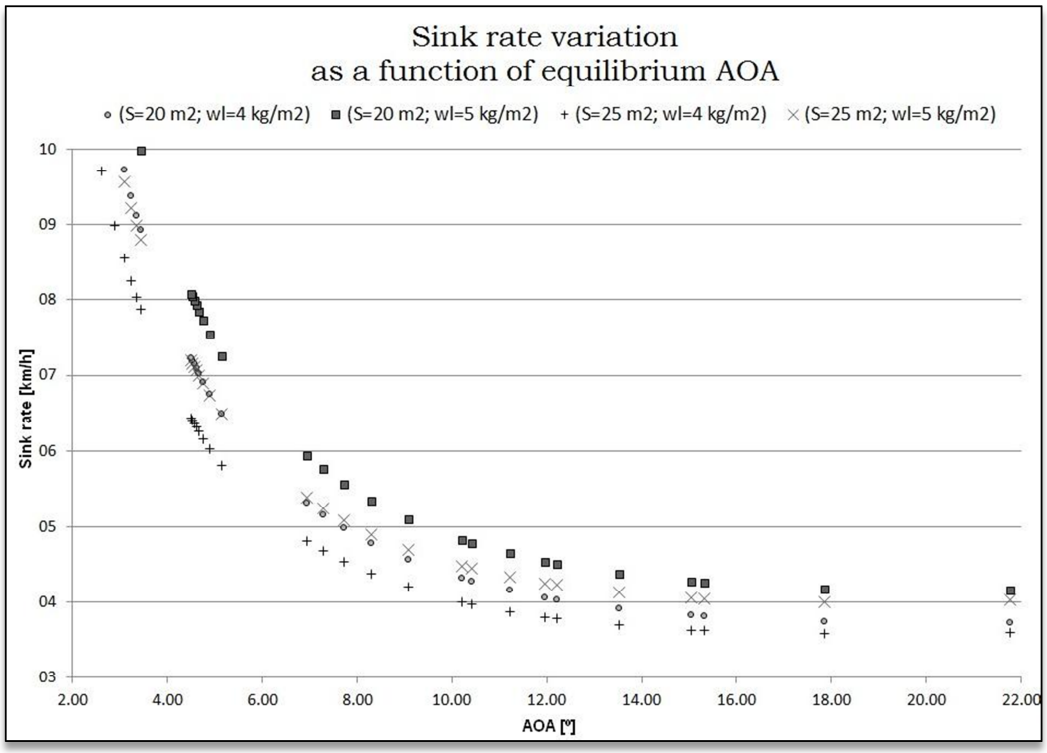

Figure 6.6 – Sink rate variation with AOA for a range of wing-load and wing-area combinations

Notice that the effect of wing-load is almost homogeneous and dominates sink rate variations for moderates and high angles of attack. For low values of AOA the wing-area effect

increases and also the sink rate itself. It is also noticeable that for sink rate there is no relevant variation above a certain AOA value, what is a useful observation for conceptual design parameters management. This observation allows concluding that there is a minimum AOA that put the vertical speeds in an acceptable range.

As proceeded for the glide ratio, it is possible to find the angle-of-attack for minimum sink rate by differentiating equation (6.17):

$$\alpha_{opt.Vsr} = i_0 + \sqrt{3 \cdot \frac{\left(D_0 + \frac{S_{CG} \cdot C_{D_{CG}}}{S}\right)}{D_2 \cdot a^2}} \tag{6.18}$$

It can be noticed that this AOA is greater then the AOA for best glide, and the distance between the AOA for maximum glide ratio and the AOA for minimum sink rate can be calculated as:

$$\Delta\alpha_{opt.} = \left(\sqrt{3} - 1\right)\sqrt{\frac{\left(D_0 + \frac{S_{CG} \cdot C_{D_{CG}}}{S}\right)}{D_2 \cdot a^2}} \tag{6.19}$$

By applying the AOA for minimum sink rate in equation (6.17) it can be calculated the minimum sink rate as:

$$V_{sr_{min}} = \sqrt[4]{\frac{2^{10} \cdot {w_l}^2 \cdot {D_2}^3}{27 \cdot \rho^2} \cdot \left(D_0 + \frac{S_{CG} \cdot C_{D_{CG}}}{S}\right)} \tag{6.20}$$

Also, in order to evaluate how far from the endurance optimization point a specific model operates, it can be defined the “Endurance Performance Index”:

$$EPI = \frac{V_{q_{min}}}{V_{q_{eq}}} \cdot 100\% \tag{6.21}$$

This index also represents the effective flight time compared to a maximum flight time.

6.1.4. Performance parameters simultaneous evaluation

As show in the last sections, the performance parameters present specific behavior and the optimization of a specific model must consider the simultaneous variation of such characteristics. Figure 6.7 below shows the simultaneous variation of glide ratio and sink rate for a range of equilibrium AOA:

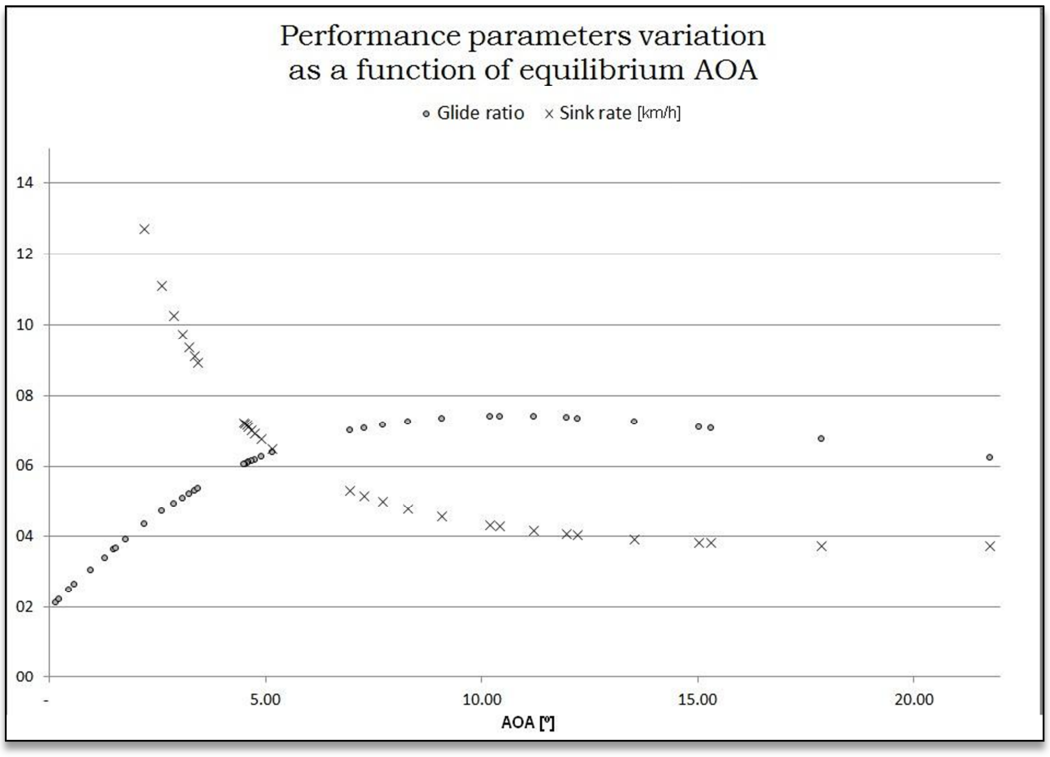

Figure 6.7 – Performance parameters variation with AOA

Based on this illustration it can be concluded that for high AOA the vertical speed do not varies relevantly. It can be also noticed that near to the glide ratio optimization point the sink rate is already in an acceptable range. Because of that, it is rational to give some priority to glide ratio optimization, using the sink rate just as an acceptability or pass criteria.

Another way to analyze glide ratio and sink rate simultaneously is by drawing the "performance curve". The descent speed can be calculated as a function of the total flight speed, by relating equations (6.10) and (6.17) as follows:

$$V_{sr} = V \cdot \left[D_2 \cdot \left(\frac{w_l}{\frac{1}{2}\rho \cdot V^2} \right) + \frac{\left(D_0 + \frac{S_{CG} \cdot C_{D_{CG}}}{S} \right)}{\left(\frac{w_l}{\frac{1}{2}\rho \cdot V^2} \right)} \right] \tag{6.22}$$

By plotting the defined speeds it is generated a curve as illustrated in figure 6.8:

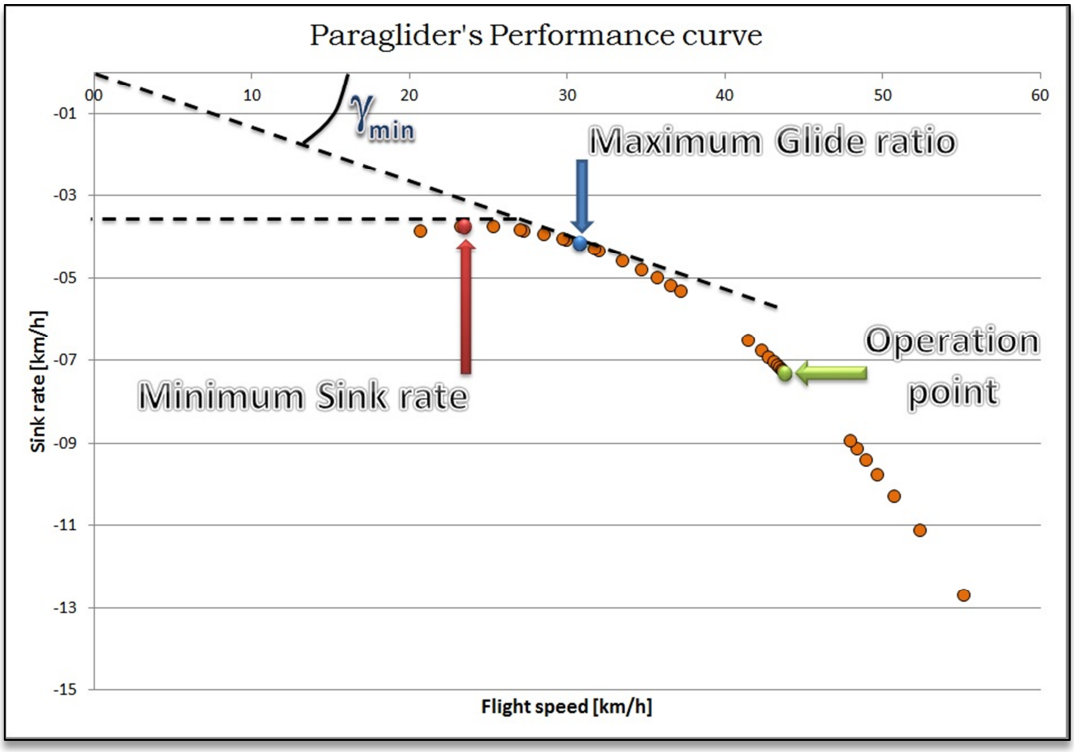

Figure 6.8 – Performance Curve

This curve can be called “the performance curve” for a specific paraglider. That’s because in this curve it can be visualized all performance parameters. The point of maximum gives the minimum sink rate. The tangent to the curve passing through the origin gives the minimum flight path and, indirectly, the maximum glide ratio. By plotting on this graph the steady flight point it can be also identified the steady flight parameters, and it is possible to have a good visualization of how far from the optimum condition the model operates.

For some kinds of analysis this graph is more interesting because it deals with speed instead of angle of attack, and normally, it is easier to have a better “feeling” about the speed range. Changing the equilibrium AOA is a way to “walk through” the curve redefining the steady flight point. By looking the performance curve it is possible to evaluate if a “slow down” or a “speed up” in the steady flight speed is suitable for performance improvements and how relevant would be such adjustments.

As already commented, it can be noticed that the distance between the two optimization points is quite small elapsing a straight speed range. This shows, once more, that the glide ratio optimization seems to be the most efficient approach.

Finally, although each performance parameters presented here have its own importance for flight characteristics, it can be said that the glide ratio is the main performance indicator, and the other two works as flight characteristics constraints.

6.2. The Equilibrium Condition

In section 6.1 above it was defined the performance parameters as a function of the equilibrium angle of attack. However, as already assessed in previous chapters, for a specific commands actuation condition there is a single equilibrium AOA which is a function of the design parameters. This equilibrium point (or operational point) will then define the operational glide ratio, flight speed and sink rate for the model. This point may vary with commands actuation but this variation is not relevant for basic performance characteristics and must be taking in account just to allow refinements on the brake mechanism design. For performance design initial evaluations it will be considered the wing flying hands-off.

It must be taking in account that calculation processes requiring iterative numerical solutions can be time consuming and introduce a major difficulty for conceptual design evaluations. Because of that, the development of simplified direct relations between the in-flight parameters and the design variables can be very useful to allow faster analysis.

As discussed previously in chapters 4 and 5 and reaffirmed in this chapter, for a defined wing, the center of gravity position can be adjusted to reach a specific angle of attack. In other words, the operational point of a paraglider can be defined by adjusting a term called the CG position reference ratio, which means, the ratio between CG and AC vertical and horizontal distances.

In chapter five it was shown how to calculate the equilibrium angle of attack in a very precise manner. Although this is an important tool, it is interesting to analyze the AOA expression using algebraic expressions. Using the sketch presented in figure 6.10, the equation representing the rotational equilibrium towards the pitch axis can be written as:

$$[L \cdot cos(\propto) + D \cdot sin(\propto)] \cdot d_0' - [L \cdot sin(\propto) - D \cdot cos(\propto)] \cdot h_0' + m_0 = 0 \quad (6.23)$$

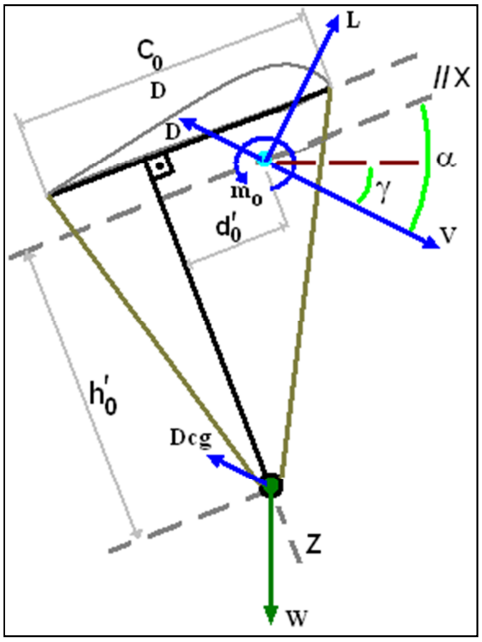

Figure 6.10 – Longitudinal Flight Parameters

In the initial stages of the design process, the geometric parameters in equation (6.23) can be successfully approximated as:

$$d_0' \approx \left(d_{CG} - \frac{1}{4}\right) \cdot C_0 = d_0 \tag{6.24}$$

$$h_0' \approx h_0 \tag{6.25}$$

By applying the basic definitions of the aerodynamic forces and moments it follows:

$$\bar{Q} \cdot S \cdot \{[C_L \cdot cos(\propto) + C_D \cdot sin(\propto)] \cdot d_0' - [C_L \cdot sin(\propto) - C_D \cdot cos(\propto)] \cdot h_0' + MAC \cdot C_{m_0}\} = 0 \tag{6.26}$$

Considering both flight path and AOA sufficiently small to allow the classical approximation: tan=sin=angle and cos=1, the equation becomes:

$$\bar{Q} \cdot S \cdot \{[C_L + C_D \cdot \propto] \cdot d_0' - [C_L \cdot \propto - C_D] \cdot h_0' + MAC \cdot C_{m_0}\} = 0 \tag{6.27}$$

Using the formulation proposed in chapter four to describe the aerodynamic coefficients the expression above can also be written as a cubic equation in alpha:

$$\propto^3+\left[-2\cdot i_0+\frac{h_0'}{d_0'}\left(1-\frac{1}{D_2\cdot a}\right)\right]\cdot\propto^2+\left[{i_0}^2+\frac{(D_0+a)}{D_2\cdot a^2}+\frac{h_0'}{d_0'}\left(\frac{i_0}{D_2\cdot a}-2\cdot i_0\right)\right]\cdot\propto+\left[\frac{h_0'}{d_0'}\left(\frac{D_0}{D_2\cdot a^2}+{i_0}^2\right)+\frac{1}{D_2\cdot a}\cdot\left(\frac{MAC\cdot Cm_0}{d_0'\cdot a}-i_0\right)\right]=0 \tag{6.29}$$

The alphas that satisfy this equation are mathematically possible equilibrium angles-of-attack, but actually, in most designs, only one AOA results in flight characteristics that comply with the basic design limits.

Although there are many methods to solve such equations, the expression is complex and the analytical investigation using such format is restricted. Therefore, some simplifications can be done to find a more suitable algebraic expression. As it is expected that the absolute values of AOA are low, the cubic term can be automatically dismissed. In this way a quadratic equation is obtained and a deeper analytical investigation can be done.

In addition, based in a dedicate statistical investigation using appropriate range of values for the variables involved in equation 6.29, it is still possible to apply some further simplifications finding a simpler relation defining the equilibrium AOA:

$$\frac{h_0'}{d_0'}(D_2\cdot a-1)\cdot{\propto_{eq}}^2+\propto_{eq}+\left(\frac{h_0'}{d_0'}\cdot\frac{D_0}{a}+\frac{MAC\cdot Cm_0}{d_0'\cdot a}-i_0\right)=0 \tag{6.30}$$

By solving the quadratic equation, it can be found the equilibrium angle of attack:

$$\propto_{eq}\approx\frac{1\pm\sqrt{1+4\cdot\frac{h_0'}{d_0'}(1-D_2\cdot a)\cdot\left(\frac{h_0'}{d_0'}\cdot\frac{D_0}{a}+\frac{MAC\cdot Cm_0}{d_0'\cdot a}-i_0\right)}}{2\cdot\frac{h_0'}{d_0'}(1-D_2\cdot a)} \tag{6.31}$$

It can be shown that the expression above presents results sufficiently accurate to allow initial evaluations and conceptual design dimensioning. It is possible to show that for conventional designs the error resulting from this expression is less than 2 degrees. In this way, equation 6.31 provides a useful approximation of the equilibrium AOA for a specific set of design parameters. It

can be seen that the equilibrium AOA do not depend on CG drag or wing-load, being basically a function of wing's aerodynamic proprieties and the CG position.

This expression is equally valid for any CG position, which means, in front of or behind the wing's aerodynamic center. Equation (6.31) shows that for high absolute values of CG position reference ratios there is a limiting AOA given by:

$$\propto_{lim} \approx \sqrt{\frac{D_0/a}{(1 - D_2 \cdot a)}} \tag{6.32}$$

Figure 6.10 below plots the above equation for a range of CG positions reference ratios, comprehending both aft and forward CG:

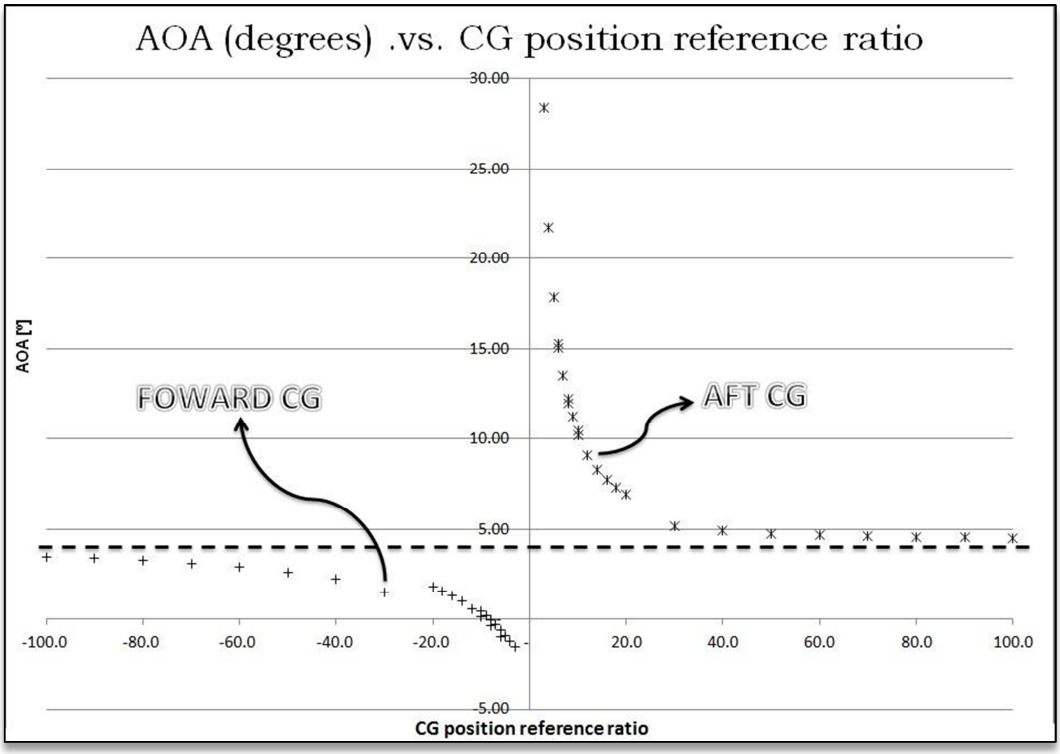

Figure 6.10 – Equilibrium AOA variation with CG position reference ratio

As can be seen on the graphic above, for both forward and aft center of gravity positions, there are limiting CG position reference ratios defined by restrictions on the angles of attack. Aft CG with low position ratios would lead to an AOA near to the stall, and forward CG, with low position ratios (in absolute value) would lead to negatives AOA.

In this way, there is a range of acceptable CG position reference ratios limited at one side by the stall and at the other side by the collapse. Notice that, comparing the two situations on figure 6.10, frontal CG positions demands greater CG heights. Also, the before mentioned tendency to an AOA limit can be visualized in both extremity of the horizontal axis, which means that over a certain CG height the AOA variation is pretty low, and for a sufficiently high CG the AOA limit will be the same regardless of the horizontal positioning.

Finally, taking in account the discussion, a CG positioning envelope can be drawn to illustrate how the selection of CG position will affect the equilibrium AOA:

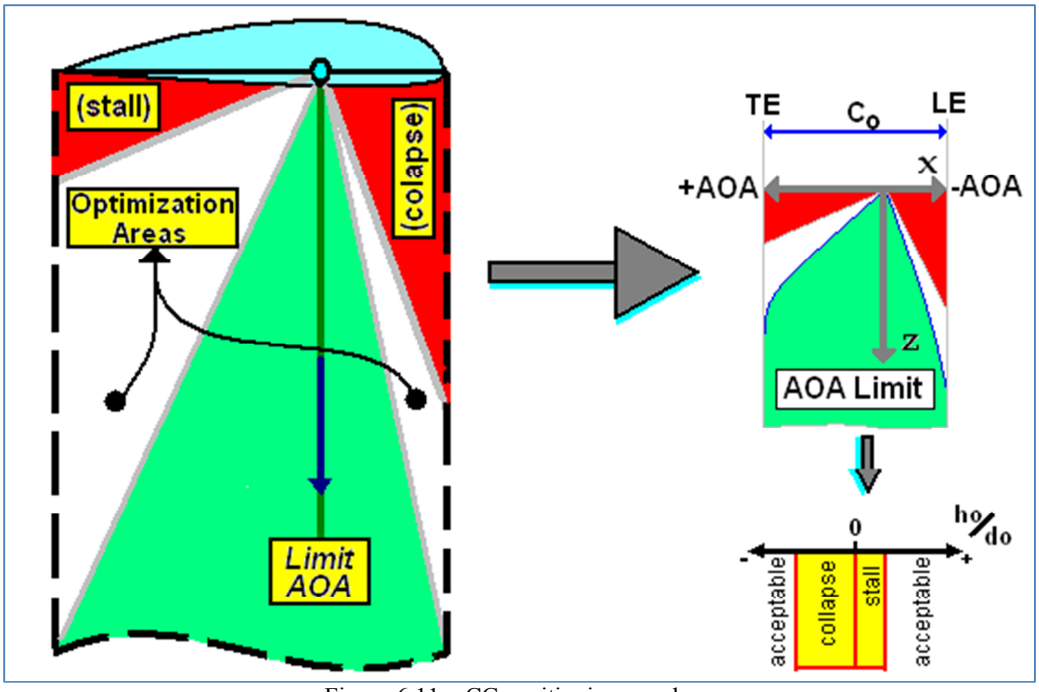

Figure 6.11 – CG positioning envelope

The CG positioning envelope shows that any location between the stall region and the collapse region is acceptable. It also illustrates how the AOA varies with CG position.

For aft CG, as more the CG moves aft and up, more the AOA increases. By varying the CG in the opposite directions, which means forward and down, up to the aerodynamic center line, a limiting low AOA is reached.

In the cases where the CG is in front of the AC, if the CG moves forward and up, the AOA may become negative. By varying the CG in the opposite directions, which means aft and down, up to the aerodynamic center line, the previously mentioned AOA limit is reached.

It is also made clear the existence of a certain CG height above which no changes on AOA is perceptible by moving the CG horizontally. This critical point can be calculated as:

$$h'_{0_{lim}} = \left.\frac{h'_0}{d'_0}\right|_{min} \cdot C_0 \tag{6.33}$$

Where, $\left.\frac{h'_0}{d'_0}\right|_{min}$ is given by the maximum point, considering absolute values, above which no variation in AOA is perceptible.

The analysis held up to here only considers AOA effects, however, the equilibrium AOA will define the other flight parameters as discussed before. In this way, the effect of CG positioning in general flight characteristics can be evaluated as shown in figure 6.12 below:

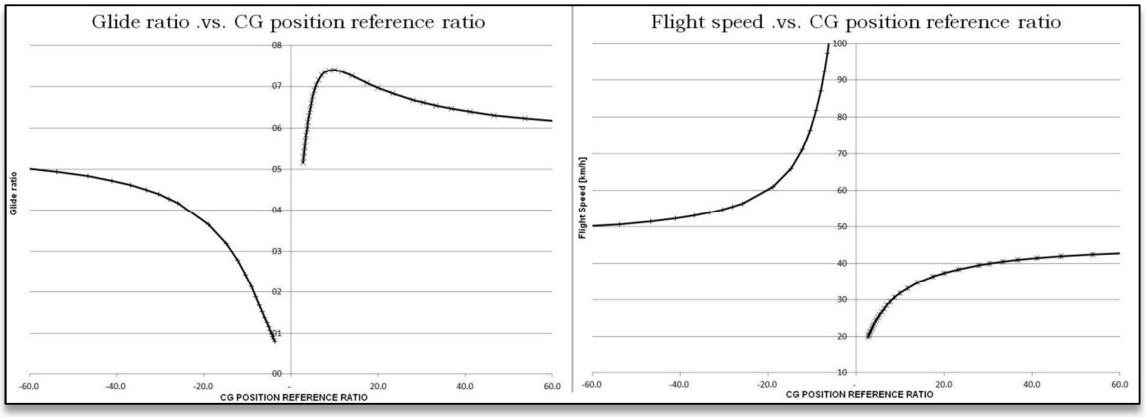

Figure 6.12 – Flight parameters variation with CG position - considering aft and forward CG

It can be concluded that after reaching a certain CG position reference ratio, no significant variation in flight parameters is observed with further increase in CG height. This is coherent with the existence of an AOA limit as demonstrated before.

It can also be noticed that for frontal CG positions the flight speeds are pretty high and the performance parameters become degraded. Because of that, it is a reasonable decision to analyze closer the situations of aft CG, which will allow more efficient design parameters management.

Figure 6.13 below shows how the equilibrium AOA varies with CG position reference ratio for common aft CG positions:

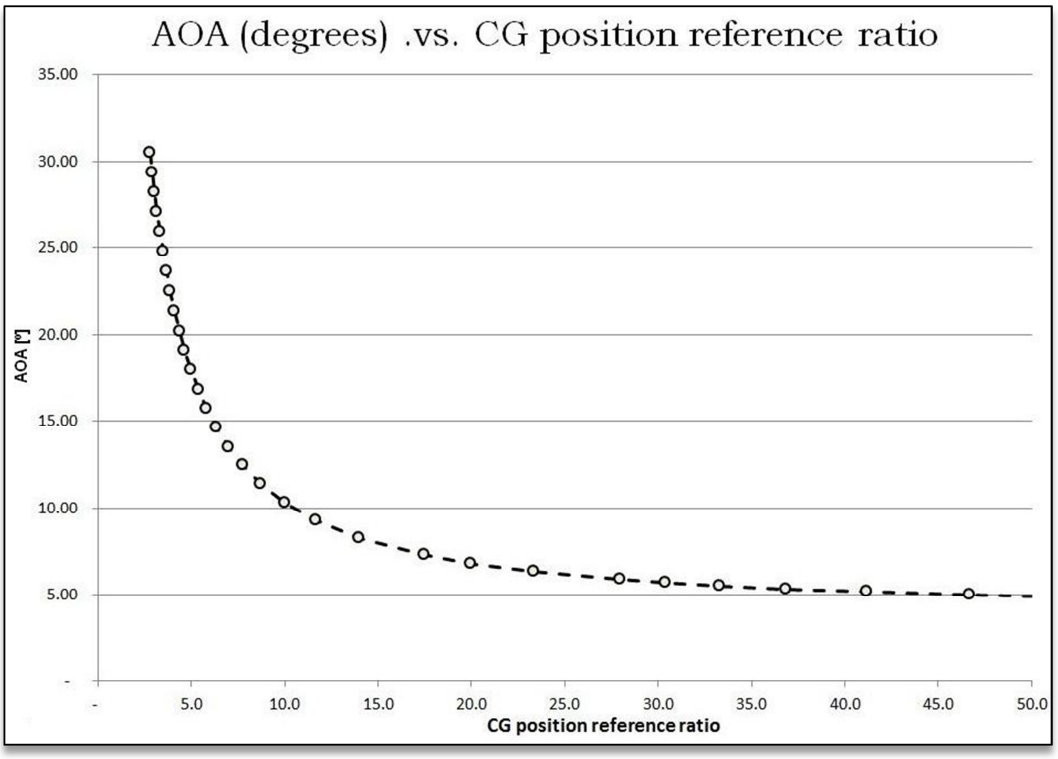

Figure 6.13 – Variation of equilibrium AOA with CG position reference ratio

It can be noticed that for aft CG position there is a good range of variation to be used as an AOA adjustment tool. Slight variations in the equilibrium AOA can result representative variations in the overall flight characteristics, therefore, the ability to specify a good CG position, can improve performance, stability and controllability.

Some other design parameters may affect the curve shown in figure 6.13, however, as shown in figure 6.14 below, the overall behavior is maintained. Notice that a increase in lift-curve slope, induced drag or zero-lift angle (in absolute value) leads to a high AOA for a same CG position reference ratio.

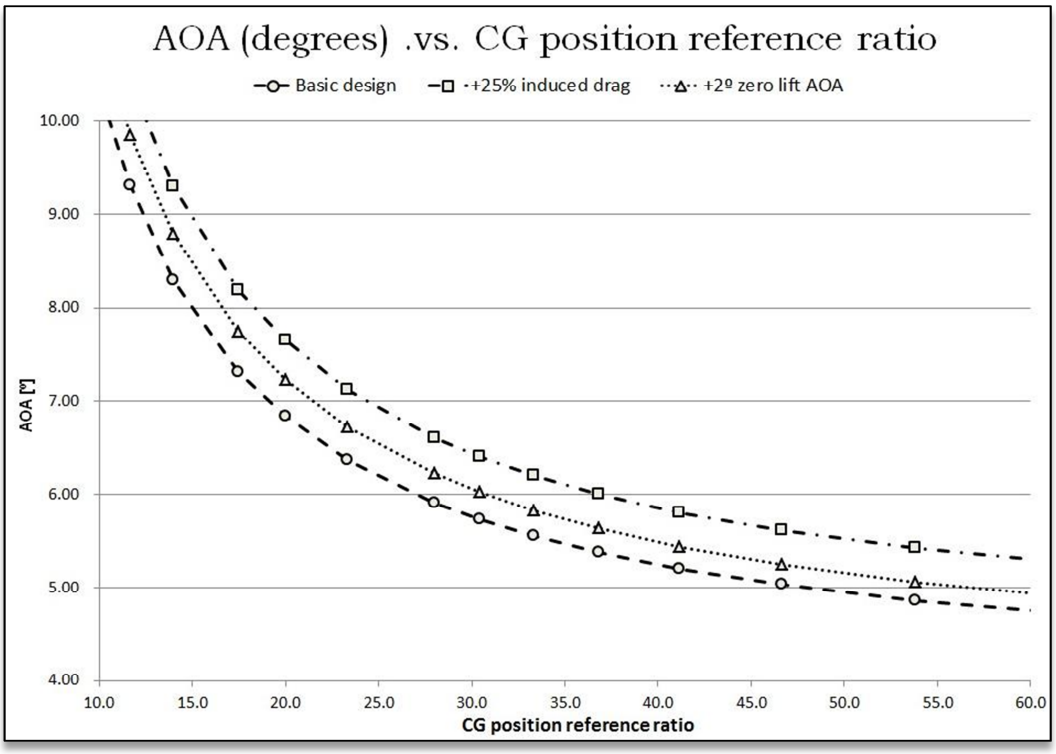

Figure 6.14 – Variation of AOA with CG position for different aerodynamics proprieties

Finally, figure 6.15 below illustrates generically the discussed variation of AOA with CG positioning for aft CG positions:

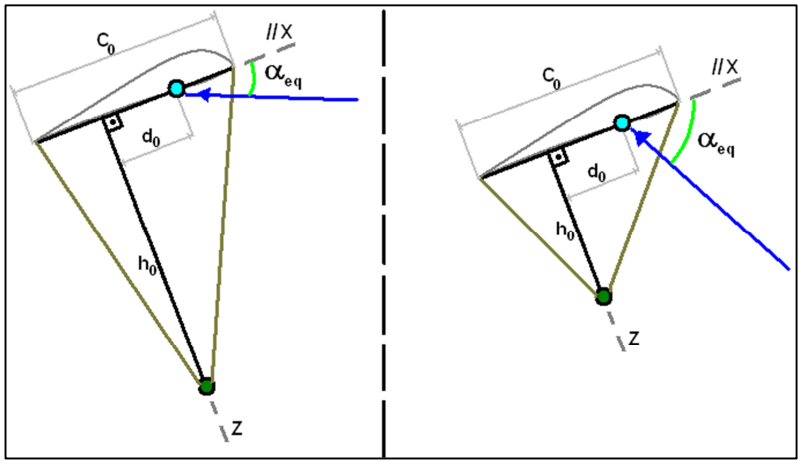

Figure 6.15 – Different equilibrium conditions of a same wing

Observing the illustration above, and taking in account that the expected variation in flight path (see glide ratio variations with AOA graph) is much smaller then possible variations in equilibrium AOA, the CG position will indirectly define the attitude angle. In this way, a high CG will lead to low attitude angles and vice-versa. This observation is relevant for human factors,

because pilot´s feel more comfortable flying with the wing aligned to the horizon. In this way it is desirable to maintain low attitudes.

6.3. Conceptual design Performance Optimization

As discussed in section 6.1.4 and illustrated in figure 6.7 the performance indicative parameters varies differently with the AOA. It is notable that over a relatively small AOA the sink rate do not varies in a relevant amount, but the glide ratio still changes considerably. Therefore, considering any performance purposes, a good approach for design definitions is to look for the best glide ratio optimization point. For most common wings the lost in endurance performance is not relevant and the gain in glide capability is far way preferable.

Following the above considerations, a performance optimization can be done by adjusting the design parameters around the "Glide-optimized condition". For a defined wing geometry, this condition is a specific CG position reference ratio which results the AOA for best glide.

The management of the design variables to improve performance is a complex iterative process that can be done better by knowing how the design variables affect the flight characteristics. In the following sections an analysis of such variations will be presented and also a flowchart for conceptual design performance evaluations.

6.3.1. The Center of gravity position optimization

As shown in equation (6.31), the CG position defines the equilibrium AOA and then the performance parameters. It must be noticed that this relation is affected by the wing area and wing-load as shown in figure 6.17 below:

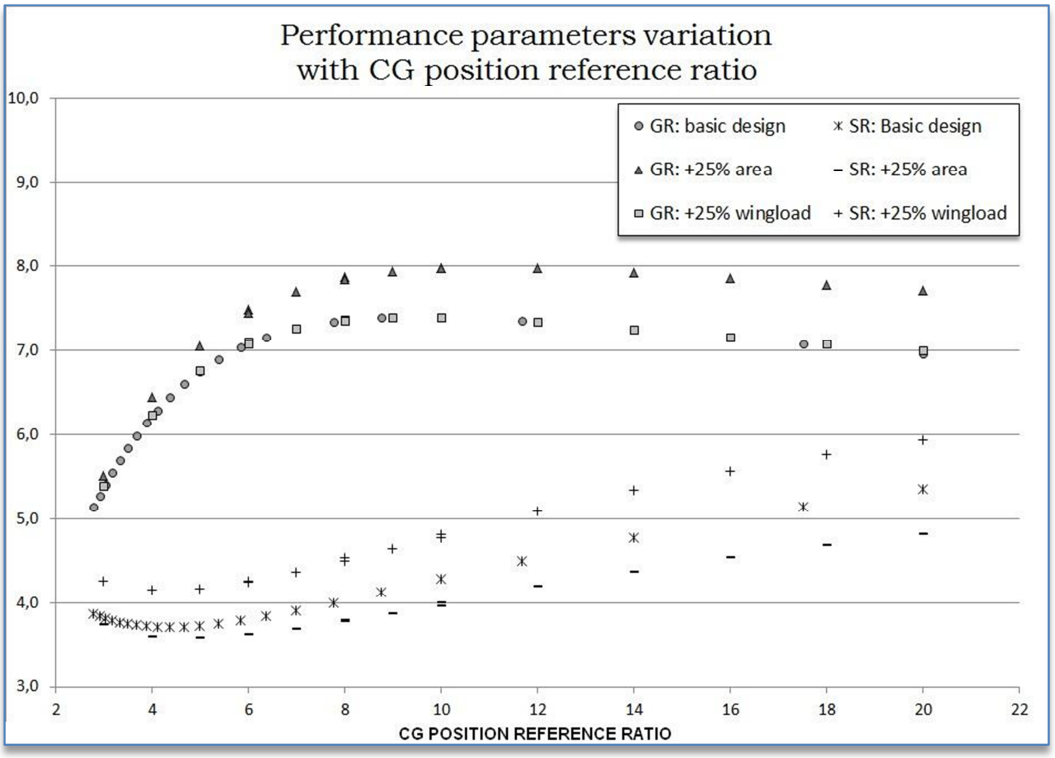

Figure 6.16 – Performance parameters variation

It can be seen that both wing area and wing-load variation causes a displacement of the basic-design curves. However it is also noticeable that the overall behavior remains unchanged. The main conclusion from this figure is that, besides CG position management optimization, the redefinition of wing area and wing-load can be a useful tool for changing the performance parameters level.

Also the performance index will change with the basic design parameters, however, those index are mainly useful for evaluation of a defined design and its use for comparisons are not indicated. Figures 6.17 and 6.18 below show the performance index variation with CG position:

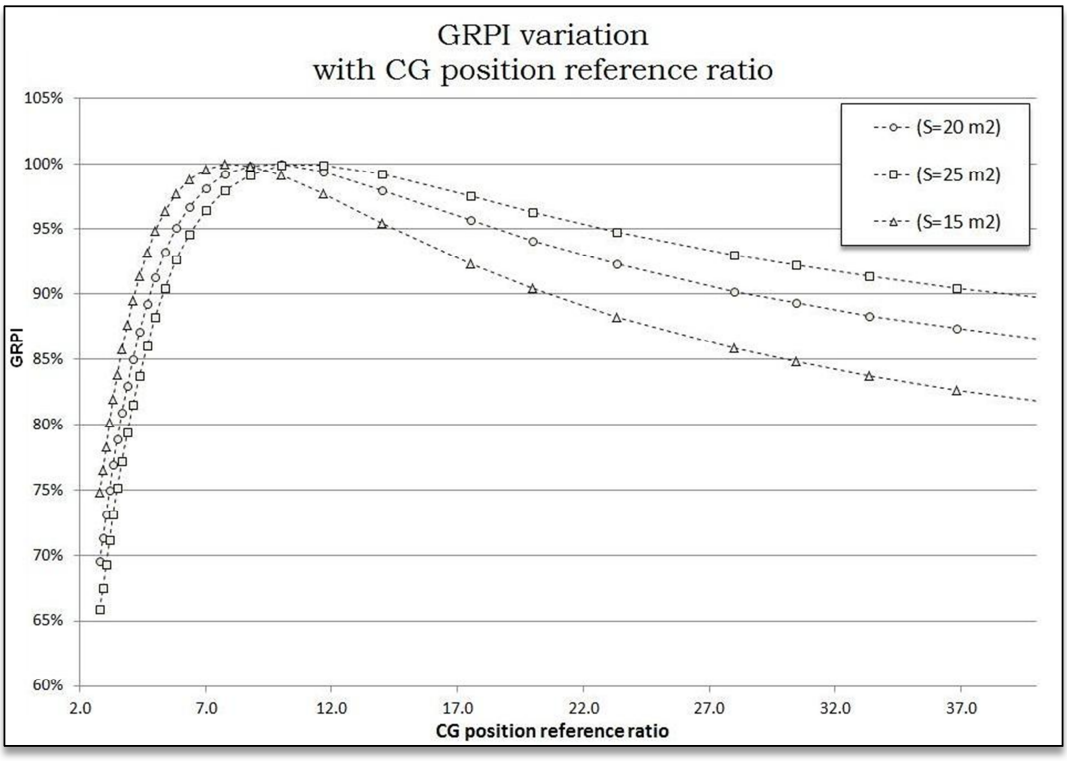

Figure 6.17 – GRPI variation with CG position

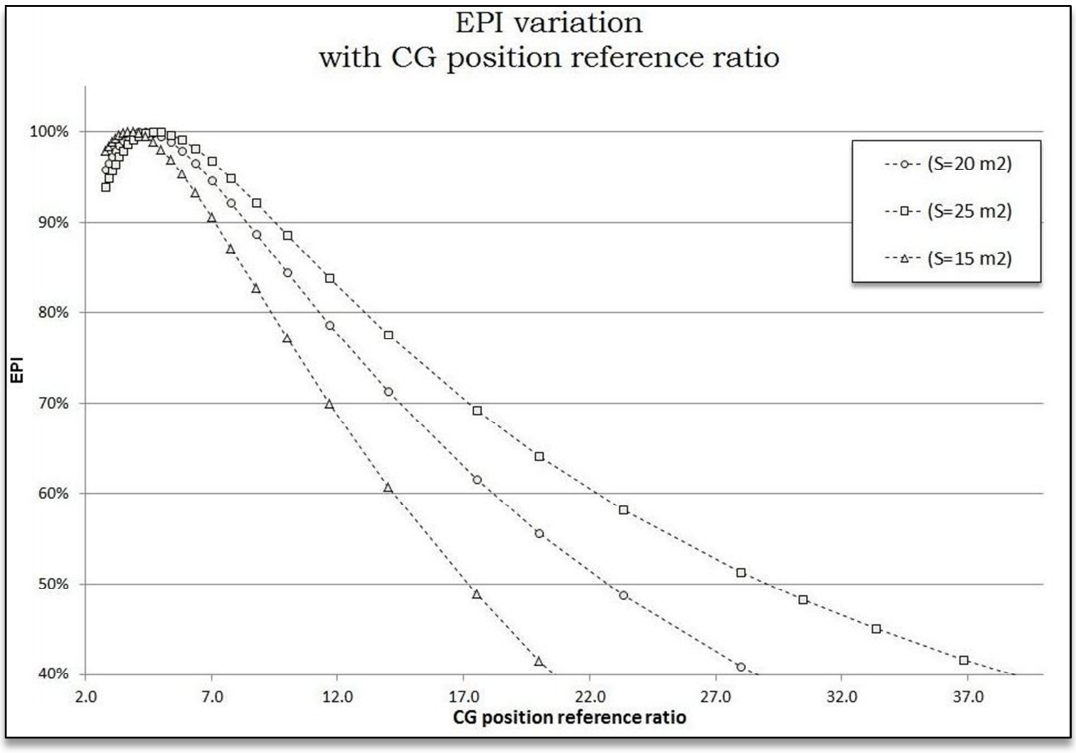

Figure 6.18 – EPI variation with CG position

It can be seen that over a specific minimum CG position reference ratio, for normal wing proprieties, the GRPI variation becomes slow. On the other hand, as the CG position ratio increases the EPI decreases considerably. These are obvious results; however, it is interesting to notice that there is a defined region where both GRPI and EPI are relatively high and this is the "optimization range". Therefore, the CG positioning must be managed respecting these proportions.

Another important evaluation is to visualize how the steady flight parameters vary with the CG position ratio. Figure 6.19 below shows the variation of flight speed and glide path with CG position reference ratio:

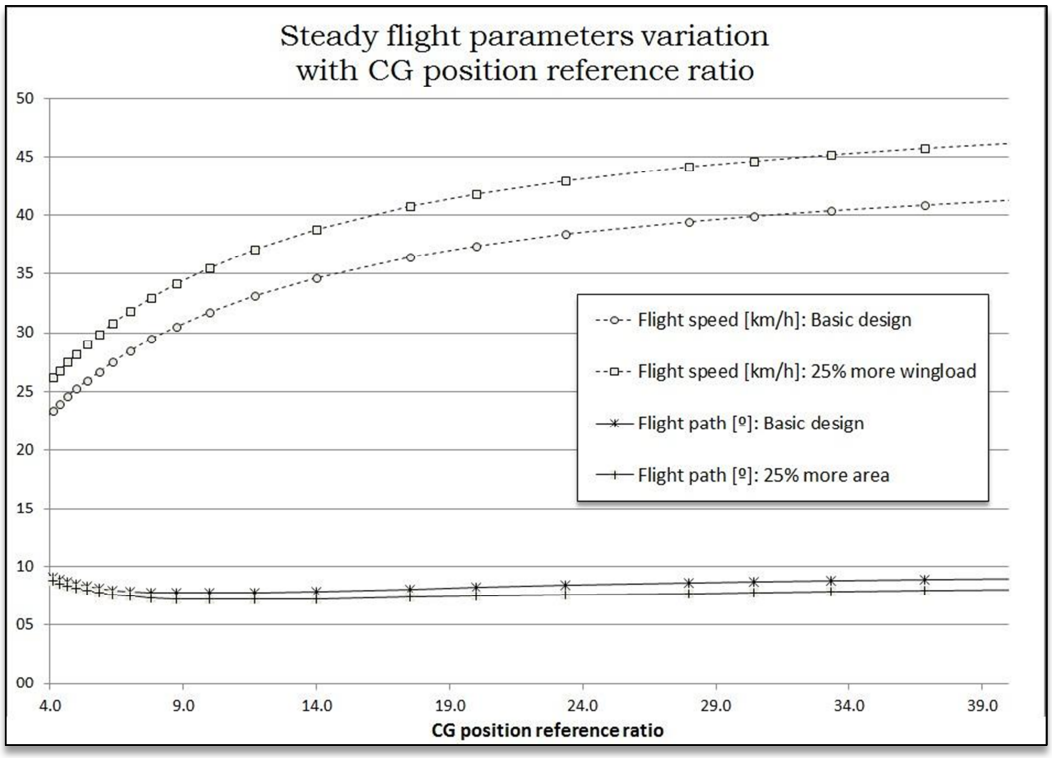

Figure 6.19 – Flight Parameters variation with CG position

Notice that, above a certain CG position, the flight path and then the glide ratio is not relevantly affected anymore. On the other hand, the flight speed keeps increasing. In this way it is possible to conclude that there is a speed limit for low–forward CG positions. For aft-high CG positions many other limits exists as: performance minimums, stall, structural stability and maneuverability. Figure 6.20 below shows another useful visualization of flight parameters.

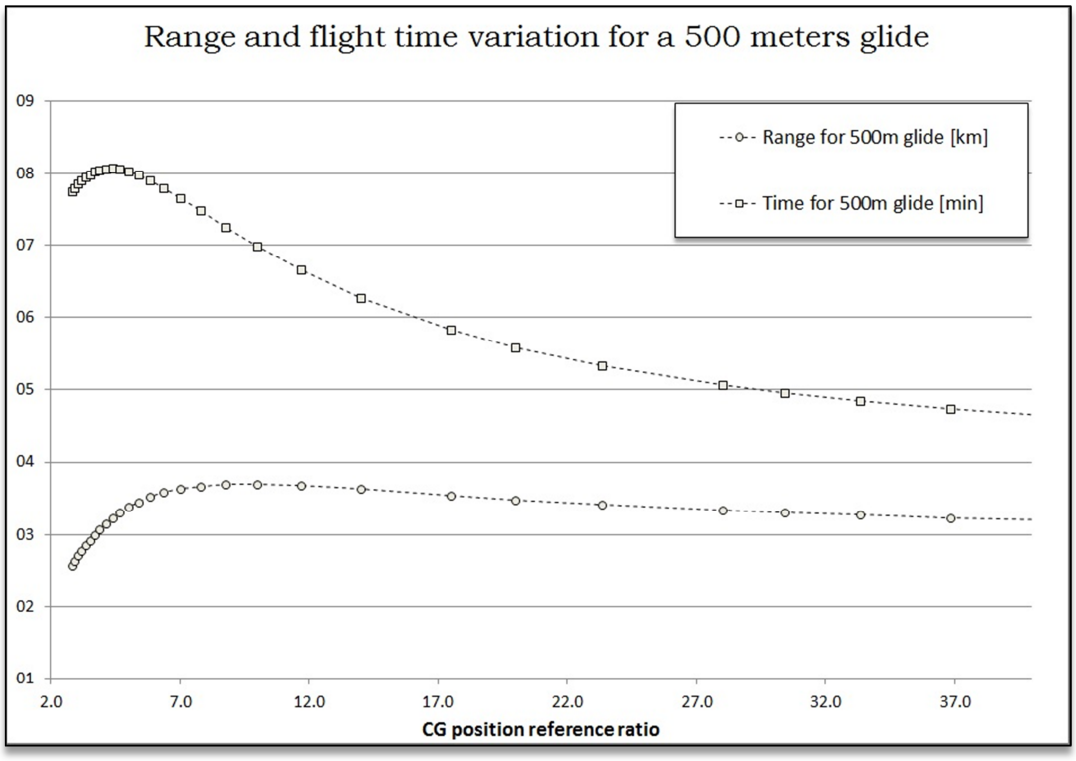

Figure 6.20 – 500m glide parameters variation with CG position

The above illustration shows the flight range and flight time supposing a steady glide from a takeoff-base with 500m height. There are no new conclusions here, however, in this graphic it can be seen that the flight time variation is not really representative, especially if we consider that the improvement of glide ratio increases thermal-hunting efficiency what will indirectly improves flight time.

Finally, as initially proposed, the CG position can be adjusted to reach the maximum glide ratio by applying the AOA for optimum glide into the CG position equation. In this way, it can be found the CG position reference ratio that optimizes the glide performance for a defined set of aerodynamic proprieties:

$$\left.\frac{h_0'}{d_0'}\right|_{opt.GR} = \frac{{\propto_{opt.GR}}^3 + -2 \cdot i_0 \cdot {\propto_{opt.GR}}^2 + \left({i_0}^2 + \frac{(D_0 + a)}{D_2 \cdot a^2}\right) \cdot \propto_{opt.GR} + \frac{1}{D_2 \cdot a} \cdot \left(\frac{MAC \cdot Cm_0}{d_0' \cdot a} - i_0\right)}{-\left[\left(1 - \frac{1}{D_2 \cdot a}\right) \cdot {\propto_{opt.GR}}^2 + \left(\frac{i_0}{D_2 \cdot a} - 2 \cdot i_0\right) \cdot \propto_{opt.GR} + \left(\frac{D_0}{D_2 \cdot a^2} + {i_0}^2\right)\right]} \tag{6.34}$$

An important observation is that the above equation does not include the wing-load, thus, weight variations do not change the optimization point, affecting only the flight speed.

6.3.2. General basic proprieties optimization

As discussed above, the CG positioning is useful for optimizing a model using a defined wing. A question that remains uncovered is how to optimize the other design parameters. Actually, this answer is quite complex and there are no mathematical formulation to easily represent these relations.

Some developments exist in this field presenting some strategies for performance improvement, mostly based in increasing wing stiffness and improving aerodynamic proprieties (Babinsky, 1999; Pagen, 2001). The most relevant approaches are constructive modifications as: Increasing the number of cells, introduction of stiffeners and ribs, and material selection. However, no mathematical relations allowing a prediction of the level of improvement are available to be used in conceptual design evaluations.

Therefore, following the developments presented in this chapter, a variation analysis can be done in other to investigate the influences of each relevant design parameters in the steady flight characteristics. Below it is presented some charts showing the most relevant influences of design variables in performance and equilibrated flight parameters considering the CG position optimized for maximum glide ratio:

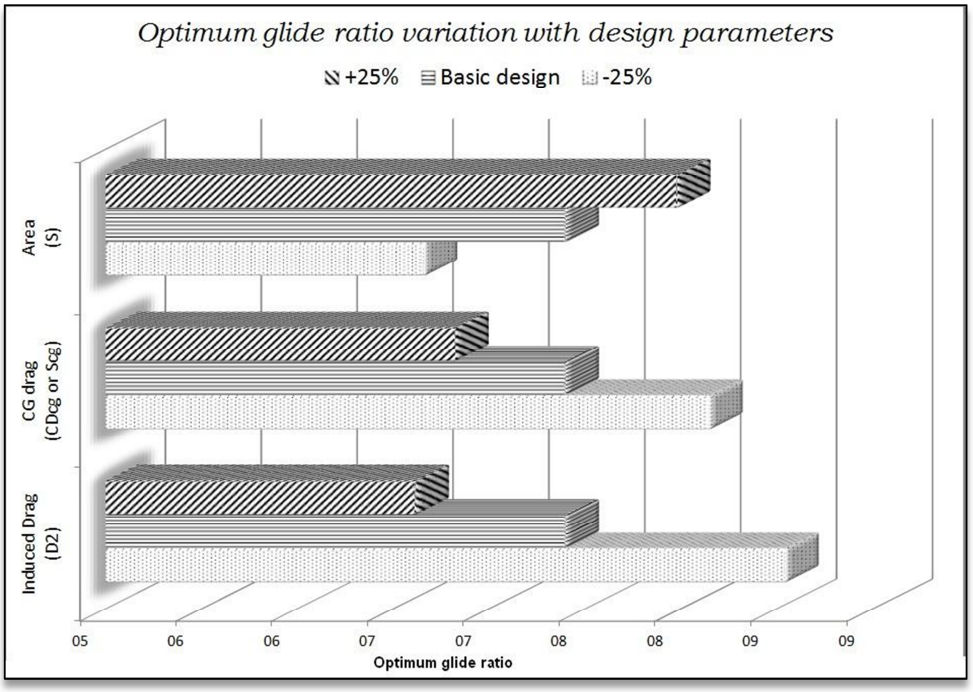

Figure 6.21 – Optimum glide ratio variation with design parameters

Figure 6.21 shows that the maximum achievable glide ratio increases with wing area and decreases with both wing's induced drag and CG drag, in comparable proportions.

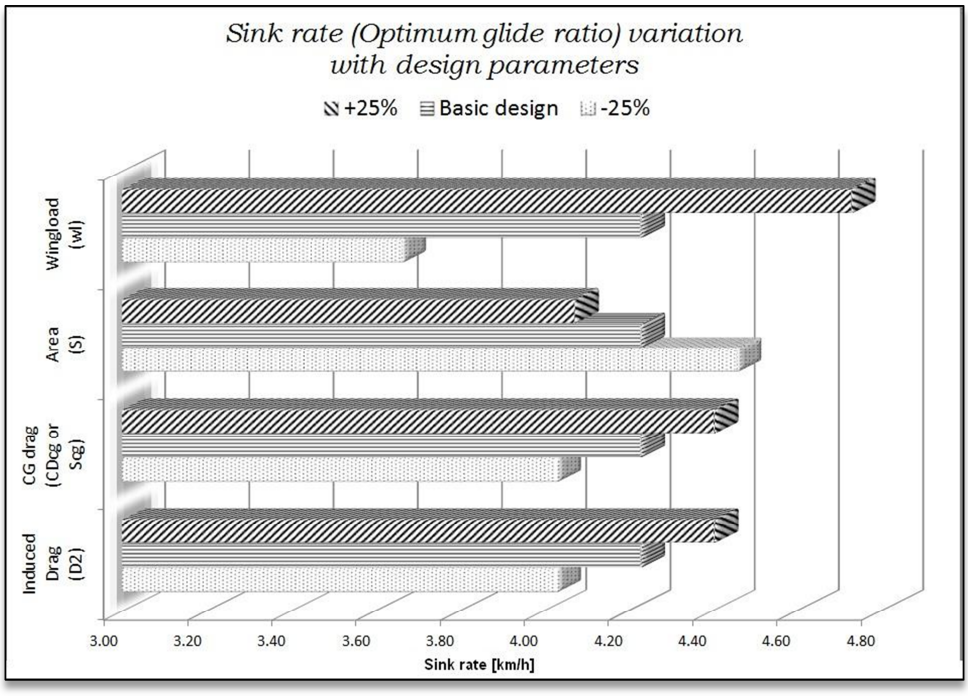

Figure 6.22 – Sink rate (glide optimized condition) variation with design parameters

Figure 6.22 shows that the sink rate for the glide-optimized condition varies specially with the wing-load, drag and reference area. This is expected once vertical speed is a component of the total speed, which is completely related to wing-load, and this component depends mostly on the path angle, which is affected by drag coefficients and reference area.

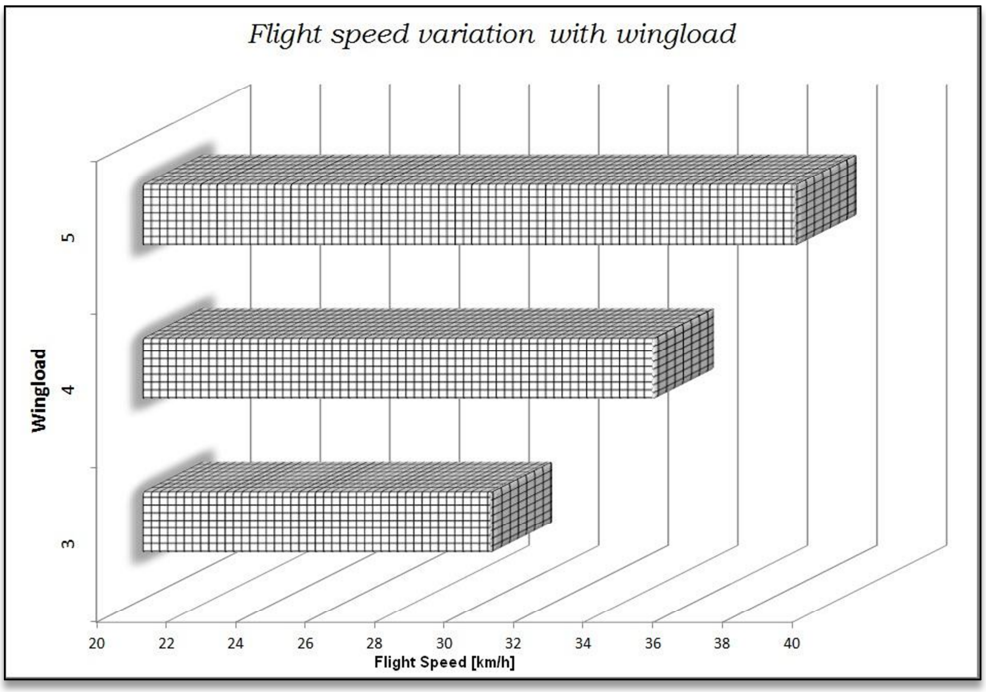

Figure 6.23 – Steady flight speed variation with design parameters

Figure 6.23 shows how wingload affects flight speed. This influence is normally more representative considering the range of variation of wing area or system's weight compared to expected variations in the lift-AOA curve slope.

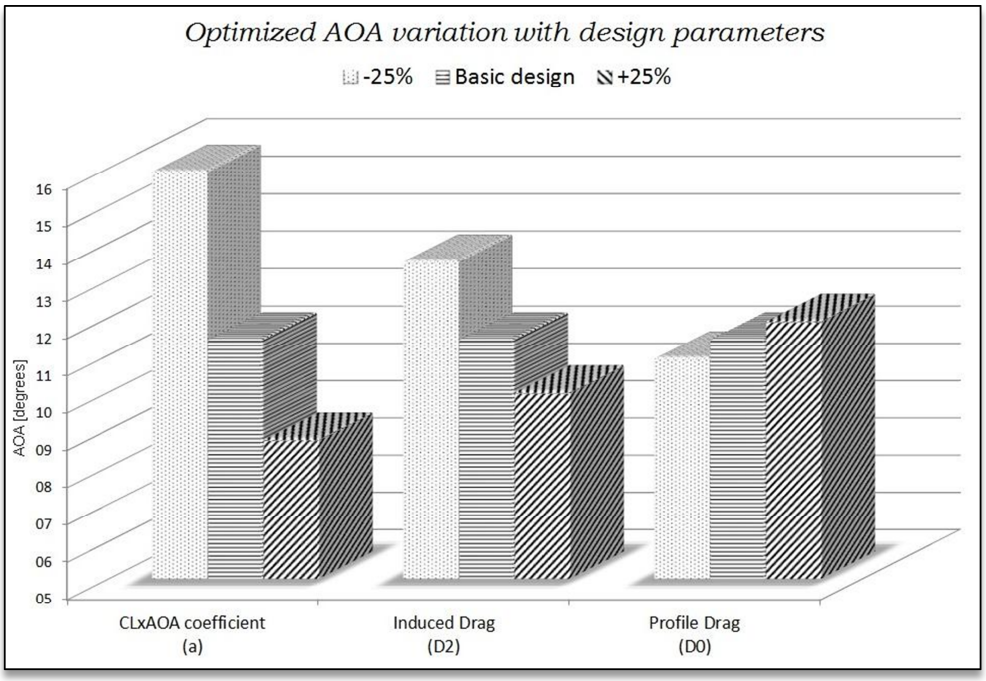

Figure 6.24 – Equilibrium AOA variation with design parameters

Figure 6.24 shows that the optimized AOA varies with aerodynamics coefficients but, specially, with the lift-curve slope. Another observation is that the AOA decreases with an increase in the induced drag term, this behavior is not obvious but can be comprehended if we consider that the representativeness of the induced drag is directly linked to the required lift coefficient.

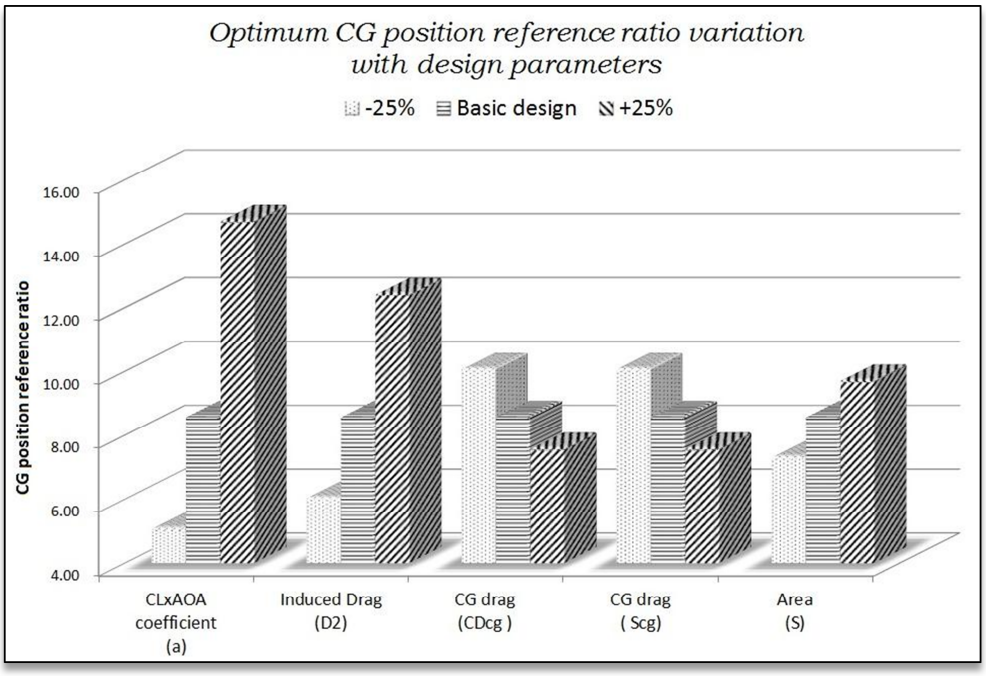

Figure 6.25 – Optimum CG position reference ratio variation with design parameters

Figure 6.25 shows that the optimum CG position present the opposite variations of the AOA with an additional light influence of the profile drag. Notice that, coherently, the variation is strongly influenced by the CL-Alpha curve slope and the induced drag.

Finally, considering all the graphics above, for a glide-optimized model the performance can be still improved by managing aerodynamic coefficients, reference area and wing-load. The aerodynamic proprieties are usually adjusted through an adaptation of wing geometry and airfoil selection. Airfoils present some variability of proprieties restricted to a plausible range of values. Also, as paragliders are normally designed for a specific weight range, the wing-load is direct linked to the definition of the wing area. In this way, by adjusting the wing geometry it is adjusted the aspect ratio, the reference area, and consequently, the CL-Alpha curve slope, the induced drag and the wing-load.

Based on the discussion until here, it can be concluded that: a good wing for performance purposes presents high values of reference area and aspect ratio, and uses high-efficiency airfoils.

6.3.3. Conceptual design Performance Refinements Strategy

Paraglider design involves the understanding of many aspects of flight including the performance parameters. However, as shown throughout this chapter, the many involved variables have different effects on different flight characteristics. Based on this situation, an iterative approach is usually necessary in order to design an efficient model.

A useful approach for performance improvements and analysis is shown below in a flowchart generated using the concepts and mathematical relations introduced:

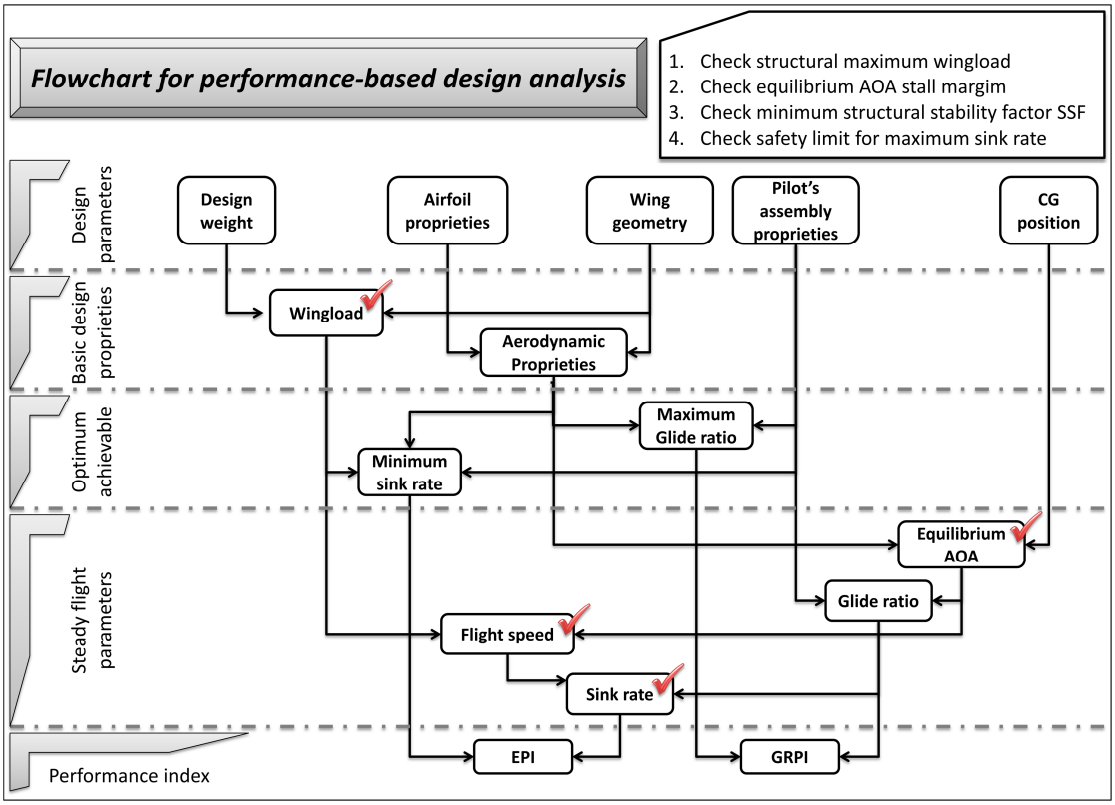

Figure 6.26 – Flowchart for performance-based design analysis

The figure above shows in a pictorial format how it become defined the flight parameters. The evaluation procedure can be described as follows:

- Define basic design parameters and limitations as structural load constraints, constructive constraints, AOA safety margin, vertical speed safety limit, structural stability constraints.
- Define model performance targets as an acceptable range of glide ratio and flight speed.
- Design the wing attempting for the relations presented in previous section

- Calculate wing-load and aerodynamic proprieties. Then, check for structural load constraints, and if the characteristics do not comply with the limits, review the basic design.
- Estimate CG area and drag using experimental data or theoretical modeling.
- Calculate maximum glide ratio and minimum sink rate and check for initial performance targets values, if the characteristics do not comply with the minimum established, review the basic design.
- Define CG position reference ratio. At the first interaction is useful to chose the optimized CG position by using equation (6.34)
- Calculate steady flight parameters, performance parameters and check for AOA margins, speed limits and performance objectives. If the characteristics are not suitable, review the CG positioning.
- Calculate the performance index. If these indicators are relevantly low, probably a better management of design variables is possible.

Using this proposition for table 6-1 initial values, the values on table 6-2 can be found:

Table 6-2: Performance parameters for a specific model

Paraglider's basic proprieties				
Geometric proprieties ->	Reference area = 20m^2		Wing-load = 4Kg/m^2	
Wing's Aerodynamic proprieties ->	l_0=-2°	a=3.6 rad^{-1}	D_0=0.017	Cm_0=-0.009
CG's proprieties ->	S-cg = 1m^2		CD-cg = 0.8	
Maximum performance ->	Glide ratio = 7.4		Sink rate = 3.7 Km/h	
Optimized CG position ->	CG position (ho/do) = 10.0			
Equilibrated flight parameters ->	AOA=10.2°	V=32Km/h	GR=7.4	SR=4.3Km/h
Performance index ->	GRPI=100%		EPI=84%	

In this case it was possible to apply the optimized CG position and reach the best glide ratio; however, it could be impossible due to other limitations. It must be remembered that until this point no stability or maneuverability characteristics are being evaluated. Therefore, it means that further limitations could appear from such analysis.

Another necessary observation is that only the CG position reference ratio is defined, and the complete definition of the CG positioning still depends on stability and controllability characteristics.

6.4 Final Comments:

In this chapter it was presented a dedicate analysis of the performance parameters applicable to paragliders using a simplified formulation of the steady flight condition. It was derived useful algebraic expressions relating performance parameters to design variables, and also defining some performance index.

With the formulation presented it was possible to identify how the different geometric features and aerodynamic proprieties may affect the performance, and then, allowing the development of a simple algorithm for conceptual design performance optimization.

7 PARAGLIDERS LONGITUDINAL STABILITY

One of the most important flight characteristics for paragliders is stability. A system is said to be stable if when slightly disturbed from a state of equilibrium, it tends to return and maintain this equilibrium estate. Particularly, the longitudinal stability represents paragliders capability to return to steady flight when submitted to a symmetrical small disturbance, and coherently, the lateral-directional stability represents paragliders capability to return to steady flight when submitted to a small asymmetrical disturbance. In this context, it is important to present some main concepts related to stability applied to paragliders before dealing with each specific kind of disturbances.

7.1 Stability Concepts Applied to Paragliders

The stability is, of course, directly related to safety because paragliders are constantly subjected to gusts, thermals and other atmospheric phenomenon which will disturb the steady glide. Because paragliders operate at low altitudes they are more susceptible to local atmospheric disturbances, which become more significant due to the low speed range of operation. The capability to recover from a disturbance is of first importance for paraglider handling qualities (Pagen, 2001). This capability is basically related to system natural response (open loop) and also related to system's controllability characteristics (closed loop).

Although there are relevant relations between stability and controllability, in most common aircrafts these two set of flight characteristics can be analyzed separately. As will be shown in chapter 9, the paraglider controllability aspects are related to how easily the pilot controls the aircraft, maintaining steady flight and also changing flight path and speed as desired. In this way, the controllability concept comprehends stability and maneuverability characteristics which commonly present opposite trends, it means, as more stable the paraglider less maneuverable it will be. Chapters 7 and 8 deal with paraglider stability (or system natural responses), that means, considering the pilot out of the loop. This system natural behavior analysis is of primary importance for controllability evaluations. It is notable that a paraglider can present an instable characteristic and still be controllable if this behavior is not hazardous and allows regain equilibrium with basic pilot's inputs. This trade-off between stability and maneuverability defines some paragliders categories rated by required pilot's skills (Deutscher Hängegleiterverband – 2009).

The classical concept of static and dynamic stability states that (Babister, 1980): the static stability is the tendency of a system to re-equilibrate when subjected to a small disturbance. This behavior is analyzed punctually around the equilibrium condition, not considering relevant changes on the dynamics components acting on the system. The dynamic stability is the capability of the system to return to the equilibrium condition after being disturbed. This last one is an analysis of system behavior responding to a disturbance, and clearly involves dynamic variations in forces and moments. It is simple to conclude that in order to be dynamically stable a system must be statically stable, however, static stability do not guarantee dynamic stability.

It can be shown that paragliders presents a natural static stability due to the pendulum nature of its movements, however, the dynamic stability of paragliders are deeply dependent on the design parameters and good characteristics are not always easy to be reached. Besides, due to the low speed range of operation and also due to the singular geometry, the classical types of motion studied in conventional aircraft stability theory may present some different characteristics and relevance for handling qualities analysis when applied to paragliders.

In this chapter the most relevant proprieties related to static and dynamic longitudinal stability are modeled as a function of the design parameters, and a comprehensive investigation about paraglider's response to longitudinal disturbances is developed identifying some useful design constraints and explaining some commonly observed in-flight characteristics.

7.2 Longitudinal Static Stability

The longitudinal static stability represents the paraglider tendency to return to steady flight when submitted to a symmetrical small disturbance. In this situation it is considered that the static forces and flight speed remains in equilibrium. For such scenario a small longitudinal disturbance can be treated as a variation in angle of attack. In this way, the stability condition demands that the pitch moments generated by this AOA variation be corrective, which means, try to restore the equilibrium AOA. The illustration in figure 7.1 represents paraglider in steady flight and the forces and moments involved.

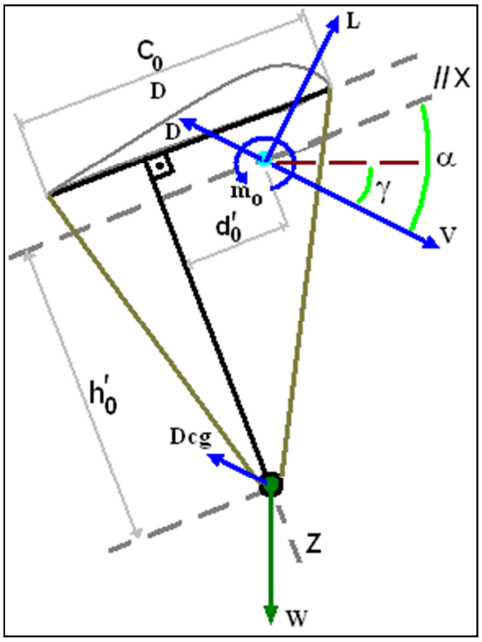

Figure 7.1 – Longitudinal Flight Parameters

To analyze the static stability conditions the equation representing the moment towards the pitch axis can be written as:

$$M_y = [L \cdot cos(\propto) + D \cdot sin(\propto)] \cdot d'_0 - [L \cdot sin(\propto) - D \cdot cos(\propto)] \cdot h'_0 + m_0 \tag{7.1}$$

Re-writing the equation in terms of aerodynamic coefficients, and considering angles of attack sufficiently small to allow the classical approximation, $tg(\propto) = sin(\propto) = \propto$ and $cos(\propto) = 1$ the expression above becomes:

$$\bar{Q} \cdot S \cdot MAC \cdot C_m = Q \cdot S \cdot \{[C_L + C_D \cdot \propto] \cdot d'_0 - [C_L \cdot \propto - C_D] \cdot h'_0 + MAC \cdot C_{m_0}\} \tag{7.2}$$

Then, it follows:

$$C_m = \frac{1}{MAC} \cdot \{[C_L + C_D \cdot \propto] \cdot d'_0 - [C_L \cdot \propto - C_D] \cdot h'_0 + MAC \cdot C_{m_0}\} \tag{7.3}$$

This coefficient is related to the pitch moment acting on the system for a particular flight condition. Consistent with the body coordinate axis definition (Etkin, 1995), if this moment

coefficient is positive the movement tendency is “pitch up”, and if it is negative the tendency is “pitch down”. Logically, in equilibrium this expression must result zero. It can be noticed that the pitch coefficient variation with AOA depends on some geometric proprieties, specially the CG position reference ratio. In this way, for a specific wing, the CG position will directly affect the moment coefficient variation with AOA, and so, the longitudinal stability proprieties.

Graph 7.2 illustrates the variation of pitch moment coefficient with angle of attack for a typical model considering different CG position reference ratios (h_0'/d_0'). Notice that, coherently, near to steady flight condition (Cm=0), if the angle of attack increases, a negative pitch moment is generated trying to restore equilibrium. However, it can be also observed a point of maximum on those curves, representing a practical static stability limit. Thus, for an AOA below this point the behavior will be inverted and the paraglider becomes instable.

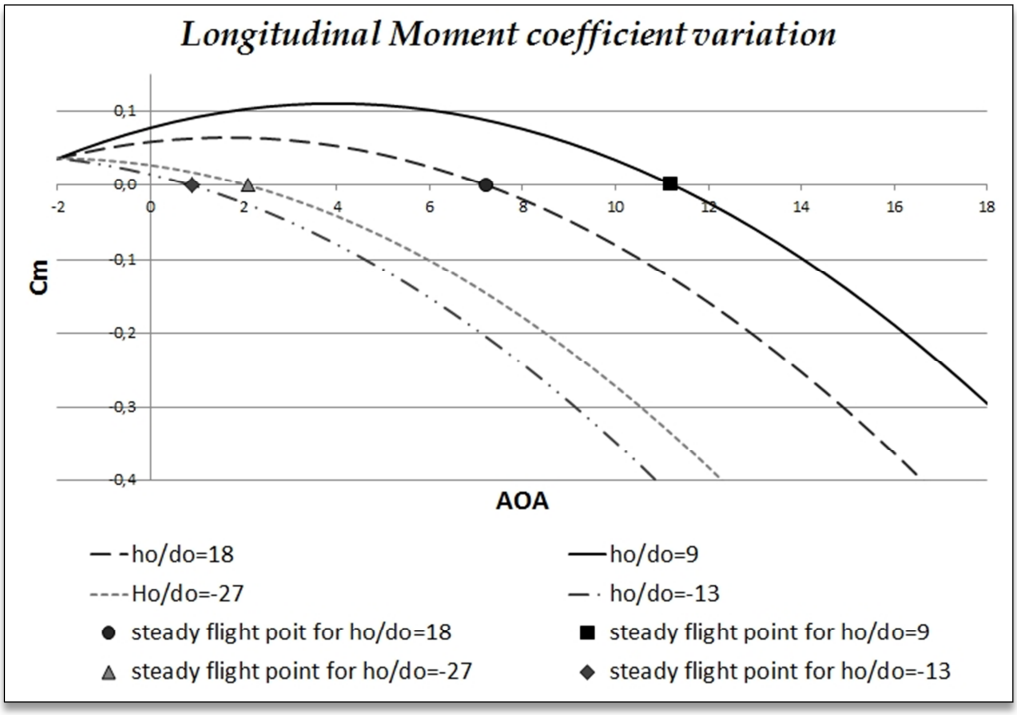

Figure 7.2 – Moment coefficient variation

The variation of the pitch moment coefficient with AOA can be mathematically expressed as:

$$\frac{dC_m}{d\propto} = \frac{1}{MAC} \cdot \left\{ \left[\frac{dC_L}{d\propto} + C_D + \frac{dC_D}{d\propto} \cdot \propto \right] \cdot d_0' - \left[C_L + \frac{dC_L}{d\propto} \cdot \propto - \frac{dC_D}{d\propto} \right] \cdot h_0' \right\} \tag{7.4}$$

Using the basic concept of static stability (Babister, 1980), the mathematical definition of the longitudinal static stability condition can be expressed as follows:

$$\frac{dC_m}{d\propto} < 0 \tag{7.5}$$

Using the expression above it yields:

For aft CG positions ($d'_0 > 0$):

$$\left[\frac{dC_L}{d\propto} + C_D + \frac{dC_D}{d\propto}\cdot\propto\right] - \left[C_L + \frac{dC_L}{d\propto}\cdot\propto - \frac{dC_D}{d\propto}\right]\cdot\frac{h'_0}{d'_0} < 0 \tag{7.6}$$

For forward CG positions ($d'_0 < 0$):

$$\left[\frac{dC_L}{d\propto} + C_D + \frac{dC_D}{d\propto}\cdot\propto\right] - \left[C_L + \frac{dC_L}{d\propto}\cdot\propto - \frac{dC_D}{d\propto}\right]\cdot\frac{h'_0}{d'_0} > 0 \tag{7.7}$$

and using the formulation proposed for the global aerodynamic coefficients in chapter 4, it can be written:

$$\begin{cases} D_2\cdot a\cdot\propto^2 - \left(D_2\cdot a\cdot i_0 + (1 - D_2\cdot a)\cdot\frac{h'_0}{d'_0}\right)\cdot\propto + \frac{1}{2}\cdot\left(1 + (1 - 2\cdot D_2\cdot a)\cdot\frac{h'_0}{d'_0}\cdot i_0\right) < 0 \quad (\forall\, d'_0 > 0) \\ D_2\cdot a\cdot\propto^2 - \left(D_2\cdot a\cdot i_0 + (1 - D_2\cdot a)\cdot\frac{h'_0}{d'_0}\right)\cdot\propto + \frac{1}{2}\cdot\left(1 + (1 - 2\cdot D_2\cdot a)\cdot\frac{h'_0}{d'_0}\cdot i_0\right) > 0 \quad (\forall\, d'_0 < 0) \end{cases} \tag{7.8;7. 9}$$

This is the equations that must be satisfied to achieve longitudinal static stability. Plotting this equation as shown in figure 7.3 it can be visualized the "level" of longitudinal static stability of a model. Notice that the stability condition states that the variation of pitch moment with AOA must be negative. Because of that, the point where the curves in illustration 7.3 cross the horizontal axis represents the limiting situation. By plotting in this same graph the points of steady flight it is possible to identify how far from the limiting situation a specific model operates. This "distance" in terms of AOA can be understood as a static stability margin.

This margin it is an important first clue to judge paraglider´s longitudinal stability characteristics. At first because common deviations in predictive design calculations and model

production may result practical deviations in the real equilibrium AOA, and care must be taken to assure that such variations will not leads to an unstable model. Also, notice that, as much narrow the distance between equilibrium AOA and critical AOA is, more easily the operational AOA will trespass the critical AOA during dynamic oscillations, what may result adverse behaviors.

On the graph presented in figure 7.3 it can be seen that the critical AOA are normally behind the equilibrium AOA. It means that the disturbances which could potentially generate longitudinal instability are those related to AOA diminishing: descendent currents, frontal gusts or sudden pitch down movements. However, frontal gusts necessary to result relevant AOA variations are normally too high, therefore, it can be concluded that the main sources of dangerous disturbances for longitudinal static stability are descendent gusts and sudden pilot's induced pitch down motions.

On the assessment above only the stability aspects were evaluated. However, the stall approximation plays a relevant part in longitudinal flight characteristics evaluation. Taking in account that any expressive "pitching up" disturbance caused by a tailwind, ascendant gust, or brake application may cause instantaneous AOA to reach high values. It is important to assure that the equilibrium AOA has sufficient margin from stall as well.

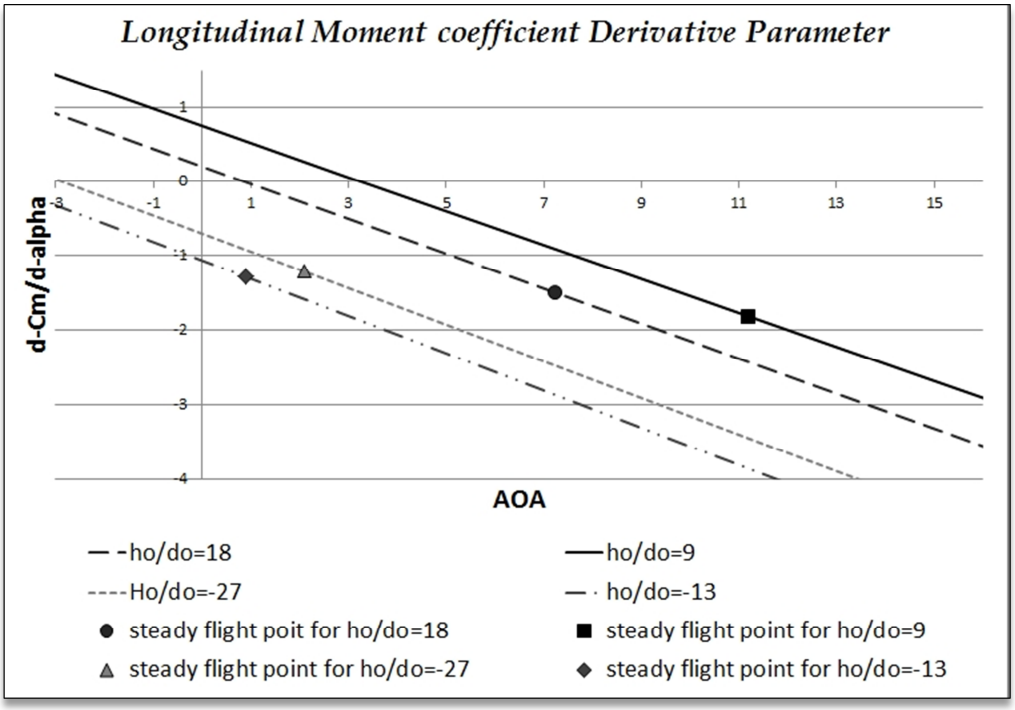

Figure 7.3 – Pitch moment coefficient derivative parameter

As corroborated by figure 7.3 above, it can be shown that for most possible paragliders models the pitch moment coefficient variation can be simplified as a linear expression as follows:

$$\begin{cases} -(1-D_2\cdot a)\cdot\dfrac{h_0^{'}}{d_0^{'}}\cdot\propto+\dfrac{1}{2}\cdot\left(1+(1-2\cdot D_2\cdot a)\cdot\dfrac{h_0^{'}}{d_0^{'}}\cdot i_0\right)<0 \quad (\forall\, d_0'>0) \\ -(1-D_2\cdot a)\cdot\dfrac{h_0^{'}}{d_0^{'}}\cdot\propto+\dfrac{1}{2}\cdot\left(1+(1-2\cdot D_2\cdot a)\cdot\dfrac{h_0^{'}}{d_0^{'}}\cdot i_0\right)>0 \quad (\forall\, d_0'<0) \end{cases} \tag{7.10}$$

the critical situation can then be expressed as:

$$\propto_c=\frac{1/_2}{(1-D_2\cdot a)\cdot\frac{h_0'}{d_0'}}+\frac{1}{2}\cdot\left(\frac{1-2\cdot D_2\cdot a}{1-D_2\cdot a}\right)\cdot i_0 \tag{7.11}$$

consequently, the "longitudinal static stability margin" can be defined as:

$$SM|_p=\propto_{eq}-\propto_c \tag{7.12}$$

The equilibrium angle of attack can be calculated solving equation (7.3) for Cm=0. This calculation is complex and an accurate result can be obtained following the procedures indicated in chapter 5. However, a very reasonable approximation can be used as proposed in chapter 6 in equation (6.31).

The longitudinal static stability margin, as explained above, gives an idea about how far from the critical situation is the equilibrium AOA. However, it is important to highlight that although an increased longitudinal margin diminishes paraglider's susceptibility to instability, it may increases stall proximity. Notice that this concept is not the same one used in classical aircraft theory (Babister, 1980), where the stability margin is related to CG position variation.

By working with an statistical evaluation using many different models it is possible to show that reaching a negative longitudinal static margin is quite improbable for common design parameters. Figure 7.4 below shows the static stability margin plotted for a range of CG positions reference ratio considering a typical paraglider.

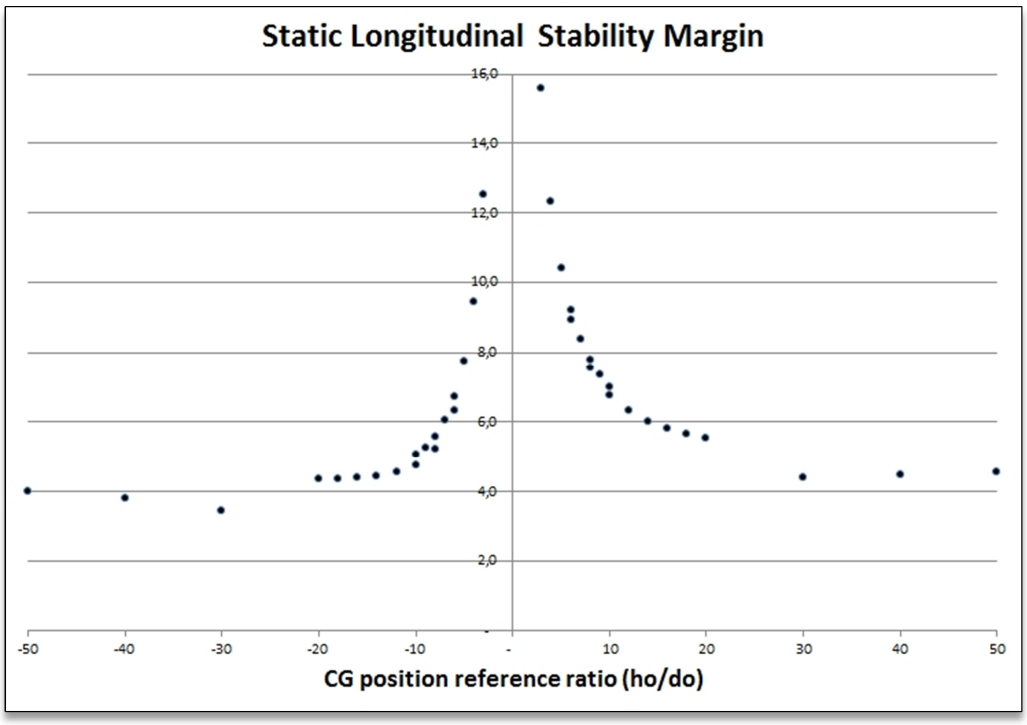

Figure 7.4 – Longitudinal static margin

Based on the above analysis, it is possible to conclude that expected positions of the CG will not generate longitudinal static instability. But it can considerably reduce the stability margin. Plotting the static margin variation with the CG position for a range of aerodynamics coefficients, it is possible to evaluate how the static stability is affected by the design parameters. This analysis is especially relevant inside the best range of optimization, which is often limited by aft CG positions, or positive CG position reference ratios.

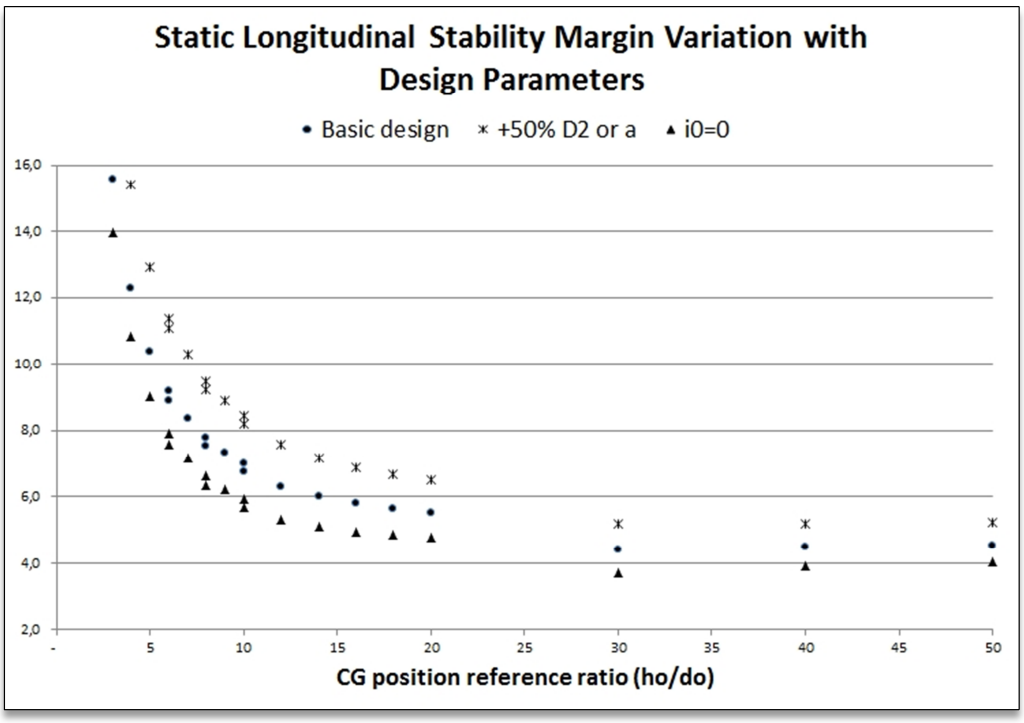

Figure 7.5 – Longitudinal static margin for aft CG positions

Observing figures 7.4 and 7.5, it is possible to see that the increase in induced drag increases stability margin. Also, it can be observed that above certain CG position reference ratio there is no significant changing in stability margin, however, low values of CG position reference ratio aggressively improves the margin. This last observation makes sense because the critical angle of attack for stability is normally a low AOA value, and low CG position reference ratios result higher equilibrium AOA providing a better margin.

7.3 Longitudinal Dynamic Stability

The longitudinal dynamic stability is characterized by the capability of the system to recover from a symmetrical disturbance. The longitudinal motion involves relevant changes in lift and drag forces, and because of that, its modeling is far more complex than static stability. When the paraglider starts to rotate in reaction to an initial disturbance, the dynamic components are heavily affected by the pitch rate, this effect is amplified by the fact that the CG is considerable distant from the AC. This propriety results in an interesting characteristic of paraglider's longitudinal response, where the classical short-period and long-period motions become unilaterally linked. As will be

shown, for paragliders, any short-period oscillation rapidly evolves to a long-period oscillation that can be considered the "dominant" vibration mode. Also, different from the static longitudinal stability proprieties analyzed previously, paragliders may present an undesirable dynamic behavior depending on the defined design parameters. In fact, as pointed out by Watanabe (2008) the low level of longitudinal damping in paragliders are known, and some attempts to overcome this characteristics has been made by designing moderns stability augmentation systems.

In practice, it can be observed that when submitted to a representative symmetric gust paragliders starts to vary attitude as a pendulum. Depending on the model's longitudinal stability characteristics, it may be able to recover itself restoring steady glide with just a couple of self-contained oscillations, or it may sustain an expressive oscillatory motion, which may also be divergent requiring active piloting to stop the oscillation before it reaches dangerous amplitudes.

The overall movement described above is mostly related to the long-period oscillatory mode, however, if the initial disturbance is a small variation in AOA, at the beginning of the movement, the short-period motion characteristics can be identified. The short-period oscillation can be noticed as a quick low-amplitude movement of the wing followed by a subsequent slower movement with increased amplitude. Actually, this slower subsequent movement corresponds to the manifestation of the long-period motion, which is rapidly induced. Therefore, it can be noticed that the short-period motion appears almost as a dead-bit oscillation, working basically as a transient to indirectly excite long-period oscillations.

Completing the practical observations, an especially dangerous and important characteristic that can be observed in real life is the pilot-induced-oscillation (PIO). This phenomenon occurs when the period of the wing's response is near to pilot's natural reaction time. In such situation pilot's inputs and wing's reactions can be resonant, then, pilots may increase the oscillation trying to end it.

The most precise approach to analyze longitudinal stability is working simultaneously with the tree equations of motion pertinent to the longitudinal plane (Yechout, 2003). Beneficiating from modern control theory (Ogata, 2003; Tewari, 2002) a complete analysis of longitudinal response will be proposed in section 7.3.1 below using the concepts of state-space variables.

7.3.1 Longitudinal motion – state-space assessment:

To obtain the longitudinal stability characteristic parameters the concepts of modern control theory can be applied using the previously derived equations of motion.
The equations of longitudinal motion are written as:

$$m \cdot \dot{U} = X_{RES} + m \cdot (R \cdot V - Q \cdot W) \tag{7.21}$$

$$m \cdot \dot{W} = Z_{RES} + m \cdot (Q \cdot U - P \cdot V) \tag{7.22}$$

$$I_y \cdot \dot{Q} = M_Y + (I_z - I_x) \cdot P \cdot R + I_{xz} \cdot (R^2 - P^2) \tag{7.23}$$

Using the concept of small disturbances it follows that:

$$U = U_{eq} + u \rightarrow \dot{U} = \dot{u} \tag{7.24}$$

$$W = W_{eq} + w \rightarrow \dot{W} = \dot{w} \tag{7.25}$$

$$\Theta = \Theta_{eq} + \theta \rightarrow \dot{\Theta} = \dot{\theta} \tag{7.26}$$

By using a linear approximation of the initial set of equations near to equilibrium, considering small disturbances and disregarding second order terms, it can be written:

$$m \cdot \dot{U} = \sum_{j=U}^{\delta_{Bl}} \frac{\partial F_{x_{RES}}}{\partial j} - m \cdot W_{eq} \cdot \dot{\theta} \tag{7.27}$$

$$m \cdot \dot{W} = \sum_{j=U}^{\delta_{Bl}} \frac{\partial F_{z_{RES}}}{\partial j} + m \cdot U_{eq} \cdot \dot{\theta} \tag{7.28}$$

$$I_y \cdot \dot{Q} = \sum_{j=U}^{\delta_{Bl}} \frac{\partial M_y}{\partial j} \tag{7.29}$$

Applying the simplified linear formulation for the system's forces and moments components as proposed in chapter 5, it yields:

$$\vec{R}_{RES} = \vec{R}_w + \vec{F}_{CG} \tag{7.30}$$

Where:

$$\begin{bmatrix} F_{x_{CG}} \\ F_{z_{CG}} \end{bmatrix} = \begin{bmatrix} F_{x_{CG_{eq}}} \\ F_{z_{CG_{eq}}} \end{bmatrix} + \begin{bmatrix} -\rho \cdot C_D \cdot S_{CG} \cdot U_{eq} & 0 & -m \cdot g \cdot cos(\Theta_{eq}) \\ 0 & -\rho \cdot C_D \cdot S_{CG} \cdot W_{eq} & -m \cdot g \cdot sen(\Theta_{eq}) \end{bmatrix} \cdot \begin{bmatrix} u \\ w \\ \theta \end{bmatrix}$$

$$\begin{bmatrix} F_{x_w} \\ F_{z_w} \\ M_{y_w} \end{bmatrix} = \begin{bmatrix} F_{x_{w_{eq}}} \\ F_{z_{w_{eq}}} \\ M_{y_{w_{eq}}} \end{bmatrix} + \begin{bmatrix} \frac{\partial F_{x_w}}{\partial U}|_{eq} & \frac{\partial F_{x_w}}{\partial W}|_{eq} & \frac{\partial F_{x_w}}{\partial Q}|_{eq} & \frac{\partial F_{x_w}}{\partial \delta_{B_r}}|_{eq} & \frac{\partial F_{x_w}}{\partial \delta_{B_l}}|_{eq} \\ \frac{\partial F_{z_w}}{\partial U}|_{eq} & \frac{\partial F_{z_w}}{\partial W}|_{eq} & \frac{\partial F_{z_w}}{\partial Q}|_{eq} & \frac{\partial F_{z_w}}{\partial \delta_{B_r}}|_{eq} & \frac{\partial F_{z_w}}{\partial \delta_{B_l}}|_{eq} \\ \frac{\partial M_{y_w}}{\partial U}|_{eq} & \frac{\partial M_{y_w}}{\partial W}|_{eq} & \frac{\partial M_{y_w}}{\partial Q}|_{eq} & \frac{\partial M_{y_w}}{\partial \delta_{B_r}}|_{eq} & \frac{\partial M_{y_w}}{\partial \delta_{B_l}}|_{eq} \end{bmatrix} \cdot \begin{bmatrix} u \\ w \\ \dot{\theta} \\ \delta_{B_r} \\ \delta_{B_l} \end{bmatrix}$$

Also, considering that the brakes mechanism is symmetric and for the longitudinal motion analysis only the symmetrical brake applications are of interest, it can be established:

$\frac{\partial J}{\partial \delta_B}|_{eq} = \frac{\partial J}{\partial \delta_{B_r}}|_{eq} = \frac{\partial J}{\partial \delta_{B_l}}|_{eq}$; and $\delta_B = \delta_{B_r} = \delta_{B_l}$

Then, the equations of motion can be rewritten as:

$$\begin{bmatrix} \dot{U} \\ \dot{W} \\ \ddot{\theta} \end{bmatrix} = \begin{bmatrix} X_u & X_w & X_{\dot{\theta}} & X_\theta & X_\delta \\ Z_u & Z_w & Z_{\dot{\theta}} & Z_\theta & Z_\delta \\ M_{Y_u} & M_{Y_w} & M_{Y_{\dot{\theta}}} & M_{Y_\theta} & M_{Y_\delta} \end{bmatrix} \cdot \begin{bmatrix} u \\ w \\ \dot{\theta} \\ \theta \\ \delta_B \end{bmatrix} \tag{7.31}$$

However, to use the benefits of classical state-space description, the system above can be re-arranged as:

$$\begin{bmatrix} \dot{u} \\ \dot{w} \\ \ddot{\theta} \\ \dot{\theta} \end{bmatrix} = \begin{bmatrix} X_u & X_w & X_{\dot{\theta}} & X_\theta \\ Z_u & Z_w & Z_{\dot{\theta}} & Z_\theta \\ M_{Y_u} & M_{Y_w} & M_{Y_{\dot{\theta}}} & M_{Y_\theta} \\ 0 & 0 & 1 & 0 \end{bmatrix} \cdot \begin{bmatrix} u \\ w \\ \dot{\theta} \\ \theta \end{bmatrix} + \begin{bmatrix} X_\delta \\ Z_\delta \\ M_{Y_\delta} \\ 0 \end{bmatrix} \cdot \delta_B \tag{7.32}$$

Which represents a standard state-space system in the form: $\left\{\dot{x}_{(t)} = A \cdot x_{(t)} + B \cdot \delta_{B(t)}\right\}$. Therefore applying Laplace's transformation and considering non-null initial conditions it can be obtained:

$$s \cdot \begin{bmatrix} U_{(s)} \\ W_{(s)} \\ \dot{\Theta}_{(s)} \\ \Theta_{(s)} \end{bmatrix} = \begin{bmatrix} X_u & X_w & X_{\dot{\theta}} & X_\theta \\ Z_u & Z_w & Z_{\dot{\theta}} & Z_\theta \\ M_{Y_u} & M_{Y_w} & M_{Y_{\dot{\theta}}} & M_{Y_\theta} \\ 0 & 0 & 1 & 0 \end{bmatrix} \cdot \begin{bmatrix} U_{(s)} \\ W_{(s)} \\ \dot{\Theta}_{(s)} \\ \Theta_{(s)} \end{bmatrix} + \begin{bmatrix} X_\delta \\ Z_\delta \\ M_{Y_\delta} \\ 0 \end{bmatrix} \cdot \delta_{B(s)} + \begin{bmatrix} u_{(0)} \\ w_{(0)} \\ \dot{\theta}_{(0)} \\ \theta_{(0)} \end{bmatrix}$$

(7.33)

Notice that the entries of the system can be divided in two groups. The effect of command actuation and initial disturbances (normally related to atmospheric activity). These two kinds of inputs can be considered separately, and, although some brakes inputs will be assessed as a source of disturbance, this chapter will focus on initial non-commanded disturbances. The equation above can be expressed in the form: $\left\{\mathrm{s} \cdot X_{(s)} = A \cdot X_{(s)} + B \cdot \delta_{B(s)} + x_{(0)}\right\}$, and is equivalent to the following presentation in time's domain:

$$\dot{x}_{(t)} = A \cdot x_{(t)} + B \cdot \delta_{B(t)} + x_{(0)} \cdot \delta(1)$$

(7.34)

Where the term $\delta(1)$ is the Dirac's delta, denoting an impulse function to represents an initial disturbed condition. As the outputs of interest are the dynamic variables itself, the output matrix is simply the unit matrix. Therefore, the system can be represented in a block diagram as follows:

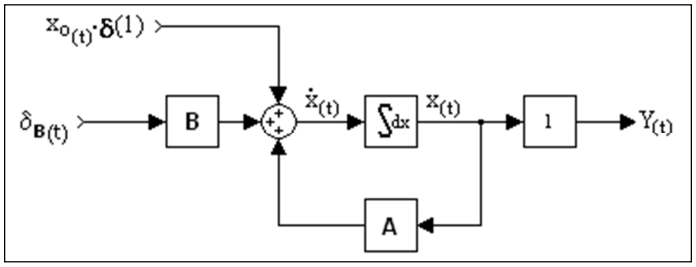

Figure 7.6 – Longitudinal motion state space model

The terms in equation (7.33) represent the longitudinal stability derivatives which are given by:

Table 7-1: Longitudinal stability derivatives

$X_u = \frac{1}{\mathrm{m}} \cdot \left(-\rho \cdot C_D \cdot S_{CG} \cdot U_{eq} + \frac{\partial X_V}{\partial U}\vert_{eq}\right)$	$Z_u = \frac{1}{\mathrm{m}} \cdot \frac{\partial Z_V}{\partial U}\vert_{eq}$	$M_{Y_u} = \frac{1}{\mathrm{I_y}} \cdot \frac{\partial M_y}{\partial U}\vert_{eq}$
$X_w = \frac{1}{\mathrm{m}} \cdot \frac{\partial X_V}{\partial W}\vert_{eq}$	$Z_w = \frac{1}{\mathrm{m}} \cdot \left(-\rho \cdot C_D \cdot S_{CG} \cdot W_{eq} + \frac{\partial Z_V}{\partial W}\vert_{eq}\right)$	$M_{Y_w} = \frac{1}{\mathrm{I_y}} \cdot \frac{\partial M_y}{\partial W}\vert_{eq}$
$X_{\dot{\theta}} = \frac{1}{\mathrm{m}} \cdot \frac{\partial X_V}{\partial Q}\vert_{eq} - W_{eq}$	$Z_{\dot{\theta}} = \frac{1}{\mathrm{m}} \cdot \frac{\partial Z_V}{\partial Q}\vert_{eq} + U_{eq}$	$M_{Y_{\dot{\theta}}} = \frac{1}{\mathrm{I_y}} \cdot \frac{\partial M_y}{\partial Q}\vert_{eq}$
$X_\theta = -g \cdot cos(\Theta_{\mathrm{eq}})$	$Z_\theta = -g \cdot sen(\Theta_{\mathrm{eq}})$	$M_{Y_\theta} = 0$
$X_\delta = \frac{1}{\mathrm{m}} \cdot \frac{\partial X_V}{\partial \delta_{\mathrm{B}}}\vert_{eq}$	$Z_\delta = \frac{1}{\mathrm{m}} \cdot \frac{\partial Z_V}{\partial \delta_{\mathrm{B}}}\vert_{eq}$	$M_{Y_\delta} = \frac{1}{\mathrm{I_y}} \cdot \frac{\partial M_y}{\partial \delta_{\mathrm{B}}}\vert_{eq}$

Where the wing's forces and moments derivative terms can be obtained as suggested in chapter 5. Considering null initial conditions, equation (7.33) can also be written as:

$$\begin{bmatrix} s - X_u & -X_w & -\left(X_{\dot{\theta}} \cdot s + X_\theta\right) \\ Z_u & s - Z_w & -\left(Z_{\dot{\theta}} \cdot s + Z_\theta\right) \\ -M_{Y_u} & -M_{Y_w} & s^2 - s \cdot M_{Y_{\dot{\theta}}} - M_{Y_\theta} \end{bmatrix} \cdot \begin{bmatrix} U_{(s)} \\ W_{(s)} \\ \Theta_{(s)} \end{bmatrix} = \begin{bmatrix} X_\delta \\ Z_\delta \\ M_{Y_\delta} \end{bmatrix} \cdot \delta_{B_{(s)}} \tag{7.35}$$

Finally, the characteristic equation do not depends on the inputs and it is given by the following determinant:

$$\begin{vmatrix} s - X_u & -X_w & -\left(X_{\dot{\theta}} \cdot s + X_\theta\right) \\ -Z_u & s - Z_w & -\left(Z_{\dot{\theta}} \cdot s + Z_\theta\right) \\ -M_{Y_u} & -M_{Y_w} & s^2 - M_{Y_{\dot{\theta}}} \cdot s \end{vmatrix} = K^4_{long} \cdot s^4 + K^3_{long} \cdot s^3 + K^2_{long} \cdot s^2 + K^1_{long} \cdot s + K^0_{long} \tag{7.36}$$

Where:

$$\begin{bmatrix} K^4_{long} \\ K^3_{long} \\ K^2_{long} \\ K^1_{long} \\ K^0_{long} \end{bmatrix} = \begin{bmatrix} 1 \\ -X_u - Z_w - M_{Y_{\dot{\theta}}} \\ (X_u \cdot Z_w - Z_u \cdot X_w) + \left(M_{Y_{\dot{\theta}}} \cdot (X_u + Z_w) - X_{\dot{\theta}} \cdot M_{Y_u} - Z_{\dot{\theta}} \cdot M_{Y_w}\right) \\ (X_w \cdot Z_u - X_u \cdot Z_w) \cdot M_{Y_{\dot{\theta}}} - M_{Y_u} \cdot (X_w \cdot Z_{\dot{\theta}} - X_{\dot{\theta}} \cdot Z_w + X_\theta) - M_{Y_w} \cdot (X_{\dot{\theta}} \cdot Z_u - X_u \cdot Z_{\dot{\theta}} + Z_\theta) \\ \left(Z_w \cdot M_{Y_u} - Z_u \cdot M_{Y_w}\right) \cdot X_\theta + \left(X_u \cdot M_{Y_w} - X_w \cdot M_{Y_u}\right) \cdot Z_\theta \end{bmatrix}$$

At this point it is already possible to determine if the system is dynamically stable by applying the Routh's criterion well explained in control theory classical literature (Ogata, 2003).

For paragliders, by solving the characteristic fourth order polynomial equation, it will be found two pairs of complex roots related to the short period and the phugoid mode:

$$\left(K^4_{long}\cdot \mathrm{s}^4 + K^3_{long}\cdot \mathrm{s}^3 + K^2_{long}\cdot \mathrm{s}^2 + K^1_{long}\cdot \mathrm{s} + K^0_{long} = 0\right) \rightarrow \left(r^R_{sp} + r^I_{sp}\cdot i\right) e \left(r^R_{ph} + r^I_{ph}\cdot i\right)$$

Using these roots, the basic parameters can be calculated as follows:

$$\omega_{n_{sp}} = \sqrt{\left(r^R_{sp}\right)^2 + \left(r^I_{sp}\right)^2} \qquad \omega_{n_{ph}} = \sqrt{\left(r^R_{ph}\right)^2 + \left(r^I_{ph}\right)^2}$$

$$\xi_{sp} = -\frac{r^R_{sp}}{\sqrt{\left(r^R_{sp}\right)^2 + \left(r^I_{sp}\right)^2}} \qquad \xi_{ph} = -\frac{r^R_{sp}}{\sqrt{\left(r^R_{ph}\right)^2 + \left(r^I_{ph}\right)^2}}$$

Finally, it can be defined the characteristic parameters for each mode as proposed in table 7-2:

Table 7-2: Longitudinal stability characteristic parameters

Oscillation Period:	Cicles to damp (reduction to 5%):
$T_{sp} = \frac{2\cdot\pi}{\omega_{n_{sp}}\cdot\sqrt{1-\xi_{sp}{}^2}}$	$CTD^{5\%}_{sp} \approx \frac{1}{2\cdot\xi_{sp}}$
$T_{ph} = \frac{2\cdot\pi}{\omega_{n_{ph}}\cdot\sqrt{1-\xi_{ph}{}^2}}$	$CTD^{5\%}_{ph} \approx \frac{1}{2\cdot\xi_{ph}}$

Both stability parameters derived here are necessary to characterize the longitudinal behavior. The period of oscillation allows judging if the motion is too fast revealing a violent response, or if it is in the range of pilot's reactions, contributing for PIO. The number of cycles to damp (CTD) gives an idea of the "level of longitudinal damping".

7.3.2 Longitudinal response analysis:

Analyzing the state-apace model presented in figure 7.6 it can be seen that two main kinds of disturbances may occur: a command input or a natural atmospheric disturbance. The longitudinal stability analysis will be concentrated in responses to gusts and transient command inputs. Command steps or continuous inputs will be analyzed more carefully under the controllability aspects analysis on chapter 9.

A natural common source of longitudinal disturbance is a quick symmetric command input, which will instantaneously change wing angle of attack. This is modeled as an impulse functions in time's domain, representing the initial input given by: $\delta_B \cdot \delta_1(t)$

Where $\delta_1(t)$ is the unitary impulse function (Dirac's delta), and δ_B is the amount of brakes applied in fraction of available length.

Considering a typical paraglider, figure 7.7 below shows system's response to a full command impulse ($\delta_B = 1$) input.

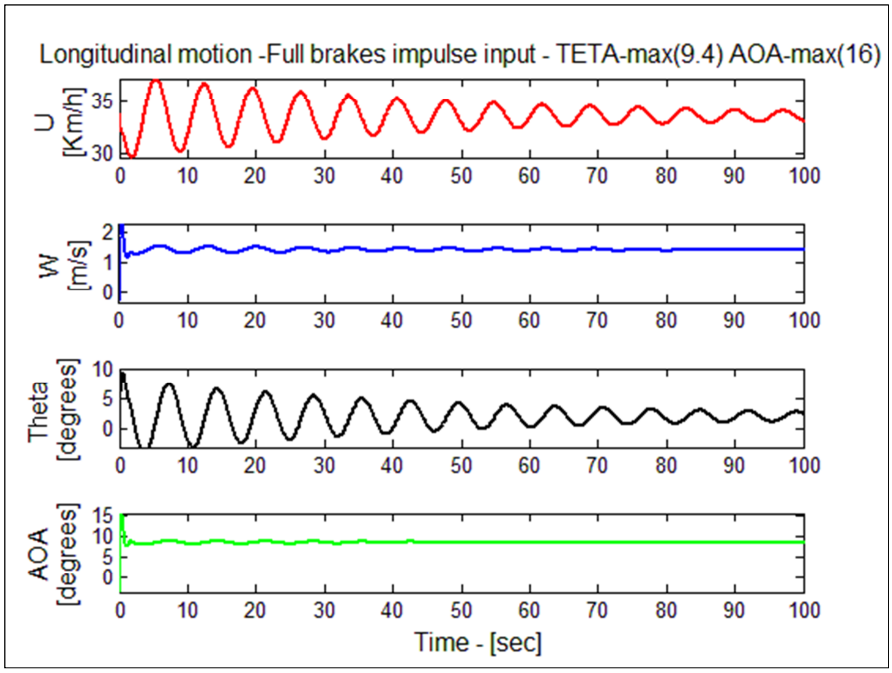

Figure 7.7 – Impulse response – General observation

As can be seen, the system recovering motion is basically a manifestation of the phugoid mode, which is characterized by an attitude and flight speed oscillation. However, by applying a zoom in the initial portion of the movement the occurrence of the short period can be visualized as show in figure 7.8 below:

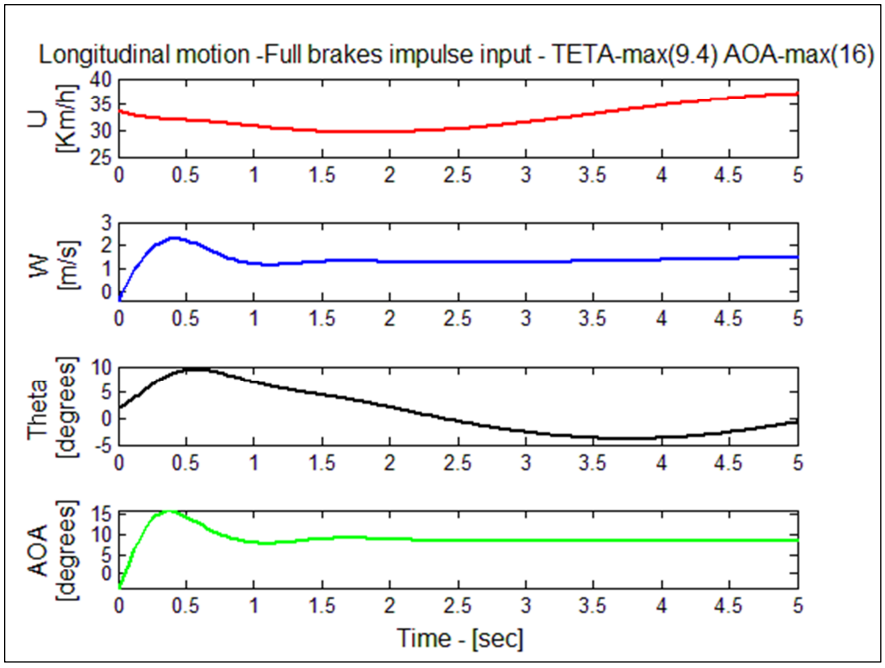

Figure 7.8 – Impulse response – Initial transient observation

The movement represented in Fig. 7.8 is the manifestation of the short-period motion, which is characterized by a rapidly suppressed oscillation in AOA.

In general, although the natural damping is not effective for the long period motion, considering the low amplitudes and the long period of the oscillations, it should not cause discomfort for the pilot or dangerous situations. In fact, this level of oscillation may pass unnoticed.

Now, to evaluate wing stability proprieties considering atmospheric disturbances susceptibility, it might be considered that the common expected longitudinal disturbances are normally originated by horizontal gusts and vertical currents. In this way, it is accurate enough to define a standardized initial disturbed condition (initial state-variable), which can be modeled in time domain as simple speed impulse functions:

$$\begin{cases} [u_0;\ 0;\ 0;\ 0] \cdot \delta_1(t) \rightarrow \text{Horizontal gust} \\ [0;\ w_0;\ 0;\ 0] \cdot \delta_1(t) \rightarrow \text{Vertical current} \end{cases}$$

For the horizontal gust, considering the basic hypotheses of small disturbances, a reasonable value to assume as a representative small disturbance is 10km/h. For the vertical currents the most relevant source of disturbances will be the thermals and local turbulences. These air currents present vertical speeds up to 8m/s depending on the local temperature and geographical characteristics (Pagen, 2001), but a reasonable value to use as a standard small disturbance is 2m/s.

Finally, as the equilibrium attitude angle is normally small, the "standard disturbances" can be described in term of speed variations using the body-coordinate-system as:

$$u_0 = 3\,{}^{m}/_{s}\,;\; w_0 = 2\,{}^{m}/_{s}$$

Using separately these standard disturbances, the system's response can be simulated as shown in figures 7.9 and 7.10 below:

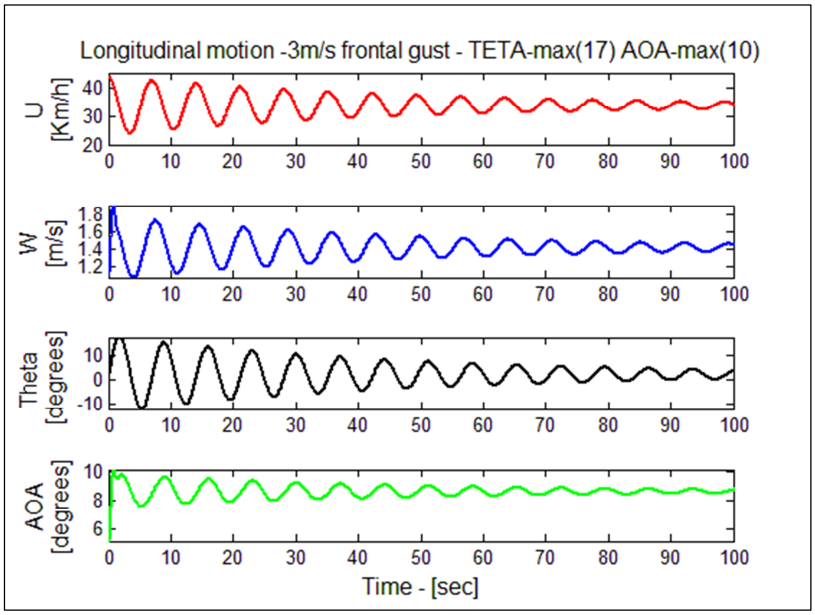

Figure 7.9 – Response to a 3m/s frontal gust

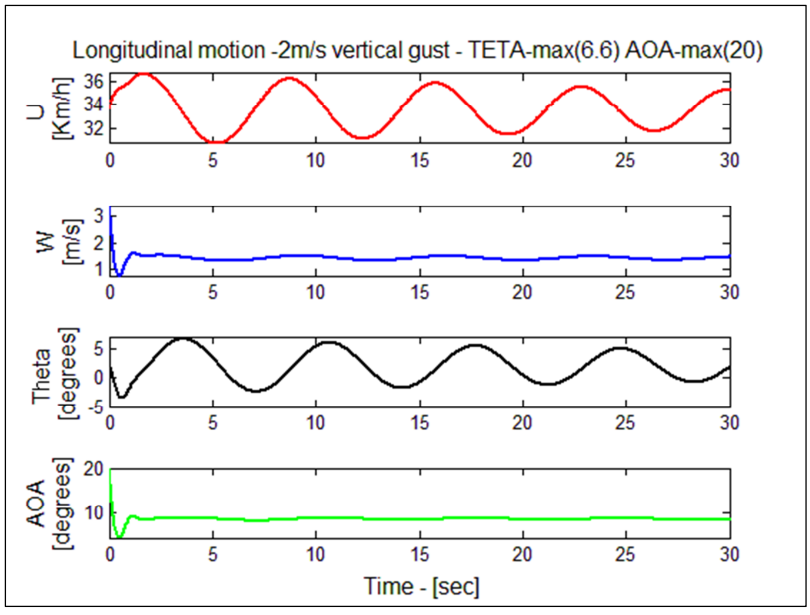

Figure 7.10 – Response to an entrance in a 2m/s vertical current

As expected, the graphics confirms the results for period and damping factor obtained from calculation using the characteristic equation. However, a new parameter is made available: The maximum amplitude of the oscillations.

The amplitude of the oscillation in attitude is an important parameter because it is related to how the pilot is exposed to the disturbance. If the oscillation is significantly large and the period of oscillation is short it means that the wing reacts violently, which is an undesirable behavior.

Notice that for the vertical gust there is an initial movement which is fast, but with moderate amplitude, and also quickly suppressed. This is the manifestation of the short period motion. As illustrated, the movement continues the phugoid takes place and a longer period motion with increased amplitude becomes dominant. This final motion is then slowly damped. For the horizontal gust, the transient is almost imperceptible and the phugoid takes place immediately.

For handling characteristics it is desirable that any short period movement be small and heavily damped, and that the phugoid be a slow subsidence, with moderate amplitudes.

A maximum attitude oscillation parameter can be defined from the responses to the standard disturbances as the greater value between:

$$\theta^{u}_{max};\ and\ \theta^{w}_{max}$$

The values of the maximum amplitudes for the case presented in figures 7.9 and 7.10 are shown below in table 7-3:

Table 7-3: Longitudinal motion maximum amplitudes

Standard oscillations maximum amplitudes					
Initial disturbance		u_{max} **km/h**	w_{max} **km/h**	θ_{max} **degrees**	$\propto_{max}$ **degrees**
Shor period	w_0*=2m/s*	37	3.1	6.6	20
Long period	u_0*=3m/s*	45	1.5	**17**	10

In this case, and as will be commonly observed, the maximum is dictated by the horizontal gust input. There are no good analytical approximations to calculate maximum amplitudes, in this way, numerical calculations (Tewari, 2002) and statistical analysis are expected to be necessary to investigate possible relations with the design parameters.

7.3.3 Analytical approximations

The methods above provides precise results about paraglider's longitudinal dynamics; however, it involves solving a fourth order equation demanding numerical methods and does not reveal practical relations between longitudinal stability characteristics and design parameters. Therefore, to allow a deeper analytical investigation of each component of longitudinal motion, a simplified approach using classical stability and control theory applied for conventional airplanes (Babister, 1980) will be carried out in sections 7.3.3.1 and 7.3.3.2 below.

7.3.3.1 – Short-Period oscillation approximation:

The short-period oscillation can be understood as a vibration mode caused by a small AOA variation where there are no significant changes on system's velocity. The paraglider is supposed to oscillate varying attitude while the CG maintain the original flight path. This kind of movement can be caused by vertical gusts, pilot's quick inputs or moderate turbulence. It is commonly presented as an AOA adjustment capability and can be felt by the pilot as an initial quick oscillation when entering into a thermal current.

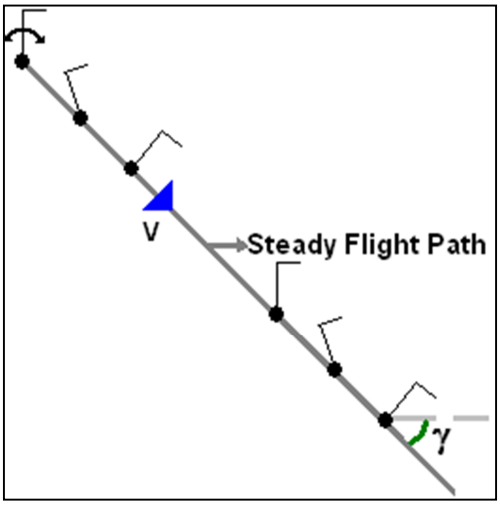

Figure 7.11 – Short Period oscillation

Figure 7.11 above illustrates the short period movement. As can be seen, this movement is characterized by a slight variation in attitude that can be related to an AOA variation, and because of that, a divergent behavior could result stalls or frontal collapses. It is interesting to mention that for conventional aircraft this motion presents a very low period of oscillation and an increased damping coefficient, characterizing a rapid suppression of any small disturbance on AOA, mostly

imperceptible for the pilot. However, for paragliders, this motion is characterized by a period of oscillation varying between 1 and 3 seconds, and a moderate-to-light damping coefficient varying between 0.2 and 0.6, resulting in theoretical accommodation times that could reach 5 seconds.

The short period oscillation can be modeled using the pitch moment equation as follows:

$$M_y = [L \cdot cos(\propto) + D \cdot sin(\propto)] \cdot d_0' - [L \cdot sin(\propto) - D \cdot cos(\propto)] \cdot h_0' + m_0$$

(7.37)

to develop a linear approximation of this expression, it can be seen that:

$$\left.\frac{\partial M_y}{\partial \alpha}\right|_{eq} = [D \cdot d_0' - L \cdot h_0'] \approx -W \cdot h_0'$$

(7.38)

disregarding total speed variation, and then, taking in account that: $\dot{\propto} \approx$ Q

$$\left.\frac{\partial M_y}{\partial \dot{\alpha}}\right|_{eq} \approx \left.\frac{\partial M_y}{\partial Q}\right|_{eq}$$

(7.39)

In this way, the initial equation can be written as:

$$I_y \cdot \ddot{\propto} = \cancel{M_{y_{eq}}} + \left.\frac{\partial M_y}{\partial Q}\right|_{eq} \cdot \dot{\propto} + \left.\frac{\partial M_y}{\partial \alpha}\right|_{eq} \cdot \propto$$

(7.40)

That yields:

$$\ddot{\propto} - M_{Y_{\dot{\theta}}} \cdot \dot{\propto} + \frac{W \cdot h_0'}{I_y} \cdot \propto = 0$$

(7.41)

The expression above defines a linear, second order, homogeneous differential equation that can be written as:

$$\ddot{\propto} + 2 \cdot \xi_{sp} \cdot \omega_{n_{sp}} \cdot \dot{\propto} + {\omega_{n_{sp}}}^2 \cdot \propto = 0$$

(7.42)

For normal design parameters, the equation above is supposed to result complex roots, representing the expected oscillatory movement. Beneficiating from classical control theory (Ogata, 2003), it is easy to obtain the natural frequency and the period of oscillation for this motion.
The natural frequency will be given by:

$$\omega_{n_{sp}} = \sqrt{\frac{W \cdot h_0'}{I_y}} \tag{7.43}$$

The damping coefficient will be:

$$\xi_{sp} = \frac{-M_{Y_{\dot{\theta}}}}{2 \cdot \omega_{n_{sp}}} \tag{7.44}$$

Then, the damped frequency will be given by:

$$\omega_{d_{sp}} = \omega_{n_{sp}} \cdot \sqrt{1 - \xi_{sp}{}^2} \tag{7.45}$$

Considering small values of damping coefficient, the characteristic short-period to be used as a reference for conceptual design evaluations can be approximated by:

$$T_{sp} = 2 \cdot \pi \cdot \sqrt{\frac{I_y}{W \cdot h_0'}} \tag{7.46}$$

The set of equations above allows some conclusions about paraglider´s short-period motion. It can be seen that the period is related to system's weight, inertia and the CG height. Notice that by increasing weight the period will be diminished and the damping factor increased, in this way, the increase of wing-load acts as a stabilizing factor. Also, it must be noticed that by increasing CG height the longitudinal inertia will also be increased, but, for normal design parameters, the final result is usually a beneficial increase in damping factor.

For the damping coefficient, the result obtained with expression (7.44) is not a good approximation, because of the relevant impact of many second order effects not taken in account in equation (7.40). However, a statistical analysis may demonstrate that no divergence in short-period oscillations is expected, and the damping capability increases with flight speed.

Regarding short period oscillations, two main characteristics would be desirable: The oscillation should be quickly damped and the period of oscillation should not be in the range of pilot's reaction in order to not increase pilot-induced-oscillations (PIO) susceptibility. Tanking in account the theoretical values for paragliders both characteristics could be problematic in a first view, because the light weight and the low speed range will cause paragliders to present periods of oscillation in the range of pilot's reactions (around 1 second) and also low damping coefficients if compared to conventional aircraft. However, for paragliders, this motion acts just as a transient between an initial AOA disturbance and a final long-period oscillation. As presented in the simulations in section 7.3.2, usually the short-period is a dead-bit oscillation that can be considered not relevant if the transition to the phugoid mode is quick.

7.3.3.2 – Long-Period oscillation (Phugoid) approximation:

The long-period oscillation, or phugoid, can be approximated as an oscillatory motion where there are a slight variation in angle of attack and a more representative variation in attitude. In this motion the speed and flight path varies oppositely causing a riding around the equilibrated flight path as illustrated in figure 7.12 below. This kind of movement can be caused by small disturbances in flight speeds due to gusts, pilot's inputs or any previous motion resulting representative pitch rate. It is commonly presented as a flight path adjustment capability and reveals itself in the form of a continuous longitudinal oscillation which may pass unnoticed by the pilots if in low amplitudes.

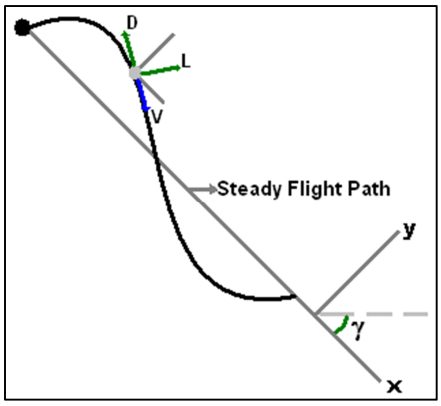

Figure 7.12 –Long-Period oscillation (Phugoid)

Figure 7.12 above illustrates the long period motion. As can be seen this movement is characterized by a variation in flight path angle that can be related to speed component variations. Oscillations with excessive high amplitude can be found in some models, but as the AOA remains under safe limits no unsafe characteristics is expected if it is provided a minimum level of controllability. For paragliders, this motion is characterized by a period of oscillation varying between 4 and 9 seconds, and a light damping factor normally below 0.1, resulting an accommodation time which can easily trespass 1 minute.

Regarding long-period oscillations, the main desirable characteristic is to have a period large enough, necessarily out of the range of pilot's reaction time to prevent pilot-induced-oscillations (PIO). For paragliders, taking in account the normal values encountered, the design parameters must be carefully managed to result good handling characteristics.

Different of the phugoid approximation normally used for conventional airplanes where only the translational equations are taken in account (Babister, 1980), in paragliders the long-period motion involves pitch rate and small variations in AOA. This is mainly due to the high distance between CG and AC. This characteristic allied to the low values of damping coefficient make some second order terms representative, and restricts the possibilities to efficiently represent this mode by a classical second-order system using linear approximations. However, the benefits of having such approximation to be applied in conceptual design evaluations, even with restricted validity, are very representative. Because of that, an approximation will be modeled disregarding the rotational equation as in classical airplane flight mechanics.

To find an approximation for the phugoid, it can be made the following considerations:

- The flight path angle and the angle of attitude are small.
- There is no changing in angle of attack.
- The total flight speed equals the speed component in the X-axis.

Using the above considerations the complete set of equations describing the longitudinal motion can be reduced suppressing the terms related to vertical speed component variations (directly related to AOA variations) and the pitch moment equation. Starting from equation (7.35) the second column and third line can be removed, what corresponds to take in consideration only the equations characterizing the center of gravity trajectory, which means, flight speed and path angle. Then, a new second order characteristic equation can be obtained by solving the following determinant:

$$\begin{vmatrix} s - X_u & -\left(X_{\dot{\theta}} \cdot s + X_\theta\right) \\ Z_u & -\left(Z_{\dot{\theta}} \cdot s + Z_\theta\right) \end{vmatrix}$$

(7.47)

Then, using the same algebraic procedures introduced previously, the natural frequency can be calculated as:

$$\omega_{n_{ph}} = \sqrt{\frac{X_\theta \cdot Z_u - X_u \cdot Z_\theta}{Z_{\dot{\theta}}}}$$

(7.48)

However, it is possible to demonstrate that, for typical design parameters, $Z_\theta \approx \mathrm{g} \cdot \sin\left(\Theta_{\mathrm{eq}}\right)$ and $X_u \approx 0$, what results: $|X_\theta \cdot Z_u| \gg |X_u \cdot Z_\theta|$. Therefore it is enough to use the formula:

$$\omega_{n_{ph}} = \sqrt{\frac{X_\theta \cdot Z_u}{Z_{\dot{\theta}}}}$$

(7.49)

Considering the small values of damping coefficient normally present in the phugoid, the characteristic period to be used as a reference for conceptual design evaluations can be approximated by:

$$T_{ph} = 2 \cdot \pi \cdot \sqrt{\frac{Z_{\dot{\theta}}}{X_\theta \cdot Z_u}}$$

(7.50)

Using the expressions for the longitudinal stability derivatives in table 7-1 it is possible to deduce the approximation:

$$T_{ph} \approx 2 \cdot \pi \cdot \sqrt{\frac{U_{eq}}{g}}$$

(7.51)

This approximation shows that the phugoid period is proportional to the squared root of the flight speed, exactly as in classical airplanes stability theory. And, as flight speeds keeps a close

relation to wing-load, it is possible to conclude that the total weight plays an important part defining longitudinal stability characteristics.

With the natural frequency calculated, following classical second order system's formulations (Ogata, 2003), the damping factor can be calculated as:

$$\xi_{sp} = \frac{-X_u - \frac{Z_\theta}{Z_{\dot{\theta}}} - X_{\dot{\theta}} \cdot \frac{Z_u}{Z_{\dot{\theta}}}}{2 \cdot \omega_{n_{sp}}} \tag{7.52}$$

However, it can also be shown that for typical design parameters values: $Z_{\dot{\theta}} \gg Z_\theta$; and $Z_{\dot{\theta}} \gg Z_u \cdot X_{\dot{\theta}}$, what results: $|X_u| \gg \left|\frac{Z_\theta}{Z_{\dot{\theta}}} + X_{\dot{\theta}} \cdot \frac{Z_u}{Z_{\dot{\theta}}}\right|$. Therefore it is enough to use the formula:

$$\xi_{sp} = \frac{-X_u}{2 \cdot \omega_{n_{sp}}} \tag{7.53}$$

Analyzing the expressions for the longitudinal stability derivatives in table 7-1, it is possible to conclude that the damping factor increases with flight speed and CG drag. Also, by working with some dynamic simulations using the model proposed in chapter 5, it is possible to observe that the damping factor coefficient diminishes if glide ratio increases. This is another proof of the fact that, most times, improving performance shall reduce stability.

Finally, it is important to highlight that both short-period and phugoid simplifications presented here are just first approximations to allow a faster calculation of longitudinal stability characteristics, and then, such formulations must be used carefully.

7.4 Conceptual design longitudinal stability evaluations:

By analyzing different models using the developments presented until this point it is possible to compare the stability characteristics and reach some valuable conclusions. Based on last sections discussions, the most relevant longitudinal stability parameters are specially affected by the

wing-load, which is always benefic for stability, and by the CG position, that must be managed carefully to adequate the performance, stability and controllability characteristics.

To evaluate the longitudinal response it is reasonable to concentrate efforts investigating the phugoid proprieties, since the short-period was shown to be harmless if it is sustained as a transient mode, what occurs for most models. In this way, for the phugoid it is desirable to have a period long enough, combined with low amplitude oscillations and resulting minimum cycles to damp if possible.

Established that improving wing-load will be beneficial for the phugoid characteristics, the most relevant variables remaining to be evaluated are the CG position and the aerodynamics proprieties. To investigate the effect of CG positioning on longitudinal stability, let's consider figure 7.13 below, which was obtained by comparing some theoretical models.

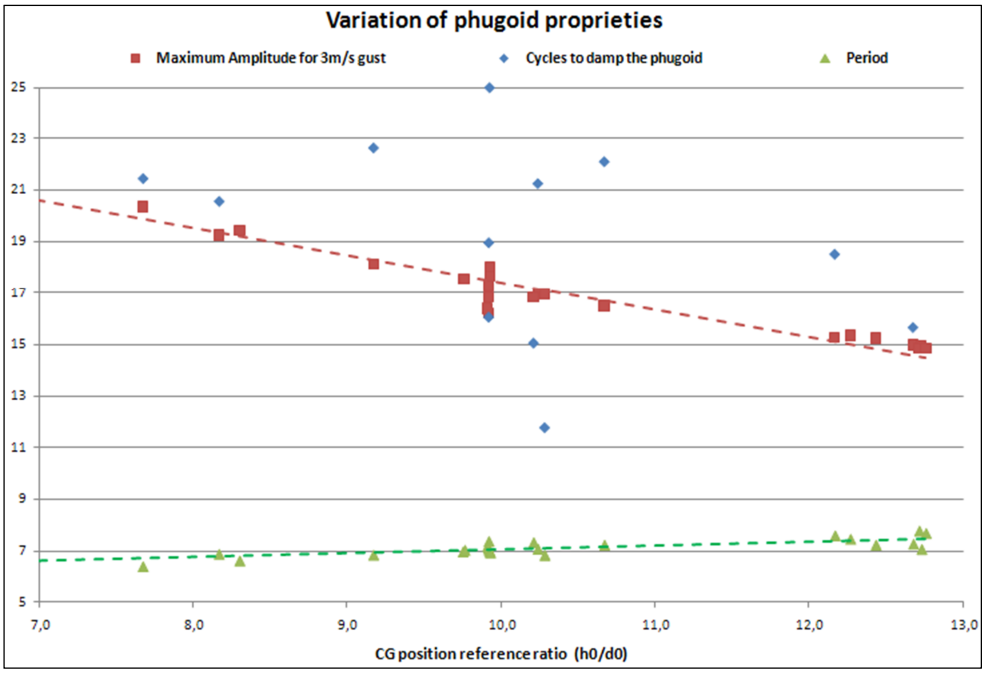

Figure 7.13 – Longitudinal Stability characteristics variation with CG position

Figure 7.13 shows a decrease in the maximum amplitude of the oscillations and a slight increase in the phugoid period driven by an increase in the CG position reference ratio. The variability of the damping efficiency showed by the increased dispersion in cycles to damp data, mostly due to the many second order effects involved in this variable, do not allow assertive relation with the CG position reference ratio. Even though, over all, it can be said that the longitudinal response characteristics improves as the CG position reference ratio increases. This is true mostly because a slow small oscillation is very controllable or may pass unnoticed.

It is worthy to mention that for a fixed CG position reference ratio the variation of the stability parameters with CG height is quite small, but it is also true that increasing CG height leads to a slight decrease in maximum amplitudes and slight increase in long-period.

Using the developments presented in chapter 6, it can be seen that the equilibrium angle of attack varies oppositely with the CG position reference ratio. Because of that the analysis above could be also presented in terms of AOA variation as illustrated in figure 7.14 below.

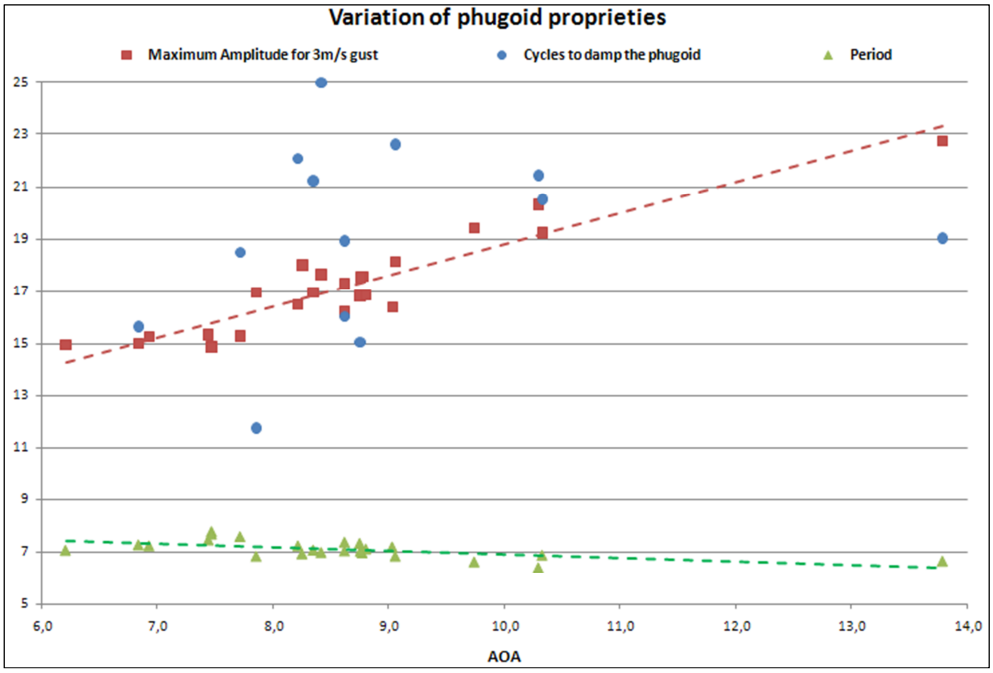

Figure 7.14 – Longitudinal Stability characteristics variation with AOA

Taking in account the assessments above, it can be concluded that selecting a CG position reference ratio far from the optimum value may improve stability but will probably degrade performance.

Also, modifications in the aerodynamic proprieties may be helpful improving damping capability and reducing the oscillatory amplitudes. However, no simplified procedures or direct algebraic relations are available, and some empirical effort investigating different combinations of airfoils and wings geometry is supposed to be necessary.

A final necessary observation is that, although the simulations of "hands-off" longitudinal disturbances present a limited natural damping coefficient, in practice, because of the period of oscillation, the pilot is able to suppress the disturbance regaining equilibrium. Figure 7.15 bellow presents a simulation considering the pilot on the loop, reacting to wing's rotation.

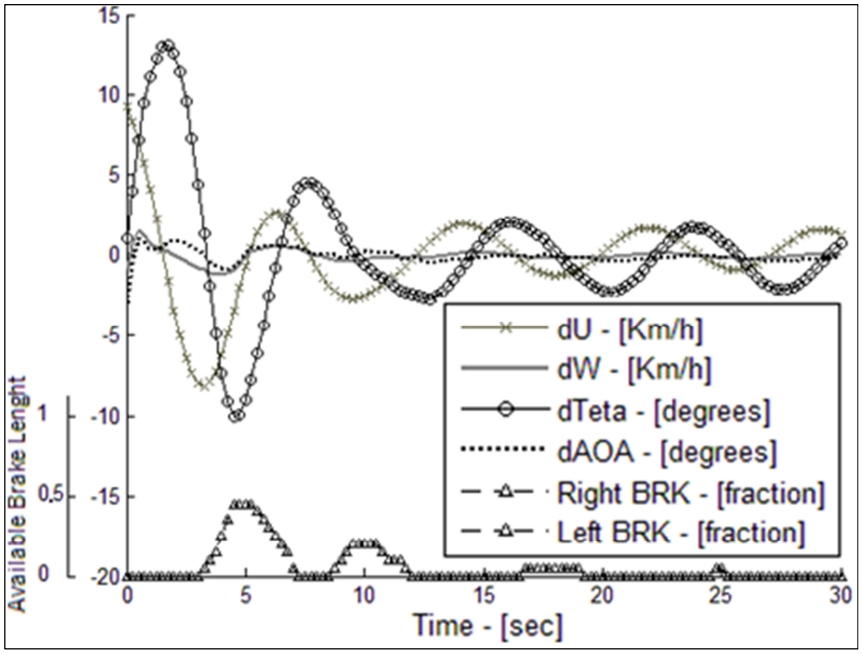

Figure 7.15 – Longitudinal dynamics – response to a 10Km/h frontal gust – Pilot in the loop

Notice that the oscillation is easily controllable with the application of expected low rate pilot's inputs.

7.5 Final Comments:

In this chapter it was presented the many reasons that make longitudinal stability characteristics important for safety and handling qualities. It was shown that any flyable paraglider will present positive static longitudinal stability, but it may present inadequate dynamic stability characteristics, mainly due to the low level of damping in pitching oscillations already reported by other autors.

It was shown that the longitudinal dynamics of paragliders is characterized by the existence of two modes, the short-period and the phugoid just as in conventional airplanes, where the short-period acts as a quickly damped transient and the phugoid acts as a continuous attitude oscillation. The analysis of each one of these movements provided some important relations between stability and design parameters.

Finally, it was possible to obtain some useful conclusions for conceptual design optimizations, showing that the longitudinal stability can be improved by increasing wing-load and flight speed. Also a methodology to evaluate paraglider's longitudinal response was presented, establishing standard disturbances which will allow a longitudinal stability characteristics rating.

8 PARAGLIDERS LATERAL-DIRECTIONAL STABILITY

The lateral-directional stability characteristics are of great relevance for paraglider's flight safety. Besides the fact that lateral-directional stability is closely related to the ability to maintain or efficiently change flight heading, the generation of yaw moments due to lateral gusts or command applications has a special effect on structural stability of flexible wings. In this way, the response characteristics following an asymmetrical disturbance must be effective enough to restore equilibrium, but not so aggressive to cause wing twists.

The analysis of lateral-directional stability can be made based on the same basic concepts discussed in section 7.1. However, the analysis will be more complex since the applicable equations involves motion in both horizontal and frontal planes. Also, differently of the assessments presented in section 7.3, approximations to find simple algebraic relations between design parameters and lateral-directional stability characteristics are not feasible and the types of movement encountered are not the same ones found in classical airplanes flight mechanics (Yechout, 2003). As will be better explained in section 8.2.1.1, paragliders present an important behavior named roll-spiral coupling which were analyzed before (Bosca, 2010; Stengel, 2010) for other aircrafts and has an important consequence in paragliders lateral-directional response characteristics.

Recording the basic concepts, the lateral-directional stability represents paragliders capability to return to steady flight when submitted to a small asymmetric disturbance. For conventional aircrafts the vertical tail plays a fundamental part in defining such characteristics (Thorpe, 1948). In paragliders, which are tailless aircrafts, other design features are responsible for providing an acceptable level of directional stability and control. In this way, it will be shown that paragliders present some specific and interesting behavior regarding lateral-directional motion.

Finally, it is important to mention that for paragliders the balance between stability and maneuverability characteristics are very critical, being one of the most important design compromise to be analyzed. In this chapter only the aspects related to stability will be assessed, the controllability and maneuverability will be investigated in chapter 9.

8.1. Lateral-Directional Static Stability

The lateral and directional static stability represents the paraglider tendency to return to steady flight when submitted to an asymmetrical small disturbance. In this situation it is considered that the static forces and flight speed remains in equilibrium. In such scenario a small lateral disturbance can be treated as an instantaneous sideslip (Babister, 1980). In this way, the stability condition demands that the roll and yaw moments generated by this sideslip be corrective. The illustration in figure 8.1 represents paraglider's dynamic components when submitted to a lateral gust:

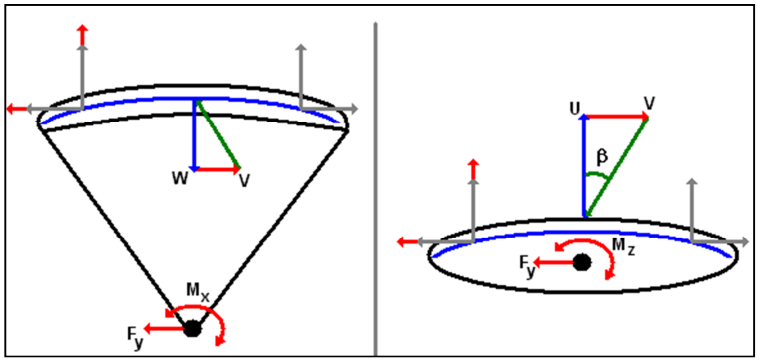

Figure 8.1 – Lateral-Directional Flight Parameters

It is natural to expect that when a positive sideslip angle (beta) is present, for wings with negative dihedral, there will be an increase on the left hand side semi-wing's aerodynamic forces due to a local increase of AOA. In this way, it is generated a lateral negative force component trying to eliminate the sideslip speed component.

Due to the considerable vertical distance of the center of gravity relatively to the wing, it is expected a resultant negative roll moment. Also, for normal combinations of span length and CG horizontal position, it is expected a positive yaw moment. The resultant rotation shall be in order to restore steady flight by eliminating sideslip; this is accomplished by accelerating the wing in the opposite direction and by aligning the wing with the relative wind.

Notice that, if the roll moment generated is positive or the yaw moment is negative the sideslip would be increased leading to an instable behavior. Also, if the yaw moment was negative the wing would rotate oppositely becoming submitted to a tailwind component, which could lead to dangerous stalling conditions.

A relevant observation is that, although the lateral response will tries to reach zero bank angle, the directional response will not try to restore the original flight heading, it only adjust the wing to be aligned with the relative wind.

The rationale above determines the lateral and directional static stability conditions, which can be translated in a more general wording as: The variation of roll moment coefficient with sideslip must be negative, and, the variation of yaw moment coefficient with sideslip must be positive (Hiraki, 2003).

Before starting a complete insight on the lateral-directional stability characteristics of paragliders it is useful to present a conceptual comparison between the lateral-directional mechanics involved in conventional airplanes and paragliders. Figures 8.2 and 8.3 below presents a qualitative assessment focusing on the importance of the CG positioning and wing curvature:

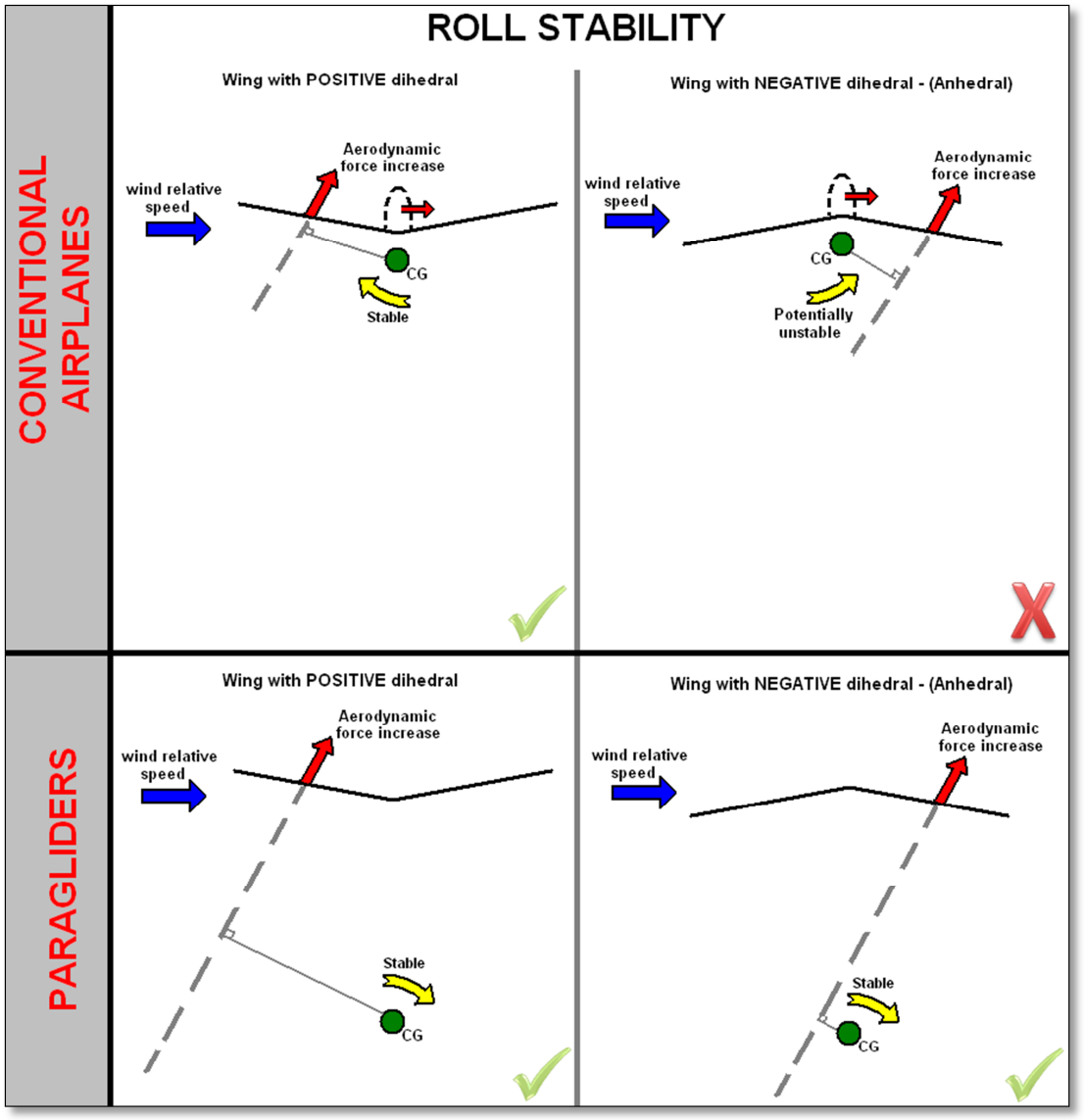

Figure 8.2– Airplanes .vs. paragliders comparison: Roll Stability

It can be seen that, considering the wing curvature and CG distance, roll stability is easily guarantied for paragliders, whereas for airplanes a tradeoff between the effects of vertical stabilizer and negative dihedral (anhedral) must be considered to reach suitable roll capability without compromising stability.

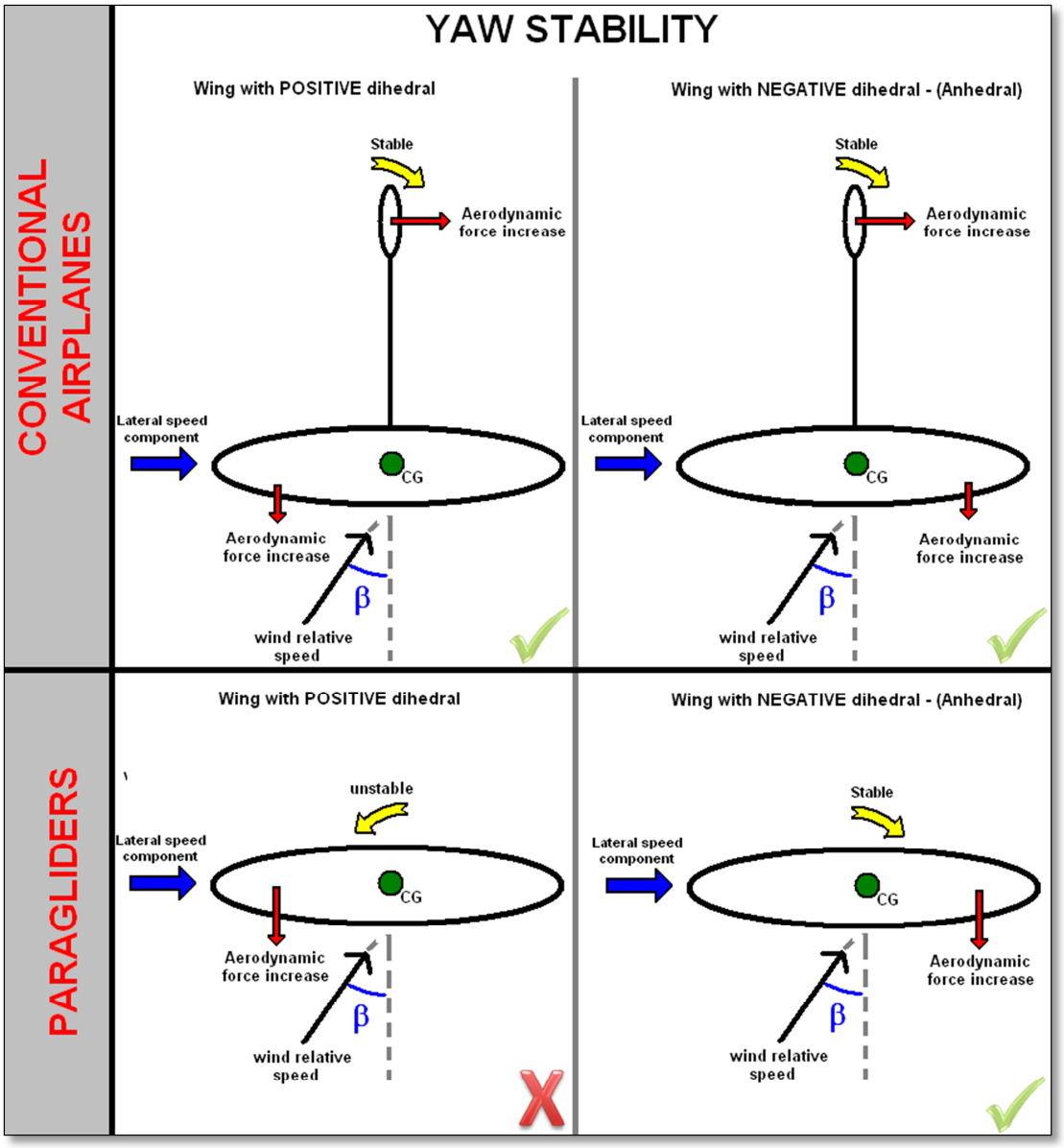

Figure 8.3 – Airplanes .vs. paragliders comparison: Yaw Stability

As illustrated in figure 8.3 negative dihedral is basically mandatory for tailless aircrafts. While in conventional airplanes the vertical stabilizer plays an important part by making the aircraft

aligned to the relative wind when submitted to a sideslip, in paragliders this effect must be reached only through an asymmetric distribution of aerodynamic forces over the wing.

Working with the model provided in chapters 4 and 5 to calculate wing's forces and moments, it is possible to demonstrate that the forces and moments generated by a sideslip are proportional to the sideslip angle (as shown in details in appendix B). In this way, it is possible to obtain the relations:

$$F_{y_w} \approx \frac{\rho}{2} \cdot {U_{eq}}^2 \cdot S \cdot \bar{a} \cdot \Gamma_{ef} \cdot \beta \tag{8.1}$$

$$Cm_{x_w} \approx \left(\frac{\bar{a}}{S \cdot MAC}\right) \cdot A_r \cdot \beta \tag{8.2}$$

$$Cm_{z_w} \approx \left(\frac{\bar{a}}{S \cdot MAC}\right) \cdot A_y \cdot \beta \tag{8.3}$$

Figure 8.4 below shows the moment coefficients variation with sideslip for a typical paraglider. As this illustration is the graphic representation of the above equations, it is easy to conclude that parameters A_r and A_y are given by the curve slopes.

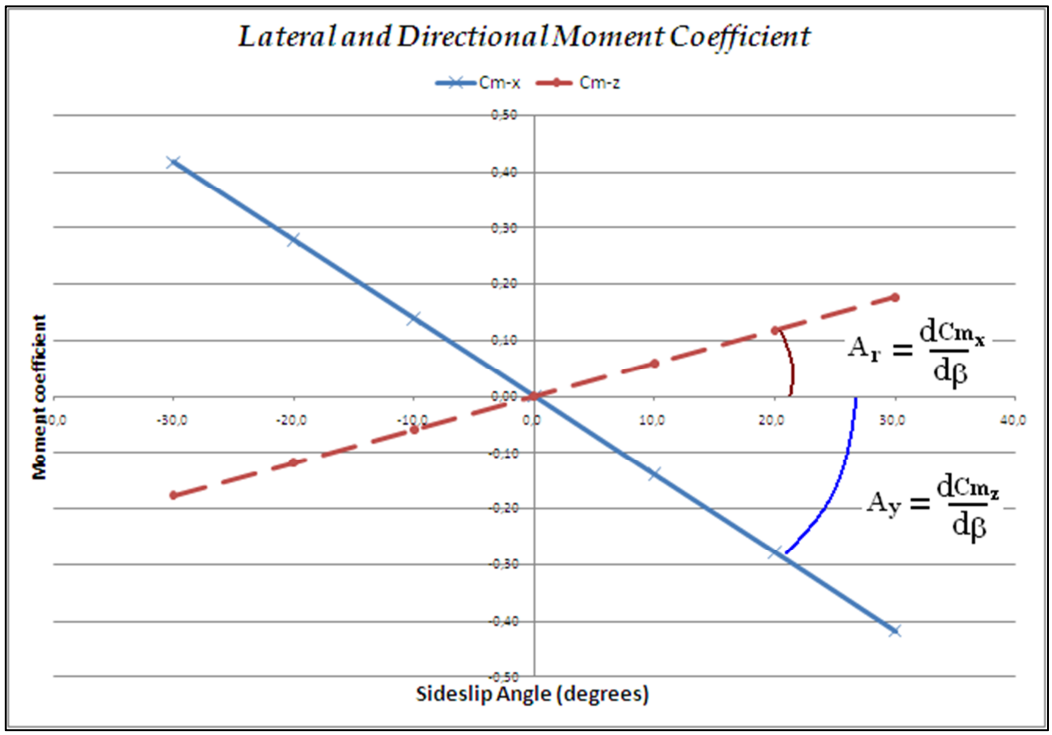

Figure 8.4 – Lateral and Directional Moment coefficients

The parameters A_r and A_y are called respectively "roll arm" and "yaw arm". This nomenclature is meaningful because these parameters can be understood as a virtual distance between the point of action of the aerodynamic force components in each semi-wing and the CG projected in each axis. These parameters can be successfully approximated by the following expressions:

$$A_r \approx \int_{-b/2}^{b/2} \left(cos(\delta) \cdot y + sin(\delta) \cdot f_z(y)\right) \cdot sin(\delta) \cdot f_c(y) \cdot dy \tag{8.4}$$

$$A_y \approx \int_{-b/2}^{b/2} \left[\left(2 \cdot (1 - D_2 \cdot \bar{a}) \cdot \propto_{eq} \cdot cos(\delta) + (1 - 2 \cdot D_2 \cdot \bar{a}) \cdot (f_\theta(y) - i_0)\right) \cdot y - sin(\delta) \cdot f_x(y)\right] \cdot sin(\delta) \cdot f_c(y) \cdot dy \tag{8.5}$$

Using the lateral and directional static stability conditions:

$$\frac{\partial Cm_{x_w}}{\partial \beta} < 0 \rightarrow A_r < 0 \tag{8.6}$$

$$\frac{\partial Cm_{z_w}}{\partial \beta} > 0 \rightarrow A_y > 0 \tag{8.7}$$

It can be noticed that both parameters depends on wing geometry, but the yaw arm depends also on aerodynamic coefficients.

The parameter Γ_{ef} is called the "effective dihedral" and it represents the wing curvature effectiveness. This parameter will determine the magnitude and direction of the lateral force caused by a lateral speed component. Although for static stability analysis the aspects related to Γ_{ef} are already accounted for in the moment coefficients discussed above, the presentation of this additional parameter can be useful to evaluate lateral response characteristics.

Notice that, paragliders presenting large "effective dihedral" will respond to a lateral gust with aggressive translational acceleration, deviating quickly from the initial flight path what can be especially dangerous for takeoff, landing, and for obstacles clearance. On the other hand, paragliders with low "effective dihedral" may be very difficult to maneuver or even lateral-directionally instable. Finally, it is an obvious observation that the value of Γ_{ef} must be negative and it is a consequence of wing curvature. Also, despite the use of the term "dihedral" which is better to generalize the nomenclature, for the reasons exposed above, normal paragliders will present "anhedral".

The lateral static stability condition establishes that A_r must be negative. Mathematically, this can be expressed as:

$$\int_{-b/2}^{b/2} |f_z(y)| \cdot sin(\delta)^2 \cdot f_c(y) \cdot dy > \int_{-b/2}^{b/2} \left(\frac{sin(2 \cdot \delta)}{2} \cdot y\right) \cdot f_c(y) \cdot dy \tag{8.8}$$

The features that contribute to satisfy this condition are the same ones observed in figure 8.5:

- Increased CG height
- Low span
- Low taper ratio
- Increased anhedral

The wing geometry completely defines the lateral static stability condition. Also, it is important to notice the obvious critical condition of zero curvature. In this point the roll arm is zero and the stability is theoretically neutral.

Figure 8.5 below shows how the variation in some design parameters may affect static lateral stability:

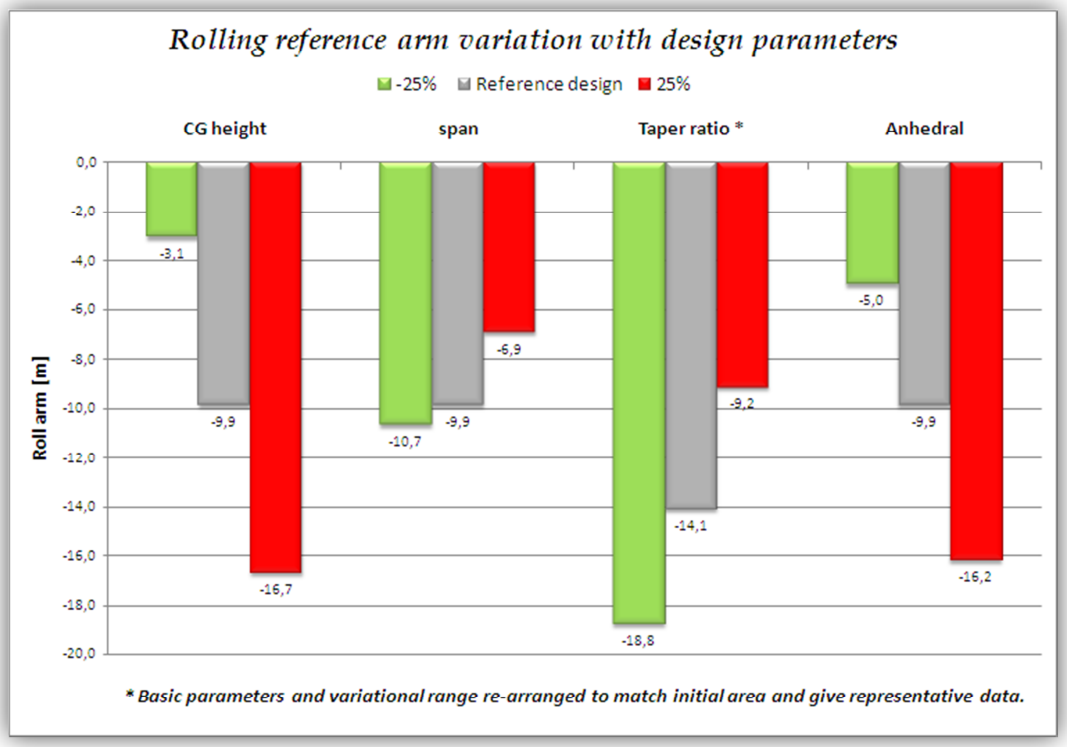

Figure 8.5 – Lateral static stability analysis – Roll arm variation with design parameters

As expected the major effect of the CG height and anhedral improving lateral stability is clear. It can also be noticed a positive effect of decreasing span and taper ratio, both related to the concentration of the aerodynamic resultants on the center of the wing.

For the directional static stability it is not easy to reach algebraic analytical expressions to mathematically represent the positive stability condition using the design parameters. However some statistical assessments based on numerical observations can help us to understand how directional static stability varies.

It is expected that forward CG positions and an increased span will improve directional static stability. And it is easy to imagine that in a tailless aircraft the span will have a major effect among all related variables. Figure 8.6 below shows how variations in the involved design parameters may affect static directional stability and corroborate the thoughts above:

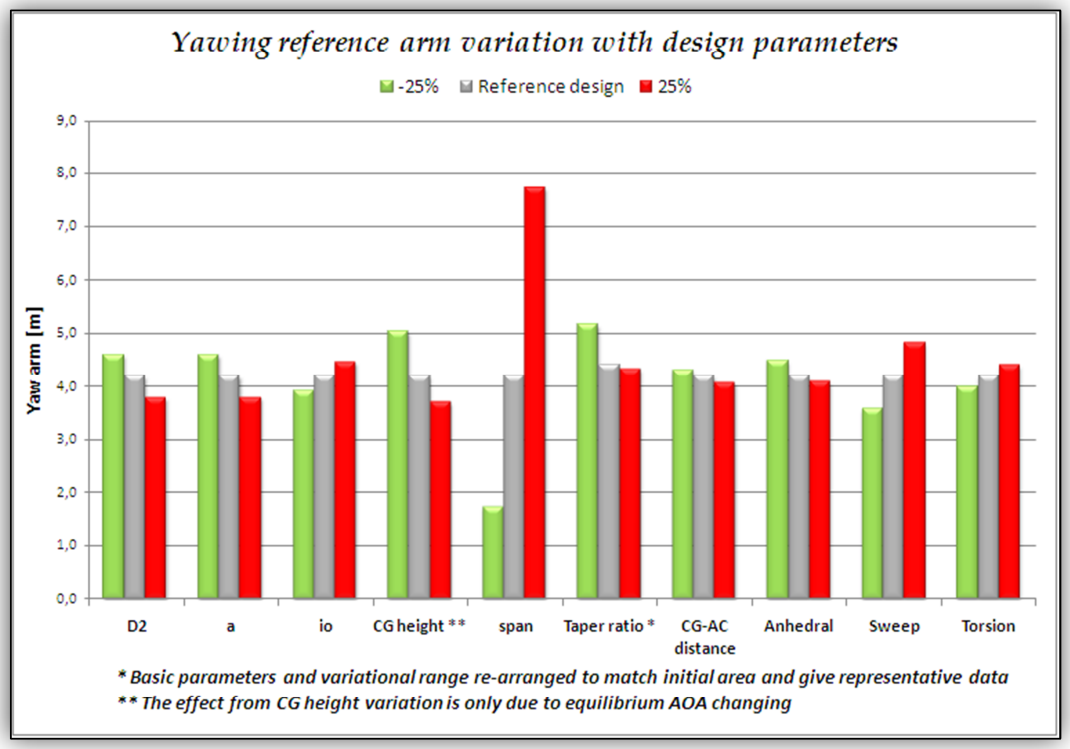

Figure 8.6 – Directional Static Stability Analysis – Yaw arm variation with design parameters

The above tendencies must not be taken as a general true. The effects show in figure 8.4 derives from a specific theoretical model and aims to show the impact of design variables adjustments for a typical wing. However, it is possible to design a directionally instable wing and the variations exhibited above would be invalid. A wing will be directionally instable for some low span and aft CG combinations, but in general this kind of situation is unlikely for normal design parameters.

Finally, it is worthy to mention that the lateral and directional static stability characteristics are not enough to judge paraglider's behavior at all. Paraglider's lateral-directional response presents a strong dependency on wing's rotational movements. As will be shown in the following sections, different combinations of design parameters will result different behaviors which cannot be related directly to the static parameters.

8.2. Lateral-Directional Dynamic Stability

The lateral-directional dynamic stability is characterized by the capability of the system to recover from an asymmetrical disturbance. The lateral and directional motions are strongly coupled, and unlike the longitudinal case it comprehends variables in different planes. In this way, simplifications using the equations of motion become more difficult to be developed and has its use more restricted.

In any aircraft the lateral and directional motions are related to asymmetrical aerodynamic forces distribution over the wing, and this effect is even more relevant in tailless aircrafts (Thorpe, 1948). In paragliders, the definition of basic design parameters as span, chord length distribution, dihedral, and CG positioning determines the general forces and moments distribution which may prioritize the lateral or the directional reaction. Because of that, for some movements, it is complicate to define general behaviors applicable for all possible designs.

In general, paragliders present a strong lateral stability due to the increased anhedral and high vertical CG position (Hiraki, 2003; Rogallo, 1960). However, the directional stability strongly depends on the design parameters and may be very poor. Another particular propriety of paragliders is the potential coupling between longitudinal and lateral-directional modes. Although the classic stability and control theory may be used to analyze paragliders giving reasonable results, the differences encountered in paraglider's lateral-directional behavior must be carefully taken into account.

By practical observation of paraglider flight, it can be seen a factual characteristics of paraglider's lateral-directional responses: When submitted to a representative asymmetrical gust, paragliders starts to roll and change heading trying to realign with the relative wind and eliminating sideslip. The quick heading response is due to the low moment of inertia in the vertical axis and lack of vertical stabilizer which degrades yaw damping capability, the representativeness of the roll rate is mostly a function of geometric characteristics linked especially to the CG height and wing anhedral, these two rotations are companied by a small attitude oscillation, which all together will be felt by the pilot as an asymmetric turbulence. For a gust coming from the right-hand side, a pressure increase on the left-hand-side semi-wing will be felt and an unsteady combination of positive yaw, negative roll and small attitude oscillations will appears. The subsequent movement depends on design characteristics and can be in two ways: For paragliders presenting lateral-directional modes as in conventional airplanes, the resultant movement could be a classic short-period lateral-directional oscillation (Dutch roll). For common paraglider presenting the roll-spiral coupling phenomenon, the

response will be a combination of two oscillatory motions, composed by the previously mentioned short-period oscillation (Dutch roll) and a second mode which is a rolling-yawing long-period oscillation know as the "lateral phugoid". Differently from conventional airplanes, the incidence of this coupled mode is the most common situation for paragliders. In fact, paragliders not presenting roll-spiral coupling are almost always instable, and presents unacceptable handling characteristics. In rare cases where there isn't roll-spiral coupling and the wing is still stable, the Dutch-roll is the dominant mode and the roll mode and spiral mode presents no relevance for the wing's response. For the most common cases where roll-spiral coupling is present, the Dutch-roll is a relatively fast transient which is heavily damped and can be understood as a sideslip adjustment oscillation which will induce the dominant lateral phugoid exhibiting a long-term combination of roll rate and yaw rate.

Making a parallel to the comments in chapter 7, an especially dangerous and important characteristic that could also be observed for lateral-directional motions are pilot-induced-oscillations (PIO). However, the strong level of lateral damping commonly observed in paragliders make such concerns unnecessary (Pagen, 2001).

To analyze lateral-directional stability the equations of motion derived in chapter 5 will be used together with classical state-space control theory (Ogata, 2003) exactly as proceeded previously in chapter 7 for the longitudinal stability study. However, due to the increased difficulties in obtaining reasonable approximations of the different types of motion, no simplified assessment will be proposed.

8.2.1 Lateral-Directional motion – state-space assessment

To obtain the lateral-directional stability characteristic parameters the concepts of modern control theory can be applied using the previously derived equations of motion and the concept of state-space variables (Tewari, 2002).

The equations of lateral-directional motion are written as:

$$\dot{V} = \frac{Y_{RES}}{m} - R \cdot U + P \cdot W \tag{8.9}$$

$$\dot{P} = \frac{(I_z \cdot M_x + I_{xz} \cdot M_z)}{(I_x \cdot I_z - {I_{xz}}^2)} + \frac{I_{xz} \cdot (I_x - I_y + I_z)}{(I_x \cdot I_z - {I_{xz}}^2)} \cdot Q \cdot P + \frac{(I_z \cdot (I_y - I_z) - {I_{xz}}^2)}{(I_x \cdot I_z - {I_{xz}}^2)} \cdot Q \cdot R \tag{8.10}$$

$$\dot{R} = \frac{(I_{xz} \cdot M_x + I_x \cdot M_z)}{(I_z \cdot I_x - {I_{xz}}^2)} - \frac{(I_x \cdot (I_y - I_x) - {I_{xz}}^2)}{(I_z \cdot I_x - {I_{xz}}^2)} \cdot Q \cdot P - \frac{I_{xz} \cdot (I_x - I_y + I_z)}{(I_z \cdot I_x - {I_{xz}}^2)} \cdot Q \cdot R$$

(8.11)

As for the lateral translational and rotational speeds the steady state values are null, the instantaneous condition and the respective disturbance are coincident.

$$\dot{V} = \dot{v}; \qquad p = P; \qquad r = R$$

(8.12)

By using a linear approximation of the initial set of equations near to the equilibrium, considering small disturbances and disregarding second order terms, it follows:

$$m \cdot \dot{V} = \sum_{j=U}^{\delta_{Bl}} \frac{\partial Y_{RES}}{\partial j} - R \cdot m \cdot U_{eq} + P \cdot m \cdot W_{eq}$$

(8.13)

$$\dot{P} = \frac{I_z}{I_x \cdot I_z - {I_{xz}}^2} \cdot \sum_{j=U}^{\delta_{Bl}} \frac{\partial M_x}{\partial j} + \frac{I_{xz}}{I_x \cdot I_z - {I_{xz}}^2} \cdot \sum_{j=U}^{\delta_{Bl}} \frac{\partial M_z}{\partial j}$$

(8.14)

$$\dot{R} = \frac{I_{xz}}{I_x \cdot I_z - {I_{xz}}^2} \cdot \sum_{j=U}^{\delta_{Bl}} \frac{\partial M_x}{\partial j} + \frac{I_x}{I_x \cdot I_z - {I_{xz}}^2} \cdot \sum_{j=U}^{\delta_{Bl}} \frac{\partial M_z}{\partial j}$$

(8.15)

Considering that the term I_{xz} is negligible, the linear approximation can be rewritten as:

$$m \cdot \dot{V} = \sum_{j=U}^{\delta_{Bl}} \frac{\partial Y_{RES}}{\partial j} - R \cdot m \cdot U_{eq} + P \cdot m \cdot W_{eq}$$

(8.16)

$$I_x \cdot \dot{P} = \sum_{j=U}^{\delta_{Bl}} \frac{\partial M_x}{\partial j}$$

(8.17)

$$I_z \cdot \dot{R} = \sum_{j=U}^{\delta_{Bl}} \frac{\partial M_z}{\partial j}$$

(8.18)

Applying the simplified formulation for the system's forces and moments components as proposed in chapter 5, it can be written:

$$\vec{R}_{RES} = \vec{R}_w + \vec{F}_{CG} \tag{8.19}$$

Where:

$$F_{y_{CG}} = m \cdot g \cdot cos(\Theta_{\mathrm{eq}}) \cdot \emptyset$$

$$\begin{bmatrix} F_{y_w} \\ M_{x_w} \\ M_{z_w} \end{bmatrix} = \begin{bmatrix} \frac{\partial F_{y_w}}{\partial U}|_{eq} & \frac{\partial F_{y_w}}{\partial P}|_{eq} & \frac{\partial F_{y_w}}{\partial R}|_{eq} & \frac{\partial F_{y_w}}{\partial \delta_{\mathrm{B}_r}}|_{eq} & \frac{\partial F_{y_w}}{\partial \delta_{\mathrm{B}_l}}|_{eq} \\ \frac{\partial M_{x_w}}{\partial V}|_{eq} & \frac{\partial M_{x_w}}{\partial P}|_{eq} & \frac{\partial M_{x_w}}{\partial R}|_{eq} & \frac{\partial M_{x_w}}{\partial \delta_{\mathrm{B}_r}}|_{eq} & \frac{\partial M_{x_w}}{\partial \delta_{\mathrm{B}_l}}|_{eq} \\ \frac{\partial M_{z_w}}{\partial V}|_{eq} & \frac{\partial M_{z_w}}{\partial P}|_{eq} & \frac{\partial M_{z_w}}{\partial R}|_{eq} & \frac{\partial M_{z_w}}{\partial \delta_{\mathrm{B}_r}}|_{eq} & \frac{\partial M_{z_w}}{\partial \delta_{\mathrm{B}_l}}|_{eq} \end{bmatrix} \cdot \begin{bmatrix} \mathrm{v} \\ \mathrm{P} \\ \mathrm{R} \\ \delta_{\mathrm{B}_r} \\ \delta_{\mathrm{B}_l} \end{bmatrix}$$

Then, the equations of motion can be rewritten as:

$$\begin{bmatrix} \dot{v} \\ \ddot{\emptyset} \\ \ddot{\psi} \end{bmatrix} = \begin{bmatrix} Y_v & Y_{\dot{\phi}} & Y_{\phi} & Y_{\dot{\psi}} & Y_{\delta_{B_l}} & Y_{\delta_{B_r}} \\ M_{X_v} & M_{X_{\dot{\phi}}} & 0 & M_{X_{\dot{\psi}}} & M_{X_{\delta_{B_l}}} & M_{X_{\delta_{B_r}}} \\ M_{Z_v} & M_{Z_{\dot{\phi}}} & 0 & M_{Z_{\dot{\psi}}} & M_{Z_{\delta_{B_l}}} & M_{Z_{\delta_{B_r}}} \end{bmatrix} \cdot \begin{bmatrix} v \\ P \\ \emptyset \\ R \\ \delta_{B_l} \\ \delta_{B_r} \end{bmatrix} \tag{8.20}$$

However, to use the benefits of classical state-space description, the system above can be re-arranged as:

$$\begin{bmatrix} \dot{v} \\ \ddot{\emptyset} \\ \ddot{\psi} \\ \dot{\emptyset} \end{bmatrix} = \begin{bmatrix} Y_v & Y_{\dot{\phi}} & Y_{\dot{\psi}} & Y_{\phi} \\ M_{X_v} & M_{X_{\dot{\phi}}} & M_{X_{\dot{\psi}}} & 0 \\ M_{Z_v} & M_{Z_{\dot{\phi}}} & M_{Z_{\dot{\psi}}} & 0 \\ 0 & 1 & 0 & 0 \end{bmatrix} \cdot \begin{bmatrix} v \\ P \\ R \\ \emptyset \end{bmatrix} + \begin{bmatrix} Y_{\delta_{B_r}} \\ M_{X_{\delta_{B_r}}} \\ M_{Z_{\delta_{B_r}}} \\ 0 \end{bmatrix} \cdot \delta_{B_r} + \begin{bmatrix} Y_{\delta_{B_l}} \\ M_{X_{\delta_{B_l}}} \\ M_{Z_{\delta_{B_l}}} \\ 0 \end{bmatrix} \cdot \delta_{B_l} \tag{8.21}$$

Which represents a standard state-space system in the form: $\left\{\dot{x}_{(t)} = A \cdot x_{(t)} + B \cdot \delta_{B_r(t)} + C \cdot \delta_{B_l(t)}\right\}$. Therefore applying Laplace's transformation (Ogata, 2003) and considering non-null initial conditions it can be obtained:

$$s \cdot \begin{bmatrix} V_{(s)} \\ P_{(s)} \\ R_{(s)} \\ \phi_{(s)} \end{bmatrix} = \begin{bmatrix} Y_v & Y_{\dot{\phi}} & Y_{\dot{\psi}} & Y_{\phi} \\ M_{X_v} & M_{X_{\dot{\phi}}} & M_{X_{\dot{\psi}}} & 0 \\ M_{Z_v} & M_{Z_{\dot{\phi}}} & M_{Z_{\dot{\psi}}} & 0 \\ 0 & 1 & 0 & 0 \end{bmatrix} \cdot \begin{bmatrix} V_{(s)} \\ P_{(s)} \\ R_{(s)} \\ \phi_{(s)} \end{bmatrix} + \begin{bmatrix} Y_{\delta_{Br}} \\ M_{X_{\delta_{Br}}} \\ M_{Z_{\delta_{Br}}} \\ 0 \end{bmatrix} \cdot \delta_{Br(s)} + \begin{bmatrix} Y_{\delta_{Bl}} \\ M_{X_{\delta_{Bl}}} \\ M_{Z_{\delta_{Bl}}} \\ 0 \end{bmatrix} \cdot \delta_{Bl(s)} + \begin{bmatrix} v_{(0)} \\ P_{(0)} \\ R_{(0)} \\ \phi_{(0)} \end{bmatrix}$$

(8.22)

Notice that the entries of the system can be divided in two groups. The effect of command actuation and initial disturbances (normally related to atmospheric activity). These two kinds of inputs can be considered separately, and, although some brakes inputs will be assessed as a source of disturbance, this chapter will focus on initial non-commanded disturbances. The equation above can be expressed in the form: $\left\{s \cdot X_{(s)} = A \cdot X_{(s)} + B \cdot \delta_{B_r(t)} + C \cdot \delta_{B_l(t)} + x_{(0)}\right\}$, and is equivalent to the following presentation in time's domain:

$$\dot{x}_{(t)} = A \cdot x_{(t)} + B \cdot \delta_{B_r(t)} + C \cdot \delta_{B_l(t)} + x_{(0)} \cdot \delta(1)$$

(8.23)

Where the term $\delta(1)$ is the Dirac's delta, denoting an impulse function to represents an initial disturbed condition. As the outputs of interest are the dynamic variables itself, the output matrix is simply the unit matrix. Therefore, the system can be represented in a block diagram as follows:

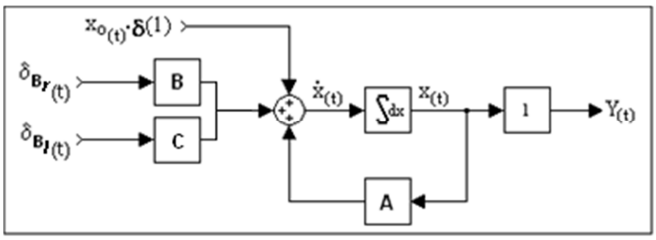

Figure 8.7 – Lateral-Directional motion state space model

The terms in the system above are given by:

Table 8-1: Lateral-Directional stability derivatives

$Y_v = \frac{1}{\mathrm{m}} \cdot \frac{\partial Y_V}{\partial v}\|_{eq}$	$M_{X_v} = \frac{\frac{\partial M_x}{\partial V}\|_{eq}}{I_x}$	$M_{Z_v} = \frac{\frac{\partial M_z}{\partial V}\|_{eq}}{I_z}$
$Y_{\dot{\phi}} = \frac{1}{\mathrm{m}} \cdot \frac{\partial Y_V}{\partial P}\|_{eq} + W_{eq}$	$M_{X_{\dot{\phi}}} = \frac{\frac{\partial M_x}{\partial P}\|_{eq}}{I_x}$	$M_{Z_{\dot{\phi}}} = \frac{\frac{\partial M_z}{\partial P}\|_{eq}}{I_z}$
$Y_{\phi} = g \cdot cos(\Theta\|_{eq})$	-	-
$Y_{\dot{\psi}} = \frac{1}{\mathrm{m}} \cdot \frac{\partial Y_V}{\partial R}\|_{eq} - U_{eq}$	$M_{X_{\dot{\psi}}} = \frac{\frac{\partial M_x}{\partial R}\|_{eq}}{I_x}$	$M_{Z_{\dot{\psi}}} = \frac{\frac{\partial M_z}{\partial R}\|_{eq}}{I_z}$
$Y_{\delta_{\mathrm{B}l}} = \frac{1}{\mathrm{m}} \cdot \frac{\partial X_V}{\partial \delta_{\mathrm{B}_l}}\|_{eq}$	$M_{X_{\delta_{\mathrm{B}l}}} = \frac{\frac{\partial M_x}{\partial \delta_{\mathrm{B}_l}}\|_{eq}}{I_x}$	$M_{Z_{\delta_{\mathrm{B}l}}} = \frac{\frac{\partial M_z}{\partial \delta_{\mathrm{B}_l}}\|_{eq}}{I_z}$
$Y_{\delta_{\mathrm{B}r}} = \frac{1}{\mathrm{m}} \cdot \frac{\partial X_V}{\partial \delta_{\mathrm{B}_r}}\|_{eq}$	$M_{X_{\delta_{\mathrm{B}r}}} = \frac{\frac{\partial M_x}{\partial \delta_{\mathrm{B}_r}}\|_{eq}}{I_x}$	$M_{Z_{\delta_{\mathrm{B}r}}} = \frac{\frac{\partial M_z}{\partial \delta_{\mathrm{B}_r}}\|_{eq}}{I_z}$

Where the derivative terms can be obtained as suggested in chapter 5.

Considering null initial conditions, equation (8.22) can also be written as:

$$\begin{bmatrix} s - Y_v & -\left(Y_{\dot{\phi}} \cdot s + Y_{\phi}\right) & -s \cdot Y_{\dot{\psi}} \\ -M_{X_v} & s^2 - s \cdot M_{X_{\dot{\phi}}} & -s \cdot M_{X_{\dot{\psi}}} \\ -M_{Z_v} & -s \cdot M_{Z_{\dot{\phi}}} & s^2 - s \cdot M_{Z_{\dot{\psi}}} \end{bmatrix} \cdot \begin{bmatrix} V_{(s)} \\ \phi_{(s)} \\ \psi_{(s)} \end{bmatrix} = \begin{bmatrix} Y_{\delta_{B_r}} \\ M_{X_{\delta_{B_r}}} \\ M_{Z_{\delta_{B_r}}} \end{bmatrix} \cdot \delta_{B_{r_{(s)}}} + \begin{bmatrix} Y_{\delta_{B_l}} \\ M_{X_{\delta_{B_l}}} \\ M_{Z_{\delta_{B_l}}} \end{bmatrix} \cdot \delta_{B_{l_{(s)}}} \tag{8.24}$$

Finally, the characteristic equation do not depends on the inputs and it is given by the following determinant:

$$\begin{vmatrix} (s - Y_v) & \left(-Y_{\dot{\phi}} \cdot s - Y_{\phi}\right) & -Y_{\dot{\psi}} \cdot s \\ -M_{X_v} & \left(s^2 - M_{X_{\dot{\phi}}} \cdot s\right) & -M_{X_{\dot{\psi}}} \cdot s \\ -M_{Z_v} & -M_{Z_{\dot{\phi}}} \cdot s & \left(s^2 - M_{Z_{\dot{\psi}}} \cdot s\right) \end{vmatrix} = K_{lat}^5 \cdot s^5 + K_{lat}^4 \cdot s^4 + K_{lat}^3 \cdot s^3 + K_{lat}^2 \cdot s^2 + K_{lat}^1 \cdot s \tag{8.25}$$

Where:

$$\begin{bmatrix} K_{lat}^5 \\ K_{at}^4 \\ K_{lat}^3 \\ K_{lat}^2 \\ K_{lat}^1 \end{bmatrix} = \begin{bmatrix} 1 \\ -\left(Y_v + M_{X_{\dot{\phi}}} + M_{Z_{\dot{\psi}}}\right) \\ Y_v \cdot \left(M_{X_{\dot{\phi}}} + M_{Z_{\dot{\psi}}}\right) + M_{X_{\dot{\phi}}} \cdot M_{Z_{\dot{\psi}}} - M_{Z_{\dot{\phi}}} \cdot M_{X_{\dot{\psi}}} - Y_{\dot{\psi}} \cdot M_{Z_v} - Y_{\dot{\phi}} \cdot M_{X_v} \\ Y_v \cdot \left(M_{Z_{\dot{\phi}}} \cdot M_{X_{\dot{\psi}}} - M_{X_{\dot{\phi}}} \cdot M_{Z_{\dot{\psi}}}\right) + Y_{\dot{\phi}} \cdot \left(M_{X_v} \cdot M_{Z_{\dot{\psi}}} - M_{X_{\dot{\psi}}} \cdot M_{Z_v}\right) + Y_{\dot{\psi}} \cdot \left(M_{Z_v} \cdot M_{X_{\dot{\phi}}} - M_{X_v} \cdot M_{Z_{\dot{\phi}}}\right) - Y_{\dot{\phi}} \cdot M_{X_v} \\ Y_{\dot{\phi}} \cdot \left(M_{X_v} \cdot M_{Z_{\dot{\psi}}} - M_{X_{\dot{\psi}}} \cdot M_{Z_v}\right) \end{bmatrix}$$

At this point it is already possible to determine if the system is dynamically stable by applying the Routh's criterion well explained in control theory classical literature (Ogata, 2003).

By solving the fifth order polynomial equation, in most cases it will be found the two pairs of complex roots related to the short period and the lateral phugoid mode, and a zero regarding to the neutral heading stability. In this situation:

$$\left(K_{lat}^5 \cdot \mathrm{s}^5 + K_{lat}^4 \cdot \mathrm{s}^4 + K_{lat}^3 \cdot \mathrm{s}^3 + K_{lat}^2 \cdot \mathrm{s}^2 + K_{lat}^1 \cdot \mathrm{s} = 0\right)$$
$$\rightarrow \left(r_{sp}^R + r_{sp}^I \cdot i\right);\ \left(r_{lp}^R + r_{lp}^I \cdot i\right);\ e\ 0$$

Using these roots, the basic parameters can be calculated as follows:

$$\omega_{n_{DR}} = \sqrt{\left(r_{sp}^R\right)^2 + \left(r_{sp}^I\right)^2} \qquad \omega_{n_{lp}} = \sqrt{\left(r_{lp}^R\right)^2 + \left(r_{lp}^I\right)^2}$$

$$\xi_{DR} = -\frac{r_{sp}^R}{\sqrt{\left(r_{sp}^R\right)^2 + \left(r_{sp}^I\right)^2}} \qquad \xi_{lp} = -\frac{r_{sp}^R}{\sqrt{\left(r_{lp}^R\right)^2 + \left(r_{lp}^I\right)^2}}$$

Finally, it can be defined the characteristic parameters for each mode as proposed in table 8-2:

Table 8-2: Lateral-Directional stability characteristic parameters

Oscillation Period:	Cicles to damp (reduction to 5%):
$T_{DR} = \frac{2 \cdot \pi}{\omega_{n_{sp}} \cdot \sqrt{1 - \xi_{sp}^2}}$	$CTD_{DR}^{5\%} \approx \frac{1}{2 \cdot \xi_{sp}}$
$T_{lp} = \frac{2 \cdot \pi}{\omega_{n_{lp}} \cdot \sqrt{1 - \xi_{lp}^2}}$	$CTD_{lp}^{5\%} \approx \frac{1}{2 \cdot \xi_{lp}}$

Both stability parameters derived here are necessary to characterize the lateral-directional behavior. The period of oscillation allows judging if the motion is too fast revealing a violent response, or if it is in the range of pilot's reactions contributing for PIO. The number of cycles to

damp gives an indication about the system's ability to re-equilibrate without pilot's action, or in other words, the "level of lateral-directional damping".

The discussion above provides the results about paraglider's lateral-directional dynamics; however, it was assumed that the characteristic equation result two pairs of complex roots. It must be investigated the cases where this hypotheses do not applies and the consequent implications.

8.2.1.1 Lateral-Directional characteristic equation possible results:

By solving the fifth order polynomial equation, it will be found a null root due to an indifferent mode relative to heading, and, depending on the design parameters: two pairs of complex roots (related to the short period and the phugoid modes); or one pairs of complex roots (relative to the short period mode) and two real roots (related to pure roll and spiral modes).

It can be noticed that the characteristic equation is pretty complicated, being hard to establishes any direct relations between design parameters and stability characteristics. However, by exploring the common proprieties of the lateral-directional derivative terms it can be revealed many important characteristics of the lateral-directional response.

It is immediate to see that the three disturbances involved in lateral-directional stability analysis are linked respectively to sideslip, roll and yaw. It is also easy to conclude that the sideslip effects are basically covered in the static analysis of section 8.1, however, the effects originated from roll and yaw deserves dedicated attention. As it is illustrated in figure 8.8 below, it is possible to make important conclusions about the derivative terms using a qualitative analysis of the physical phenomenon involved.

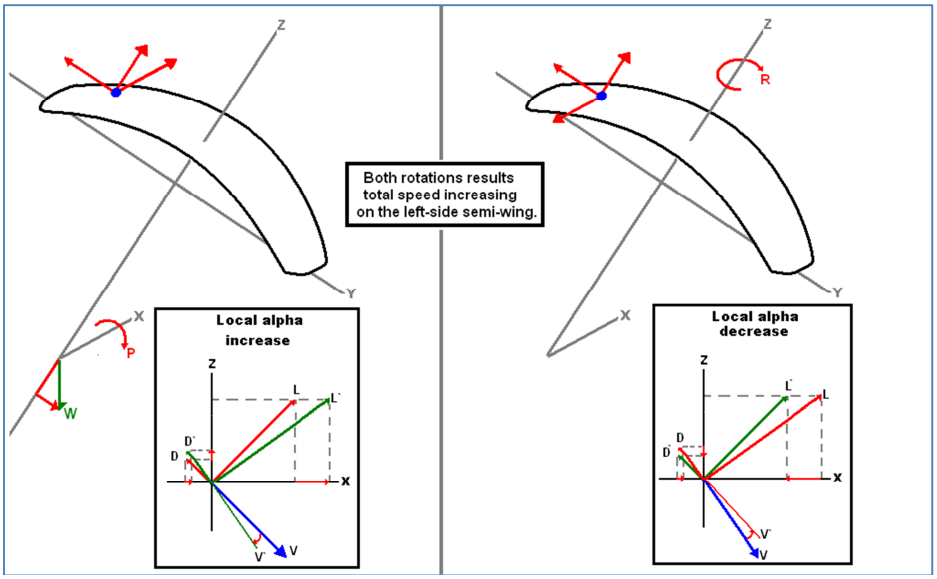

Figure 8.8 – Roll and Yaw rate effects on lateral-directional resultants.

Using the previous developments up to this point it is possible to observe that:

- Y_v is always negative because the incidence of a positive lateral speed component will obviously increase the aerodynamic reactions in the opposite direction, both at the wing and at the CG.

- M_{X_v} is always negative for laterally stable wings as discussed in section 8.1.

- M_{Z_v} is always positive for directionally stable wings as discussed in section 8.1.

- $Y_{\dot{\phi}}$ can be ether positive or negative. A positive roll rate will generate a positive lateral speed component which results a negative lateral aerodynamic force component. Also, a positive force component will be generated as a component of the gravitational force due to the bank angle. A positive resultant will be the case only if the weight force component be greater than the lateral wing`s resultant aerodynamic force originated by the asymmetrical lift distribution. Such case will occur for wings with low effective dihedral and low CG height.

- $M_{X_{\dot{\phi}}}$ must be negative to provide "roll-rate" stability. Besides, although there is a chance to have this term positive for a combination of low dihedral, large span and reduced CG height, this kind of design would be limited by many other flight characteristics, and thus, it is valid to say that this term will be always negative for acceptable design parameters.

- $M_{Z\dot{\phi}}$ can be ether positive or negative. A positive roll rate can be understood as an increase in local AOA on the tips of the left side wing. It generates an aerodynamic resultants increase that will produce: a positive yaw moment due to the increase in X-axis resultant force on the left side, and may produce a negative or positive yaw moment due to the Y-axis resultant force depending on the relative position of the CG. Therefore, the resultant yaw moment will be positive for wings with forward CG positions, high sweep angle, and large span; and negative for wings with aft CG positions, low sweep angle, and small span. Commonly the span contribution is predominant for yaw, and thus, this term is often positive.

- $M_{X\dot{\psi}}$ is normally negative. A positive yaw rate can be understood as an increase in local penetration speed and consequent AOA reduction on the left side wing. The total speed increase combined with the AOA reduction will practically maintain the aerodynamic resultant modulus; however, it will be relatively rotated increasing the local Z-axis components and decreasing the X-axis components on that semi-wing. In this way, it will produce: a positive roll moment due to an increase in Z-axis resultant force on the left side, and a negative roll moment due to a lateral negative resultant in Y-axis. Because the contribution of the lateral force is commonly dominant for stable wings, this term is often negative.

- $M_{Z\dot{\psi}}$ is always negative. A positive yaw rate can be understood as an increase in local penetration speed and consequent AOA reduction on the left side wing. The total speed increase combined with the AOA reduction will practically maintain the aerodynamic resultant modulus; however, it will be relatively rotated increasing the local Z-axis components and decreasing the X-axis components on that semi-wing. In this way, it will produces: a negative yaw moment due to a relative increase in X-axis resultant force on the right side, and may produce a negative or positive yaw moment due to the Y-axis resultant force depending on the relative position of the CG. However, for normal design parameters the CG is behind AC and the contribution of the lateral component is also negative, besides, the contribution of the X-axis force potentiated by the wingspan is always dominant. Thus, this term is always negative.

It can be seen that the parameters above are basically driven by three geometric proprieties:

- The effective dihedral;

- The ratio between CG height and span, that will be called “PLP – Primary lateral proportion”;

- The ratio between span and CG to AC horizontal distance (measured from the AC to the CG as positive sense)

Among the parameters above, only $Y_{\dot{\phi}}$ and $M_{Z_{\dot{\phi}}}$ are expected to vary in signal. $Y_{\dot{\phi}}$ Will become positive for low effective dihedrals and $M_{Z_{\dot{\phi}}}$ will become negative for low values of CG to AC horizontal distances (d_0'). In this way, by inspecting the characteristic equation (8.22) some useful conclusions can be reached:

- K_{lat}^4 is always positive
- K_{lat}^3 is normally positive
- K_{lat}^2 can be ether positive or negative, and this term will normally determine the convergence or divergence of the dominant oscillatory mode. Because of that dedicated attention will be given to it.
- K_{lat}^1 is normally positive for stable wings

After some empirical investigations using normally expected values for the design parameters, it is possible to conclude that the occurrence of roll-spiral coupling is conditioned to the existence of relatively low values of the ratios $\frac{K_{lat}^4}{K_{lat}^1} and \frac{K_{lat}^2}{K_{lat}^1}$. For paragliders, the first ratio is normally a low positive value (varying between 0.1 and 2), and the second relation generally varies between -2 and 2. As a practical guidance, the possible occurrence of roll-spiral coupling can be pre-evaluated as follows:

- $if \ \frac{K_{lat}^2}{K_{lat}^1} \geq 2 \ OR \ \frac{K_{lat}^4}{K_{lat}^1} \geq 1 \rightarrow conventional \ roots$
- $if \ \frac{K_{lat}^4}{K_{lat}^1} < 2 \ and \ \frac{K_{lat}^4}{K_{lat}^1} < 1 \rightarrow coupled \ roots$

In this way, taking a deeper look into the both terms that may cause coupling it is possible to associate them to a main representative design parameter called the "lateral-coupling modulus":

$$L_c = \frac{180}{\pi} \cdot \left| \Gamma_{ef} \cdot \frac{h_0'}{b} \right| \tag{8.26}$$

This parameter can be understood as a measurement of the dominance of the rolling stability over yaw stability due to the accentuated curvature and high CG vertical distance. Considering the term above in degrees, when L_c reaches values above 5 (approximately) the coupling is likely to happen. As will be assessed below, for conventional airplanes this value is not supposed to trespass 2 but for paragliders it is normally above 5.

Comparing to conventional small airplanes, the parameter above will present a relatively higher absolute value. Notice that, for airplanes, because of the representativeness of the wingspan compared to CG high, the above parameter present very low values, what is aggravated by the low values of dihedral – negative or positive. On the other hand, paragliders will normally present increased negative dihedral combined with comparable values of CG high and wingspan.

Physically, a paragliders presenting roll-spiral coupling will present the short period mode (Dutch-roll) as a transient mode, just as the short period oscillation in paraglider`s longitudinal motion (see chapter 7). In this case, the transient will only initiate the lateral phugoid oscillation which will be the dominant and relevant oscillation.

8.2.2 Lateral-Directional response analysis:

The common expected lateral-directional disturbances are due to lateral gusts or turning maneuvers. The lateral-directional stability analysis will be concentrated in responses to gusts and other external disturbances. Command inputs will be better analyzed under controllability aspects on chapter 9.

A natural common source of longitudinal disturbance is a quick asymmetric command input, which will instantaneously change wing's force distribution. This is modeled as an impulse functions in time's domain, representing the initial inputs given by: $\delta_{B_r} \cdot \delta_1(t)$ or $\delta_{B_l} \cdot \delta_1(t)$

Where $\delta_1(t)$ is the unitary impulse function (Dirac's delta), and δ_B is the amount of brakes applied in fraction of available length in each side.

Considering a typical paraglider, figure 8.9 below shows system's response to a full right-side command impulse ($\delta_{B_r} = 1$) input.

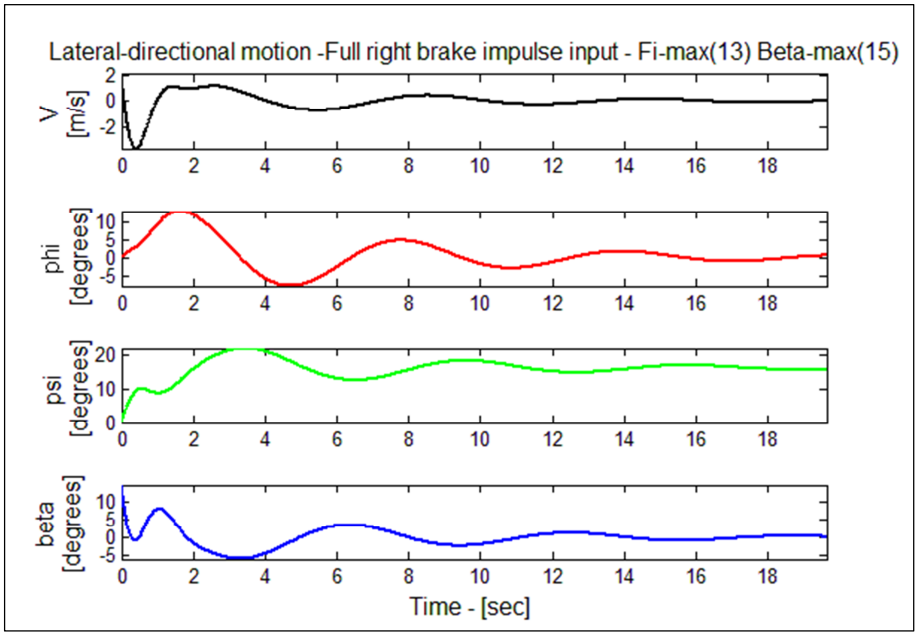

Figure 8.9 – Impulse response – General observation

As can be seen, the system recovering is very efficient, and it is clear the manifestation of an initial beta-adjustment followed by a medium-term lateral-directional oscillation. Applying a zoom in the initial portion of the movement the occurrence of the short period become more obvious as show in figure 8.10 below:

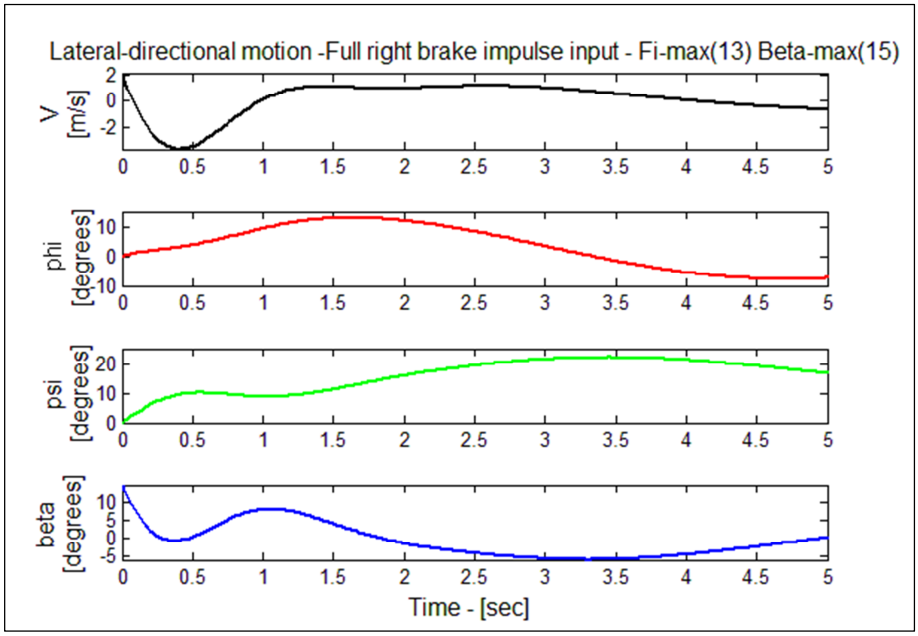

Figure 8.10 – Impulse response – Initial transient observation

In general, it can be seen that the asymmetric command impulse generates a damped and controllable oscillation. Actually, it is a fact that paraglider's presents very good lateral-directional stability due to the increased CG height.

Now, to evaluate wing's stability proprieties considering atmospheric disturbances susceptibility, it might be considered that the common expected lateral disturbances are normally originated by lateral gusts. In this way, it is accurate enough to define a standardized initial disturbed condition (initial state-variable), which can be modeled in time domain as a simple speed impulse function:

$$[0;\ v_0;\ 0;\ 0] \cdot \delta_1(t) \rightarrow \text{Lateral gust}$$

For the lateral gust, a reasonable value to assume as a representative disturbance is around 10km/h. Then, the "standard disturbance" can be approximated as:

$$v_0 = 3\ {}^{m}/_{s};$$

Using this standard disturbance, the system's responses can be simulated for systems presenting lateral coupling or conventional roots:

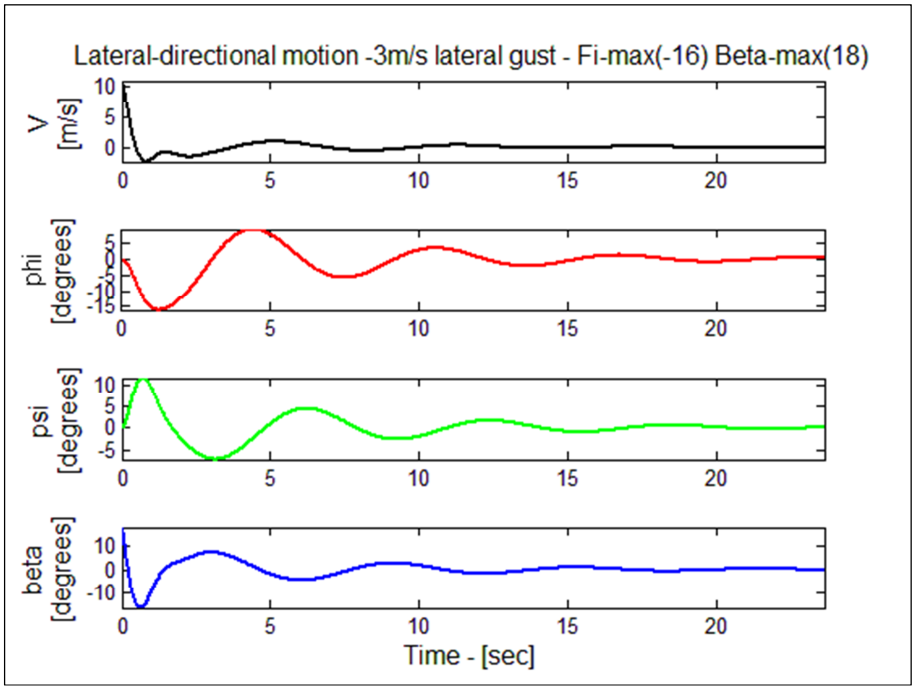

Figure 8.11 – Lateral-Directional Response to a 3m/s lateral gust – Coupled roots

For models presenting roll-spiral coupling it can be observed an efficient suppression of sideslip. Also, it can be seen that taking in account the rolling amplitudes the motion is felt basically as a single rolling response combined with a heading adjustment. This kind of reaction reveals a good lateral-directional behavior.

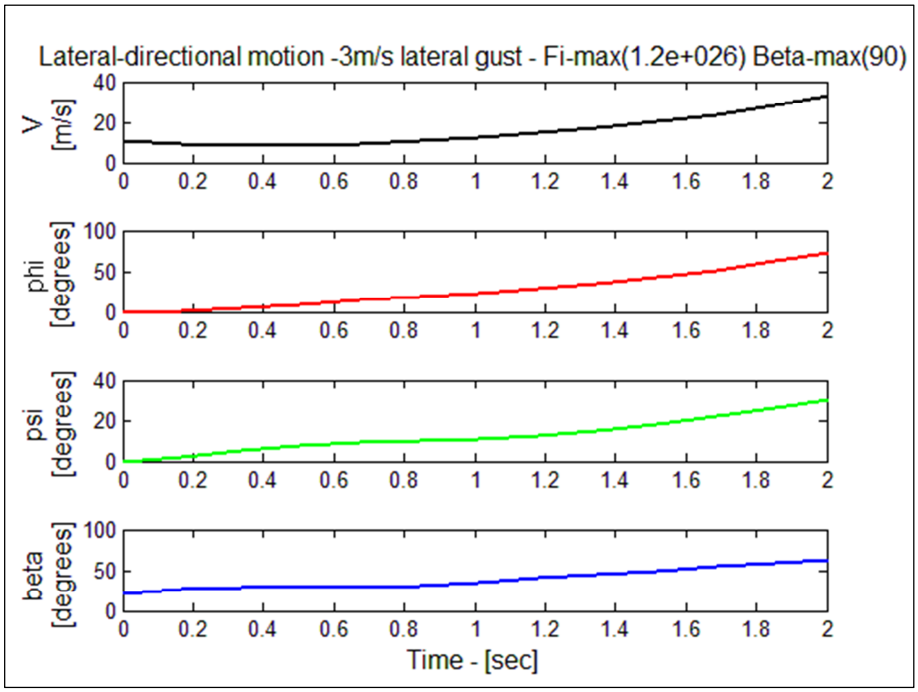

Figure 8.12 – Lateral-Directional Response to a 3m/s lateral gust – Conventional roots

For models presenting conventional roots it can be observed that the yawing response becomes more relevant, causing a rolling moment which do not counteract sideslip. It is a fact that no good yaw damping characteristics exists for tailless aircrafts, especially for those presenting low yawing inertias. Then, although there is an ineffective attempt to suppress sideslip at the beginning of the motion, the wing goes into a deep spiral where the yaw rate aggravates roll rate leading to an unstable behavior.

Taking in account the assessments up to here, it is possible to assume that no acceptable handling qualities will be achieved with paragliders presenting conventional roots. Then, the following analysis will only consider models which presents the roll-spiral coupling phenomenon.

As expected, the graphs confirm the results obtained from calculation using the characteristic equation and a new parameter is made available: The maximum amplitude of the oscillations.

The amplitude of the oscillation in bank and heading are important parameter because it is related to how the pilot is exposed to the disturbance. If the oscillation is significantly large and

the period of oscillation is short it means that the wing reacts violently, which is an undesirable behavior and, for lateral motions, it can result wing's asymmetric collapse.

The maximum attitude oscillation parameter can be defined using the sideslip input as:

$$\phi_{max} \; and \; \psi_{max}$$

The values of the maximum amplitudes for the case presented in figures 8.11 is shown below in table 8-3:

Table 8-3: Longitudinal motion maximum amplitudes

Standard oscillations maximum amplitudes					
Initial disturbance		v_{max} **km/h**	β_{max} **degrees**	ϕ_{max} **degrees**	ψ_{max} **degrees**
Sideslip	w_0=*3m/s*	10	18	-16	12

There are no good analytical approximations to calculate maximum amplitudes, in this way, numerical calculations are expected to be necessary to investigate relations with the design parameters. It can be noticed in table above that the tree angles stays in comparable ranges, however, the bank angle can be said to be more relevant for flight qualities analysis.

8.2.3 Conceptual design lateral-directional stability evaluations:

By analyzing different models using the developments presented until this point it is possible to compare the stability characteristics and take some valuable conclusions. Based on last sections discussions, the lateral-directional stability parameters are specially affected by the coupling modulus introduced in equation (8.26). Figure 8.13 below present the variation of lateral phugoid proprieties for some theoretical models.

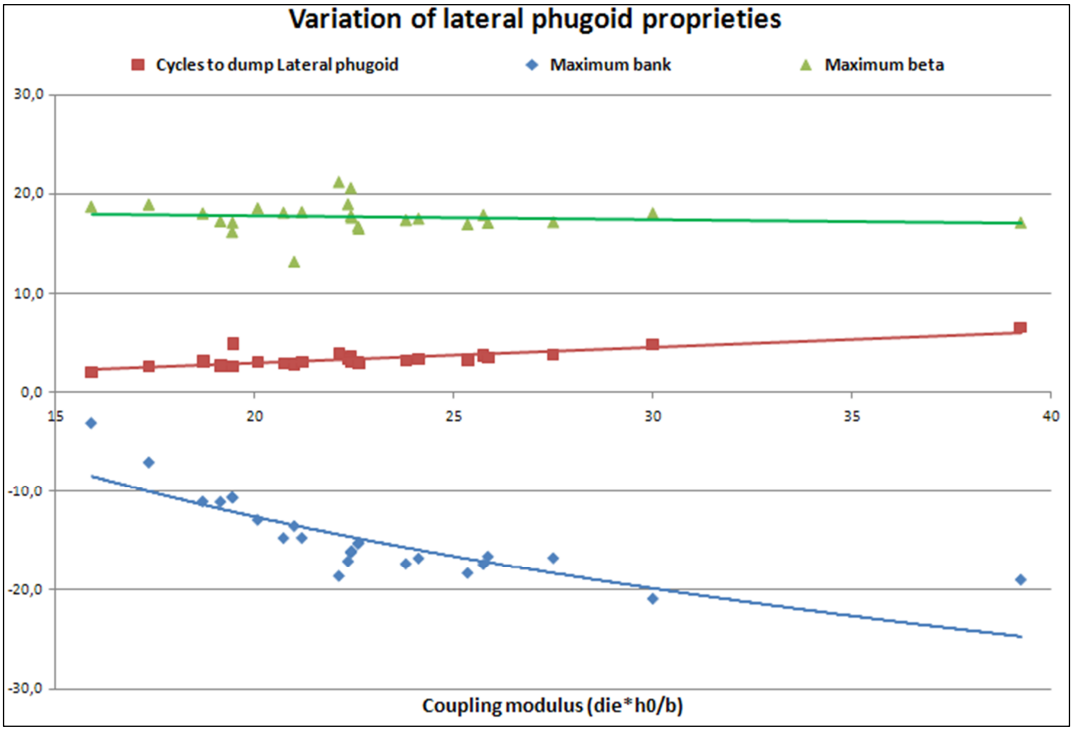

Figure 8.13 – Lateral-Phugoid proprieties variation with coupling modulus

It is noticeable that, both the maximum bank angle and number of cycles to damp increase relevantly as coupling modulus increases. Although there is a diminishing in maximum sideslip angle, the final result is for sure undesirable. In this way, it can be concluded that the lateral response characteristics could be improved by reducing the coupling modulus. However, it requires some constraints. When the coupling modulus diminishes the possibility to reach an uncoupled and unstable configuration becomes more likely. In this way, the observation here is valid up to values where the system's basic characteristics remain unchanged.

It is important to notice that, for a fixed horizontal CG position, by moving the CG down the longitudinal oscillatory amplitudes are diminished as presented in chapter 7, but the lateral-directional oscillatory amplitudes will be increased as shown in figure 8.13. Because of that, and also because there is no much freedom for dislocating CG horizontally, there is an important tradeoff between longitudinal and lateral-directional stability characteristics when defining CG height.

A final observation is that, for both lateral-directional or longitudinal stability, modifications in the aerodynamic proprieties may be helpful improving damping capability and reducing the oscillatory amplitudes. However, no simplified procedures or direct relations are available, and some empirical effort investigating different combinations of airfoils and wing geometry is supposed to be necessary.

8.3 Final Comments:

In this chapter it was presented the most important aspects of the lateral-directional stability characteristics of paragliders. It was presented the dynamics of lateral and directional responses and the parameters affecting the lateral-directional movements. In special, it was possible to verify that paragliders usually presents good lateral-directional stability characteristics due to the efficient roll damping capability.

It was shown that, due to the occurrence of a roll-spiral coupling phenomenon, the lateral-directional dynamics of common paragliders is characterized by the existence of two modes, the short-period and the lateral phugoid. This last mode substitutes the roll subsidence and the slow spiral movements, usually found in common airplanes, by another oscillatory mode. It was also shown that the short-period, or Dutch-roll, acts as a quickly damped transient and the lateral phugoid acts as a continuous rolling-yawing oscillation with good handling characteristics.

Finally, it was possible analyze some relations for conceptual design investigations, showing that the lateral-directional stability can be improved by working with variations in CG height, span and dihedral proportions.

9 PARAGLIDERS CONTROLLABILITY

The controllability is related to the capability to change heading, varying speed or recovering from an abnormal situation. It is obvious that controllability is a necessary capability of any aircraft, and especially for paragliders which are subjected to many local atmospheric disturbances and flies very close to the ground, controllability is also related to safety. Sometimes it is common to separate the concepts “controllability” and “maneuverability”, where, controllability denotes the ability to overcome disturbances sustaining equilibrated flight and maneuverability denotes the ability of efficiently change heading or generate bank angle. Actually, for flight dynamics analysis there are no differences in these concepts because the physical mechanisms that provide both capabilities are basically the same (Yechout, 2003).

For paragliders there are available three types of “commands”: The brakes, the accelerator (or speed-bar) and the CG shift. The last one is not exactly a “command” because it is not an independent mechanism, however, CG shifting is often used to supplement brakes effectiveness, and then, it can be understood as a supplementary control mean.

The available commands can be also divided regarding the plane of action. In this case it is easy to see that symmetric applications of brakes and any use of accelerator can be classified as longitudinal controls, whereas, asymmetric brakes application and cg shifting can be classified as lateral-directional controls. Such classification is useful to work separately with the longitudinal and lateral-directional characteristics as presented in chapters 7 and 8.

Finally, the controllability analysis can focus on specific common tasks. Those tasks are the most usual maneuvers present in paraglider flight. It can be established that the most relevant maneuvers to be analyzed are: Takeoff, Landing, Turning, longitudinal disturbance recovery, and Lateral-directional disturbance recovery.

In this chapter each one of the above mentioned control mechanisms and the related maneuvers will be analyzed in order to identify how the design parameters may affect paragliders controllability.

9.1. Flight Controls Modeling

To analyze the characteristics related to controllability, the flight controls mechanisms must be someway introduced into the dynamic model. The difficulties involved begins with the fact that, being the wing a flexible structure, any alteration in wing shape changes the aerodynamics characteristics, and then, the entire structure used to derive the dynamic model as proposed in chapter 5.

Below is discussed a proposition for simply modeling the flight controls in order to obtain reasonable basic results for conceptual design evaluations:

9.1.1 Brakes

The brakes system is basically a set of lines and pulleys linked to the wing's trailing edge. When these lines are pulled down, the wing presents a variable camber increase and local incidence angle changing. A simplified model relating brakes actuation to local AOA variation was proposed in chapter 5 to permit accounting for brakes inputs into the dynamic model. However, although such approach is enough to represent small and transient inputs, to properly evaluate controllability characteristics considering continuous full-brakes applications it would be necessary to consider the changing in aerodynamic proprieties caused by wing deformation. As commented by Slegers (2004), parafoil-payloads systems may present even command reversals at accentuated brake applications. Clearly, the efforts to develop a methodology to predict changes in aerodynamic coefficients due to brakes actuations would demand some advanced investigation technics as CFD and wind-tunnel tests which are out of the scope of this work.

Then, to allow reaching the objective to simply evaluate brakes application on a pre-design phase, the best option is to present an analytical assessment using the many conclusions and simplifications about paragliders dynamics obtained up to this point allied to the dynamic model generated to analyze system's stability.

The first parameter that must be derived to evaluate braking capability is the potential maximum angle of attack that can be achieved when brakes are applied. For that, the approximation given in chapter 6 relating the wing proprieties, CG position and AOA can be used adapting the zero-lift angle of attack to take in account an averaged effect of brakes actuation:

$$\propto_{eq} \approx \left[\frac{1}{\frac{h_0'}{d_0'} \cdot (1 - D_2 \cdot a)} - \frac{i_0 - \widetilde{\Delta\propto}(\delta_B)}{\left(\frac{1}{D_2 \cdot a} - 1\right)} \right] \tag{9.1}$$

Where, considering the model presented in chapter 5, $\widetilde{\Delta\propto}\,(\delta_B)$ represents an averaged effect of brakes application obtained as:

$$\widetilde{\Delta\propto}\,(\delta_B) = \frac{1}{b} \cdot \int_{-b/2}^{b/2} \left[\delta_B \cdot \delta_M \cdot \left(\left(\frac{100}{\delta_f} \right)^{\left(\frac{y}{b} - \frac{1}{2}\right)} + \left(\frac{100}{\delta_f} \right)^{\left(-\frac{y}{b} - \frac{1}{2}\right)} \right) \right] \cdot dy \tag{9.2}$$

Table 9-1 below presents the values of commanded AOA for different levels of brake inputs considering two different available brake lengths for a typical paraglider with en equilibrium AOA of 8.8°.

Table 9-1: Effect of symmetric brake application in equilibrium AOA

	Portion of brakes applied			
	25%	***50%***	***75%***	***100%***
20cm of available brake length	8.9°	9.5°	10.0°	10.4°
60cm of available brake length	10.3°	11.0°	11.8°	12.6°

With the new AOA, the flight speed can be recalculated considering the aerodynamic coefficients unchanged. Then, using the expression derived in chapter 6 relating flight speed to wing-load and lift coefficient, it can be applied:

$$V = \sqrt{\frac{w_l}{\frac{1}{2} \rho \cdot a \cdot \left(\alpha_{eq} - i_0 + \widetilde{\Delta\propto}(\delta_B) \right)}} \tag{9.3}$$

For a wing with initial flight speed of 34Km/h, this expression results the final flight speeds presented in table 9-2 below:

Table 9-2: Effect of symmetric brake application in flight speed

	Portion of brakes applied			
	25%	***50%***	***75%***	***100%***
20cm of available brake length	31.5 km/h	30.0 km/h	28.5 km/h	27.7 km/h
60cm of available brake length	28.0 km/h	27.4 km/h	26.7 km/h	24.8 km/h

It can be noticed a maximum reduction in flight speed around 5km/h, what is very reasonable considering practical observations (Pagen, 2001). The results above could be also obtained using a simulation with the dynamic model as presented in figure 9.1 below:

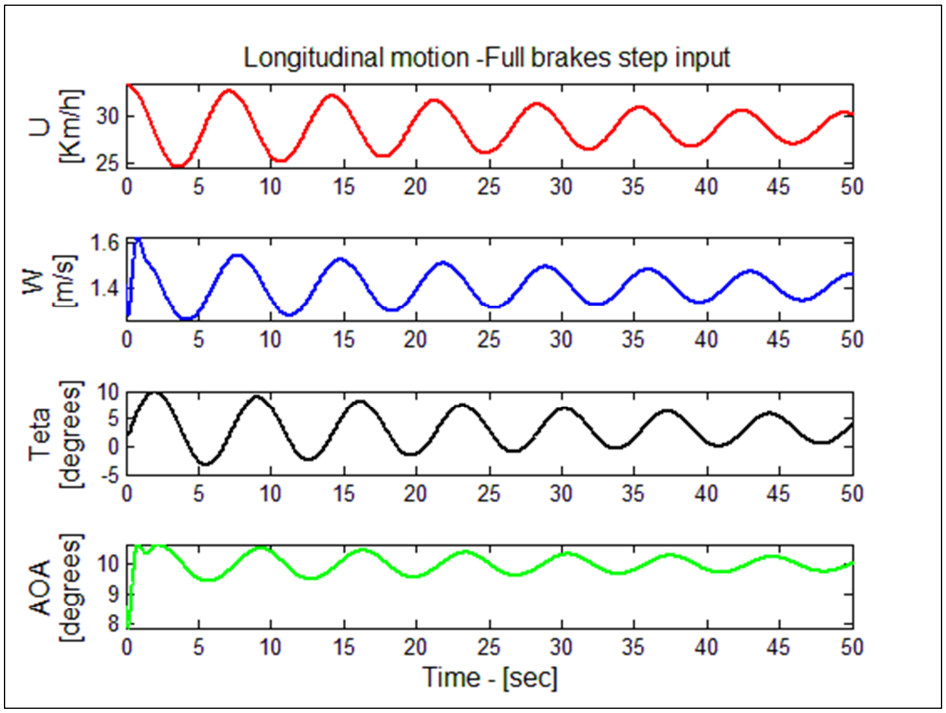

Figure 9.1 – Full brakes step input

The simulation of full brakes application shows comparable final results, however, it shows an unrealistic oscillation which is not compatible with practical observation. This is mainly due to the fact that when brakes are applied the aerodynamics coefficients changes, especially increasing damping capability which is already a relevant source of error in the derived linear model.

Finally, with the results up to here, it is possible for a defined available brake length to have a good idea about the control authority of a model. It is important to notice that up to this point only the symmetric actuation was analyzed. That's because it make sense to parameterize the control limits for equilibrated conditions. However, assessments about asymmetric inputs and turning performance will be carried out in section 9.2.3.

9.1.2 Accelerator

The accelerator, or speed bar, consists of a system of lines and pulleys linked to the leading edge of the wing. When this device is actuated the leading edge comes down diminishing the

angle of attack and speeding up the wing. It is possible to use the same strategy used to evaluate brakes applications, which means, to use an adaptation of the simplified formulation from chapter 6. However, for the accelerator it is easier to define the averaged variation in angle of attack as illustrated in figure 9.2 below:

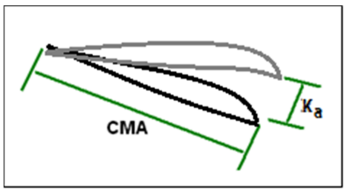

Figure 9.2 – Accelerator actuation

The standardized maximum AOA variation can be estimated using the available accelerator length κ_a and the mean aerodynamic chord (MAC) as follows:

$$\delta_M = -atan\left(\frac{\kappa_a}{MAC}\right) \tag{9.4}$$

Just as proceeded for the brakes system, the angle of attack variation can be expressed as:

$$\widetilde{\Delta\propto}\,(\delta_a) = \delta_a \cdot \delta_M \tag{9.5}$$

And then, equations (9.1) and (9.3) can be used again to determine the AOA and flight speed. Table 9-3 below presents the results of accelerator application in a typical model.

Table 9-3: Effect of accelerator application in flight speed and AOA

	Portion of accelerator applied			
	25%	***50%***	***75%***	***100%***
20cm of available accelerator length	8.4°	8.2°	8.0°	7.7°
	35.1 km/h	37.7 km/h	39.0 km/h	41.6 km/h
40cm of available accelerator length	8.0°	7.4°	6.9°	6.2°
	39.0 km/h	46.1 km/h	54.4 km/h	61.0 km/h

It can be seen a potential increase of 10km/h in flight speed for 60cm of available accelerator length, which indicates a good authority in speed. In general, the formulation above provides means to pre evaluate the design of the accelerator device, and, together with the brakes proprieties discussed in section 9.1.1 allows to define the range of speed variation for a defined

model. With these limits established, a curve can be plotted representing the "level of speed authority" as illustrated in figure 9.3 below:

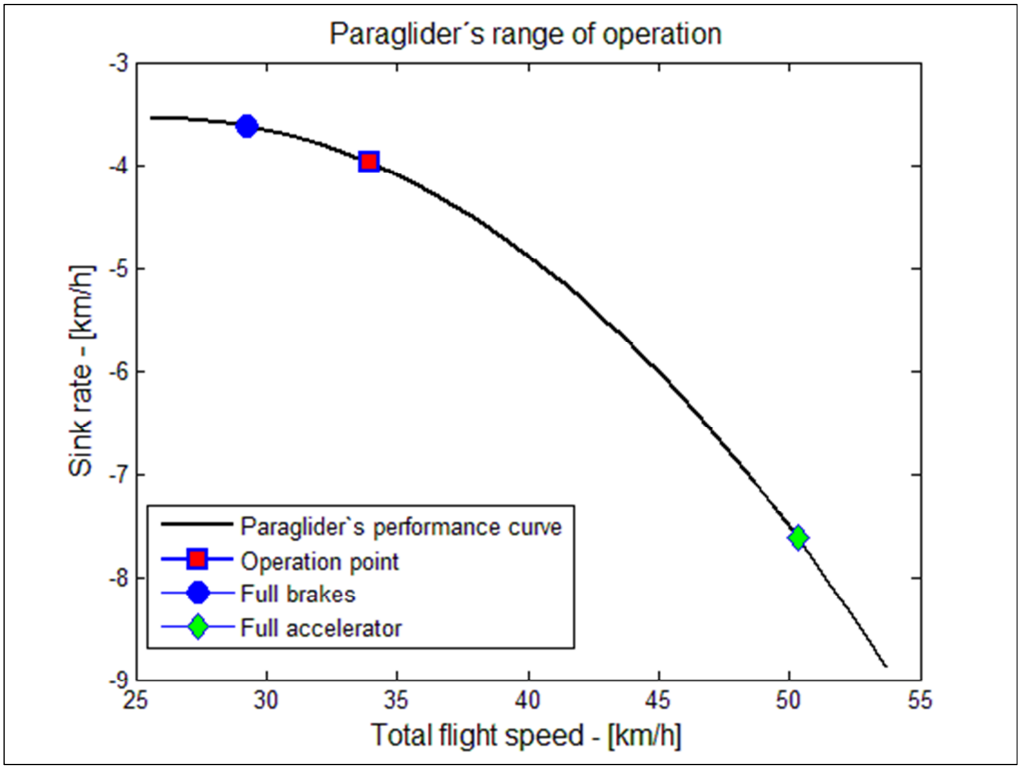

Figure 9.3 – Paraglider's speed range

9.1.3 CG shift

A common way to supplement asymmetric brake inputs is using corporal displacement, or CG shifting. Although it will be treated as a "flight control" option, it does not involve any devices or mechanisms. Also, the formulation associated to the modeling of this control consists only in determine a reasonable range of lateral displacement of the center of gravity.

Considering the general proportions of typical models, a standard value to be established as a maximum CG shift is 30cm. This value allows efficiently evaluating how the wing responds to lateral CG variations. The main variables involved in CG shifting controllability are related to wing's lateral-directional derivative parameters. In general, wings presenting a combination of low anhedral, and increased CG height present good responsiveness to CG shifting.

To modeling CG shifting using a simplified approach, the lateral-directional state-space model presented in chapter 8 can be adapted including a component of roll moment due to CG displacement. It is reasonable to consider that, when the CG is laterally dislocated, the total lift,

which is no longer aligned with the CG, will generate a rolling moment trying to rebalance the system. This can be mathematically expressed as:

$$\begin{bmatrix} \dot{v} \\ \dot{P} \\ \dot{R} \\ \dot{\emptyset} \end{bmatrix} = \begin{bmatrix} Y_v & Y_{\dot{\phi}} & Y_{\dot{\psi}} & Y_{\phi} \\ M_{X_v} & M_{X_{\dot{\phi}}} & M_{X_{\dot{\psi}}} & -\frac{W}{I_x} \cdot h_0' \\ M_{Z_v} & M_{Z_{\dot{\phi}}} & M_{Z_{\dot{\psi}}} & 0 \\ 0 & 1 & 0 & 0 \end{bmatrix} \cdot \begin{bmatrix} v \\ P \\ R \\ \emptyset \end{bmatrix} + \begin{bmatrix} 0 \\ \frac{W}{I_x} \\ 0 \\ 0 \end{bmatrix} \cdot \delta_{CG} \tag{9.6}$$

Then, it can be concluded that the potential to maneuver with CG shifting is proportional to system's weight and inversely proportional to the wing's roll inertia. Figure 9.4 below presents a simulation of 30cm CG shifting in a typical paraglider.

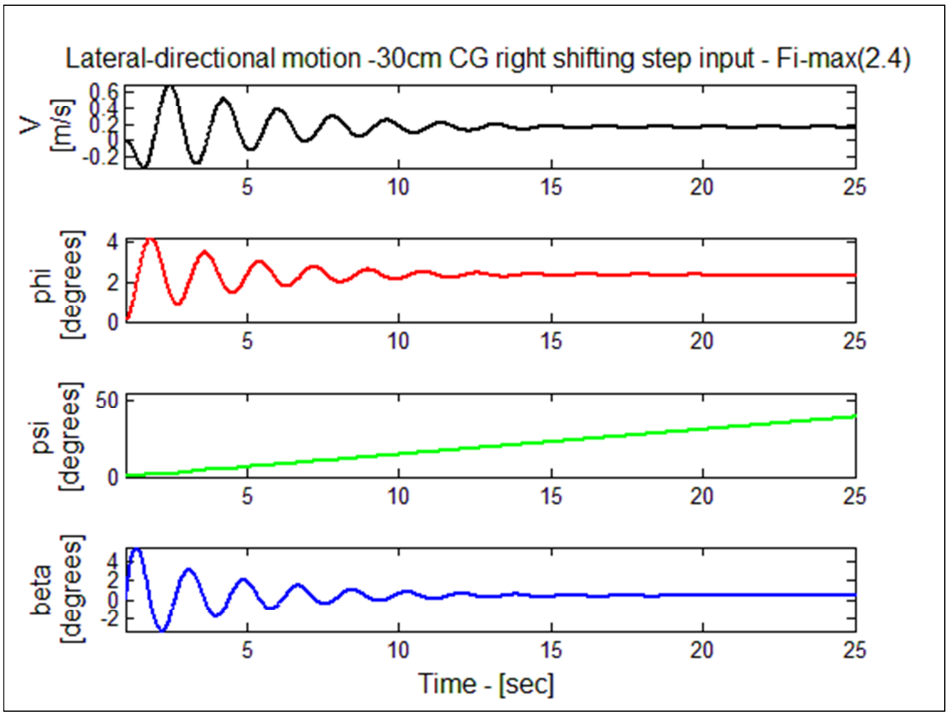

Figure 9.4 – CG shifting turn

It can be noticed that the turn is slow, presenting a small bank angle. However, when this effect is combined with braking application a much more representative roll rate is observed compared to the application of brakes alone. In this way, supplementing braking commands with CG shifting can be very efficient to improve turning performance.

9.2. Paraglider's Basic Maneuvers

Although the dynamic models intended to describe any systems is built focusing in its equilibrium condition, some important situations out-of-equilibrium deserves special attention because it reveals important characteristics and limitations of a particular model.

For obvious reasons, paragliders must be able to efficiently takeoff, landing and make turns. Then, in the sections below will be analyzed the mechanics of such maneuvers and how the design proprieties are related to those capabilities.

9.2.1 Takeoff

The takeoff is a critical flight phase in which the paraglider must be leaded through an energy transient and stabilized overhead with a sufficient level of relative-wind speed. Many hazardous accidents happen during takeoffs, being the most common causes: the occurrence of gusts, wind direction abrupt changes and wing deflation due to loss of wing kinetic energy.

The takeoff maneuver depends both on pilot's technique and wing design proprieties. There are different procedures to execute a takeoff and they are well explained in many pilots training manuals (Pagen, 2001), but all of them rely in providing an initial speed to the wing and stabilize it overhead.

The mechanics involved in the takeoff maneuver consist in causing some negative pitch rate and translational speed in order to provide the necessary amount of relative speed. In some cases, the wind itself can provide all the energy necessary to inflate the wing and the pilot has only to keep it under control while bringing the wing overhead. Otherwise, with low wind, some kinetic energy must be artificially added combining a rotational pull with a decided run.

Although a good technique is mandatory for a safe takeoff, the design proprieties can make the task much easier. In this way, it is valuable to investigate how the design characteristics are related to the capability of a paraglider to be easily controlled during takeoff.

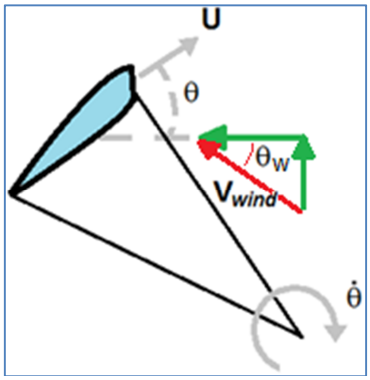

Figure 9.5 – Takeoff maneuver sketch

Figure 9.5 presents a simplified illustration of a classical takeoff condition. In this situation it is supposed no lateral wind, which means, the wing is sufficiently aligned with the relative wind. The relative wind speed may present a vertical component which mainly depends on the local hill slope. It must be noticed that wind speed helps wing inflation in two different ways. The "pressure drag" provides some structural stiffness helping the inflation of the wing at the beginning of the maneuver, and the wind-speed component assist the wing to come up by generating effective angle of attack during the pitching transient. However, takeoffs with no wind are still possible, provided a minimum relative speed combined with an expressive takeoff pitch rate impulse given by a fast short run.

Because of the need of reaching structural stability minimums during the takeoff, the frontal speed component can be considered a decisive parameter. Based on Figure 9.2 this parameter can be approximated as:

$$U_{(t)} \approx h_0' \cdot q_{(t)} + V_w \cdot cos\left(\theta_0 + \theta_w - q_{(t)} \cdot t\right) \tag{9.7}$$

In a successful takeoff, at the moment when the wing gets aligned to the horizon, the frontal relative speed must be enough to provide a minimum level of wing's structural stability but not so large that could result a dangerous over-pitching.

$$U_{TO} \approx h_0' \cdot q_{av} + V_w \tag{9.8}$$

$$U_{min} < U_{TO} < U_{max} \tag{9.9}$$

To define a minimum level of wing's structural stability the concepts explored in chapter 4 can be used, and a minimum "structural stability factor" of one can be established. Then, the minimum speed to provide such margin can be calculated as follows:

$$U_{min} \approx \sqrt{SSF_{min} \cdot 2 \cdot g \cdot \frac{\rho_w}{\rho_{air}} \cdot \frac{s}{s_f}} \approx \sqrt{2 \cdot g \cdot \frac{\rho_w}{\rho_{air}} \cdot \frac{s}{s_f}} \tag{9.10}$$

Also, to preventing from over-pitching, a maximum speed must be defined based in the longitudinal response characteristics of the model. However, as it would be unnecessarily complex to define a specific over-speed limit for each model, a standardized value of a quarter of the equilibrated flight speed is enough to investigate handling characteristics. In this way the maximum frontal speed becomes:

$$U_{max} \approx U_{eq} + \Delta_u^{max} \tag{9.11}$$

$$\Delta_u^{max} = \frac{1}{4} \cdot U_{eq} \tag{9.12}$$

Notice that equation (9.8) uses an averaged takeoff pitch rate. The takeoff pitch rate is an extremely important parameter in the takeoff dynamics, and it is not really constant. It depends both on the pilot's inputs in the frontal risers and on the aerodynamic reactions on the wing. This make it obvious that the takeoff pitch rate is a function of the technique applied for takeoff, then, it's quite hard to mathematically describe such scenario. Even though, some assessments about the influence of design parameters on the achievable takeoff pitch rate can be very useful to help evaluating paraglider's takeoff characteristics

The wing rotation dynamics can be described as proposed below:

$$I_y \cdot \ddot{\theta}_{(t)} = \frac{1}{2} \cdot \rho \cdot {U_{(t)}}^2 \cdot S \cdot \begin{pmatrix} \left(C_{L_{(\propto)}} \cdot cos(\propto) + C_{D_{(\propto)}} \cdot sin(\propto)\right) \cdot d_0' \\ -\left(C_{L_{(\propto)}} \cdot sin(\propto) - C_{D_{(\propto)}} \cdot cos(\propto)\right) \cdot h_0' + MAC \cdot C_{m_0} \end{pmatrix} + \tau_{input_{(t)}} \tag{9.13}$$

Where $\tau_{\text{input}_{(t)}}$ denotes the pilot's inputted torque as a function of time, and the instantaneous angle of attack , which will be a function of the instantaneous speed and wing position, can be described as follow:

$$\alpha_{(t)} = \frac{V_w \cdot sin(\theta_{(t)} + \theta_w)}{\sqrt{\left(h_0' \cdot \dot{\theta}_{(t)} + V_w \cdot cos(\theta_{(t)} + \theta_w)\right)^2 + \left(V_w \cdot sin(\theta_{(t)} + \theta_w)\right)^2}} \tag{9.14}$$

These two equations provide an idea about how fast is the rotation of the wing in a general condition. Inspecting equation (9.13), it can be seen that the gain in pitch rate is inversely proportional to the inertia, which is related to the material of the wing and also to the CG height. The right side of the same equation can be seen as a measurement of the pitching "responsiveness" or "sensibility" of the wing, which depends on geometric and aerodynamic parameters. Finally, equation (9.14) shows that the variation in angle of attack directly depends on the wind speed.

Notice that substituting expression (9.14) in equation (9.13), it will results a nonlinear differential equation. Numerically integrating (Chapra, 2001) this equation it can be obtained the function $\dot{\theta}_{(t)}$ giving the pitch rate in each moment between the beginning of the takeoff and the moment when the wing is aligned with the horizon. Then, an averaged value can be obtained calculating:

$$q_{av} = \frac{\int_0^t \dot{\theta}_{(t)} \cdot dt}{t} \tag{9.15}$$

It is pretty clear that the calculation process described above is complex and timing consuming. Not mentioning inaccurate, because the aerodynamic coefficients cannot be efficiently determined in such conditions and the term accounting for pilot's input cannot be precisely modeled. Anyway, the presentation was useful to drive valid conclusions about the effects of design parameters in takeoff pitch rate. Moving forward, instead of going through numerical calculations that would have to be repeated for each model under analysis, a practical observation of normal takeoffs can reveal a reasonable range of takeoff pitch rate in which it is expected a variation related to either model proprieties and takeoff techniques. Using such approach, the range of average pitch rate can be defined as:

$$20°/s \leq q_{av} \leq 45°/s$$

(9.16)

Consequently, considering a range of averaged takeoff pitch rates, the two limiting conditions for frontal flight speed can be expressed as:

$$\begin{cases} V_w > U_{min} - h'_0 \cdot q_{av} \\ V_w < U_{max} - h'_0 \cdot q_{av} \end{cases}$$

(9.17)

These limits allow plotting a safe-takeoff-chart, where the wind is limited as a function of the takeoff pitch rate. Figure 9.6 presents a safe-takeoff-chart for a typical paraglider.

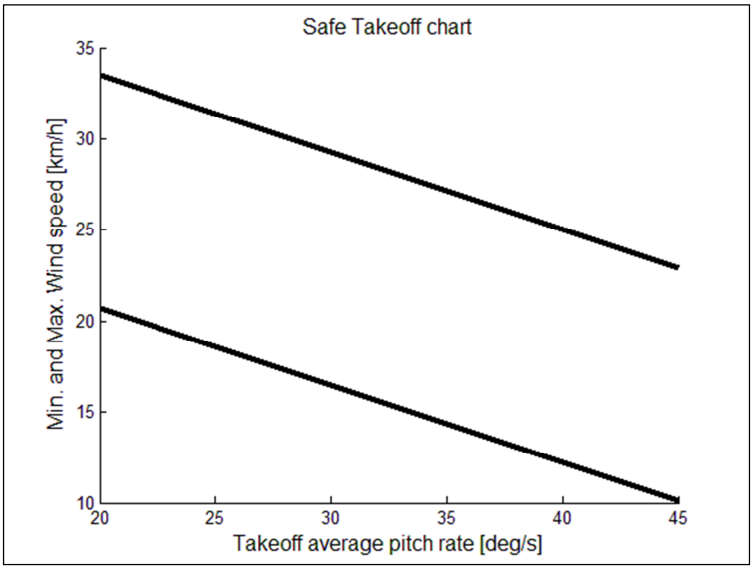

Figure 9.6 – Safe-Takeoff-chart for a typical paraglider

Figure 9.6 shows that, even with a good takeoff pith rate, a minimum "wind" is required to takeoff; however, it was already made clear that this speed component may be easily provided by a short run.

Conclusively, it can be seen that light material wings with reduced CG height and good aerodynamic efficiency are easier to rotate and also demands a minor relative speed to get structural stability. However, the reactions are faster and the susceptibility to over rotation (over pitching) is increased demanding active piloting for stabilization. Meanwhile, an initial investigation of the takeoff capability can be done with the assessments presented. Nevertheless, flight test evaluations are completely necessary to corroborate the findings and classify the handling characteristics.

9.2.2 Landing

There are some different techniques to execute approximations to landing, which can be found in pilots training manuals (Pagen, 2001), but the final landing is basically accomplished by a continuous application of symmetric brakes in order to bleed speed, especially sink rate, up to the ground. Although it is a simple task from a flight mechanics viewpoint, the majority of the incidents occur on landings, mainly due to the different kinds of disturbances that might disturb the final glide.

Depending on weather conditions and local topography expressive wind gradients may be present contributing to a hard landing or a dangerous pilot-induced-oscillation (PIO) near to the ground. Considering landing in headwind, the paraglider will maintain the relative speed but the wind component will diminishes with ground proximity causing an unexpected feeling of "ground speed acceleration". If pilots do not react to that, maintaining the approach glide, the speed gradient may result a landing in excessive speed. On the other hand, if pilots reacts applying brakes and retarding the touchdown, the paraglider may regain some altitude, and a subsequent releasing in brakes trying to reestablishes sink rate can begin a "fighting" behavior. Such induced oscillations near to the ground can be dangerous because it may leads to a stall situation or to a touchdown in high kinetic energy. The condition analyzed here also applies for symmetric gusts or excessive brakes inputs at landing, which can cause or aggravate this scenario.

A good compromise between control authority and stability will define the adequacy of handling characteristics at landing. A wing with increased brakes authority can bleed an expressive amount of flight speed permitting a soft landing; however, it also may contribute for over-reactions and stall approximations at landing. A good level of stability is also desirable for a stable approaching to the ground. Overall, no analytical assessment is efficient to predict landing characteristics being flight tests completely necessary to evaluate such capabilities. Nevertheless, to allow some design driven thoughts, it can be concluded that the parameters to be evaluated to improve landing capability are: the equilibrium sink rate, the minimum sink rate achievable with full brakes, the static longitudinal stability margin (as explained in chapter 7), and the level of longitudinal damping.

9.2.3 Turning

The capability to change heading is of first importance for paragliders flight, not only to control flight direction, but also to permit avoidance maneuvers and thermals ascending. When in

turns, paragliders present certain amount of bank angle, pitch angle and yaw rate as illustrated in figure 9.7 below.

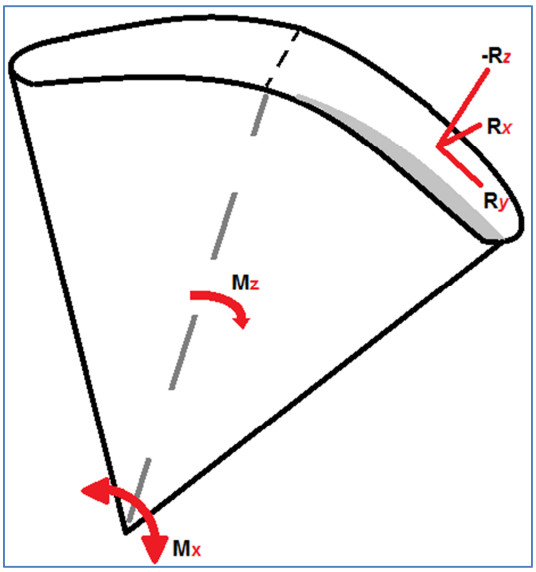

Figure 9.7 – Turning Flight Sketch

The mechanics involved in turning is somewhat simple. When one-side brakes are pulled down, a wing distortion can be seen progressively rotating the commanded tip, increasing the incidence of this semi-wing. The increase in angle of attack at the actuated side causes an initial increase in lift and drag, which combined with the rotation of the aerodynamic components backwards, reduces the final frontal resultant causing a deceleration on the actuated semi-wing and an increase in the lateral force component in this same side. As the movement goes on, the non-actuated side becomes faster and the major lift component in that side contributes for a progressive banking which will be maintained as long as command remains applied. Notice that, when in a stabilized bank angle the sink rate will contribute with a sideslip component which helps to maintain yaw rate. It is important take in account the combinations of contradictory trends here, while the right brake actuation generates moments trying to increase positively bank and yaw rates, these rates and the sideslip component will generate moments components in the opposite direction. That's why, if the commands are released, the wing will try to re-level and maintain a steady heading. These conclusions can be made clearer consulting the wing derivatives presented in chapter 5 and the concepts of lateral-directional stability discussed in chapter 8.

Due to the singular characteristics of paragliders and the difficulties to derive precise theoretical models for commands application, establishing parameters which would allow an initial evaluation of turning capability based in design parameters is quite a hard task. However, it is logical

to assume that the rate of turn achievable with full asymmetric brake application is a valid parameter to measure turning capability. This rate of turn can be understood as the rate of yaw, and it depends on many paraglider's design characteristics.

The braking actuation model proposed in chapter 5 can be used to evaluate the potential rate of turn of a particular model, however, the limitations about such approach already discussed in section 9.1.1 also applies here. Then, without specifying any model to mathematically modeling braking actuation, the mechanics of a turn can be analyzed using the equations of motion presented in chapter 5:

Rotational dynamics:

$$\dot{P} = \frac{(I_z \cdot M_x + I_{xz} \cdot M_z)}{(I_x \cdot I_z - {I_{xz}}^2)} + \frac{I_{xz} \cdot (I_x - I_y + I_z)}{(I_x \cdot I_z - {I_{xz}}^2)} \cdot Q \cdot P + \frac{(I_z \cdot (I_y - I_z) - {I_{xz}}^2)}{(I_x \cdot I_z - {I_{xz}}^2)} \cdot Q \cdot R \tag{9.18}$$

$$\dot{Q} = \frac{1}{I_y} \cdot M_Y + \frac{(I_z - I_x)}{I_y} \cdot P \cdot R + \frac{I_{xz}}{I_y} \cdot R^2 - \frac{I_{xz}}{I_y} \cdot P^2 \tag{9.19}$$

$$\dot{R} = \frac{(I_{xz} \cdot M_x + I_x \cdot M_z)}{(I_z \cdot I_x - {I_{xz}}^2)} - \frac{(I_x \cdot (I_y - I_x) - {I_{xz}}^2)}{(I_z \cdot I_x - {I_{xz}}^2)} \cdot Q \cdot P - \frac{I_{xz} \cdot (I_x - I_y + I_z)}{(I_z \cdot I_x - {I_{xz}}^2)} \cdot Q \cdot R \tag{9.20}$$

Kinematic equations for spatial orientation:

$$\dot{\Phi} = P + sen(\Phi) \cdot tan(\Theta) \cdot Q + cos(\Phi) \cdot tan(\Theta) \cdot R \tag{9.21}$$

$$\dot{\theta} = cos(\Phi) \cdot Q - sen(\Phi) \cdot R \tag{9.22}$$

$$\dot{\Psi} = \frac{sen(\Phi)}{cos(\Theta)} \cdot Q + \frac{cos(\Phi)}{cos(\Theta)} \cdot R \tag{9.23}$$

Equations (9.18) through (9.23) represent the turning dynamics. Disregarding the specificities of a particular brakes mechanisms and wing design, it can be concluded from those equations that the heading acceleration will be increased by diminishing wing inertias, and by

increasing wing responsiveness to asymmetric inputs. Assuming a stabilized curve, where no changes in bank or pitch exists, equations (9.21) and (9.22) above provides equilibrium conditions relating yaw rate, roll rate and pitch rate:

$$P = -\frac{tan(\Theta)}{cos(\Phi)} \cdot R \tag{9.24}$$

$$Q = tan(\Phi) \cdot R \tag{9.25}$$

In the dynamic equations the resultant moments are function of the instantaneous flight condition, including the amount of applied brakes. A parameter that can be used in a first investigation of turning capability is the "initial yaw acceleration", which can be defined as the instantaneous acceleration in yaw when full right brake is applied with initial equilibrated flight conditions. This parameter can be approximated as suggested below:

$$\dot{R} = \frac{M_z}{I_z} \approx \frac{\frac{\partial M_z}{\partial \delta_{B_r}}|_{eq}}{I_z} \tag{9.26}$$

The parameter $\frac{\partial M_z}{\partial \delta_{B_r}}|_{eq}$ depends on wing geometry, aerodynamic proprieties and brake mechanism. Therefore, no good algebraic approximations can be provided for this term. However, in general, it can be notice that a wing with a great anhedral and increased span will present a high "initial yaw acceleration", and thus, a good in-turning initial responsiveness. Even though, it is necessary to be extremely careful with excessive values of in-turning initial responsiveness because it increases the susceptibility to wing twists. Unfortunately, due to the many variables involved, an efficient reference value cannot be provided.

The "initial yaw acceleration" itself do not provide all information needed to evaluate turning performance. In fact, even presenting a good level of initial yaw rate, if the wing is too stable, the continuation of the turn may be slow and inefficient. The only way to have a first idea of the potential turning performance is using a simplified model as proposed in chapter 5. Then, assuming a linear approximation around equilibrium, the response to application of full right brake can be obtained as shown in figure 9.8.

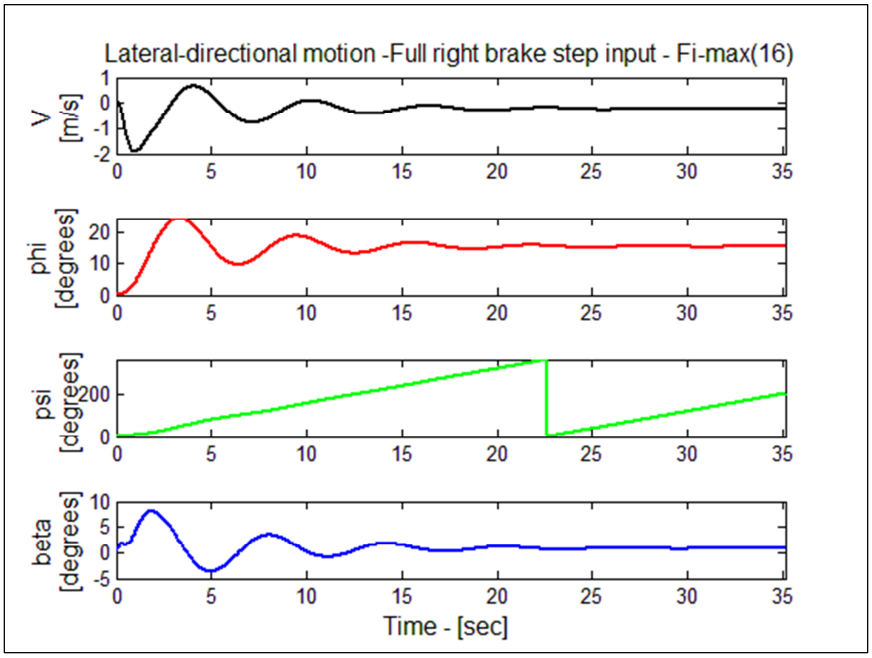

Figure 9.8 – Turning maneuver

From figure 9.8 two important parameters are made available: the final or stabilized rate of turn (16.4 degrees per second) and the bank angle (15 degrees). It is important to remember that this simulation uses the aerodynamic derivatives obtained in equilibrium conditions, but these parameters changes dramatically as the flight conditions goes far from the equilibrium situation. Then, the simulations as presented above are more reasonable for small inputs, or for analyzing just the initial portions of the movement.

Actually, for most paragliders the continuous application of brakes drives the wing into a deep spiral where the wing rotates almost horizontally (in front of the pilot). The capability to entry and get out from such maneuver is a common test used to evaluate paraglider's controllability and handling qualities (Deutscher Hängegleiterverband – 2009).

Finally, the assessments made regarding lateral-directional stability and the parameters introduced here may allow an evaluation of the potential controllability and maneuverability in turns. However, a flight test based evaluation is completely necessary to refine the design and corroborates any theoretical conclusion.

9.2.4 Disturbances Recovering

The paraglider responses to atmospheric disturbances were analyzed in chapters 7 and 8, and the conclusions obtained can be used here to compose the conclusions about how handling qualities can be improved with a reasonable tradeoff between stability and controllability.

When a paraglider is shown to be very stable, it results a very passive piloting. Such characteristics is not always desirable because a wing too passive lose maneuverability, what can be dangerous, especially when for some reason the wing is put in a condition considerable out of equilibrium. In such scenario, the low maneuverability shall difficult the recovering because the commands inputs has low effectiveness.

On the other hand, fast, maneuverable paragliders tends to present very dynamic responses to any kind of input. In this way, simple commands or atmospheric disturbances may induce dangerous movements which demands immediate pilot's reactions. These wings are normally purposed to be used in acrobatics flight and performance competitions.

Basically, the ability to efficiently recover from any disturbances depends both on the dynamic stability characteristics and the available command authority. However, human factors aspects play an important part in such evaluation making the best trade-off between command efficiency and wing's natural reaction completely not obvious.

It can be noticed, for example, that, sometimes, reducing the number of oscillations may increase the maximum amplitude. Also, increasing speed to get better stability characteristics may result faster reactions for command actuations. Therefore, no means exists to correctly tuning a flight control mechanism without flight tests.

However, to drive further improvements based on flight tests observations, it is enough to mention that, generally, an increased CG height, a faster equilibrium flight speed, and an increased aspect ratio will improve commands effectiveness.

9.3 Final Comments:

In this chapter it was presented the concepts of controllability and maneuverability applied to paragliders. The main aspects of paragliders controlled flight were analyzed, including the description of the basic maneuvers.

Although it has being defined some approximated parameters to be used in conceptual design evaluations, it was explained that paragliders handling qualities assessments considering the tradeoff between stability and controllability cannot be made without flight testing because it strongly depends on subjective evaluations.

Finally, the fundamentals of the different control mechanisms were explained and it was possible to analyze some relations between design parameters and control efficiency revealing some useful tools for conceptual design optimizations.

10 CONCLUSIONS

A complete description of the fundamentals of paragliders flight dynamics was developed allowing the prediction of paragliders flight characteristics based in theoretical design parameters, and then, making available a useful optimization tool to be applied in conceptual design phases. Also, throughout the many discussions from chapter 2 to 9 some important conclusions about the characteristics of paragliders motion were reached as summarized below:

- ✓ Performance and stability may be improved by optimizing wing geometry and relative CG position.
- ✓ Performance improvement consists basically in providing maximum glide ratio while sustaining sufficient flight speed to guarantee structural stability.
- ✓ Longitudinal dynamics shows a transient short-period mode and a dominant induced phugoid with reduced damping factor.
- ✓ Lateral-Directional dynamics shows a transient short-period mode and a heavily damped lateral-phugoid characterizing a roll-spiral coupling phenomenon.
- ✓ Controllability can be adjusted by management of wing forces and moments distributions and CG positioning.

Additionally, looking forward to further improvements of the present work and new developments to contribute to paragliders engineering science, below it is presented a list of suggestions:

- ✓ To develop dedicate methodology for paraglider instrumentation and flight testing.
- ✓ To validate the developed theory by flight testing real models.
- ✓ To improve the dynamic model by introducing adjustments derived from flight tests.
- ✓ To develop precise CFD methods to acuratelly estimate paraglider’s aerodynamics coefficients.

APPENDIX A- PARAGLIDERS ANALYSIS TOOL (PAT):

Below it is presented a computational tool for paragliders conceptual design analysis built in MATLAB® using the concepts and developments established in this work.

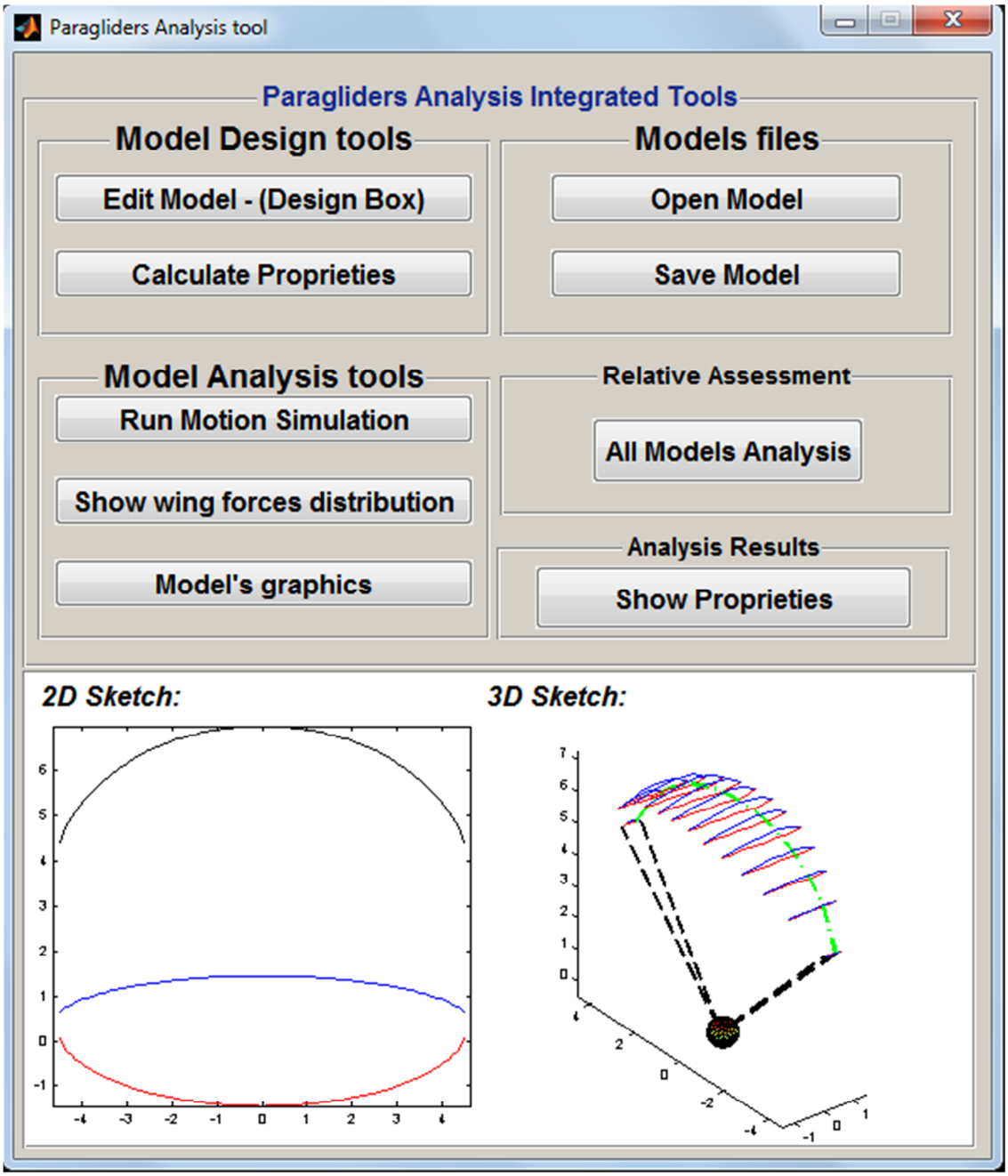

Figure A.1 – PAT - main screen

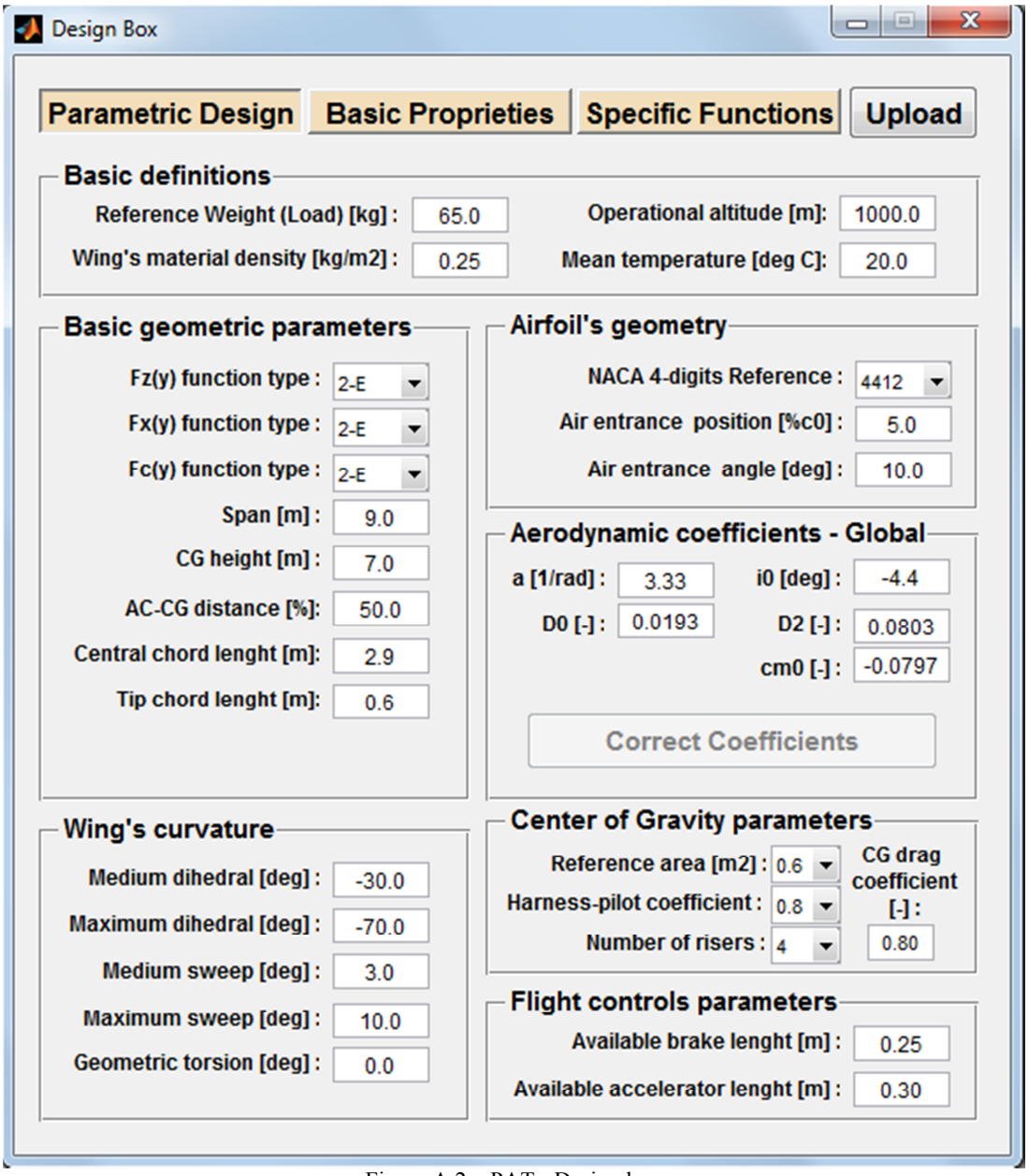

Figure A.2 – PAT - Design box

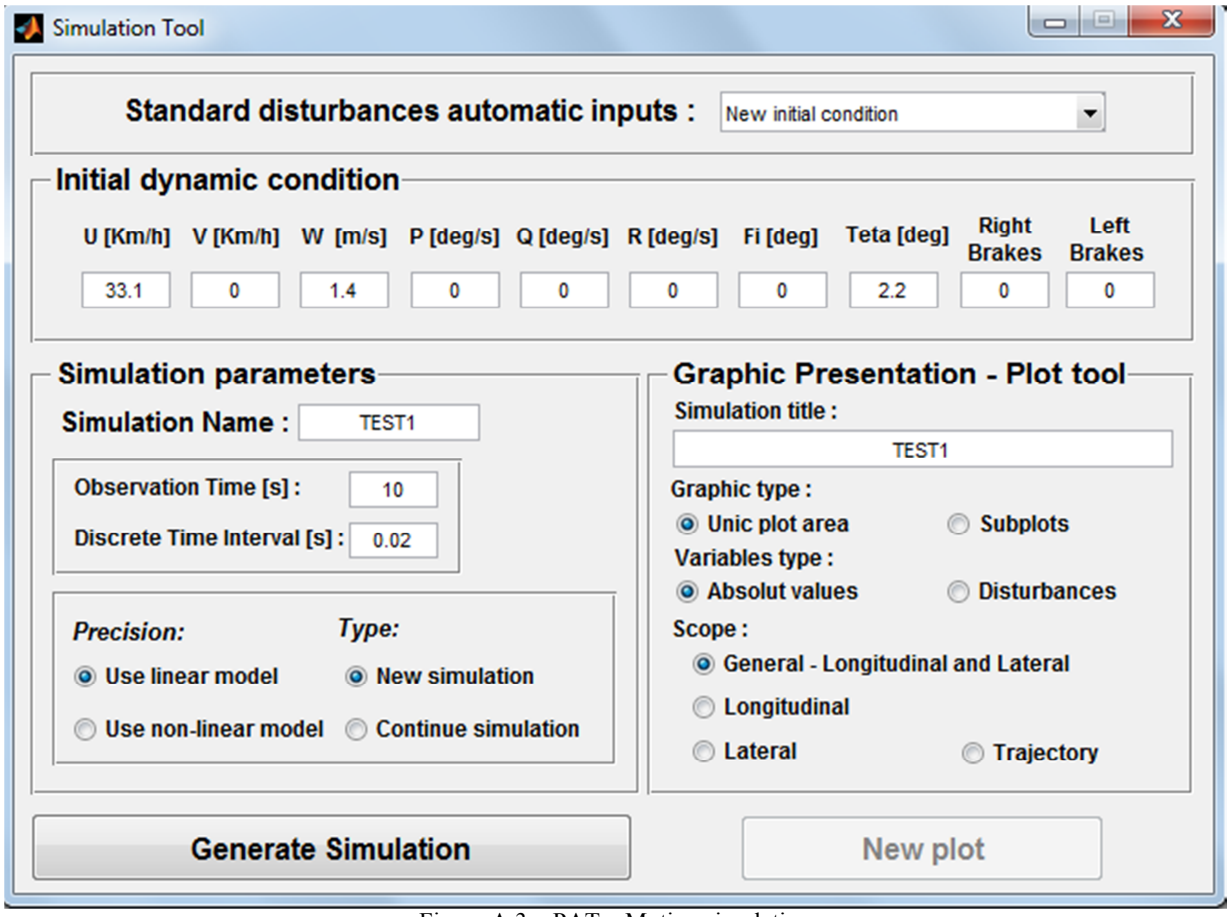

Figure A.3 – PAT – Motion simulation

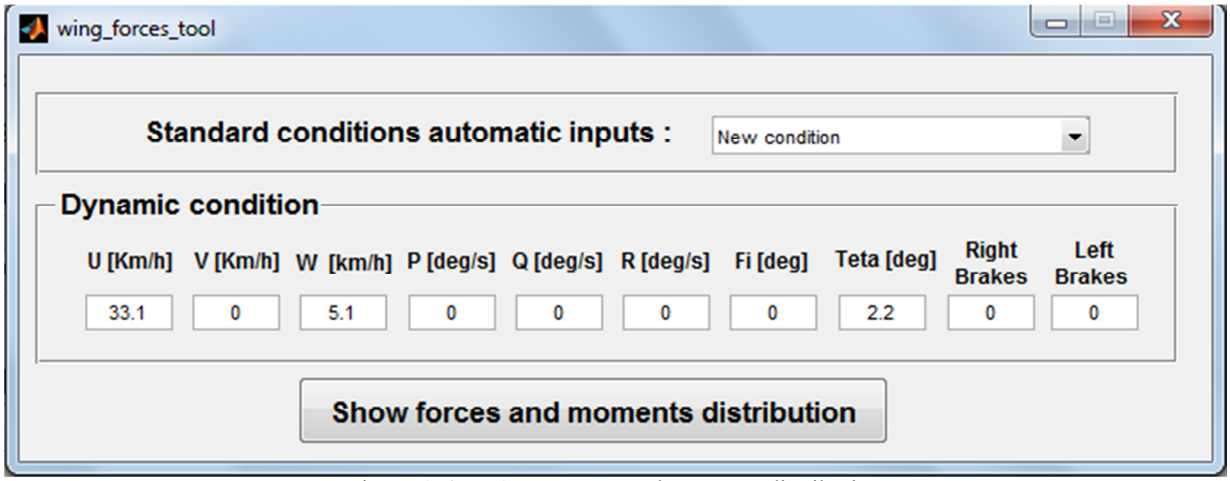

Figure A.4 – PAT – Forces and moments distribution

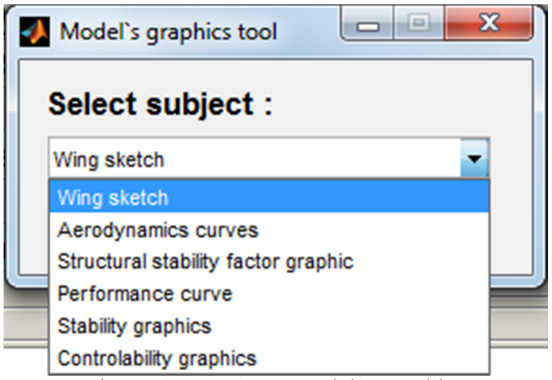

Figure A.5 – PAT – Model's graphics

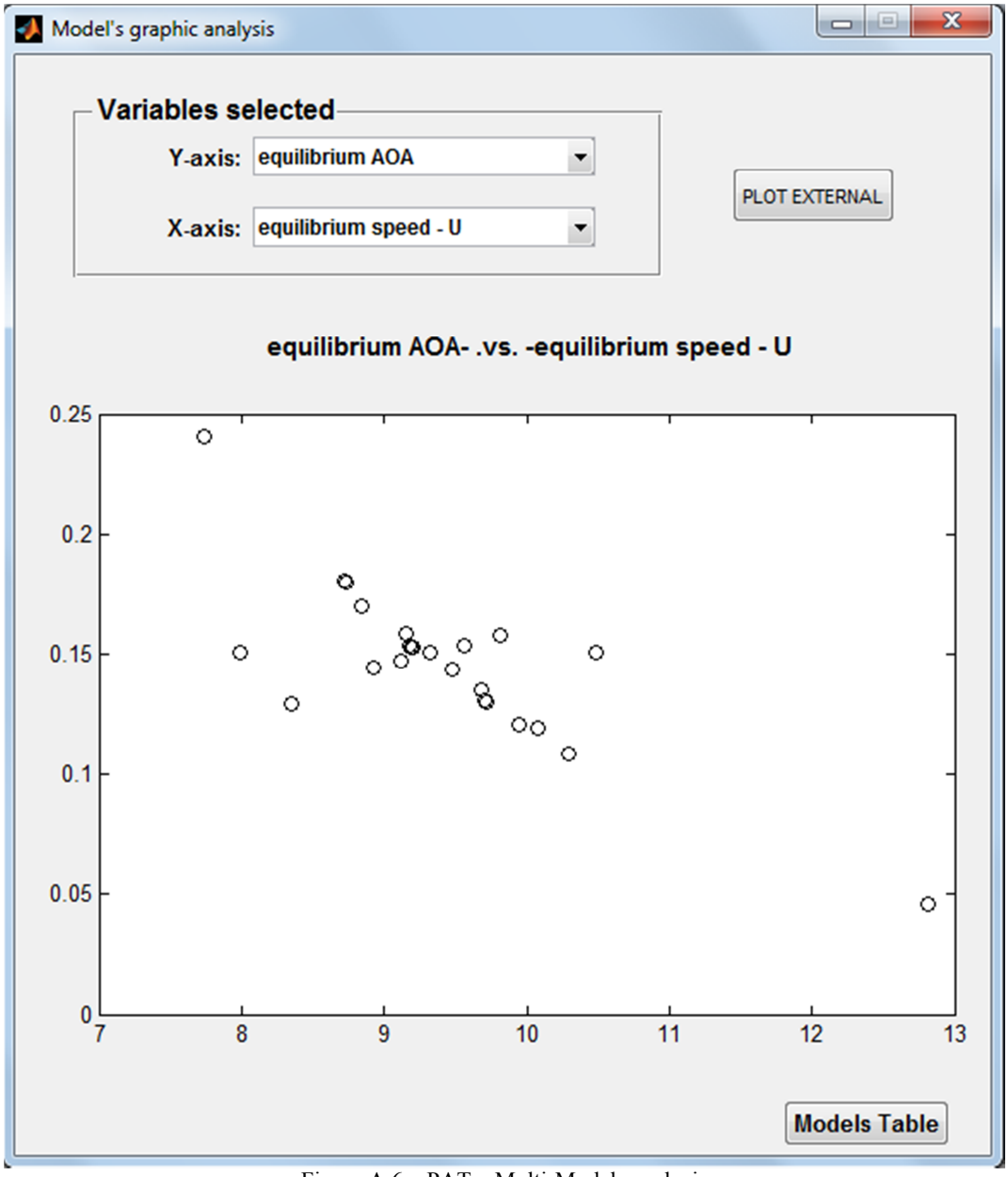

Figure A.6 – PAT – Multi-Models analysis

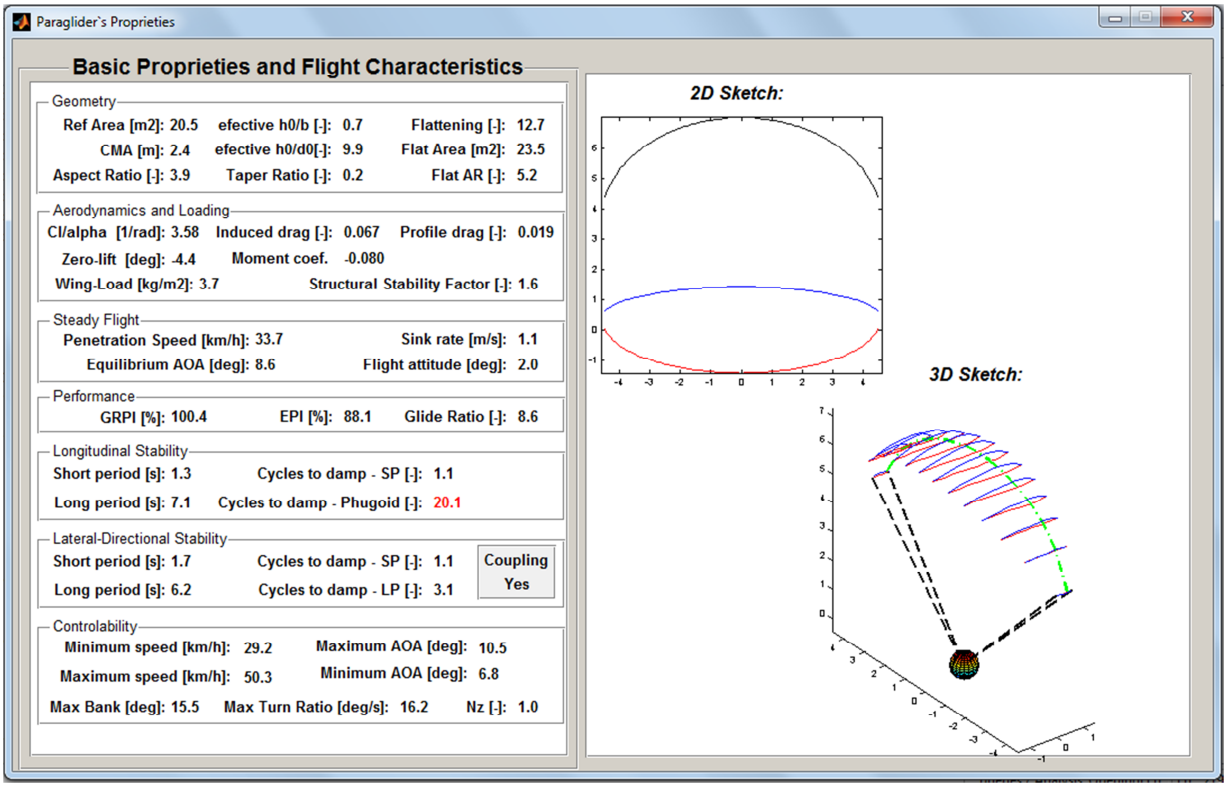

Figure A.7 – PAT – Model's proprieties

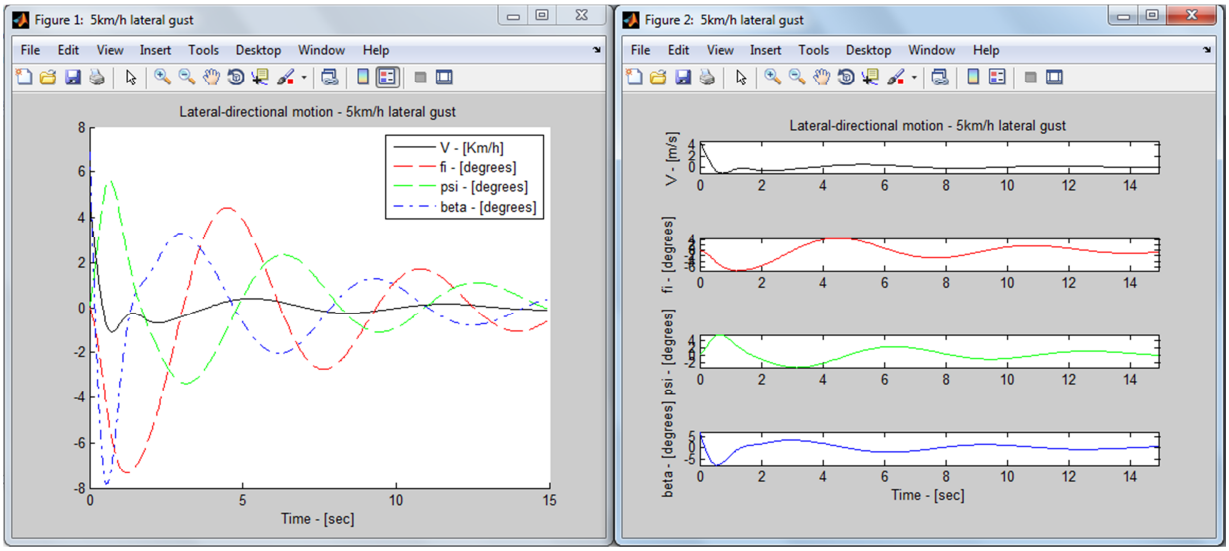

Figure A.8 – Different types of simulations plotting

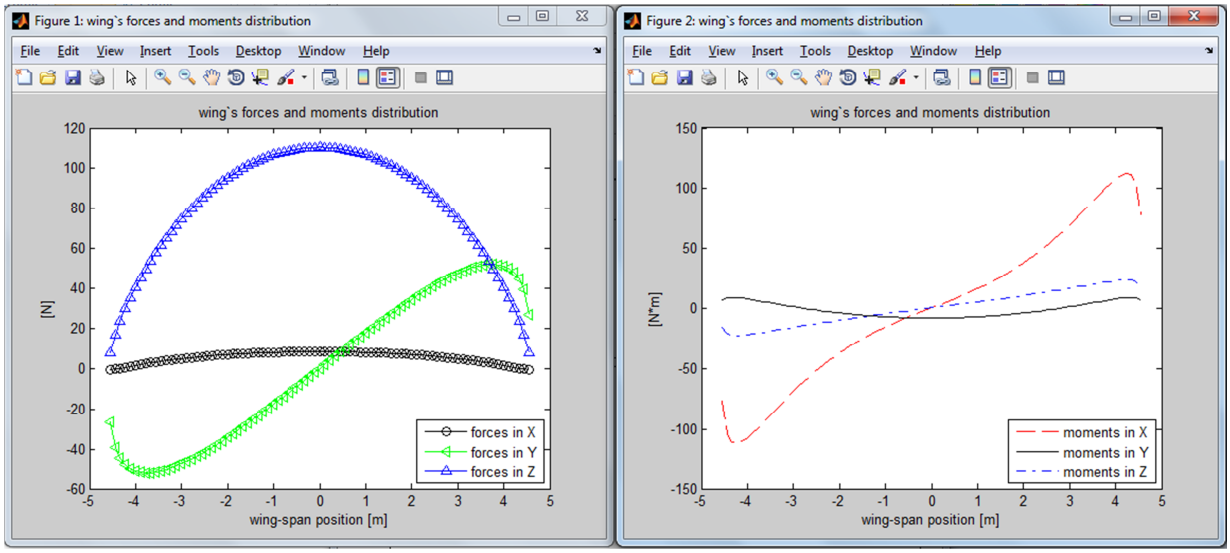

Figure A.9 – Forces and moments distribution visualization

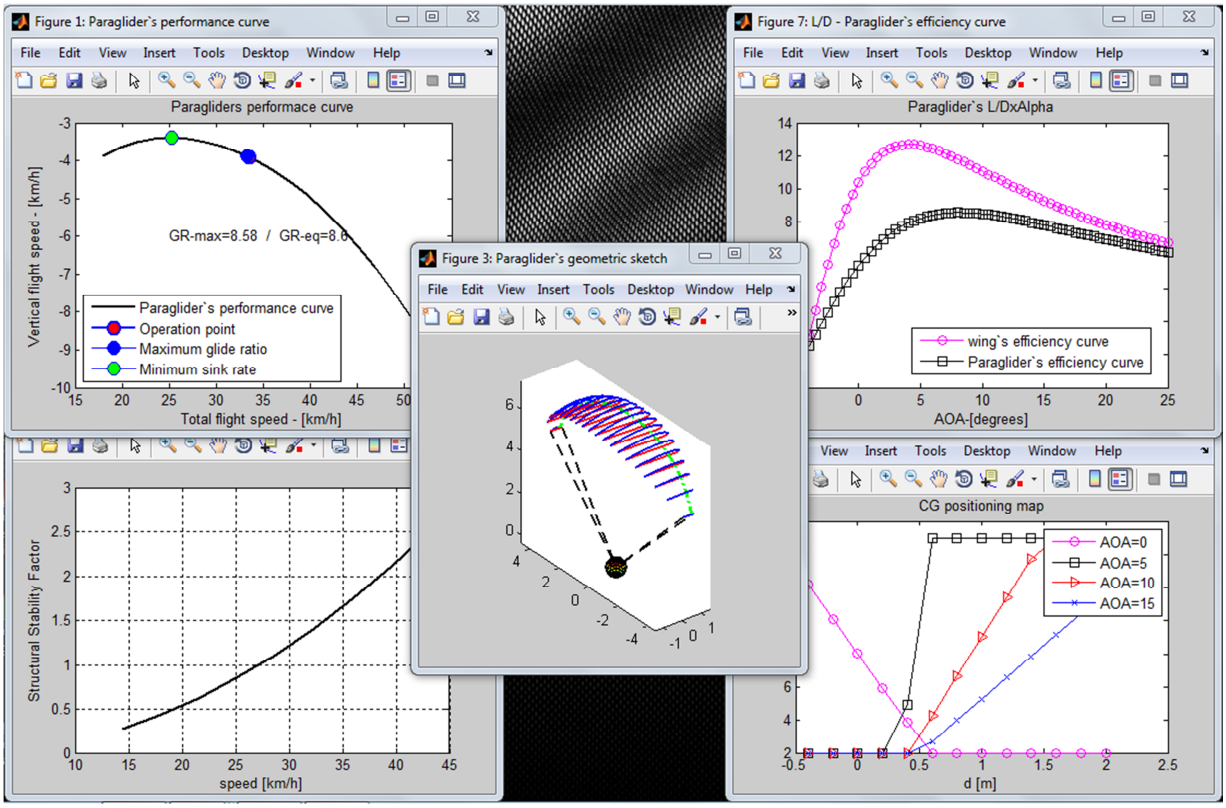

Figure A.10 – General curves and draws

APPENDIX B- DERIVATION OF LATERAL-DIRECTIONAL STATIC STABILITY SIMPLIFIED PARAMETERS:

Below it is presented the derivation of a simplified model to calculate lateral and directional forces and moments caused by sideslips for paraglider's lateral-directional dynamics analysis based on design parameters:

With the geometric description presented in chapter 3 and the forces and moments calculation model presented in chapter 4, the following development can be applied:

B.1 – Moment equations derivation:

Each cell presents a particular bank angle:

$$\delta = \operatorname{atan}\left(\frac{df_z(y)}{dy}\right)$$

In equilibrium, with no sideslip, in each cell we have:

$$u_i = U_{eq}$$

$$w_i = W_{eq} \cdot \cos(\delta)$$

$$\propto_{eq} \approx \frac{W_{eq}}{U_{eq}}$$

$$\propto_{i_{\mathrm{eq}}} \approx \frac{W_{eq}}{U_{eq}} \cdot \cos(\delta) + f_\theta(y)$$

If a sideslip speed is added, the velocity components in each cell are affected, leading to a different AOA:

$$\beta = \frac{V_g}{U_{eq}}$$

$$w_i = W_{eq} \cdot \cos(\delta) - V_g \cdot \sin(\delta)$$

$$\propto_i \approx \propto_{eq} \cdot \cos(\delta) - \beta \cdot \sin(\delta) + f_\theta(y)$$

$$\frac{w_i}{u_i} = \propto_{eq} \cdot \cos(\delta) - \beta \cdot \sin(\delta)$$

The cell's resultants can be expressed by separating the steady flight term and the sideslip term as follows:

$$L_i = \frac{\rho}{2} \cdot {U_{eq}}^2 \cdot (1 + {\propto_i}^2) \cdot \bar{a} \cdot (\propto_i - i_0) \cdot f_c(y) \cdot dy \approx L_{i_{\text{eq}}} - \frac{\rho}{2} \cdot {U_{eq}}^2 \cdot \bar{a} \cdot \beta \cdot \sin(\delta) \cdot f_c(y) \cdot dy$$

$$\begin{aligned} D_i = \frac{\rho}{2} \cdot {U_{eq}}^2 \cdot (1 + {\propto_i}^2) \cdot \left[D_2 \cdot \left(\bar{a} \cdot (\propto_i - i_0)\right)^2 + D_0\right] \cdot f_c(y) \cdot dy \\ \approx D_{i_{\text{eq}}} - \frac{\rho}{2} \cdot {U_{eq}}^2 \cdot D_2 \cdot \bar{a}^2 \cdot \left[2 \cdot \left(\propto_{eq} \cdot \cos(\delta) + f_\theta(y) - i_0\right) - \beta \cdot \sin(\delta)\right] \cdot \beta \cdot \sin(\delta) \cdot f_c(y) \\ \cdot dy \end{aligned}$$

$$m_{0_i} = \frac{\rho}{2} \cdot {U_{eq}}^2 \cdot (1 + {\propto_i}^2) \cdot c_{m_0} \cdot \left(f_c(y)\right)^2 \cdot dy \approx \frac{\rho}{2} \cdot {U_{eq}}^2 \cdot c_{m_0} \cdot \left(f_c(y)\right)^2 \cdot dy = m_{0_{i_{\text{eq}}}}$$

The local forces expressed on the body reference coordinate system can be calculated as follows:

$$\begin{aligned} X_L \approx L_i \cdot \left(\frac{w_i}{u_i}\right) - D_i \\ = X_{i_{\text{eq}}} - \frac{\rho}{2} \cdot {U_{eq}}^2 \cdot \bar{a} \\ \cdot \left[2 \cdot (1 - D_2 \cdot \bar{a}) \cdot \propto_{eq} \cdot \cos(\delta) + (1 - 2 \cdot D_2 \cdot \bar{a}) \cdot (f_\theta(y) - i_0) - (1 - D_2 \cdot \bar{a}) \cdot \beta \cdot \sin(\delta)\right] \\ \cdot \beta \cdot \sin(\delta) \cdot f_c(y) \cdot dy \end{aligned}$$

$$Y_L \approx \left(L_i + D_i \cdot \left(\frac{w_i}{u_i}\right)\right) \cdot \sin(\delta)$$
$$= -\frac{\rho}{2} \cdot {U_{eq}}^2 \cdot \bar{a}$$
$$\cdot \left[1 + {D_0}/{\bar{a}} + D_2 \cdot \bar{a} \cdot \left(\propto_{eq} \cdot \cos(\delta) + f_\theta(y) - i_0\right) \cdot \left(3 \cdot \propto_{eq} \cdot \cos(\delta) + f_\theta(y) - i_0\right) - D_2 \cdot \bar{a}\right.$$
$$\left. \cdot \left(3 \cdot \propto_{eq} \cdot \cos(\delta) + 2 \cdot (f_\theta(y) - i_0)\right) \cdot \beta \cdot \sin(\delta) + D_2 \cdot \bar{a} \cdot (\beta \cdot \sin(\delta))^2\right] \cdot \beta \cdot \sin(\delta) \cdot \sin(\delta)$$
$$\cdot f_c(y) \cdot dy$$

$$Z_L \approx -\left(L_i + D_i \cdot \left(\frac{w_i}{u_i}\right)\right) \cdot \sin(\delta)$$
$$= Z_{i_{\mathrm{eq}}} + \frac{\rho}{2} \cdot {U_{eq}}^2 \cdot \bar{a}$$
$$\cdot \left[1 + {D_0}/{\bar{a}} + D_2 \cdot \bar{a} \cdot \left(\propto_{eq} \cdot \cos(\delta) + f_\theta(y) - i_0\right) \cdot \left(3 \cdot \propto_{eq} \cdot \cos(\delta) + f_\theta(y) - i_0\right) - D_2 \cdot \bar{a}\right.$$
$$\left. \cdot \left(3 \cdot \propto_{eq} \cdot \cos(\delta) + 2 \cdot (f_\theta(y) - i_0)\right) \cdot \beta \cdot \sin(\delta) + D_2 \cdot \bar{a} \cdot (\beta \cdot \sin(\delta))^2\right] \cdot \beta \cdot \sin(\delta) \cdot \cos(\delta)$$
$$\cdot f_c(y) \cdot dy$$

The local moment is:

$$m_{y_i} = m_{0_i}$$

Applying some intuitive simplifications it follows:

$$X_L = X_{i_{\mathrm{eq}}} - \frac{\rho}{2} \cdot {U_{eq}}^2 \cdot \bar{a}$$
$$\cdot \left[\left(2 \cdot (1 - D_2 \cdot \bar{a}) \cdot \propto_{eq} \cdot \cos(\delta) + (1 - 2 \cdot D_2 \cdot \bar{a}) \cdot (f_\theta(y) - i_0)\right) \cdot \sin(\delta) \cdot \beta\right.$$
$$\left. - (1 - D_2 \cdot \bar{a}) \cdot \sin(\delta)^2 \cdot \beta^2\right] \cdot f_c(y) \cdot dy$$

$$Y_L \approx -\frac{\rho}{2} \cdot {U_{eq}}^2 \cdot \bar{a}$$
$$\cdot \left[\left(1 + D_2 \cdot \bar{a} \cdot \left(\propto_{eq} \cdot \cos(\delta) + f_\theta(y) - i_0\right) \cdot \left(3 \cdot \propto_{eq} \cdot \cos(\delta) + f_\theta(y) - i_0\right)\right) \cdot \sin(\delta)^2\right.$$
$$\left. \cdot \beta - D_2 \cdot \bar{a} \cdot \left(3 \cdot \propto_{eq} \cdot \cos(\delta) + 2 \cdot (f_\theta(y) - i_0)\right) \cdot \sin(\delta)^3 \cdot \beta^2\right] \cdot f_c(y) \cdot dy$$

$$Z_L \approx Z_{i_{\mathrm{eq}}} + \frac{\rho}{2} \cdot {U_{eq}}^2 \cdot \bar{a} \cdot \Big[\Big(1 + D_2 \cdot \bar{a} \cdot \big(\propto_{eq} \cdot \cos(\delta) + f_\theta(y) - i_0\big) \cdot \big(3 \cdot \propto_{eq} \cdot \cos(\delta) + f_\theta(y) - i_0\big)\Big) \cdot \sin(\delta) \cdot \cos(\delta) \cdot \beta - D_2 \cdot \bar{a} \cdot \Big(3 \cdot \propto_{eq} \cdot \cos(\delta) + 2 \cdot (f_\theta(y) - i_0)\Big) \cdot \sin(\delta)^2 \cdot \cos(\delta) \cdot \beta^2\Big] \cdot f_c(y) \cdot dy$$

Calculating the lateral force and the rolling and yawing moments, taking in account that the integration of the "equilibrium" terms is zero, we have:

$$F_{y_w} = \int_{-b/2}^{b/2} Y_L$$

$$F_{y_w} = \int_{-b/2}^{b/2} -\frac{\rho}{2} \cdot {U_{eq}}^2 \cdot \bar{a} \cdot \Big[\Big(1 + D_2 \cdot \bar{a} \cdot \big(\propto_{eq} \cdot \cos(\delta) + f_\theta(y) - i_0\big) \cdot \big(3 \cdot \propto_{eq} \cdot \cos(\delta) + f_\theta(y) - i_0\big)\Big) \cdot \sin(\delta)^2 \cdot \beta - D_2 \cdot \bar{a} \cdot \Big(3 \cdot \propto_{eq} \cdot \cos(\delta) + 2 \cdot (f_\theta(y) - i_0)\Big) \cdot \sin(\delta)^3 \cdot \beta^2\Big] \cdot f_c(y) \cdot dy$$

$$M_{x_w} = \int_{-b/2}^{b/2} -Y_L \cdot f_z(y) + Z_L \cdot y$$

$$M_{x_w} = \frac{\rho}{2} \cdot {U_{eq}}^2 \cdot \bar{a} \cdot \Bigg(\beta \cdot \int_{-b/2}^{b/2} \Big(1 + D_2 \cdot \bar{a} \cdot \big(\propto_{eq} \cdot \cos(\delta) + f_\theta(y) - i_0\big) \cdot \big(3 \cdot \propto_{eq} \cdot \cos(\delta) + f_\theta(y) - i_0\big)\Big) \cdot \big(\cos(\delta) \cdot y + \sin(\delta) \cdot f_z(y)\big) \cdot \sin(\delta) \cdot f_c(y) \cdot dy - \beta^2 \cdot \int_{-b/2}^{b/2} D_2 \cdot \bar{a} \cdot \Big(3 \cdot \propto_{eq} \cdot \cos(\delta) + 2 \cdot (f_\theta(y) - i_0)\Big) \cdot \big(\cos(\delta) \cdot y + \sin(\delta) \cdot f_z(y)\big) \cdot \sin(\delta)^2 \cdot f_c(y) \cdot dy\Bigg)$$

$$M_{z_w} = \int_{-b/2}^{b/2} -X_L \cdot y + Y_L \cdot f_x(y) + m_{y_i} \cdot \sin(\delta)$$

$$M_{z_w} = \frac{\rho}{2} \cdot {U_{eq}}^2 \cdot \bar{a} \Bigg(\beta \cdot \int_{-b/2}^{b/2} \Big[\Big(2 \cdot (1 - D_2 \cdot \bar{a}) \cdot \propto_{eq} \cdot \cos(\delta) + (1 - 2 \cdot D_2 \cdot \bar{a}) \cdot (f_\theta(y) - i_0) \Big) \cdot y - \Big(1 + D_2 \cdot \bar{a} \cdot (\propto_{eq} \cdot \cos(\delta) + f_\theta(y) - i_0) \cdot \big(3 \cdot \propto_{eq} \cdot \cos(\delta) + f_\theta(y) - i_0 \big) \Big) \cdot \sin(\delta) \cdot f_x(y) \Big] \cdot \sin(\delta) \cdot f_c(y) \cdot dy - \beta^2 \cdot \int_{-b/2}^{b/2} \Big[(1 - D_2 \cdot \bar{a}) \cdot y - D_2 \cdot \bar{a} \cdot \Big(3 \cdot \propto_{eq} \cdot \cos(\delta) + 2 \cdot (f_\theta(y) - i_0) \Big) \cdot \sin(\delta) \cdot f_x(y) \Big] \cdot \sin(\delta)^2 \cdot f_c(y) \cdot dy \Bigg)$$

B.2 – Lateral-Directional reference parameters

The expressions above can me modeled as a linear function of the sideslip angle by applying some simplifications on the above equations. These simplifications do not affect considerably the results, as tested for a certain number of models with a comprehensive range of design parameters values; it can be shown that the error for the resultant force and moments remains below 5%. In this way, an "effective dihedral", a "roll arm" and a "yaw arm" can be defined as follows:

<u>B.2.1 – The effective dihedral:</u>

Disregarding the superior order terms in the expression derived for F_{y_w} this can be simplified to:

$$F_{y_w} \approx \frac{\rho}{2} \cdot {U_{eq}}^2 \cdot \bar{a} \cdot \mathrm{S} \cdot \Gamma_{\mathrm{ef}} \cdot \beta$$

Where "Γ_{ef}" can be seen as an "effective dihedral", because it determines approximately the amount of lateral force generated by a defined sideslip. Thus, the effective dihedral is defined as:

$$\Gamma_{\mathrm{ef}} = -\frac{1}{\mathrm{S}} \cdot \int_{-b/2}^{b/2} \left[1 + D_2 \cdot \bar{a} \cdot \left(\propto_{eq} \cdot \cos(\delta) + f_\theta(y) - i_0\right) \cdot \left(3 \cdot \propto_{eq} \cdot \cos(\delta) + f_\theta(y) - i_0\right)\right] \cdot \sin(\delta)^2 \cdot f_c(y) \cdot dy$$

It is possible to show that for normal design parameters a reasonable approximation for the "effective dihedral" is:

$$\Gamma_{\mathrm{ef}} \approx -\frac{1}{\mathrm{S}} \cdot \int_{-b/2}^{b/2} \sin(\delta)^2 \cdot f_c(y) \cdot dy$$

B.2.2 – The roll arm:

Disregarding the superior order terms in the expression derived for M_{x_w} this can be simplified to:

$$M_{x_w} = \frac{\rho}{2} \cdot {U_{eq}}^2 \cdot \bar{a} \cdot \mathrm{S} \cdot \mathrm{A_r} \cdot \beta$$

Thus, the roll arm is defined as:

$$\mathrm{A_r} = \frac{1}{\mathrm{S}} \cdot \int_{-b/2}^{b/2} \left(1 + D_2 \cdot \bar{a} \cdot \left(\propto_{eq} \cdot \cos(\delta) + f_\theta(y) - i_0\right) \cdot \left(3 \cdot \propto_{eq} \cdot \cos(\delta) + f_\theta(y) - i_0\right)\right) \cdot \left(\cos(\delta) \cdot y + \sin(\delta) \cdot f_z(y)\right) \cdot \sin(\delta) \cdot f_c(y) \cdot dy$$

It is possible to show that for normal design parameters a very good approximation for the "roll arm" can be found using the expression:

$$\mathrm{A_r} \approx \frac{1}{\mathrm{S}} \cdot \int_{-b/2}^{b/2} \left(\cos(\delta) \cdot y + \sin(\delta) \cdot f_z(y)\right) \cdot \sin(\delta) \cdot f_c(y) \cdot dy$$

Analyzing this expression it is possible to conclude that the reference lateral arm, or "roll arm" is a direct function of the geometry. This is an important result, because it shows that it is possible to guarantee static lateral stability only managing geometry.

B.2.3 – The yaw arm:

Disregarding the superior order terms in the expression derived for M_{z_w} it can be simplified to:

$$M_{z_w} = \frac{\rho}{2} \cdot {U_{eq}}^2 \cdot \bar{a} \cdot \mathrm{S} \cdot \mathrm{A_y} \cdot \beta$$

Thus, the yaw arm is defined as:

$$\mathrm{A_y} = \frac{1}{\mathrm{S}} \cdot \int_{-b/2}^{b/2} \Big[\Big(2 \cdot (1 - D_2 \cdot \bar{a}) \cdot \propto_{eq} \cdot \cos(\delta) + (1 - 2 \cdot D_2 \cdot \bar{a}) \cdot (f_\theta(y) - i_0) \Big) \cdot y - \Big(1 + D_2 \cdot \bar{a} \cdot \big(\propto_{eq} \cdot \cos(\delta) + f_\theta(y) - i_0 \big) \cdot \big(3 \cdot \propto_{eq} \cdot \cos(\delta) + f_\theta(y) - i_0 \big) \Big) \cdot \sin(\delta) \cdot f_x(y) \Big] \cdot \sin(\delta) \cdot f_c(y) \cdot dy$$

It is possible to show that for normal design parameters a very good approximation for the "yaw arm" can be found using the expression:

$$\mathrm{A_y} \approx \frac{1}{\mathrm{S}} \cdot \int_{-b/2}^{b/2} \Big[\Big(2 \cdot (1 - D_2 \cdot \bar{a}) \cdot \propto_{eq} \cdot \cos(\delta) + (1 - 2 \cdot D_2 \cdot \bar{a}) \cdot (f_\theta(y) - i_0) \Big) \cdot y - \sin(\delta) \cdot f_x(y) \Big] \cdot \sin(\delta) \cdot f_c(y) \cdot dy$$

Differently of the "roll arm" case, this expression shows that the reference directional arm, or "yaw arm" depends not only of the geometry but also on the aerodynamic proprieties and equilibrium AOA. In this way it can be seen that the analysis of the directional static stability is more complex.

Finally, it must be remembered that the moment coefficients can be immediately derived using the definition:

$$Cm_w = \frac{M_w}{\frac{\rho}{2} \cdot {U_{eq}}^2 \cdot \mathrm{S} \cdot \mathrm{MAC}}$$

And thus,

$$Cm_{x_w} \approx \bar{a} \cdot \frac{\mathrm{A_r}}{\mathrm{MAC}} \cdot \beta$$

$$Cm_{z_w} \approx \bar{a} \cdot \frac{\mathrm{A_y}}{\mathrm{MAC}} \cdot \beta$$